PB-214 539

KINETICS OF OXIDATION AND QUENCHING OF COMBUSTIBLES IN EXHAUST SYSTEMS OF GASOLINE ENGINES

D. J. Patterson, et al

Michigan University

Prepared for:

Coordinating Research Council

22 August 1972

DISTRIBUTED BY:

NTIS
National Technical Information Service
U. S. DEPARTMENT OF COMMERCE
5285 Port Royal Road, Springfield Va. 22151

310830-3-F

PB 214 539

Annual Progress Report No. 3
(Final)

Kinetics of Oxidation and Quenching of Combustibles in Exhaust Systems of Gasoline Engines

D. J. PATTERSON, R. H. KADLEC
B. CARNAHAN
H. A. LORD
J. J. MARTIN
W. MIRSKY
E. SONDREAL

PERIOD: February 24, 1971 to August 22, 1972

1971 - 1972

This project is under the technical supervision of the:
Coordinating Research Council
APRAC-CAPE 8-68 Steering Committee

and is work performed by the:
Departments of Mechanical and Chemical Engineering
The University of Michigan
Ann Arbor, Michigan

Under Contract No. CAPE-8-68(1-68)-CRC
and Contract No. CPA-22-69-51-HEW

Reproduced by
NATIONAL TECHNICAL
INFORMATION SERVICE
U S Department of Commerce
Springfield VA 22151

294

BIBLIOGRAPHIC DATA SHEET

1. Report No. CRC-APRAC-CAPE-8-3

2.

3. Recipient's Accession No. PB-214 539

4. Title and Subtitle

Kinetics of Oxidation and Quenching of Combustibles in Exhaust Systems of Gasoline Engines

5. Report Date August 22, 1972

6.

7. Author(s) D.J. Patterson, R.H. Kadlec; B. Carnahan; H.A. Lord; J.J. Martin; W. Mirsky; and E. Sondreal

8. Performing Organization Rept. No. U of M 310830-3-F

9. Performing Organization Name and Address

Departments of Mechanical and Chemical Engineering
The University of Michigan
Ann Arbor, Michigan

10. Project/Task/Work Unit No.

11. Contract/Grant No.

12. Sponsoring Organization Name and Address

The Coordinating Research Council, Inc., 30 Rockefeller Plaza, N.Y., N.Y. 10020 and The Environmental Protection Agency, Research Triangle Park, North Carolina 27711

13. Type of Report & Period Covered Final (2/71-8/72)

14.

15. Supplementary Notes

Releasable to the public after December 15, 1972

16. Abstracts

A comprehensive analytical and experiemental study of thermal reactors has been made. Arbitrary reactor configurations may be explored in regard to the steady-state and warm-up extent of oxidation of hydrocarbons, carbon monoxide, and hydrogen with perfrect of imperfect mixing and the detrimental effects of heat losses. Reactor size, shape, and material as well as start-up temperature may be explored for their effect on reactor lightoff time with various levels of exhaust HC, CO, and H_2. This experimental and analytical program focused on the Chevrolet 350 in.^{3} engine -- duPont Model V reactor combination. An experimental technique was developed which permits an assessment of the completeness of mixing between exhaust and injected air within a thermal reactor and is expected to be useful as a design aid. In addition to oxidation results for CO, H_2 and hydrocarbons as a whole, measurements were made to determine any changes in nitric oxide, aldehydes and olefin, paraffin, and aromatic class proportion affected by the thermal reactor at selected operating conditions. Finally separate studies were conducted in a stirred tank reactor to determine global oxidation kinetics for exhaust CO, HC and H_2 to be used in the computer simulation.

17. Key Words and Document Analysis. 17a. Descriptors

Hydrocarbons
Carbon Monoxide
Hydrogen
Nitric Oxide
Air Pollution
Aldehydes
Olefin
Paraffin

17b. Identifiers/Open-Ended Terms

Chevrolet 350 in.^{3} engine -- duPont Model V reactor combination

17c. COSATI Field/Group 7b; 7c; 11i; 11j; 13b.

18. Availability Statement Releasable to the general public

19. Security Class (This Report) UNCLASSIFIED

20. Security Class (This Page UNCLASSIFIED

21. No. of Pages 286

22. Price

THIS FORM MAY BE REPRODUCED

ANNUAL PROGRESS REPORT NO. 3

(Final)

KINETICS OF OXIDATION AND QUENCHING OF COMBUSTIBLES IN EXHAUST SYSTEMS OF GASOLINE ENGINES

D. J. Patterson, R. H. Kadlec
B. Carnahan
H. A. Lord
J. J. Martin
W. Mirsky
E. A. Sondreal

PERIOD: February 24, 1971 to August 22, 1972

1971 - 1972

This project is under the technical supervision of the:

Coordinating Research Council
APRAC-CAPE 8-68 Steering Committee

and is work performed by the:

Departments of Mechanical and Chemical Engineering
The University of Michigan
Ann Arbor, Michigan

Under Contract No. CAPE-8-68(1-68)-CRC
and Contract No. CPA-22-68-51-HEW

ACKNOWLEDGMENTS

We wish to thank the APRAC-CAPE 8-68 project group, Dr. P. R. Ryason, Chairman, who on behalf of the Coordinating Research Council guided the progress of this work and made many helpful suggestions. Their names are listed in the Distribution List at the end of this report. There is little doubt that the cooperative efforts of industry and The University of Michigan in this applied research area produced a synergistic effect.

Further, we wish to acknowledge the assistance of the numerous students who worked on the project. Their diligence and attention to detail were a significant factor in the success of this effort.

TABLE OF CONTENTS

Page

LIST OF TABLES viii
LIST OF FIGURES x
ABSTRACT xviii
INTRODUCTION 1
COMPREHENSIVE SUMMARY 2
MAJOR CONCLUSIONS 6
AREAS FOR FUTURE WORK 8

DETAILED PROGRESS - PHASE I

MULTICYLINDER AND SINGLE CYLINDER ENGINE MOUNTED REACTOR EXPERIMENTAL EVALUATIONS

A. MULTICYLINDER CONVENTIONAL REACTOR 11
    1. Objectives 11
    2. Experimental System 11
        a. Engine-reactor system 11
        b. Instrumentation 14
    3. Experimental Results 14
        a. Warm-up limitations on reaction 16
        b. Mixing limitations to steady performance 25
        c. Reactor combustion luminosity 42

B. SINGLE MULTICYLINDER EXPERIMENTAL REACTOR STUDY 49
    1. Objectives 49
    2. Experimental Apparatus 49
    3. Experimental Results 51
        a. Summary of CO oxidation rate results 51
        b. Summary of HC oxidation rate results 57
        c. Summary of H_2 oxidation rate results 58

C. REFERENCES FOR PHASE I 64

TABLE OF CONTENTS (Continued)

Page

DETAILED PROGRESS - PHASE II

COMPUTER MODEL DEVELOPMENT

FOREWORD 69

INTRODUCTION TO THE THERMAL REACTOR PROBLEM 71

MODEL BUILDING AND PARAMETER EVALUATION FOR STATIONARY STATE OPERATION 81

- I. Mixing Coupled with Reaction 81
  - A. Review on mixing in chemical reactor design 82
  - B. The pattern of flow micromixing simulation 89
  - C. Simplified mixing simulations 97
- II. General Parameter Evaluation 105
  - A. Simulations run on mixing with instantaneous reaction 108
  - B. Coupled mixing and kinetics at steady flow: parameter study on "MICROMIX II" 121

SIMULATIONS ON STATIONARY STATE REACTOR OPERATION: COMPARISON WITH EXPERIMENTAL STUDIES 140

- III. Estimates of the Coalescence Parameter, I_m 140
- IV. Simulations on the Kinetics Test Reactor 144
- V. Simulations on the DuPont Model V Reactor 150
  - A. Maximum conversions for instantaneous reaction—"MIXONLY POF" 150
  - B. Comparison dilution ratio on changes in air 155
  - C. Approach to a high temperature limit on conversion of carbon monoxide 157
  - D. Sensitivity to residence time distribution and micromixedness (I_m) 166

MODELING REACTOR OPERATION DURING WARM-UP 172

- VI. Model Building for Unsteady State Operation 172
  - A. Key features and assumptions 172
  - B. Reactor parts temperature simulation 173
  - C. Solutions for multiple oxidations in a "CSTR" 177
- VII. Base Case Warm-Up Simulations for the DuPont Model V Reactor 186
  - A. Warm-up without reaction—thermal parameter evaluation 186
  - B. Warm-up with lightoff 191

TABLE OF CONTENTS (Continued)

Page

VIII. Variations on the Base Case Warm-Up Simulation 195
  A. Design and operation 195
  B. Lightoff at time zero 200
  C. Summary on ignition effects 202

CONCLUSIONS AND USE OF RESULTS 207

  IX. Summary and Conclusions 207
  X. Use of Results 212

APPENDIX A. MIXING AND REACTOR THEORY 214

  1. Mixing in Reactor Design 214
  2. Theory of an Idealized Turbulent Mixer 221
  3. Selection of a Model Type for Exhaust Reactor Simulation 224

APPENDIX B. MOMENTS OF THE CONCENTRATION DISTRIBUTION FOR CURL'S RANDOM COALESCENCE MODEL APPLIED TO A REACTION VELOCITY OF ORDER η, $r = -kc^\eta$ 230

APPENDIX C. DANCKWERTS' "J" FACTOR FOR STIRRED TANKS IN SERIES AT $I_m = \infty$ 234

REFERENCES FOR PHASE II 237

NOMENCLATURE FOR PHASE II 241

DETAILED PROGRESS - PHASE III

SPECIAL INSTRUMENTATION DEVELOPMENT AND MEASUREMENTS

A. SUBTRACTIVE COLUMN HYDROCARBON ANALYSIS 249

  1. Purpose 249
  2. Equipment 249
  3. Experimental Verification 251
    A. Gas chromatographic comparison 251
    B. Calibration gas comparison 253
  4. Conclusions 253

TABLE OF CONTENTS (Concluded)

Page

B. GAS CHROMATOGRAPHIC STUDIES OF EXHAUST ACETYLENE 255

1. Purpose 255
2. Sampling Technique 255
3. Gas Chromatograph Operation 255
4. Data Analysis 257
5. Conclusion 259

C. MEASUREMENT OF INSTANTANEOUS ENGINE EXHAUST VELOCITY AND TEMPERATURE 265

1. The Measurement of Engine Exhaust Velocity 265
2. The Attempted Measurement of Instantaneous Exhaust Temperature 273

DISTRIBUTION LIST 280

LIST OF TABLES

Table | Page

PHASE I

I. Chevrolet Engine Characteristics 12

II. DuPont Type V Reactor Characteristics 12

III. Gas Analysis Techniques 15

IV. Multicylinder Engine-Reactor Performance 16

V. Warm-Up Test Results 24

VI. Range of Parameters (Carbon Monoxide Oxidation) 51

VII. Regression Program Results, CO Oxidation Rates 53

VIII. Comparison of Experimental CO Oxidation Rates with Two Wall Materials and Two Sparger Tubes 55

IX. Range of Parameters (Hydrocarbon Oxidation) 57

X. Hydrocarbon Oxidation Regression Results 59

XI. Range of Parameters (Hydrogen Oxidation) 59

XII. Hydrogen Oxidation Regression Results 61

PHASE II

I. Conversions of "A" for Mixing with Instantaneous Reaction of Separate Reactant Streams in "n" Equal Size Cell-Wise Stirred Tanks in Series 117

II. Conditions for Testing Parameters of MICROMIX II 122

III. Comparison of High Temperature Experimental Conversion with "MIXONLY TOF" Simulations of Mixing with Instantaneous Reaction 152

IV. Time to Lightoff for Variations to the DuPont Model V Base Case 196

LIST OF TABLES (Concluded)

Table Page

PHASE III

I. Substractive Column—G.C. Comparisons 252
II. FID and Subtractive Column Analyses 256
III. Hexane Equivalent of Components Determined by GC Analysis 258
IV. Corrected Olefin Content of Samples 260
V. Engine Specifications 272

LIST OF FIGURES

Figure | Page

PHASE I

1. DuPont type V reactor mounted on the Chevrolet 350 in.^{3} engine for test. 15

2. Type V DuPont exhaust manifold reactor. 15

3. DuPont Model V exhaust manifold reactor showing thermocouple locations. 17

4. Hydrocarbon, CO, and NO emissions as well as reactor centerline gas temperature and outer skin temperature versus time for a 70°F cold start. 18

5. Torque, bsfc and air/fuel ratio provided to the engine as a function of time. 19

6. Hydrocarbon, CO, and NO emissions versus time for engine conditions of 1200 rpm, 40 BHP, MBT spark, 17:1 air/fuel ratio, no air injection. 21

7. Reactor temperatures versus time. 22

8. Torque, bsfc and air/fuel ratio provided to the engine as a function of time. 23

9. Exhaust emissions with DuPont reactors as a function of air-injection fraction. 26

10. Extent of reaction vs. reactor temperature. 27

11. Conditions similar to Figure 10 except higher CO and H_2 reactor input. 29

12. Conditions similar to Figure 11 except air injection fraction doubled to F = 0.2. 30

13. Air injection manifold pressure minus exhaust port pressure versus crankangle. 32

14. Mass flow through air injection tube for cylinder number 1. 33

LIST OF FIGURES (Continued)

Figure | Page
15. Conditions similar to Figure 12 except the engine is run lean enough to provide the same reactor mixture ratio without air injection. 35
16. Effect of reactor temperature on the concentration of O_2, HC, and CO in the exhaust of a lean running engine, 1% = 10,000 ppm. 36
17. Extent of reaction vs. reactor temperature. 38
18. Same as Figure 17, except air injection fraction increased to approximately 0.15. 39
19. Effect of air injection fraction on CO conversion and reactor temperature. 40
20. Same as Figure 19 for hydrocarbon conversion. 41
21. Chevrolet 350 in.^{3} engine, 1200 rpm, 30 hp, 12.5:1 air-fuel ratio, air injection fraction .22, reactor temperature approximately 1650°F. 43
22. Repeatability of light emission. 43
23. Location of light emission peaks with respect to cycle effects for cylinders 1, 3, 5, and 7. 44
24. Repeatability of light emission. 46
25. Repeatability of light emission. 46
26. Spectrogram of luminous blue flame appearing in exhaust gas reactor. 47
27. Two-tank experimental reactor system schematic. 50
28. Predicted rates for CO oxidation for a mixture containing 1% CO, 1% O_2, and 500 ppm NO. 54
29. Conversions of hydrogen corrected to 20 lb exhaust/hr and .006 mole fraction hydrogen entering, $r_{H_2} = 12{,}660\ e^{-52{,}000/RT}$. 63

LIST OF FIGURES (Continued)

Figure Page

PHASE II

1. Schematic of exhaust flow from one cylinder through a thermal reactor exhaust system. 72

2. Characteristic variation in cyclic exhaust flow from a single cylinder spark ignition engine. 75

3. Combined normalized flow for cylinders 1, 3, 5, and 7 of a V-8 engine. 76

4. Characteristic variation in cyclic mass flow through air injection tube during a 720° engine cycle. 77

5. Assumed variation in cyclic exhaust temperature based on coincidence with measured peak flow. 79

6. Characteristic variation in cyclic hydrocarbon concentration. 80

7. Illustrative module network for simulation "MMPOF." 89

8. Schematic on the compiling of the inlet cell roster. 91

9. Flow and mixing in non-ideal stirred tank modules within "MICROMIX PATTERN OF FLOW." 93

10. Flow and mixing in non-ideal plug flow modules within "MICROMIX PATTERN OF FLOW." 95

11. Mole fraction integration showing disappearance of species. 97

12. Mixing with instantaneous reaction, $A + B \rightarrow 2C$. 104

13. The effect of a small number of cells in the reactor, N_c, on conversion for a stirred-tank simulation of mixing with instantaneous reaction, $A + 1/2B \rightarrow C$. 105

14. The effect of a small number of cells in the reactor, N_c, on the conversion for a stirred-tank simulation of mixing with instantaneous reaction, $A + 1/2B \rightarrow C$. 106

15. Stirred-tank mixing with instantaneous reaction, $A + 1/2B \rightarrow C$. 109

LIST OF FIGURES (Continued)

Figure | Page

16. Stirred-tank mixing with instantaneous reaction, $A + 1/2B \rightarrow C$. 110

17. Effect of feed stoichiometric ratio, SR, on stirred-tank cell mixing with instantaneous reaction, $A + 1/2B \rightarrow C$. 111

18. Effect of dilution ratio (stream 2/stream 1) on stirred-tank cell mixing with instantaneous reaction, $A + 1/2B \rightarrow C$. 112

19. Plug-flow cell mixing with instantaneous reaction, $A + 1/2B \rightarrow C$. 113

20. Effect of feed stoichiometric ratio on plug flow cell mixing with instantaneous reaction, $A + 1/2B \rightarrow C$. 114

21. Effect of dilution ratio, DR, on plug-flow mixing with instantaneous reaction, $A + 1/2B \rightarrow C$. 115

22. Mixing with instantaneous reaction for "n" equal size cell-wise stirred tanks. 118

23. Danckwerts' "J" factor for cell-wise mixed stirred tanks in series. 119

24. Influence of Danckwerts' "J" on fraction "A" converted for instantaneous reaction of "A" in cell-wise mixed tanks in series. 120

25. Comparison of stirred-tank conversion for zero order and .269 order CO kinetics at $I_m = \infty$. 123

26. Material and energy balance curves for coupled reaction and mixing, $I_m = 1$ to ∞, in a cell-wise mixed stirred tank at dilution ratio, DR = .1. 124

27. Material and energy balance curves for coupled reaction and mixing, $I_m = 1$ to ∞, in a cell-wise mixed stirred tank at dilution ratio, DR = .25. 125

28. Material and energy balance curves for coupled reaction and mixing, $I_m = 1$ to ∞, in a cell-wise mixed stirred tank at dilution ratio, DR = .50. 126

LIST OF FIGURES (Continued)

Figure Page

29. Material and energy balance curves for coupled reaction and mixing, $I_m = 1$ to ∞, in a cell-wise mixed stirred tank at dilution ratio, DR = 1. 127

30. Material and energy balance curves for coupled reaction and mixing, $I_m = 1$ to ∞, in a cell-wise mixed stirred tank at a feed stoichiometric ratio (B:A), SR = 1. 129

31. Material and energy balance curves for coupled reaction and mixing, $I_m = 1$ to ∞, in a cell-wise mixed stirred tank at a feed stoichiometric ratio (B:A), SR = 2. 130

32. Material and energy balance curves for coupled reaction and mixing, $I_m = 1$ to ∞, in a cell-wise mixed stirred tank at a feed stoichiometric ratio (B:A), SR = 5. 131

33. Material and energy balance curves for coupled reaction and mixing, $I_m = 1$ to ∞, in a cell-wise mixed stirred tank at a feed stoichiometric ratio (B:A), SR = 15. 132

34. Material and energy balance curves for coupled reaction and mixing, $I_m = 1$ to ∞, in a cell-wise mixed stirred tank at activation energy, E = 10,000 cal/g mole. 134

35. Material and energy balance curves for coupled reaction and mixing, $I_m = 1$ to ∞, in a cell-wise mixed stirred tank at activation energy, E = 50,000 cal/g mole. 135

36. Material and energy balance curves for coupled reaction and mixing, $I_m = 1$ to ∞, in a cell-wise mixed stirred tank for first order reaction. 136

37. Material and energy balance curves for coupled reaction and mixing, $I_m = 1$ to ∞, in a cell-wise mixed stirred tank for second order reaction. 137

38. Material and energy balance curves for coupled reaction and mixing, $I_m = 1$ to ∞, in a cell-wise mixed stirred tank at a mean residence time, $\tau = .002$ sec at 1500°F. 138

39. Material and energy balance curves for coupled reaction and mixing, $I_m = 1$ to ∞, in a cell-wise mixed stirred tank at a mean residence time, $\tau = .150$ sec at 1500°F. 139

LIST OF FIGURES (Continued)

Figure		Page
40.	Simulation of CO conversions in the kinetic test reactor.	145
41.	Experimental conversions from kinetics test data plotted on the cell-wise mixing simulation of Figure 40.	146
42.	The effect of mixing parameter (I_m) on hydrogen conversion.	147
43.	Patterns of flow run to simulate the DuPont Model V reactor.	151
44.	Stirred-tank simulation of the effect of air injection fraction at a mixing parameter value of $I_m = 8$.	154
45.	Simulation of the effect of air injection fraction using the pattern of cell flow shown in Figure 43.	156
46.	Simulation of the approach to high-temperature mixing-limited conversion for CO using a stirred tank cell mixing model.	159
47.	Simulation of the approach to high-temperature conversion for CO using the cell pattern of flow shown in Figure 43.	160
48.	Simulation of the approach to high-temperature conversion for CO using the cell pattern of flow shown in Figure 43.	161
49.	Cell mixed plug flow simulation.	162
50.	Residence time distribution for the simulation shown in Figure 47 and item 2, Figure 43.	163
51.	The effect of inlet exhaust temperature span (cyclic) on conversion.	167
52.	Simulation of a half reactor assuming symmetry.	168
53.	Sensitivity of simulation conversions to the mixing parameter, I_m.	169
54.	Comparison of the stirred tank-with-plug-flow simulation with cell-wise stirred tanks in series.	171
55.	Thermal conductance network for the DuPont Model V reactor with external insulation.	174

LIST OF FIGURES (Continued)

Figure Page

56. Conversions of carbon monoxide corrected to 30 lb exhaust/hr and .02 mole fraction CO entering. 184

57. Conversions of hydrocarbon corrected to 20 lb exhaust/hr and 400 ppm hydrocarbon entering. 185

58. Simulated steady-state heat loss measured as drop in exhaust temperature. 187

59. Steady-state metal temperature profiles. 188

60. Warm-up of the DuPont Model V. 189

61. Comparison of experimental and typical simulated warm-up for the DuPont Model V reactor. 192

62. Simulation of lightoff for the DuPont Model V reactor. 194

63. Deviations in time to lightoff for variations to the DuPont Model V base case. 199

64. Approach to immediate lightoff. 201

65. Simulated lightoff for insulated empty can. 203

66. Warm-up simulation of inlet properties required to achieve immediate ignition with stoichiometric air at 100°F. 204

67. A summary of typical ignition behavior for a zero order CSTR simulation. 205

PHASE III

1. Flow schematic of University of Michigan subtractive column-flame ionization hydrocarbon analysis system. 250

2. Results for samples without after-reaction. 261

3. Results for samples with after-reaction. 262

4. Results for samples without after-reaction. 263

LIST OF FIGURES (Concluded)

Figure | Page
5. Results for samples with after-reaction. 264
6. Schematic diagram of laser-schlieren optical system. 266
7. Streak schlieren photograph showing the start of the exhaust process. 267
8. Exhaust velocity measurement system. 268
9. Electrical schematic. 269
10. Velocity as a function of crankangle. 270
11. Exhaust gas velocity vs. crankangle. 271
12. Photodiode amplifier circuit. 274
13. Dimensions of Hewlett-Packard pin photodiode 5082-4205. 274
14. Spark circuit. 275
15. Speed of sound in exhaust gas as a function of temperature and equivalence ratio. 276
16. Photodiode signals from velocity of sound measurements in room air at 72°F. 277
17. Photodiode signals with expanded time scale. 277
18. Photodiode signals showing repeatability. 277

ABSTRACT

A comprehensive analytical and experimental study of thermal reactors has been made. The findings have been incorporated into a computer model capable of simulating reactor performance both during warm-up and steady-state operation. Arbitrary reactor configurations may be explored in regard to the steady-state and warm-up extent of oxidation of hydrocarbons, carbon monoxide, and hydrogen with perfect or imperfect mixing and the detrimental effects of heat losses. Reactor size, shape, and material as well as start-up temperature may be explored for their effect on reactor lightoff time with various levels of exhaust HC, CO, and H_2.

This experimental and analytical program focused on the Chevrolet 350 in.^{3} engine—duPont Model V reactor combination. Experimental and calculated results are presented and compared where possible. Analytical models for the duPont reactor were developed each of which treated the exhaust ports, core, and annulus differently. An experimental technique was developed which permits an assessment of the completeness of mixing between exhaust and injected air within a thermal reactor and is expected to be useful as a design aid.

In addition to oxidation results for CO, H_2, and hydrocarbons as a whole, measurements were made to determine any changes in nitric oxide, aldehydes and olefin, paraffin, and aromatic class proportion affected by the thermal reactor at selected operating conditions. Finally separate studies were conducted in a stirred tank reactor to determine global oxidation kinetics for exhaust CO, HC, and H_2 to be used in the computer simulation.

Results of this study are incorporated in three annual progress reports to the Coordinating Research Council of which this report is the third and final.

Computer programs are available as an appendix to this report. Order PB 215-633, $3.00 in paper copy, $.95 in microfiche from NTIS.

INTRODUCTION

This exhaust thermal reactor program, which has been conducted within the Departments of Mechanical and Chemical Engineering at The University of Michigan over a three-year period has had the following broad objectives:

- To quantify the effects that the various chemical and physical processes have on emission characteristics of exhaust thermal reactors installed on selected typical engines operating at various conditions on a dynamometer test stand.

- To obtain concentration measurements of pertinent chemical species and classes at the entrance to, within, and at the exit from thermal reactors, and from this data to determine gross chemical reaction rates.

- To obtain information which will be helpful in predicting the design of gasoline engine exhaust reactors.

- To develop a computer model for the thermal reactors.

The program has been divided into three phases of study. These were:

Phase I. Multicylinder and Single Cylinder Engine Mounted Reactor Experimental Evaluations.

Phase II. Computer Model Development.

Phase III. Special Instrumentation Development and Measurements.

This report details progress made primarily during the third and final year of the program. In some cases information contained in prior annual reports has been included to improve readability. In other cases reference is made to the First and Second Annual Progress Reports for additional details. Below are the comprehensive summary and major conclusions of the program.

COMPREHENSIVE SUMMARY

PHASE I. MULTICYLINDER AND SINGLE CYLINDER ENGINE MOUNTED REACTOR EXPERIMENTAL EVALUATIONS

A Chevrolet 350 in.^{3} engine was procured and baseline performance and emission data obtained. Variables included mixture ratio, ignition timing, speed, and load. Subsequently a pair of duPont Model V thermal reactors were installed on the engine and evaluated for emission reduction performance.

Studies were made to determine factors which limited conversion of hydrogen, carbon monoxide, and hydrocarbons in the reactor during both warm-up and steady-state operation. Variables explored were mixture ratio, spark timing, and air injection quantity. For a given flowrate (residence time) oxidation of these compounds was found to depend on temperature, exhaust feed composition, air injection quantity, and mixing. Conversions between 0 and 100% were observed for hydrogen, 0 and 98% for hydrocarbons, and 0 to 95% for CO. In every case CO was the most difficult specie to oxidize because of its relatively slow reaction rate. It was a common observation that above 1600°F conversion was a maximum and no additional oxidation of any specie measured occurred as temperature increased. On the other hand, below 1200°F conversion was nil. On the average, nitric oxide concentration was not affected by the Model V reactor even though its concentration was found to correlate with CO and HC global oxidation rates determined in a separate study described later. This apparent paradox may be explained, at least in part, by the global rate assumptions themselves.

Variations in composition and temperatures within the reactor show that maximum conversion was undoubtedly mixing limited during hot steady operation. Experiments in which the air was injected steadily using a critical flow orifice strengthened the mixing limitation conclusion. Low conversion during warm-up suggested that the reactor was primarily rate limited during this mode of operation.

Under certain nonoptimum conditions of air injection and temperature, olefin and aldehyde compounds emitted from the reactor increased even though total hydrocarbons decreased. This increase was relative to the emissions without the after-reaction afforded by the thermal reactor when the injected air was terminated. The aldehyde increase was deemed potentially serious. A tenfold increase was observed in one test. Olefin increase was typically 20-30% under these nonoptimum conditions.

Our conclusion is that under warmed up conditions and especially as the reactor temperature approaches 1600°F, maximum conversion is mixing limited. Thus mixing simulation must be a key aspect in any steady-state simulation model. In contrast, during warm-up when temperatures are below 1200°F, reactors are rate limited as a result of heat transfer from the hot exhaust gas to the cold reactor surfaces. Future reactor designs should stress improved mixing and reduced thermal inertia and heat loss.

Concurrently with the multicylinder engine study, a single cylinder CFR engine-reactor study was undertaken to determine gross hydrocarbon, carbon monoxide, and hydrogen oxidation kinetics in actual engine exhaust under the controlled conditions possible with a single cylinder engine and reactor. The rate expressions determined were used in the computer models developed in Phase II.

The single cylinder thermal reactor was designed to be a continuously stirred tank reactor (CSTR). A helium tracer hot-wire anemometer technique was employed to assess residence time distribution. It indicated design changes needed to approach CSTR behavior. Rate equations were formulated which correlated CO oxidation rate with CO and O_2 concentrations in one case and with CO and O_2 and NO concentrations in the other; the latter providing a slightly better correlation. Reaction order was low, about 1/4 in either case. Hydrocarbon oxidation rate was correlated with hydrocarbon, oxygen, and nitric oxide concentration in one case, and additionally with CO in the other, the latter providing a significant improvement. Reaction order was between one and two in these hydrocarbon correlations. Hydrogen oxidation data were quite scattered and a zero-order rate expression was selected to predict the observed results. Water vapor was not included in these oxidation correlations since water vapor concentration is relatively high and constant in engine exhaust. A near zero-order dependence is the result in the global correlations.

PHASE II. COMPUTER MODEL DEVELOPMENT

The simulation efforts have been divided into two main areas of reactor performance: steady operation and warm-up. The primary goal of the steady operation effort has been the correct implementation of mixing imperfections whereas the primary goal of the warm-up study has been to describe the start-up of a cold reactor.

The warm-up simulation consisted of a program termed "RTEMP" which accepted warm-up of an arbitrary number of metal surfaces in a reactor and which accepted values of gas temperature from a simple stirred tank kinetics program. This approach assumes that conversion during warm-up is reaction rate (temperature) limited rather than mixing limited. Warm-up simulations have been run using steady-state reactor inputs. For the warm-up computations, steady mass averaged reactor exhaust inputs were found to yield results virtually identical to those obtained with staggered pulsed inputs characteristic of single or multicylinder gasoline engine exhaust. To speed computation, the rate data of Phase I were fitted with zero-order expressions. This did not affect the predicted time to light off, but did give a more abrupt light off than observed experimentally. Reasonable correlation with the results of Phase I were obtained. It must be noted that all warm-up runs, both experimental and calculated, were made with a constant (or nearly so in the experimental runs) fuel-air ratio. Thus warm-up rates and light off times do not reflect conventional cold start choked engine operation. Choked operation would be expected to accelerate the warm-up process. Rather, our results are closer to simulating a hot start where the choke is off.

The simulation of steady-state performance encompassed several programs depending on the sophistication desired. Initially a program termed "EXHAUST" was developed. It predicted the performance of a stirred tank reactor and was capable of accepting staggered pulse-type exhaust inputs. Studies in Phase I soon suggested that steady performance was mixing limited. Consequently, this aspect was added to the simulation. Since both macromixing (residence time distribution) and micromixing (localized reactant segregation) are important, our simulations have included both.

The first generation of programs incorporating mixing limitations assumed a perfectly macromixed reactor with imperfect micromixing. Three levels of capability were developed using a random coalescence mixing model. The most complicated was MICROMIX I which treated the (batch) kinetics occurring in a single packet or cell with generality and employed multiple-step integration. A more economical model to run, MICROMIX II was restricted to combustion reactions and used a single step integration for updating projections. The simplest and fastest was MIXONLY (several versions), which assumed very fast reactions which go to completion. Here, conversion was limited by mixing only.

The second generation of programs dealt in addition with imperfect macromixing. Initially efforts were aimed at developing a generalized program in which an arbitrary residence time distribution could be entered to simulate a particular reactor configuration. For this work a model for a micromixed limited plug-flow reactor was developed "MMPF." This general approach was subsequently abandoned in favor of a pattern of flow (POF) model which simulated the reactor with a series and parallel combination of stirred tank and plug-flow elements. The patterns of flow model used with one of the micromixing programs and appropriate rate expressions is the final package recommended for simulating real steady reactor performance. The degree of micromixing may vary from element to element. The program may be used with staggered pulsed inputs and these effects become more significant as the residence time distribution departs from that for a stirred tank.

PHASE III. SPECIAL INSTRUMENTATION DEVELOPMENT AND MEASUREMENTS

A. Gas Analysis

Several gas analysis instruments and procedures were constructed or developed in the course of this program. These were:

1. Hydrocarbon class analysis by subtractive columns—discussed herein in Detailed Progress - Phase III.

2. Hydrogen concentration by thermal conductivity—discussed in the Second Annual Progress Report.

3. Aldehyde analysis by DNPH.

4. Light hydrocarbon identification by gas chromatograph—discussed herein in Detailed Progress - Phase III.

As indicated, numerous experimental results and procedural details for the above instrumentation were included in the First and Second Annual Progress Reports as well as in this report.

B. Exhaust Velocity Measurement

A laser-schlieren technique has been developed to measure instantaneous exhaust gas velocity. Successful results were obtained by photographing the schlieren image of an exhaust stream eddy passing through the exhaust pipe. Results from a firing single cylinder CFR engine at 600 and 1000 rpm, wot, showed instantaneous exhaust velocity reached about 200 ft/sec with flow reversals reaching 60 ft/sec midway through the exhaust process. Similar efforts to measure instantaneous exhaust temperature by detecting the passage of spark-induced pressure waves did not prove successful.

MAJOR CONCLUSIONS

Although the automotive-type thermal reactor is similar to classical chemical reactor models, a number of important differences arise. These are: (1) the staggered pulse-type segregated feed, (2) the numerous reacting species in the feed stream, (3) the importance of transient low temperature rate limited operation, and (4) imperfect mixing within the reactor. Therefore, the complete reactor simulation must not only account for the effects of temperature, composition, reaction rate, residence time, and heat loss, but also provide for the above four additional factors. In addition the simulation must provide for a description of the often complex reactor and heat transfer geometry required in multicylinder engine applications. The experimental and analytical results of this study have shown that:

1. Under steady warmed up conditions, oxidation of exhaust combustibles can be predicted reasonably well by the simulation as temperature, feed composition, and residence time change. The simulation is most useful for determining directions for design modifications.

2. Peak conversions of exhaust hydrocarbons and carbon monoxide can reach 95% in the duPont Model V reactor. Conversion is ultimately precluded from being complete by imperfect mixing. Both theoretical and experimental results support this conclusion.

3. The simulation has shown that the character of the pulsed staggered exhaust inputs to the reactor can greatly affect oxidation of combustibles for reactors which are not well macromixed.

4. The simulation results show virtually no oxidation occurring in the exhaust port. This arises from segregation of injection air and exhaust in the port and the short residence time there.

5. Experimental results showed that reactive hydrocarbons and aldehydes may or may not be largely eliminated in a thermal reactor and, in fact may be increased under certain nonoptimum conditions, even while total hydrocarbons have decreased.

6. For air-injected reactors, a mixing volume followed by a plug-flow element is expected to be an effective reactor configuration.

7. Experimental time to light off may be predicted reasonably well by a simulation at least for the unchoked constant mixture ratio cases explored.

8. Rapid reactor warm-up is enhanced by:

a. Low thermal inertia of reactor parts and minimum heat losses.

b. Maximization of exhaust gas temperature through, for example, retarding engine spark timing.

c. Maximization of exhaust combustibles through severe engine choking at start-up and thereafter.

d. Diversion of cool injected air until reactor temperature reaches 1200°F, a typical light-off temperature. This last conclusion applies to an unchoked or lightly choked engine.

9. Results from the stirred tank experimental reactor operating on actual exhaust have yielded reaction orders for exhaust combustibles which are considerably lower than literature values.

10. A reasonable estimate of mixing intensity can be made from design data. Reactor and engine dimensions, together with flowrate information, yield upper and lower bounds on mixing intensity.

11. The extent of conversion at high reactor temperatures is recommended as a design aid to indicate the thoroughness of mixing of exhaust and injected air within the reactor. Retarding the spark at a fixed mixture ratio and air injection quantity, the approach used in Phase I of this report may be used to increase reactor temperature for this mixing assessment.

AREAS FOR FUTURE WORK

Results obtained thus far suggest the following areas for future study:

1. Further verification of the model with other reactor designs.
2. Effect of severe choking or hot-spot ignition on warm-up time for an experimental engine reactor system.
3. Effect of fuel hydrogen to carbon ratio on warm-up.
4. Optimization of reactor warm-up through programmed changes in engine operating variables.
5. Reactor performance and optimization for Wankel engines.

DETAILED PROGRESS - PHASE I

MULTICYLINDER AND SINGLE CYLINDER ENGINE MOUNTED REACTOR EXPERIMENTAL EVALUATIONS

A. MULTICYLINDER CONVENTIONAL REACTOR

1. Objectives

The overall objectives of the multicylinder engine reactor study were: (1) to determine the emission characteristics of a typical engine-reactor system operating at various conditions on a dynamometer test stand during both warm-up and steady state operation; (2) to determine concentrations of pertinent chemical species and classes entering, within, and exiting the reactor; (3) to explore factors which limit thermal reactor performance; and (4) to obtain thermal reactor data against which the computer mode could be tested.

2. Experimental System

a. ENGINE-REACTOR SYSTEM

A production Chevrolet 350 in.^{3} V-8 engine with duPont Model V exhaust reactors was used for the multicylinder work. Selected engine characteristics are listed in Table I. The engine was installed with the vehicle exhaust system.

The duPont Model V reactor is shown in Figure 1. It is mounted in place of the production exhaust manifold. One reactor is used for each bank of the engine. Figure 2 shows a schematic of the type V reactor. The reactor consists of an outer shell in which is mounted a tubular core and a radiation shield to insulate the hot core from the cooler outer shell. Air is injected into each exhaust port counter to the exhaust flow. The exhaust gas-air mixture is swept into the reactor core during the exhaust stroke as the arrows suggest. When conditions are favorable vigorous chemical reactions occur which convert hydrocarbon and carbon monoxide compounds to carbon dioxide and water vapor. The hot gases still reacting then flow around the radiation shield into the exhaust system. References 1-5 describe the reactors and their performance on vehicles in more detail. Key characteristics are listed in Table II.

In our tests, stainless steel quench coils were installed in each entrance port of the reactor. These provide cooling of the exhaust and suppression of exhaust after-reaction. The composition of the cooled mixed unreacted gases leaving the exhaust reactor has been used as a measure of the reactor input. Each coil was made from a 4-ft length of 1/8 in. stainless steel tubing

Preceding page blank

TABLE I

CHEVROLET ENGINE CHARACTERISTICS

Model year	1969
Displacement	350 in.^3
Compression ratio	9.0:1
No. of cylinders	8
Bore	4.0 in.
Stroke	3.48 in.
Con. rod length	5.7 in.
Firing order	1-8-4-3-6-5-7-2
Fuel specification	regular
Carburetion	Rochester 2-bbl
Emission control	AIR
Rated power	255 BHP at 4200 rpm
Rated torque	365 lb ft at 1600 rpm
Exhaust opening	66° BBC
Exhaust closing	32° ATC
Intake opening	16° BTC
Intake closing	70° ABC
Left exhaust manifold	13 lb/64.6 in.^3
Right exhaust mainfold	13.25 lb/73 in.^3
Exhaust port volume	3.66 in.^3/cyl

TABLE II

DuPONT TYPE V REACTOR CHARACTERISTICS

Year received	1969
Overall length	21.375 in.
Overall diameter (exc. port)	5.5 in.
Overall internal vol, flange-to-flange	259 in.^3/reactor
Inner core volume	60 in.^3/reactor
Weight	26 lb/reactor
Primary material	310 stainless
Maximum recommended core temperature*	1750°F

---

*Materials are available which permit higher temperature operation.

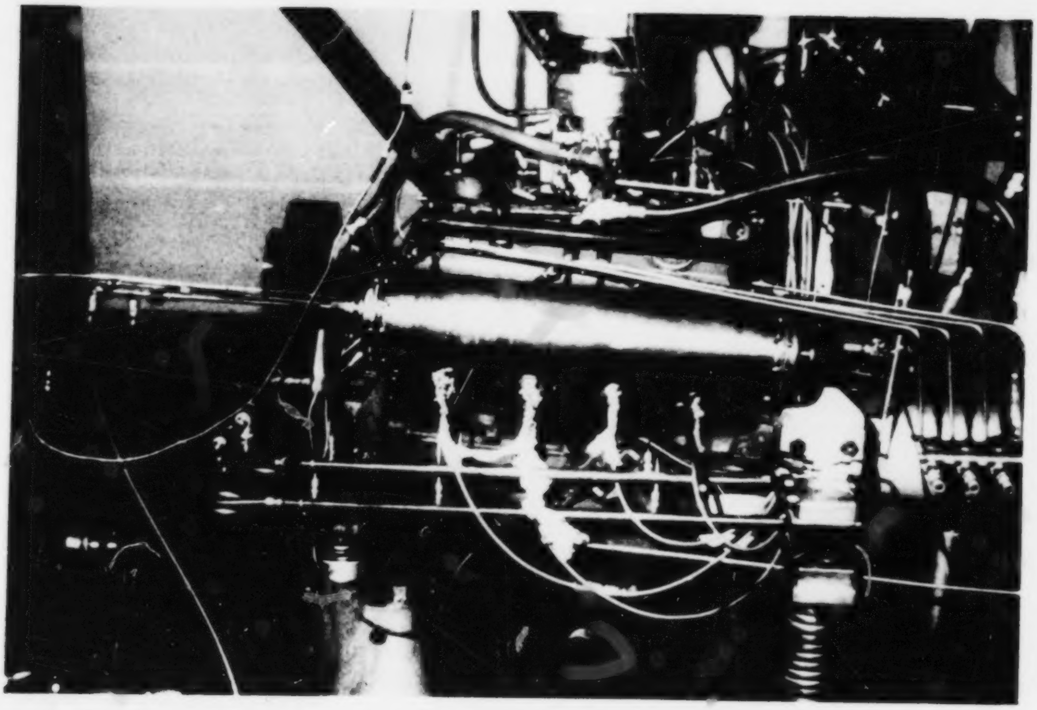

Figure 1. DuPont type V reactor mounted on the Chevrolet 350 in.^{3} engine for test in Room 243 of the Automotive Engineering Laboratory.

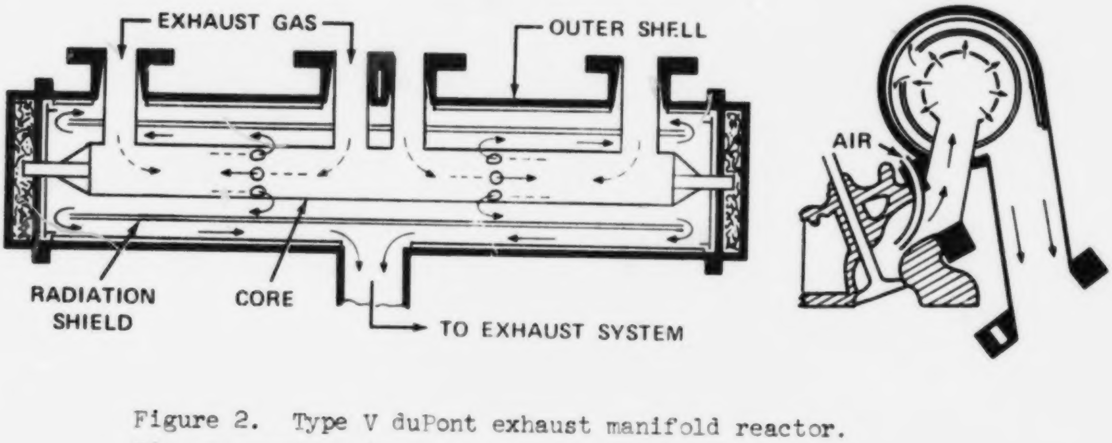
EXHAUST GAS
OUTER SHELL
AIR
RADIATION SHIELD
CORE
TO EXHAUST SYSTEM

Figure 2. Type V duPont exhaust manifold reactor. Figure courtesy duPont Corporation.

through which cold water at 65 psi circulated. Typically a 200° temperature drop could be obtained with the coils.

An engine change required for optimum reactor operation involved modifying the intake manifold heating system. The conventional exhaust gas crossover passage entrances were blocked. Instead, hot water was routed to the crossover. This conserved reactor energy while providing manifold heat. An intake manifold properly modified was supplied by duPont.

One of the reactors was modified to accept quartz windows at the center of each end of the reactor. This provided a straight optical path through the hot core. One window was large enough (1-3/4 in. dia) to allow a visual inspection of the combustion process. The other window was smaller (3/4 in. dia). Additional photographs of the reactor were included in the First Annual Progress Report."

b. INSTRUMENTATION

(1) Engine

Engine power was measured by a Westinghouse 200 hp electric dynamometer. Fuel flow was measured by a General Motors displacement-type burette system. Fuel-air ratio was controlled by pressurization or evacuation of the carburetor float bowl. Air flow was measured by a 1000 CFM Meriam laminar flowmeter. A large tank was mounted above the engine to minimize pulsation effects. Mercury manometers were used to measure the intake and exhuast system average pressures. Continuous gas sampling taps were installed at each port, at the exhaust wye, and at the tailpipe. Various thermocouples measured engine and reactor local temperatures.

(2) Gas Analysis

Gas analyses were made with a variety of instrumentation. Table III lists this equipment. The O_2 analyzer as well as nondispersive IR analyzers for CO, CO_2, NO, and HC have been incorporated into a large semiportable cart. Additional details of the gas analysis system including schematics are included in the First and Second Annual Progress Reports.[11,12]

3. Experimental Results

In the course of this investigation a variety of experimental data have been gathered on the Chevrolet 350 in.^{3} engine and the duPont Model V reactor.

TABLE III

GAS ANALYSIS TECHNIQUES

Specie	Technique	Manufacturer	Range
Carbon monoxide	NDIR[1,2]	Beckman Inst. Model 315A	0-10%
Carbon dioxide	NDIR[1,2]	Beckman Inst. Model 315A	0-15%
Nitric oxide	NDIR[1,3]	Beckman Inst. Model 315A	0-4000 ppm
Hydrocarbon	NDIR[1]	Beckman Inst. Model 315A	0-1000 ppm
Hydrocarbon	FID[4]	Beckman Inst. Model 109A	0-3000 ppm
O_2	Amperometric	Beckman Inst. Model 715	0-5% or 0-25%
Aldehydes	DNPH[5]	Wet chemical and Bausch & Lomb Spectronic 20 spectrophotometer	
Hydrocarbon classes	Subtractive column plus FID	Homemade—after Sigsby (Ref. 6) (see also Ref. 11, p. 27 and Phase III of this report)	
Individual hydrocarbons	Gas chromatograph	Perkin-Elmer 800 (see Phase III of this report)	
Hydrogen	Thermal conductivity	Homemade (discussed in Ref. 12, p. 35)	0-5%

---

1. NDIR - Nondispersive infrared.
2. Orsat used as check of calibration gases.
3. Modified Saltzman used as check of calibration gases (Ref. 10)
4. FID - Flame ionization detector.
5. DNPH - Dinitrophenylhydrazone wet chemical method—colorimetric procedure (Refs. 7-9)

Table IV summarizes the work performed during the first and second year, and where discussions can be located.

The present report contains data and analyses for work performed during the final year. The topics covered herein are:

- warm-up limitations on reaction
- mixing limitations to steady performance
- reactor combustion luminosity

In some cases the data have been corrected for the dilution effect of air injection. This correction was made based on a dry exhaust carbon balance with and without air injection. Emission results corrected for dilution are so designated.

TABLE IV

MULTICYLINDER ENGINE-REACTOR PERFORMANCE

Type of Test	Annual Report Reference
Baseline engine performance and emissions	
Varying air/fuel ratio, spark timing, speed, and load	1st, pp. 4-8
Steady-state engine-reactor performance	
Hydrocarbon and carbon monoxide oxidation, hysteresis effects	2nd, pp. 8-10
Nitric oxide emission	2nd, p. 10
Aldehyde emission	2nd, pp. 10-11
Reactor mixing	2nd, pp. 11-13
Air injection distribution	2nd, p. 13

a. WARM-UP LIMITATIONS ON REACTION

Warm-up is an important mode of thermal reactor performance because of the emphasis on cold start in Federal vehicle exhaust emission procedures. In order to simulate warm-up on our dynamometer tests, the engine was allowed to cool overnight (16 hr) to room temperature (about 70°F). For each test the engine mixture ratio, throttle, and spark settings were established the afternoon proceeding the test. They were adjusted to give 30 BHP at 1200 rpm for the warmed-up engine. Twelve tests were run with various mixture ratios, spark timings, loads, and air injection rates (see Table V). Because relatively constant mixture ratios were used results do not reflect conventional choked engine operation.

In order to measure reactor gas and metal temperatures during warm-up, thermocouples were installed in the right-hand reactor. Four chromel/alumel immersion-type thermocouples were attached to the reactor inner surfaces. These had a sheath diameter of 1/16 in. and a response time of approximately 1/4 sec. A fifth identical but shielded couple was installed to measure gas temperature. Three additional couples were attached to measure the outer skin temperature of the outer skin temperature of the reactor. The thermocouple locations are shown in Figure 3.

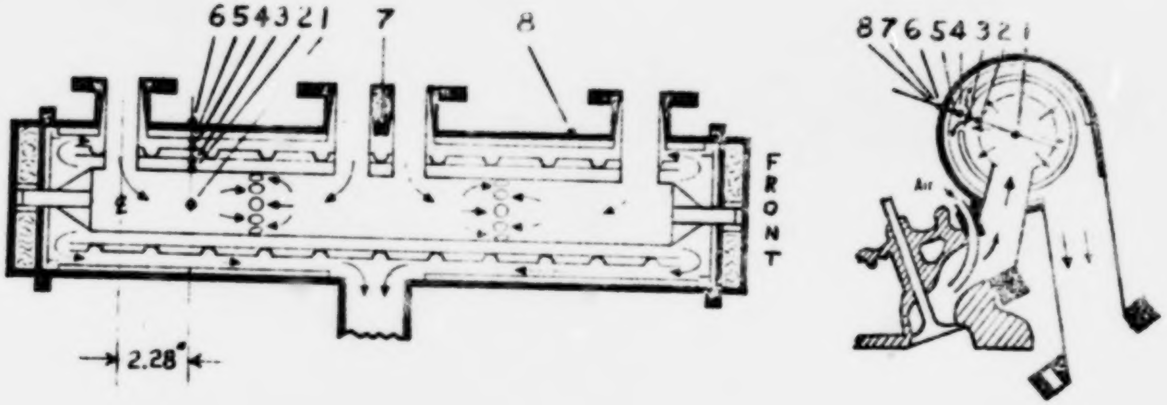

1 - Reactor centerline (gas temperature)
2 - Outside of first shell
3 - Inside of second shell
4 - Outside of second shell
5 - Inside of reactor casing
6,7,8 - Outside of reactor casing

Figure 3. DuPont Model V exhaust manifold reactor showing thermocouple locations.

After the 16-hr soak, the engine was brought up to 1200 rpm by the dynamometer and the fuel and ignition turned on. No choke was used so that mixture ratio was established by the preset carburetor settings. FID hydrocarbons and NDIR CO emissions as well as reactor temperatures were recorded on strip chart recorders. Other emission data and engine performance data were taken as rapidly as possible by hand. No changes in throttle, spark, or mixture were made by the dynamometer operator.

Figure 4 shows warm-up results at 1200 rpm, 12.5:1 air/fuel ratio, 30 BHP load, and MBT spark. Air injection was 0.3. Air injection fraction, F, is the injected air expressed as a mole fraction of the exhaust flow. Upon starting, HC emissions were high and CO low. As the engine warmed up the mixture appeared to richen as judged from the exhaust composition (Spindt method); but did not change much as judged from input air/fuel ratio measurements shown on Figure 5. In cold starting, it is likely that some fuel passes through the engine unburned. Thus the combustion air/fuel ratio was leaner than that provided by the carburetor. This unevaporated fuel probably accounts for the high hydrocarbon readings measured at start-up. As the engine warmed up, the combustion air/fuel ratio richened, reactor gas temperature rose and at about 1200°F, light off occurred as judged by the inflection point on the gas temperature curve in Figure 4. At light off the CO level emitted from the reactor dropped over a relatively short time period and the reactor gas temperature climbed to nearly 1600°F where it stabilized. Light off occurred after

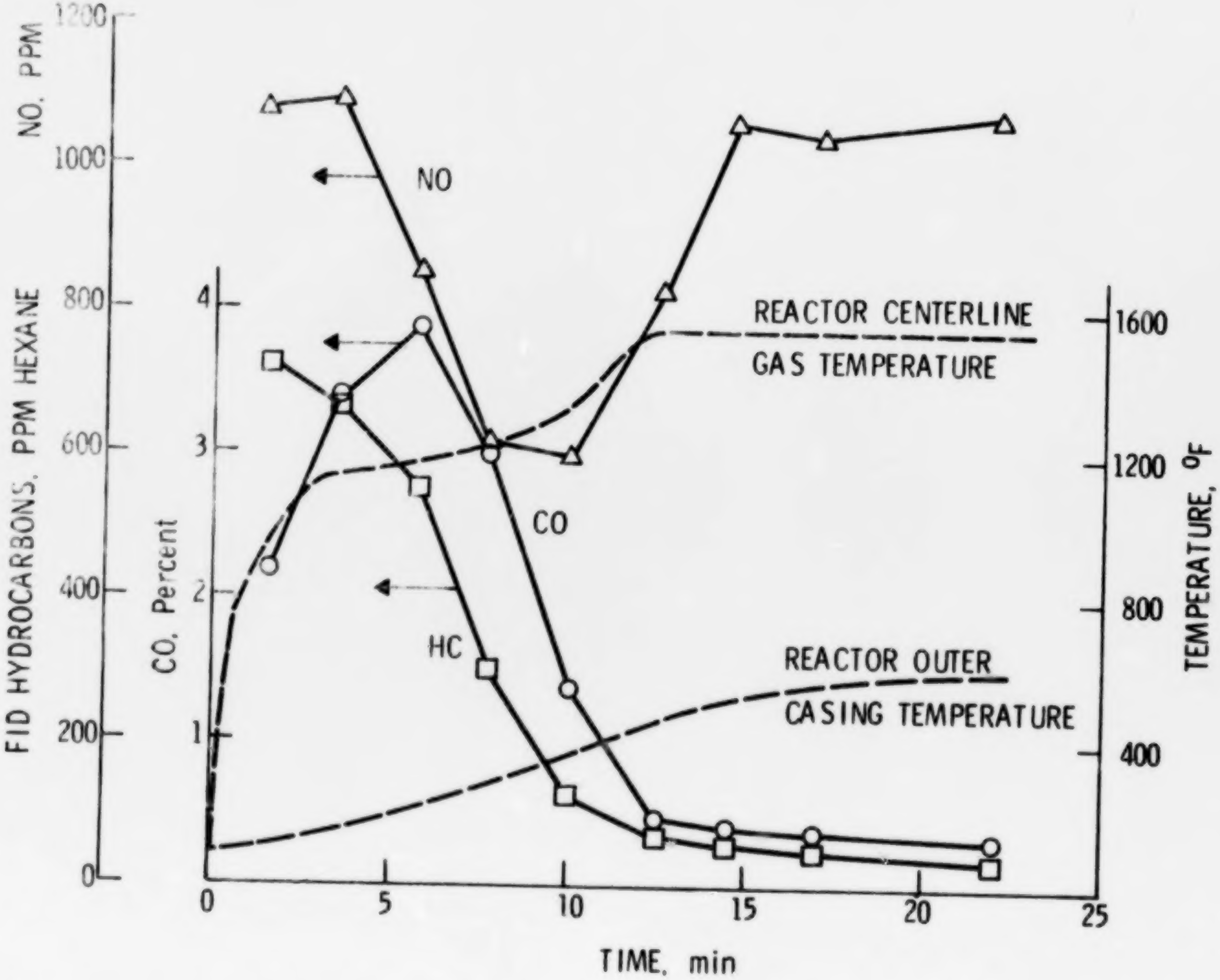

Figure 4. Hydrocarbon, CO, and NO emissions as well as reactor centerline gas temperature and outer skin temperature versus time for a 70°F cold start. Engine conditions were set at 1200 rpm, 30 BHP, MBT spark 12.5:1 air/fuel ratio, air injection fraction of 0.3.

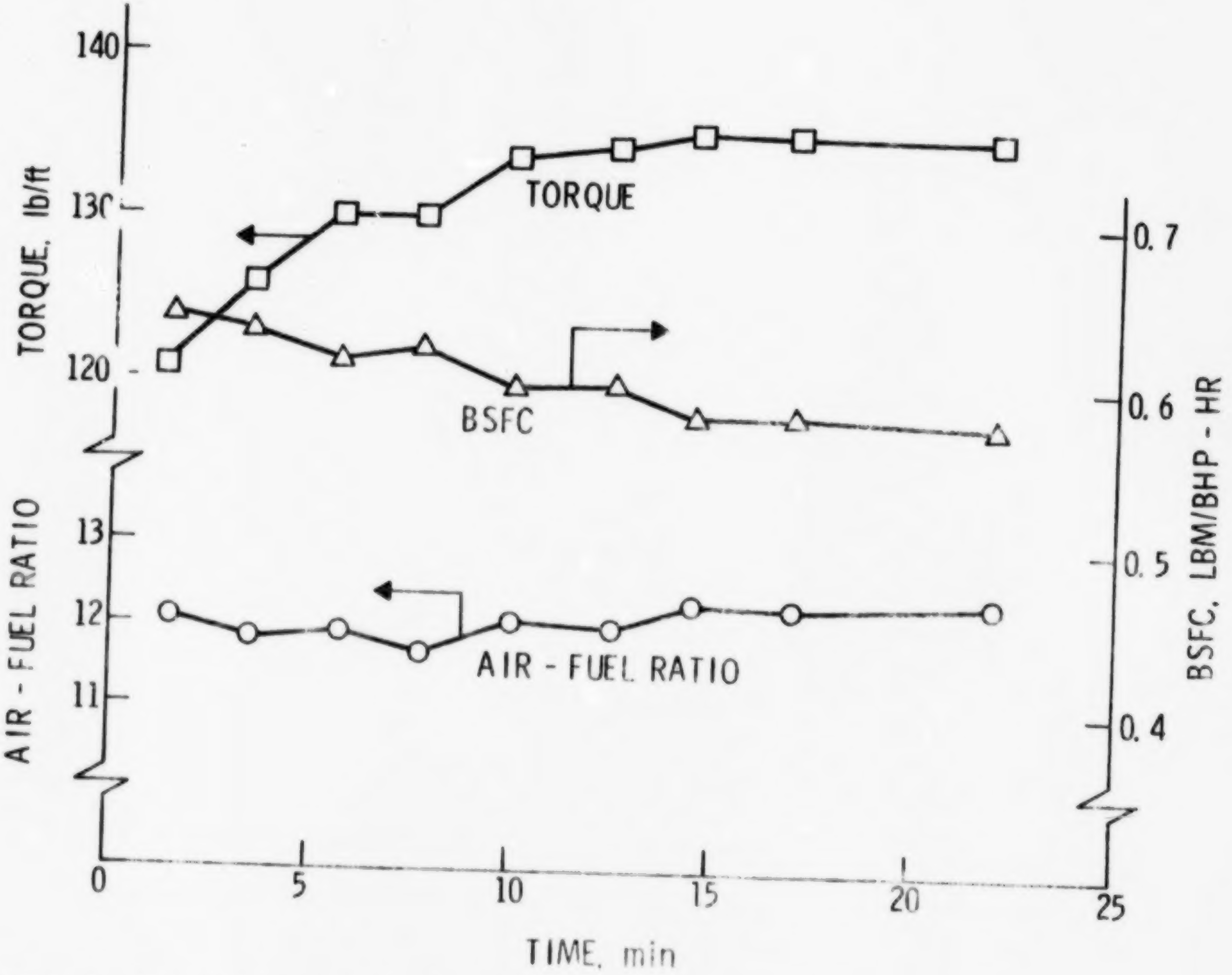

Figure 5. Torque, bsfc and air/fuel ratio provided to the engine as a function of time.

about 5 min and stabilization was not achieved until nearly 12 min. Hydrocarbon reduction preceded CO reduction in time. The observed variations in NO were thought to arise from the slight variations in mixture ratio shown in Figure 5. These emission results are typical of all rich mixture operation with air injected. As Table V shows time to light off decreased as mixture ratio was richened or as reactor input temperature was increased by retarding the timing. Low reaction rate during reactor warm-up severely limits oxidation. It was typical observation that little reaction occurred until gas temperature reached 1200°F.

Figure 6 shows emissions for a similar test run at 17:1 air/fuel ratio without air injection. This mixture ratio was selected to give the same reactor product distribution as the preceeding test at 12.5:1; namely, the products of a 12.5:1 engine air/fuel ratio plus 30% air injection. Figure 7 shows the temperature results. No light off occurred on this test. It is noteworthy that even though reactor temperature rose to 1350°F, relatively little hydrocarbon oxidation occurred. The result is typical of lean operation. Light off does not occur since the heat release of a few hundred ppm hydrocarbons is very small.

Figures 5 and 8 show the engine torque and BSFC as the engine warmed up for these rich and lean tests. This result can be attributed to high friction and excessive heat loss to the walls of the combustion chamber before the engine is fully warmed up.

One final observation is that reactor skin temperature reached 500-600°F in these tests. This was a typical temperature for the duPont reactor. Temperatures this high on such large surfaces may pose a serious problem with respect to evaporative losses and hot fuel handling.

Table V summarized results from several additional tests including those discussed in detail already. From these results and the original data, one concludes:

1. The richer the carburetion the shorter the light off time. Runs 308, 377, 375, 302, 306.

2. Retarding the spark which increases reactor inlet gas temperature shortens light off time. Runs 382, 387.

3. The half life for HC disappearance is always shorter than that for CO.

4. Hydrocarbon light off can occur without CO light off. Run 303.

The light off times observed in this study are very long compared to light off times in vehicle mounted engines which may be only a few seconds. The basic

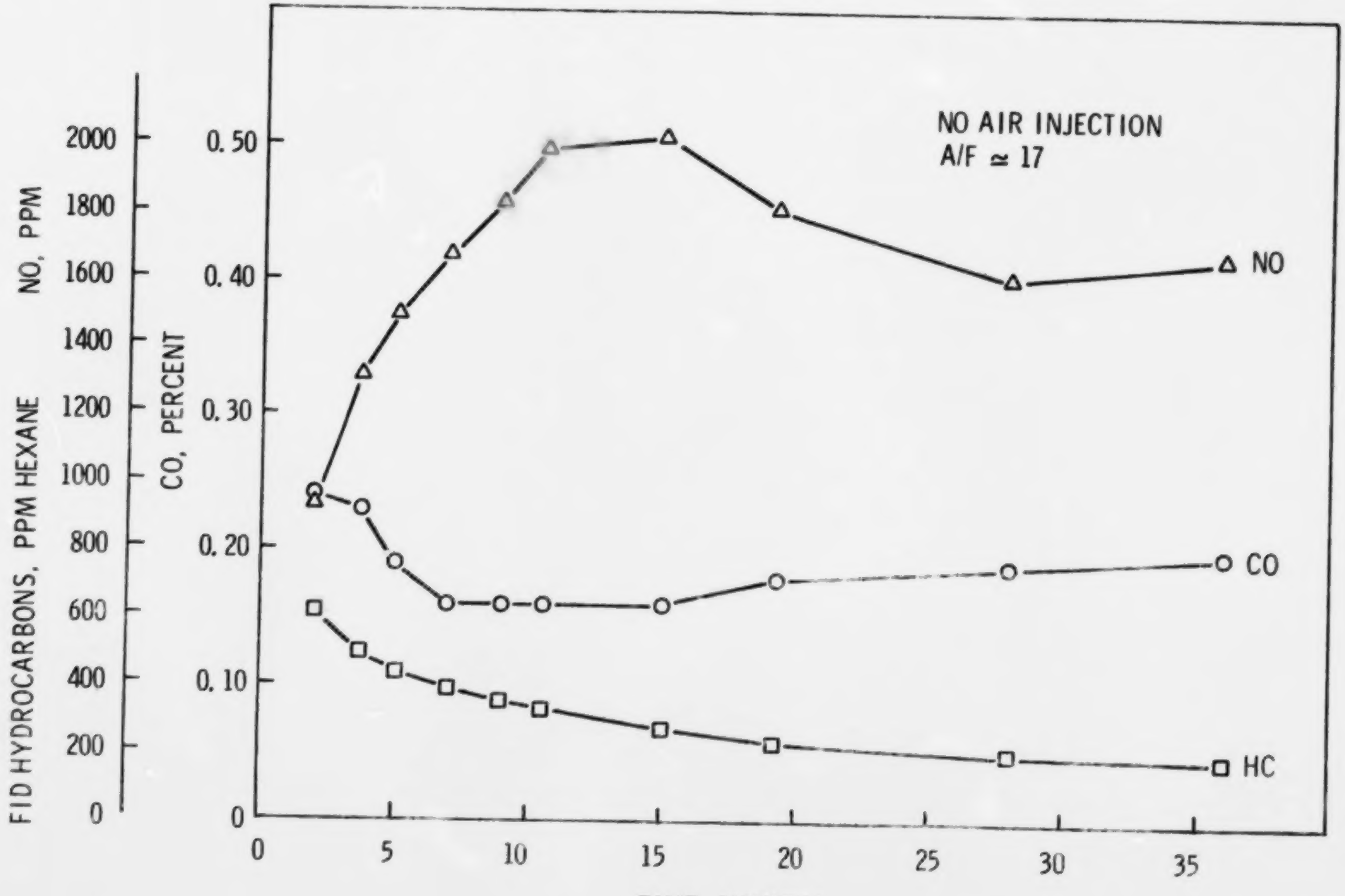

Figure 6. Hydrocarbon, CO, and NO emissions versus time for engine conditions of 1200 rpm, 30 BHP, MBT spark, 17:1 air/fuel ratio, no air injection. The products in the reactor reflect the same air/fuel ratio as the former test at 12.5:1 with 0.3 air injection fraction.

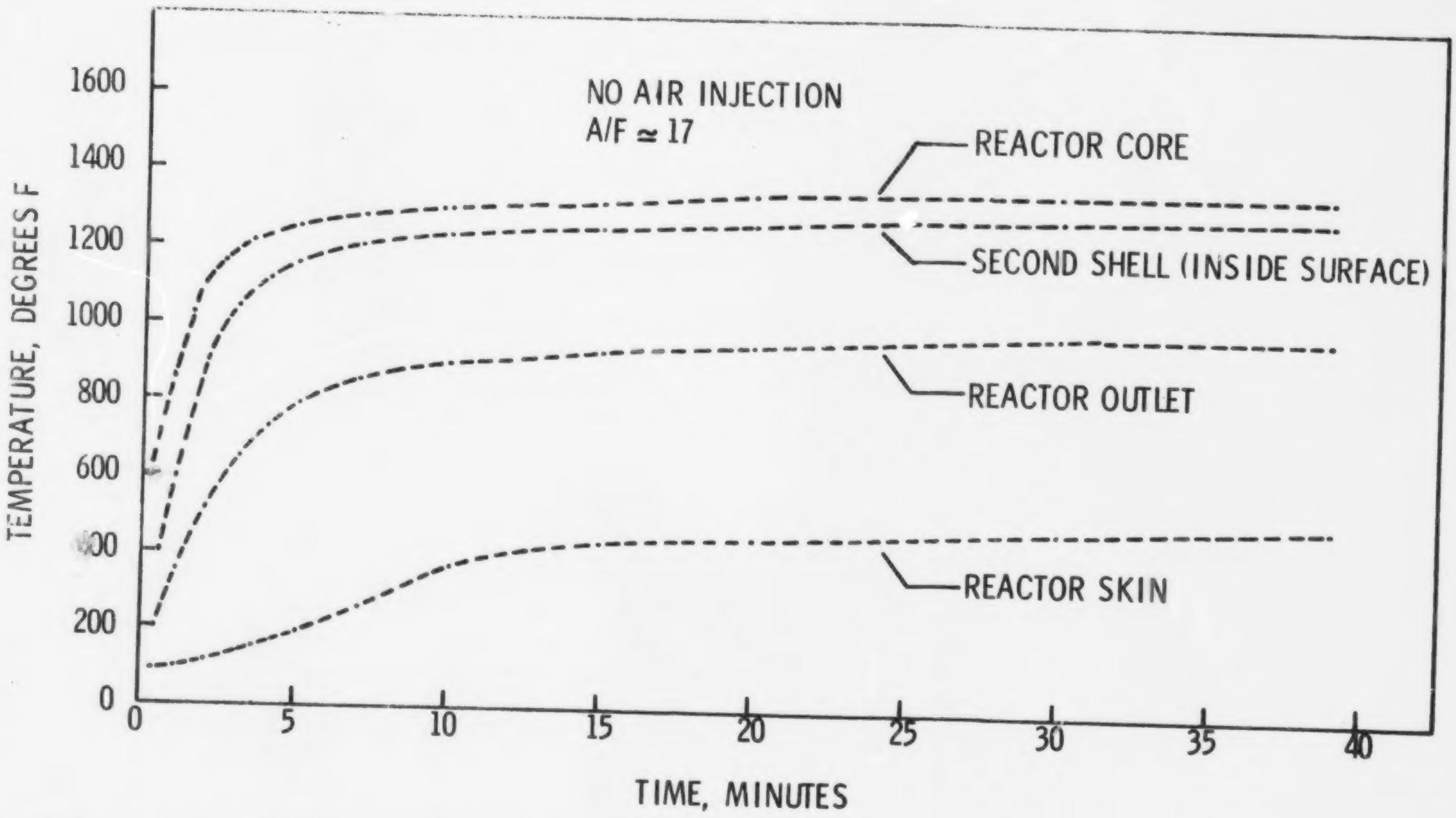

Figure 7. Reactor temperatures versus time. The thermocouple for the first reactor shell was broken for this test.

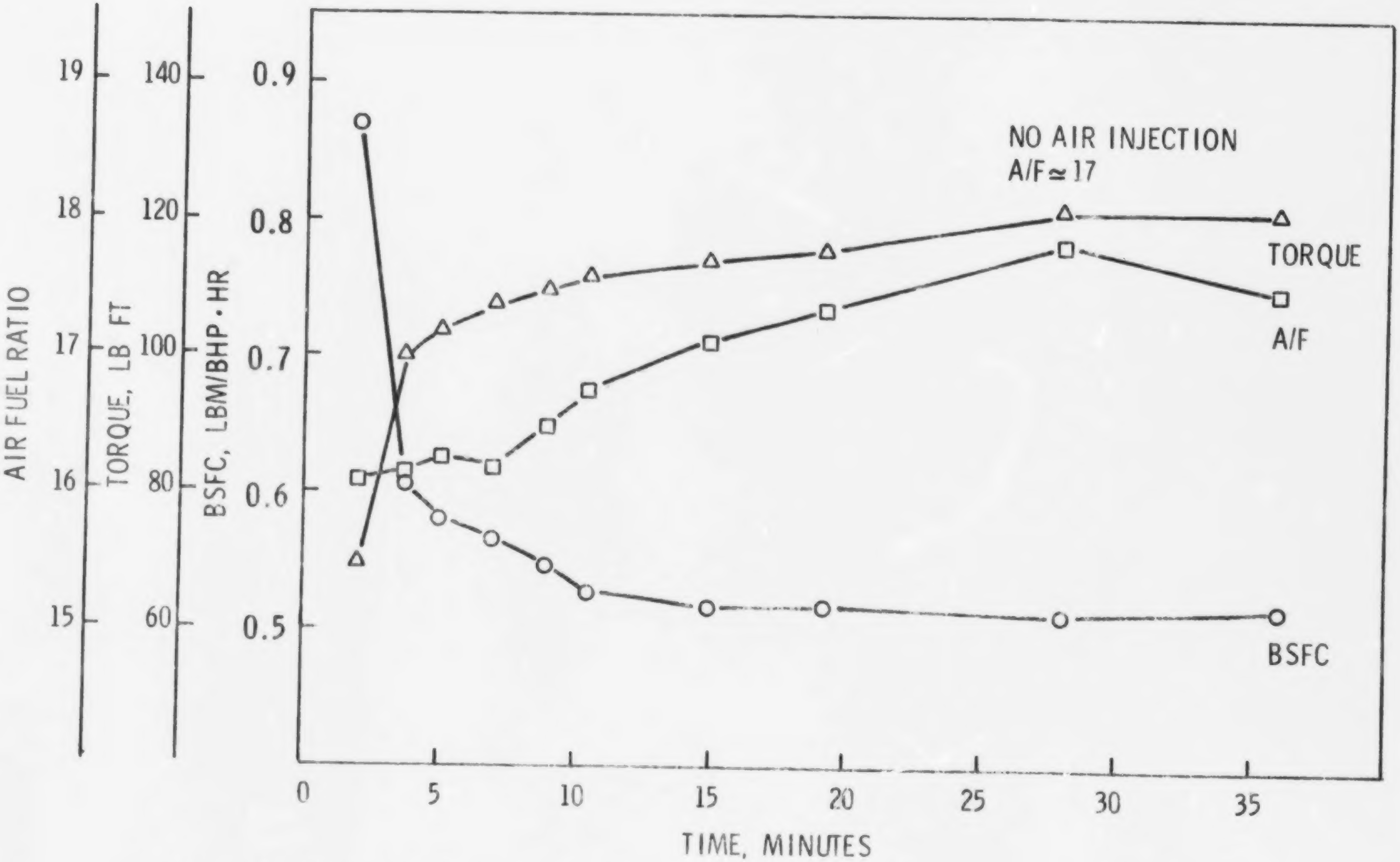

Figure 8. Torque, bsfc and air/fuel ratio provided to the engine as a function of time.

TABLE V

WARM-UP TEST RESULTS

Run No.	Engine, A/F	Reactor* Centerline Temp, °F	Light Off Time, min	Air Injection Fraction	Spark Adv.	Warmed Up, hp	HC Disappearance, half life, min/ final level, ppm	CO Disappearance, half life, min/ final level, %
501	12.5	1650	15	.36	MBT	30	11/15	19/0.2
502	12.5	1650	8	.36	MBT	30	9/45	ND/ND
503	12.5	1300	NE	.60	MBT	15	14.8/390	NE/1.75
504	12.5	1750	6	.2	MBT	47	9/42	10/0.4
506	12.5	1540	6	.3	MBT	30	7/20	9/0.35
507	17.1	1325	NE	.0	20° retard	30	11/ND	NE/ND
577	13.0	1740	14	.3	MBT	30	ND/ND	17/0.32
578	13.0	1780	14	.3	MBT	31	ND/ND	18/0.4
580	13.8	1575	22	.3	MBT	30	10/20	23/0.45
582	13.1	1730	4	.3	20° retard	30	2.3/52	3.3/0.25
585	13.1	1660	16	.3	MBT	30	12/26	15/0.4
587	14.3	1520	~0	.43	20° retard	30	2/28	3.5/0.28

NE - no change evident ND - no data
*Stabilized

difference is that in the vehicle the choke provides a very rich mixture initially. Our warm-up results are a better simulation for a hot start in which the choke is off.

Our conclusion is that when adequate oxygen is present, low reaction rate primarily limits conversion of HC, CO, and H_2 during warm-up.

b. MIXING LIMITATIONS TO STEADY PERFORMANCE

The Second Annual Progress Report contained curves of emission concentration versus air injection fraction. Figure 9 reproduces a typical curve for rich engine operation. Emission values were corrected for air injection using an exhaust carbon balance with and without air injection. Note that even under optimum conditions, carbon monoxide and hydrocarbon emissions are not necessarily zero. In such tests, the reactor operating point is a balance between the extent of reaction as determined by reaction rate, residence time and mixing and the temperature rise due to oxidation. References 13 and 14 develop the theory. The lack of complete combustion at the highest temperature was concluded to arise from incomplete micromixing of exhaust combustibles and oxygen.

To explore the effect of incomplete mixing on extent of reaction, tests were run in which the spark was retarded while keeping fixed all other variables including mixture ratio, throttle, and speed. This served to heat up the reactor gases to a point where reaction rate was no longer a limit to conversion and any unconverted carbon monoxide, hydrocarbons, or hydrogen was deemed to result from incomplete mixing. As a design aid the extent of imperfect mixing may be judged by the conversion efficiency plataeu attained at the highest temperature. Theoretical support for the existence of a mixing limited plateau is included in Detailed Progress - Phase II.

(1) Rich Carburetion Plus Air Injection

For rich reactor studies, air was injected into the engine exhaust port. A production Chevrolet air manifold was used and supplied with shop air. Long high volume lines were used to simulate the low pressure system typical of a vehicle.

Figure 10 shows extent of conversion of HC, CO, and H_2 as a function of reactor temperature. Input CO was 1.91%. Reactor temperature was varied by changing the spark timing. Initially the reactor was warmed to 1640°F by retarding the spark to 10° BTC. The spark was then advanced incrementally to cool the reactor. Maximum advance in this test was 30° BTC which was MBT Reactor input was taken to be the well mixed CO, HC and H_2 concentration emitted from the reactor at 30° spark advance with cooling coils in the exhaust to

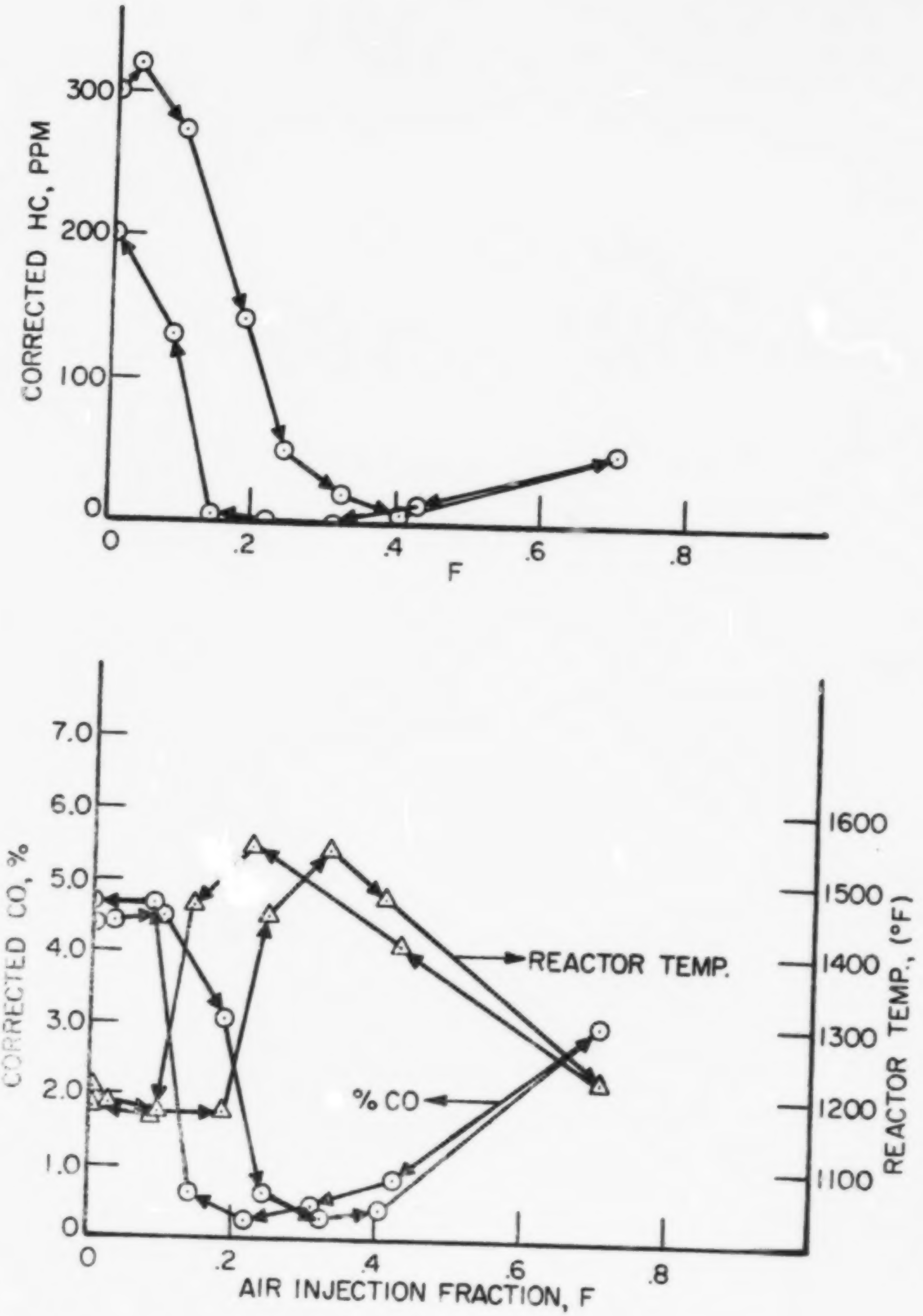

Figure 9. Exhaust emissions with duPont reactors as a function of air-injection fraction. 1200 rpm, 30 hp, 12.5:1 air/fuel ratio, MBT spark of 33°. Indolene 30 fuel.

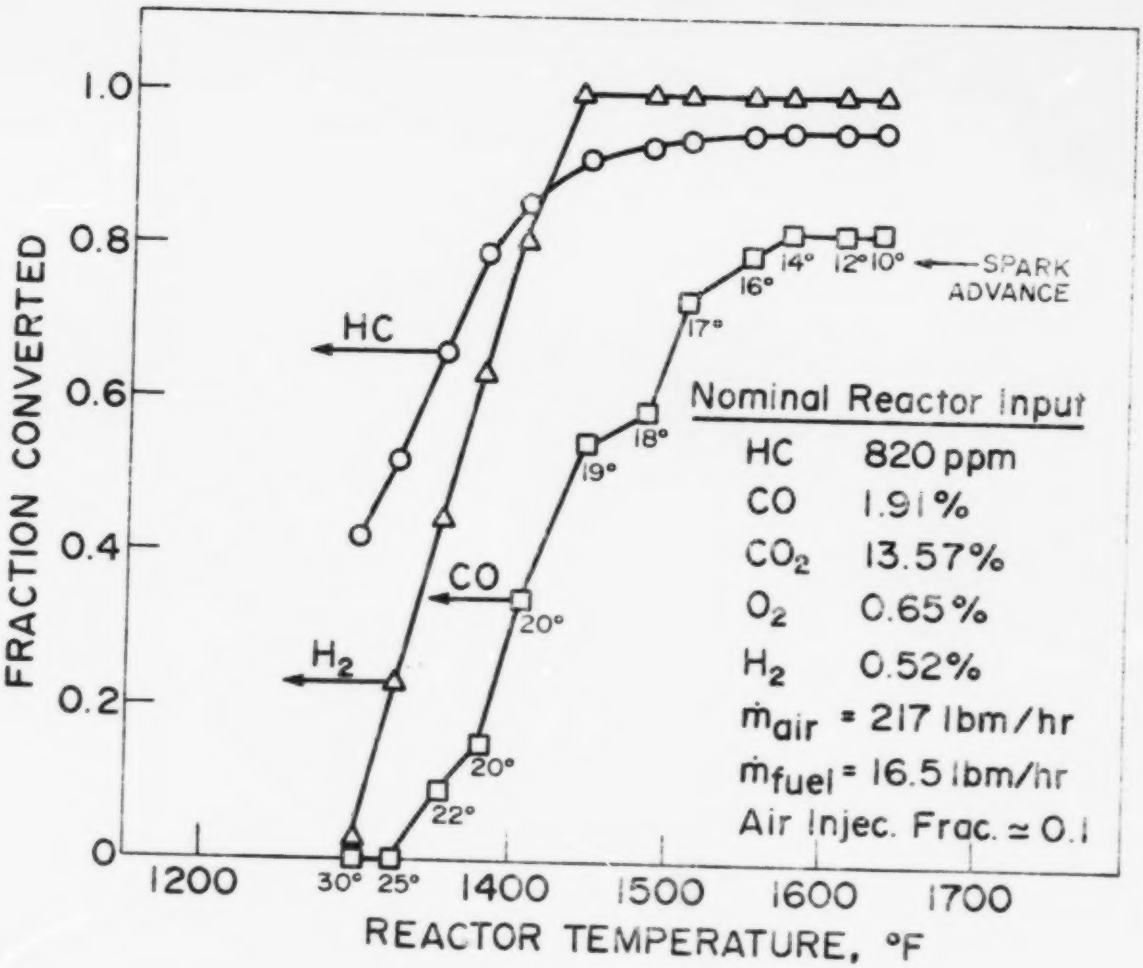

Figure 10. Extent of reaction vs. reactor temperature. Engine conditions 1200 rpm, 30 hp at 30° BTC spark timing. Total engine air flow 217 lbm/hr and fuel flow 16.5 lbm/hr. Air injection fraction approximately 0.1.

suppress after-reaction. Extent of conversion is defined as one minus the ratio of emitted to input specie concentration. Of significance is the extent of reaction at the highest temperature where it is reasonable to assume the reactor is not kinetically limited but only mixing limited. In this test the experimental limit of conversion was 82% for CO, 95% for HC and 100% for hydrogen.

Figure 11 shows similar results for richer engine operation, 2.8% CO input to the reactor but with the same air injection fraction. With more CO the extent of conversion curves were shifted to the right with respect to temperature. CO conversion was only 75% and HC 93% complete in the limit in spite of the fact that the overall reactor mixture ratio was slightly leaner than chemically correct. Hydrogen was reacted completely.

Figure 12 shows results for operating conditions similar to Figure 11 but with twice as much air injection. An increase in air quantity increased reaction rate and shifted the extent of reaction curves to the left and upward. CO conversion was 93%, HC was 97% and H_2 was 100% complete. One can conclude that when mixing is poor, flooding the reactor with excess air will always help conversion if the temperature is maintained at a given level. Poorly mixed reactors are expected to require more air and more spark retard to achieve a given level of performance.

The difference between the extent of conversion for CO and H_2 at the limit is thought to arise from the fact that because of a higher reaction rate, the hydrogen is consumed prior to the CO, closer to the reactor entrance. As a result the hydrogen reacts in a more oxygen enriched environment and thus reacts more completely. Note that the reported extent of conversion for hydrocarbons is inaccurate. This is because spark timing affects HC concentration emitted from the cylinder and the HC concentration at each retarded timing without after reaction was not obtained. Thus the extend of conversion for HC with retarded timing is overestimated since it is based on the high quenched value. If one makes the reasonable assumption that the HC emitted from the cylinder decreased by less than a factor of two due to spark retard over the range of this experiment then the true fraction HC unconverted is no more than twice the observed value and for the data of Figures 10, 11, and 12, the CO oxidation is not only apparently less complete but is actually less complete than the HC oxidation.

Consequently of the three choices, incomplete carbon monoxide oxidation is the most reliable indicator of poor mixing in a rich thermal reactor for the type of experiment described herein. As a more general conclusion, the spark retard method is recommended for assessing the goodness of mixing in a rich thermal reactor with CO conversion as an indicator.

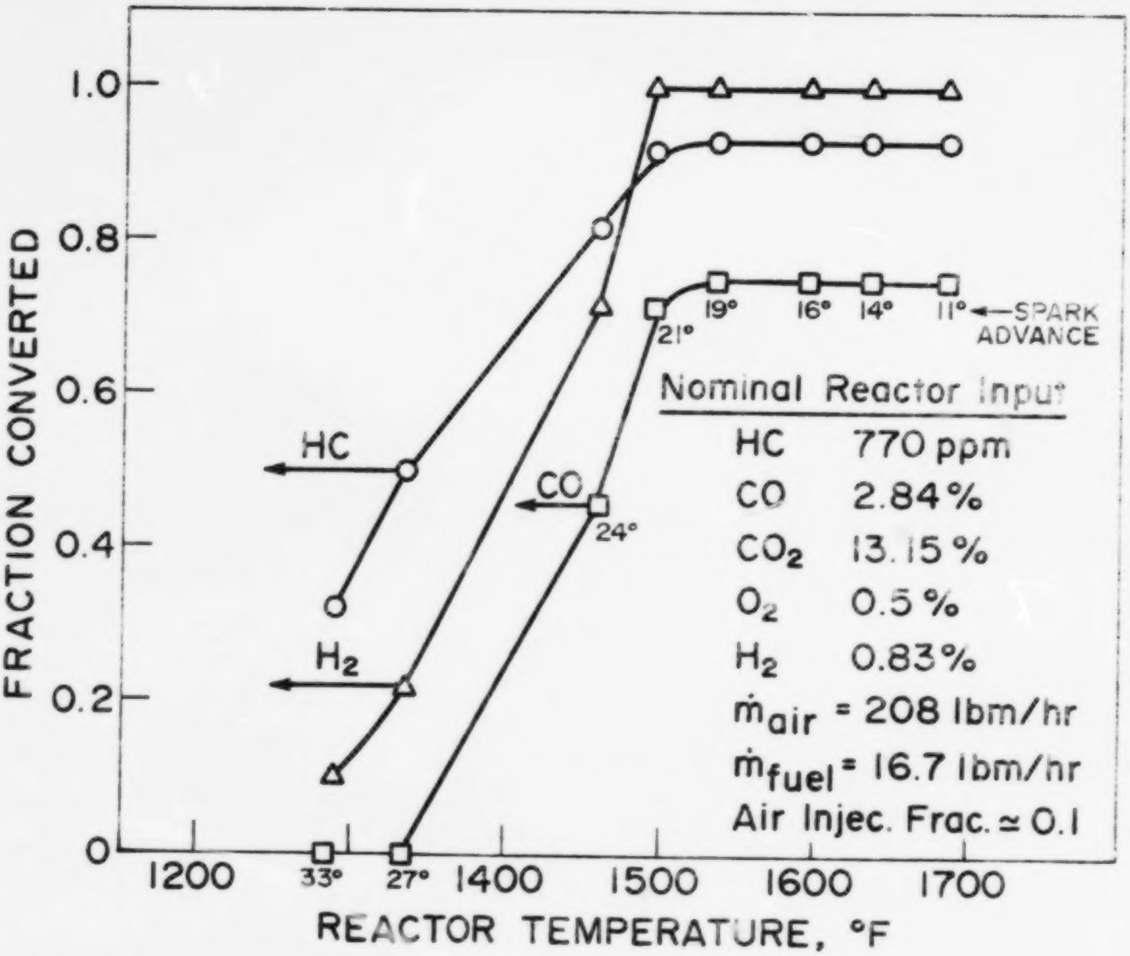

Figure 11. Conditions similar to Figure 10 except higher CO and H_2 reactor input.

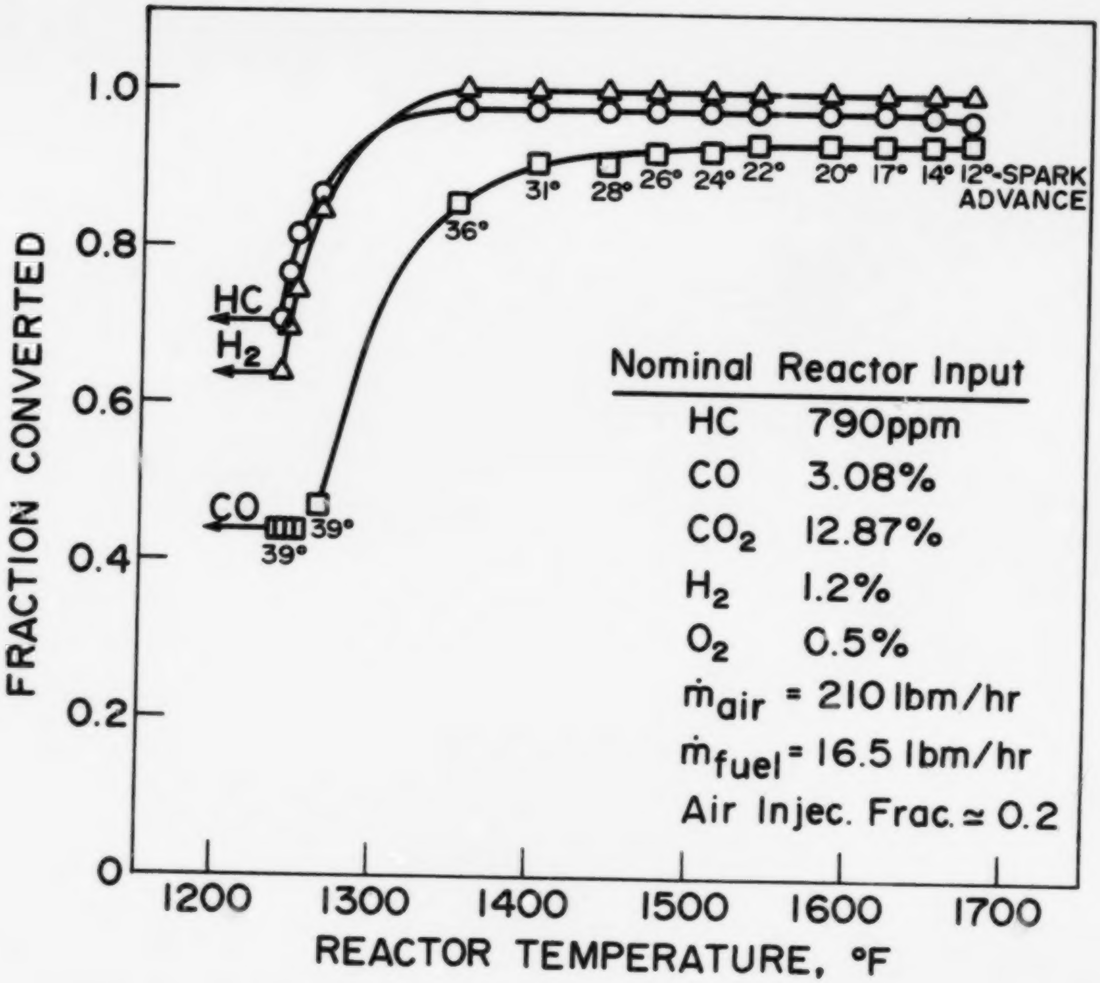

Figure 12. Conditions similar to Figure 11 except air injection fraction doubled to F = 0.2.

(2) Air Injection Flow Characteristics

The lack of mixing between combustibles and air may be thought of as arising from two sources, incomplete micro- and macromixing. Commonly air and exhaust do not enter the reactor at the same time and the exhaust composition varies during the cycle. This reactant segregation naturally results from the exhaust and air injection flow characteristics of reciprocating engines. A high degree of micromixing within the reactor is required to homogenize the reactants and achieve complete combustion. The incomplete micromixing is one cause of reactor inefficiency. The other source of incomplete mixing arises from the patterns of flow within the reactor coupled with the segregated input. Depending on the residence time distribution within the reactor, it may not be possible for various elements of gas to intermix in spite of a high level of micromixing. This effect, termed incomplete macromixing, is most evident for a plug flow reactor. Reactants which enter early are precluded from mixing with those entering later.

The segregation of air and exhaust arise from the unsteady exhaust flow characteristic of reciprocating engines and the air flow variations of low pressure continuous air injection systems. The exhaust volume flow variations are indicated by the exhaust velocity variations measured in Phase III, and shown in Figure 28 of that section.

One measurement was made of the variation in velocity of the injected air in the air injection tube under running conditions. For this a hot-wire anemometer was installed in the air injection tube for cylinder 1. The wire was located about 5 in. from the discharge end of the tube. A 0.0002-in. diameter tungsten wire was employed. The instantaneous pressure difference between the air injection manifold and exhaust port was also measured (A Statham strain gage transducer with a range of ± 5 psi peak to peak was used.)

Figure 13 shows the pressure difference between the air injection manifold and the exhaust port as a function of crank angle. Figure 14 shows the calculated mass flow based on the velocity measurements made by the hot wire anemometer. Constant air density was as summed.

As a result of the blowdown process in cylinder 1, Figures 13 and 14 show a pressure and flow reversal occurred in the air injection tube. Some slowing of the air flow appeared to occur also as a result of rapid explusion of exhaust gas when the pistion velocity reached its maximum value. Some flow perturbation is noted as well from events in other cylinders. In these situations the air is diverted to the other three exhaust ports. These measurements show that the air injection flow lagged the engine events by about 45°.

Indicated on Figure 14 are the measured average value of air injection flow (computed from one-eighth of the known air and fuel flow to the engine and air injection fraction) and the integrated average of Figure 14. Their difference is about 10%.

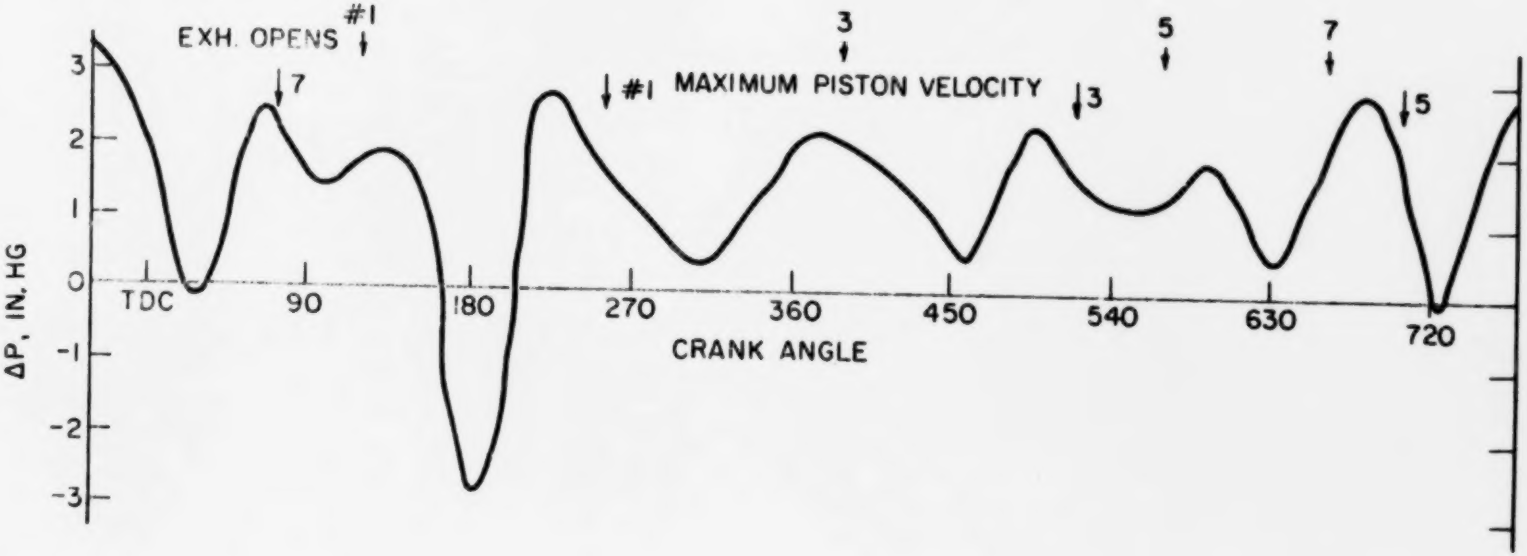

Figure 13. Air injection manifold pressure minus exhaust port pressure versus crankangle. A positive pressure difference indicates air flow to the engine.

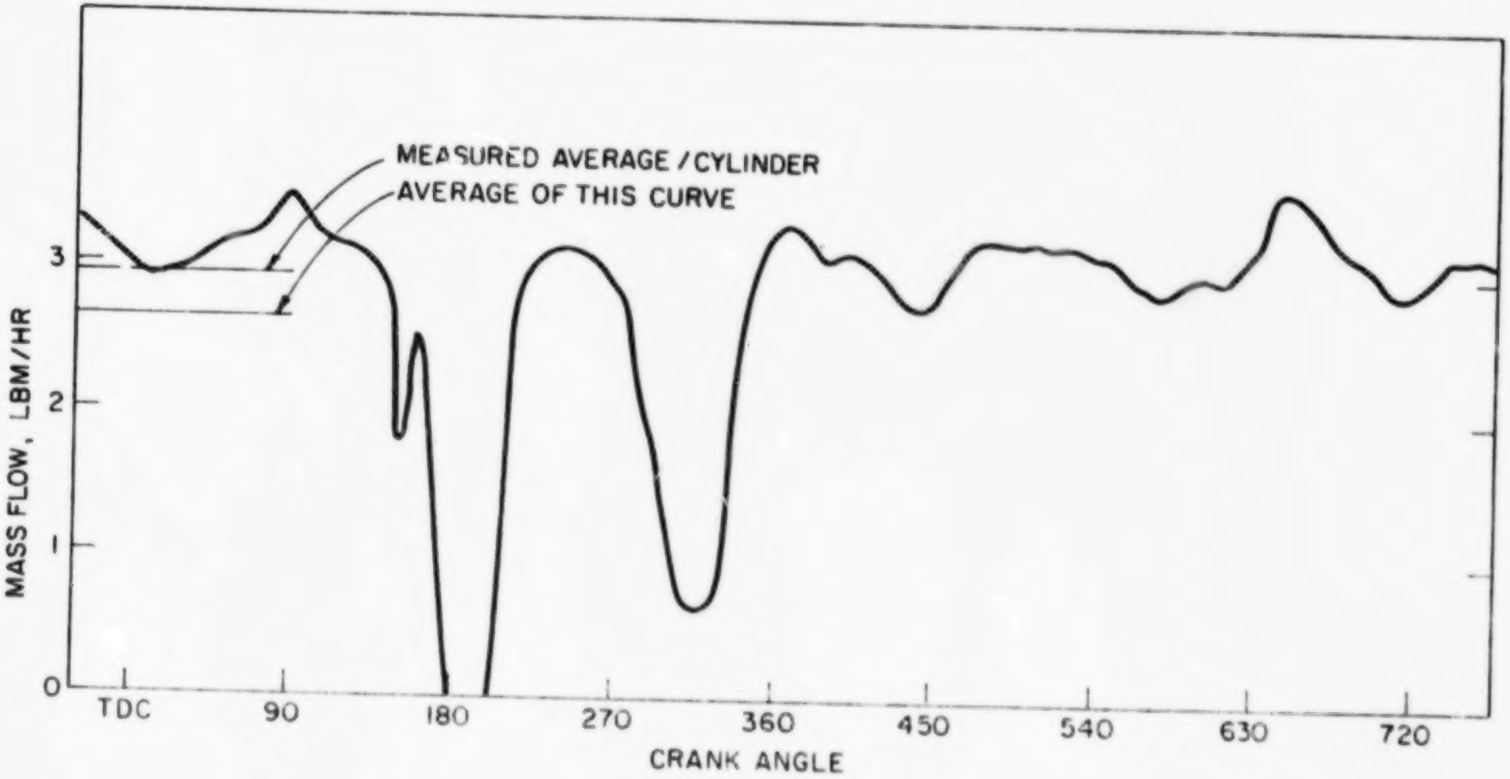

Figure 14. Mass flow through air injection tube for cylinder number 1. 350 CID Chevrolet, 1200 rpm, 30 hp, MBT spark, air injection fraction 0.3.

The variations in air injection flow and particularly the slowing or reversal of air flow just when exhaust flow is maximum is a major factor leading to segregation of oxygen and combustibles. For optimum reactor performance the ratio of air flow to exhaust flow should be nearly constant at each crank angle.

(3) Lean Carburetion—No Injection

Figure 15 shows the extent of conversion for a lean engine without air injection. Exhaust CO was very low (less than 3000 ppm and difficult to measure with NDIR analyzer of this experiment) and H_2 was zero. The conditions were chosen such that the reactor air-fuel ratio was the same as that of Figure 12 where air was added to a rich mixture exhaust. Compared to Figure 12, the HC entent of conversion curve was shifted to the right but reached the same limiting conversion of 97%. With lean operation, it was anticipated that the conversion would be complete since without air injection, oxygen is well mixed with the exhaust. Perhaps the result can be attributed to imperfect mixing arising in this case from a uniformly distributed oxygen quantity being mixed with a nonuniform hydrocarbon emission profile whose span may be a factor of 10. The hydrocarbon containing boundary layer is expected to be quite rich in hydrocarbons since a portion of its contents arises from the evaporation of liquid droplets which impinge and collect on combustion chamber surfaces and deposits. Consequently even a lean reactor may benefit from air injection especially if it is timed to coincide with the end of the exhaust stroke where HC concentration is high.

A very interesting result of this lean reactor experiment is shown in Figure 16. Plotted on a semilog scale are the CO, HC, and oxygen concentrations. The oxygen in the exhaust was 2.65%. The oxygen value plotted in Figure 16 is the actual oxygen reading minus 2.05% excess O_2 not required for complete combustion of the emitted CO and HC. Plotting in this way amplifies the fluctuations in oxygen.

The low temperature (975°F) points were measured with exhaust cooling coils turned on to suppress after-reaction and are assumed to be the reactor input. As reactor temperature was increased, CO emission first increased and then decreased. The CO increase is thought to arise from the HC oxidation in which CO is an intermediate. HC oxidation proceeded more rapidly above 1300°F, but the CO was not rapidly oxidized to CO_2 until a temperature above 1400°F was reached in the reactor.

The partial oxidation of unburned hydrocarbons to CO in the exhaust may be one source of the exhaust CO commonly found in lean running engines. Two other sources are mixture maldistribution and slow atom recombination reactions during expansion leading to nonequilibrium CO concentration. Normally maldistribution masks the other effects.

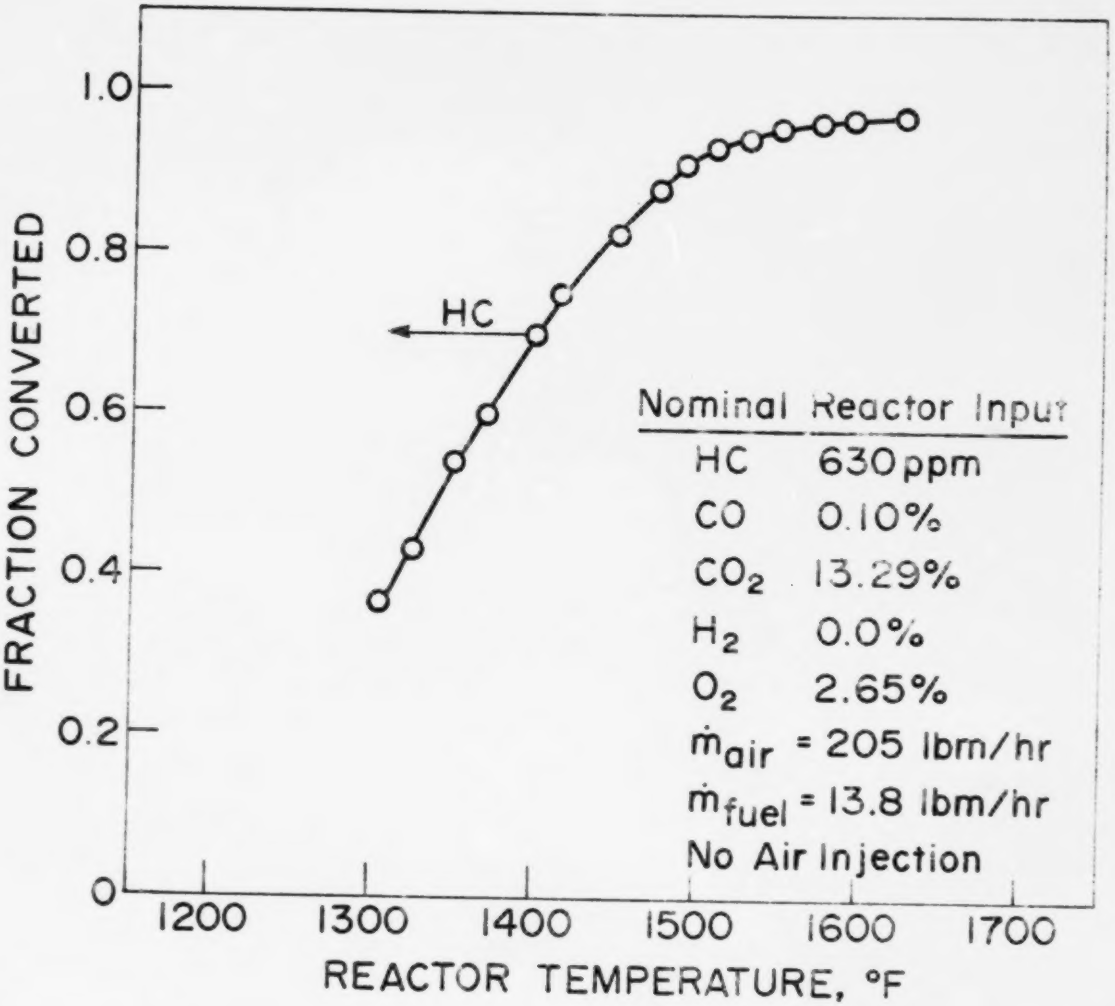

Figure 15. Conditions similar to Figure 12 except the engine is run lean enough to provide the same reactor mixture ratio without air injection.

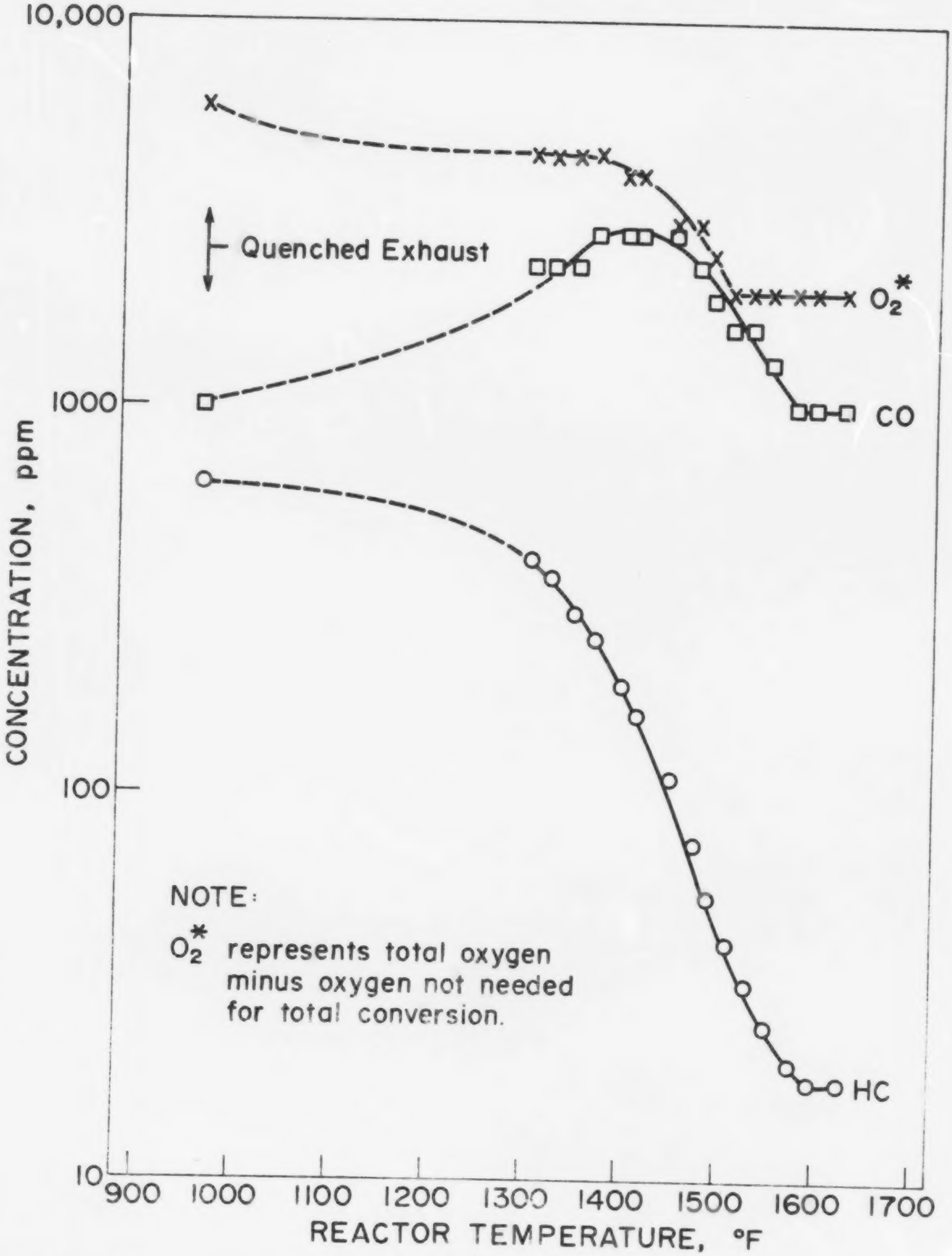

Figure 16. Effect of reactor temperature on the concentration of O_2, HC, and CO in the exhaust of a lean running engine, 1% = 10,000 ppm. Oxidation of HC leaves CO as a product at the lower temperatures. Engine conditions of Figure 1[illegible].

(4) Rich carburetion Plus Critical Flow Air Injection

A critical flow air injection system was incorporated by installing a small orifice in the air injection line about 5 in. the discharge from point. Orifice size was adjusted until each cylinder received the same air quantity. The shop supply was used to supply the high pressure air required. The purpose was to improve the mixing of air and exhaust by injecting air at a constant rate. Obviously this was a partial step since the instantaneous exhaust flow variations were unchanged.

Tests were run to explore conversion gains possible with the better mixing provided by the critical flow system. Figure 17 shows the fraction converted as a function of reactor temperature for the critical flow system at an engine operating condition of 3% exhaust CO and about 0.09 air injection fraction. Maximum conversion was H_2 100%, HC 93%, and CO 86% This may be compared to the low pressure air injection results in Figure 11 where maximum conversions were 100%, 93%, and 75%, respectively, for a similar mixture ratio and air injection fraction. CO oxidation was significantly improved with critical flow air injection. At temperatures between 1300° and 1500°F, H_2 oxidation was significantly improved with critical flow injection and HC oxidation was improved slightly.

Figure 18 shows similar results at a 50% increased air injection quantity of F = .15. In the limit conversion was H_2 100%, HC 98%, and CO 96%. These data may be compared to Figure 12 which shows data for F = .2. These maximum conversions were 100%, 97%, and 93%, respectively. Normally an air injection fraction of 0.2 would be expected to provide better oxidation than one of 0.15. However, critical flow injection yielded better results at the lower air quantity. In this test, it was impossible to stop light off by advancing the spark (to 39°).

Figures 19 and 20 show additional comparisions with and without critical flow air injection as air injection fraction was varied. The limitations of our critical flow system precluded air fractions greater than 0.375. Note that with the critical flow system light off occurred at a lower air injection fraction and produced a higher temperature (less dilution), and yielded more complete oxidation. In this comparison minimum CO was reduced from about 0.4% to 0.2%, a 50% improvement. Minimum HC emissions were also reduced from about 30 to 20-25 ppm.

These results further demonstrate that incomplete mixing of air and exhaust limits peak reactor conversion in the duPont reactor. The critical flow air system increased the unformity of the instantaneous ratio of air to exhaust by making the air rate constant. Of course the exhaust flow rate remained variable so only an improvement was made in reactant segregation. Some form of timed air distribution is required to achieve perfect uniformity of instantaneous air to exhaust ratio. Favorable results with timed air

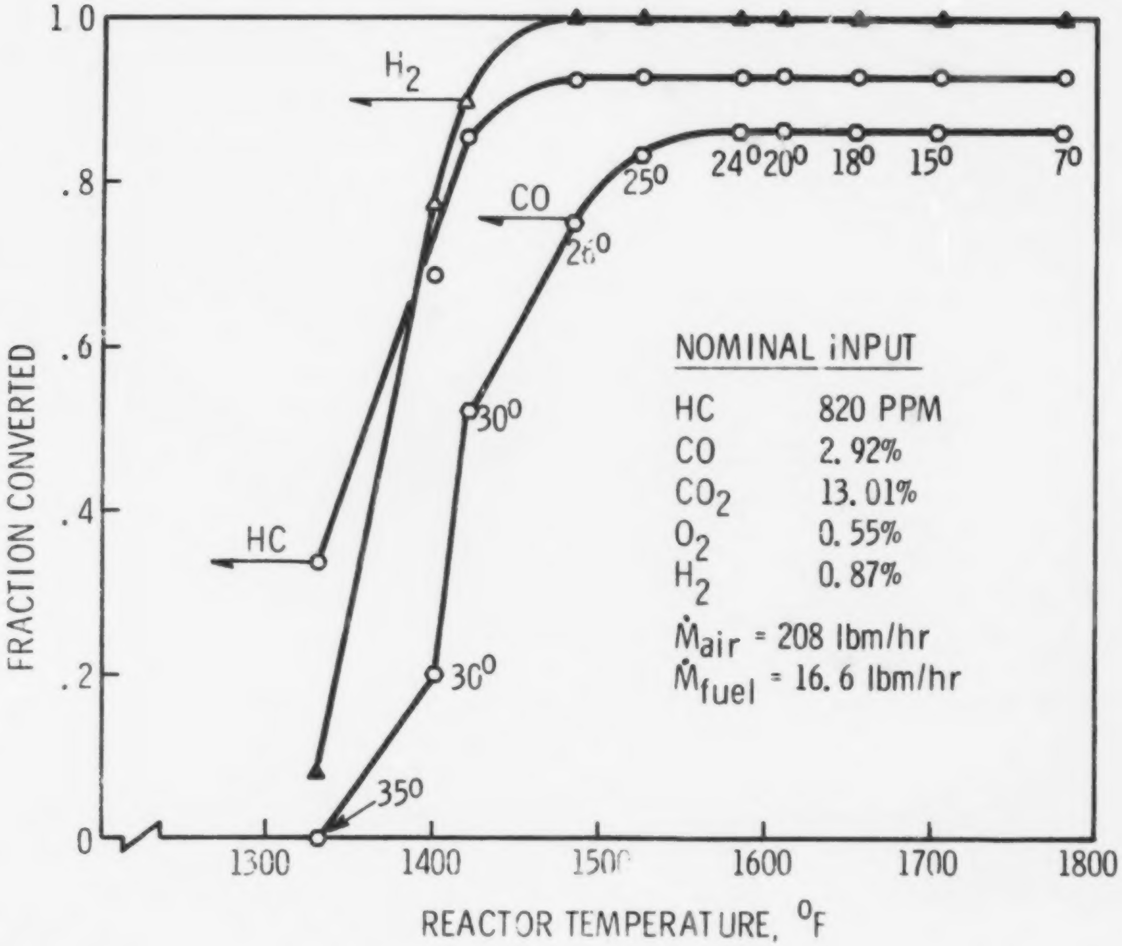

Figure 17. Extent of reaction vs. reactor temperature. Engine conditions 1200 rpm, 30 hp at 30° BTC spark timing. Total engine air flow 208 lbm/hr and fuel flow 16.6 lbm/hr. Air injection fraction approximately 0.0[illegible].

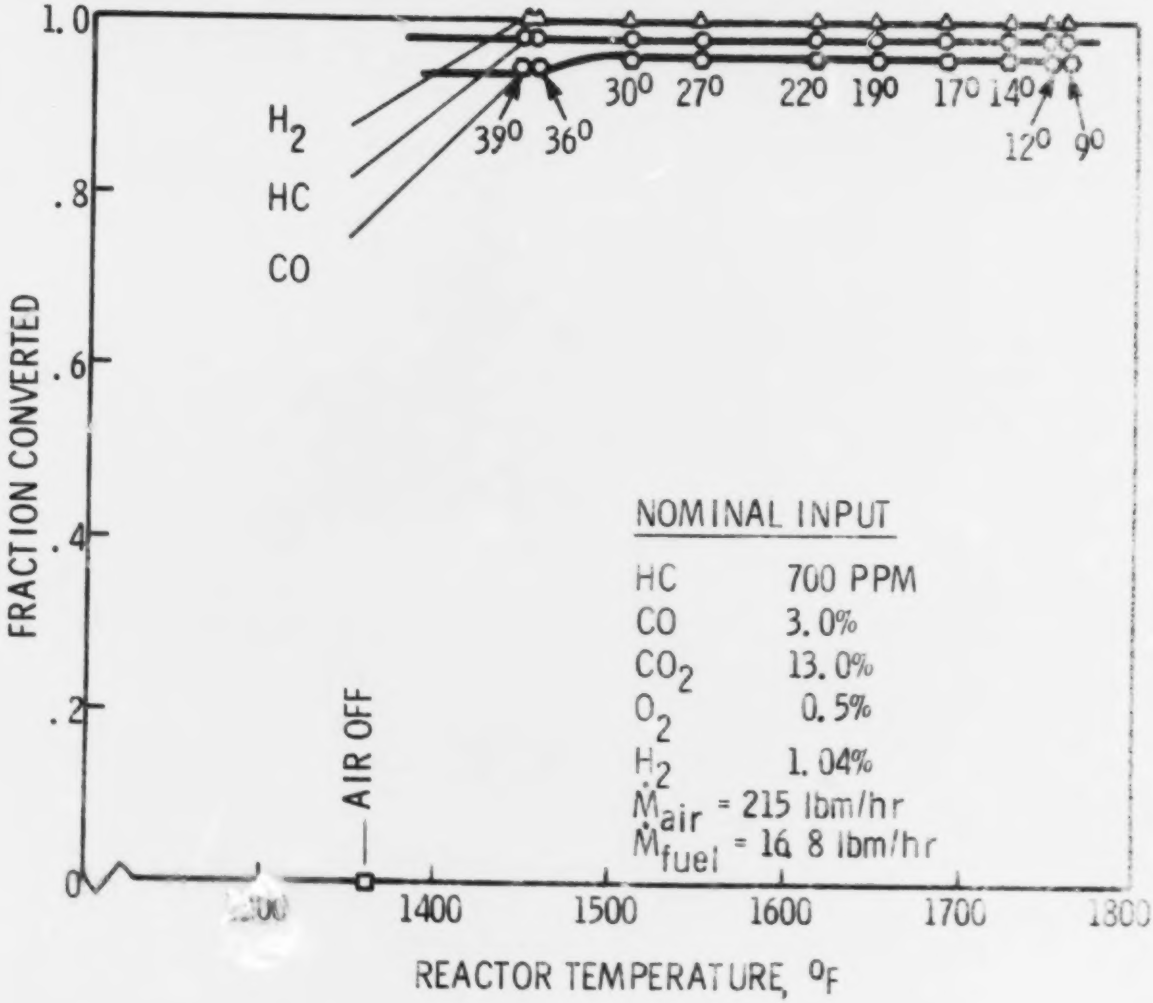

Figure 18. Same as Figure 17, except air injection fraction increased to approximately 0.15.

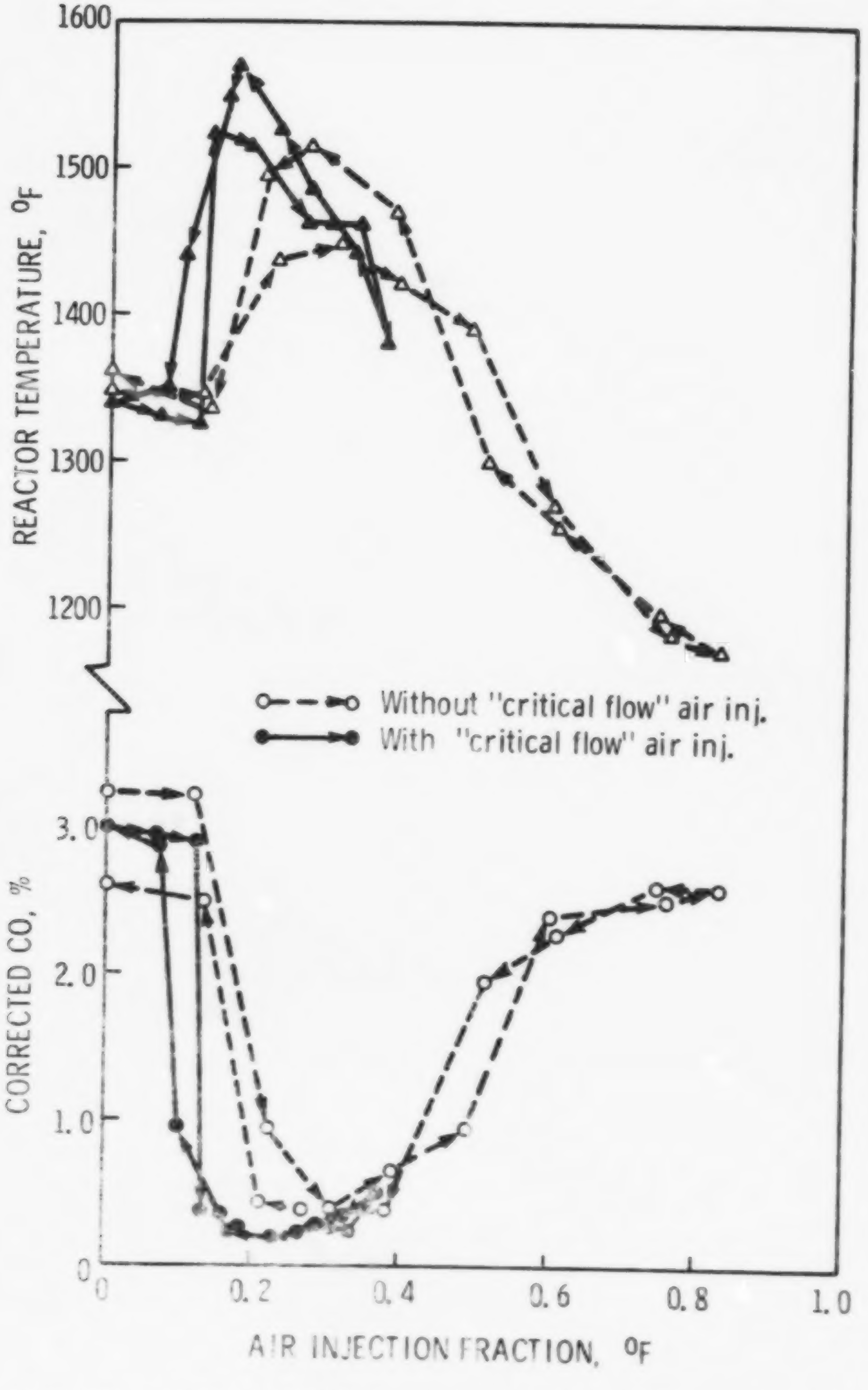

Figure 19. Effect of air injection fraction on CO conversion and reactor temperature. The conventional air injection system is compared to an experimental critical flow system. Engine conditions same as for Figure 17.

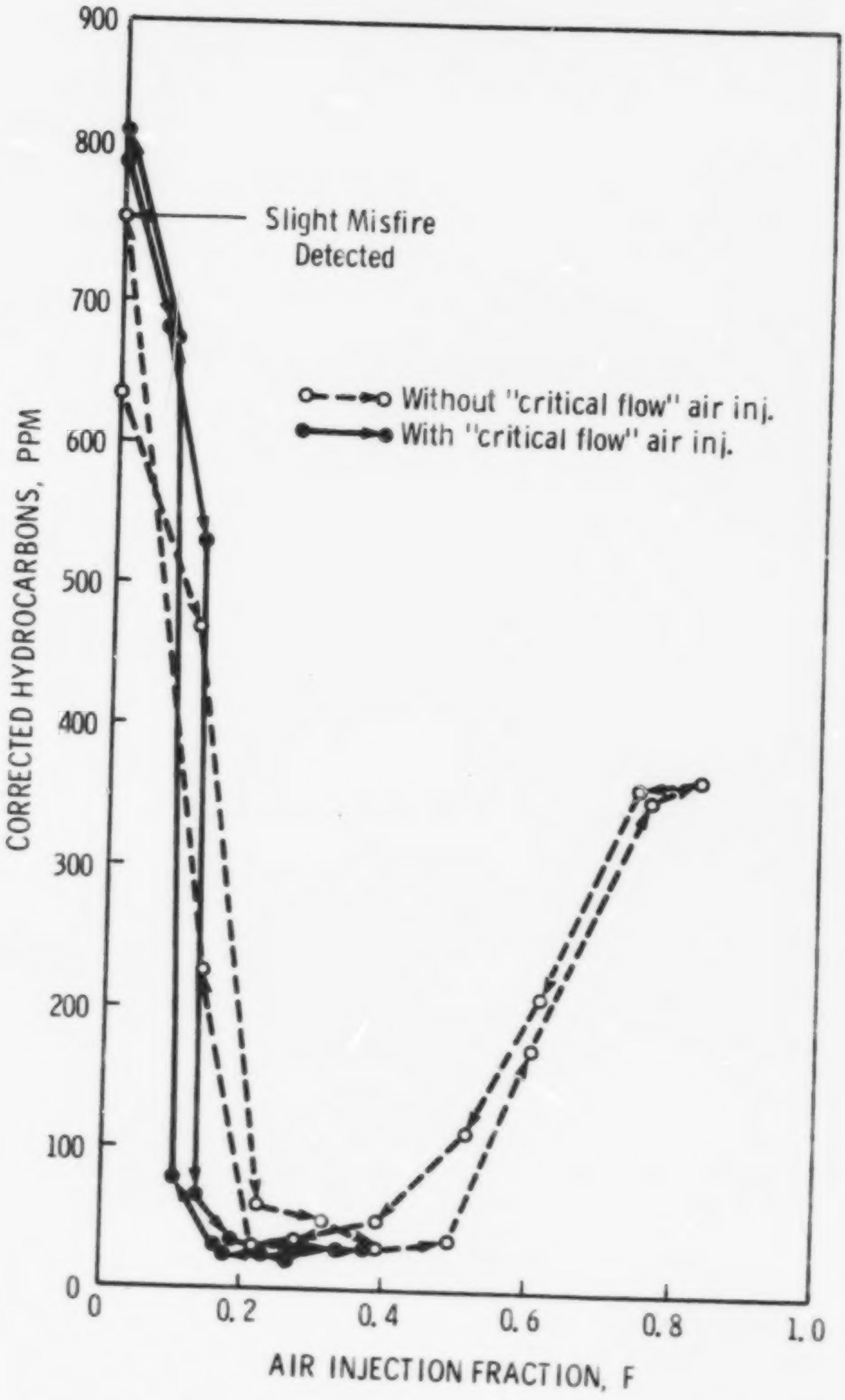

Figure 20. Same as Figure 19 for hydrocarbon conversion.

injection on a vehicle have been reported by Glass.[15] The incentive is a lower air requirement for light off, higher reactor temperature, and better conversion of exhaust combustibles. It is antipated that mixing limitations will be more evident with Wankel engine thermal reactor thermal reactor systems, since the higher exhaust temperature of the Wankel will minimize kinetic limitations to complete conversion.

c. REACTOR COMBUSTION LUMINOSITY

(1) General

As described in the First Annual Progress Report,[11] page 3, one duPont reactor used in this study was modified to accept quartz windows at either end. During operation where extensive carbon monoxide was oxidized, a bluish-gray light was observed in the reactor core. Studies were made to determine the intensity versus time of the light and also its spectrum. Overall brightness as a function of time was measured with an IP-21 photomultiplier. The light emission spectrum was measured with a home made spectrometer with the assistance of Dr. Joseph Harrington of the Ford Motor Company Scientific Laboratory.

(2) Photomultiplier Results

Overall reactor brightness was measured with the IP-21 photomultiplier tube. The phototube was located about 18 in. from the rear of the left-hand reactor and was closest to cylinder 7.

To the eye the flame in the reactor appeared blue-gray. The IP-21 has a strong sensitivity to blue light, its maximum response being at 4000 ± 500 angstroms.

The upper trace of Figure 21 shows the output of the phototube as a function of time. The lower trace shows timing marks 45° apart. As each cylinder exhausts two light peaks arise. The first and largest corresponds to blowdown. The second corresponds to the maximum piston velocity. At both times, relatively large amounts of gas enter the reactor. Referring to Figure 21, the left-most peak is blowdown for cylinder 7. The next peak is blowdown for cylinder 1. Note that this has a double hump. One hump is the blowdown for cylinder 1 and the other corresponds to the maximum piston velocity for cylinder 7. Double humps are evident for cylinders 3 and 5 as well. The second hump for 5 is nearly masked by the blowdown from 7.

The uneven spacing of the pulses reflects the order of exhaust valve opening. The location of the peaks with respect to the cycle events is shown in Figure 23. The large peak from each cylinder occurs slightly after

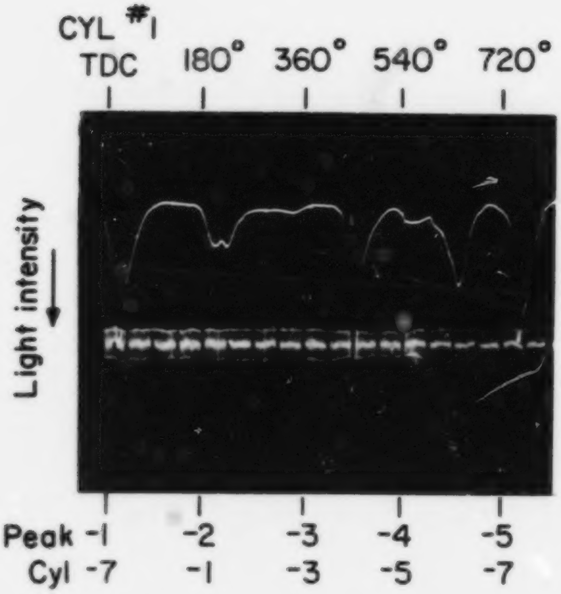

Figure 21. Chevrolet 350 in.^{3} engine, 1200 rpm, 30 hp, 12.5:1 air-fuel ratio, air injection fraction .22, reactor temperature approximately 1650°F. Upper trace: Light emission as function of time. Lower trace: 45° timing marks.

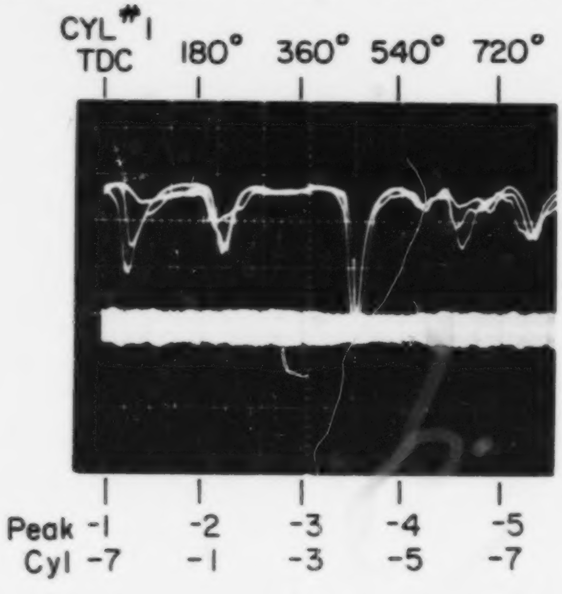

Figure 22. Repeatability of light emission.

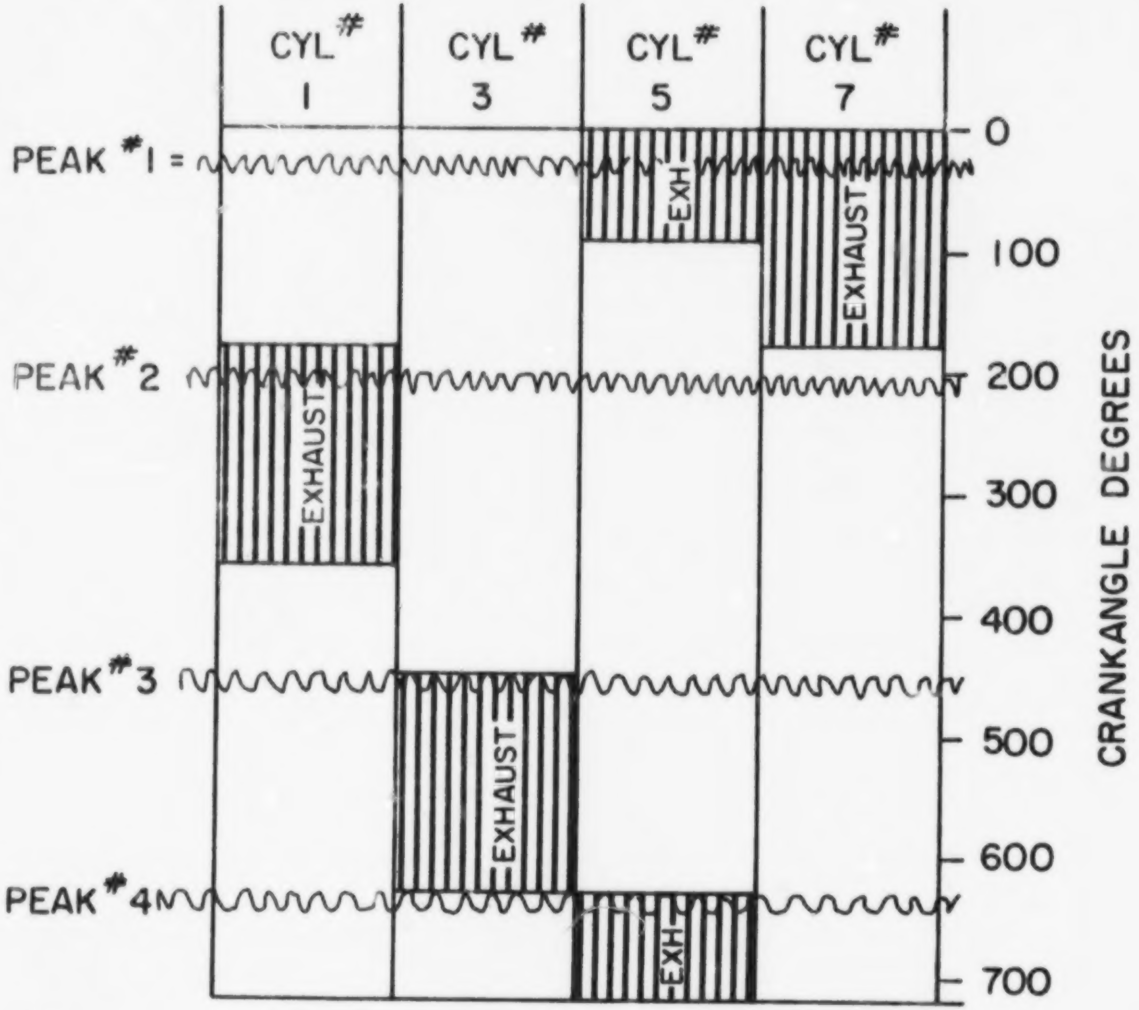

Figure 23. Location of light emission peaks with respect to cycle events for cylinders 1, 3, 5, and 7.

bottom center. The variations in height reflect both variations in exhaust temperature between cylinders and the location of the port with respect to the photomultiplier tube.

Figures 22 and 24 show data repeatibility. Differences in light emission from cycle-to-cycle for a given cylinder primarily reflect differences in gas temperature at the end of expansion. Temperature variations result from combustion variations in the cylinder. Figure 24 shows an often observed phenomena of growing and diminishing overall light intensity. On this photograph there are two brighter regions. The frequency of these brighter regions appears to be about 2 cps which is near the surge frequency of a vehicle! Note that the light signal from cylinder 1 disappears during the low-intensity period. Cylinder 1 is the second blip after the TDC timing mark which is on the lower trace. Cylinder 5 was generally the highest in this run. For this test the photomultiplier was mounted in front of the engine, recording light emitted from the large front window in the reactor.

Figure 25 shows additional data similar to Figure 22. The second bright region during the exhaust of cylinders 1 and 3 is very evident. Note also that cycles with lower peak light intensities began emitting later in time. Cylinders which emit strongly tended to be strong each cycle.

Upon starting the engine, there is no light. After a minute or so, an occasional flicker is noted. The flicker frequency gradually increases in an apparently erratic manner until a relatively steady light is obtained. Even at steady state however, there is a perceptible flicker. This arises from the uneven frequency of exhaust valve opening which leads to one brighter and one darker period per two revolutions of the crankshaft. At 1200 rpm, the test condition, this leads to a 10 cps flicker which is easily detected with the eye.

(3) Spectral Studies

A spectrum of the light emission was obtained from the spectrograph. Calibration was made with a mercury lamp. Figure 26 shows a typical result. Maximum intensity was near 4000 angstroms. It was surprising to find that all the detectible lines were lead or lead oxide. Perhaps engines running on unleaded fuel do not have the high intensity luminous reactions observed in these tests. Running for 20 hr on unleaded gasoline did not diminish the light emitted from our reactor. Perhaps too much lead had accumulated in the engine and reactor to be eliminated in this short time.

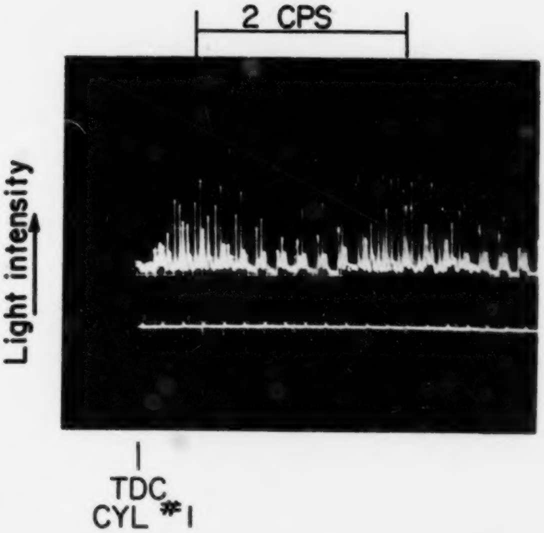

Figure 24. Repeatability of light emission.

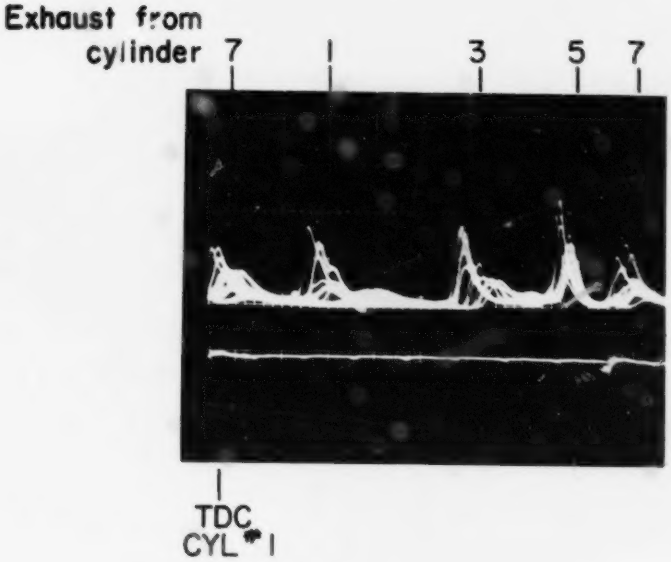

Figure 25. Repeatability of light emission. Timing marks on lower trace are 90° apart.

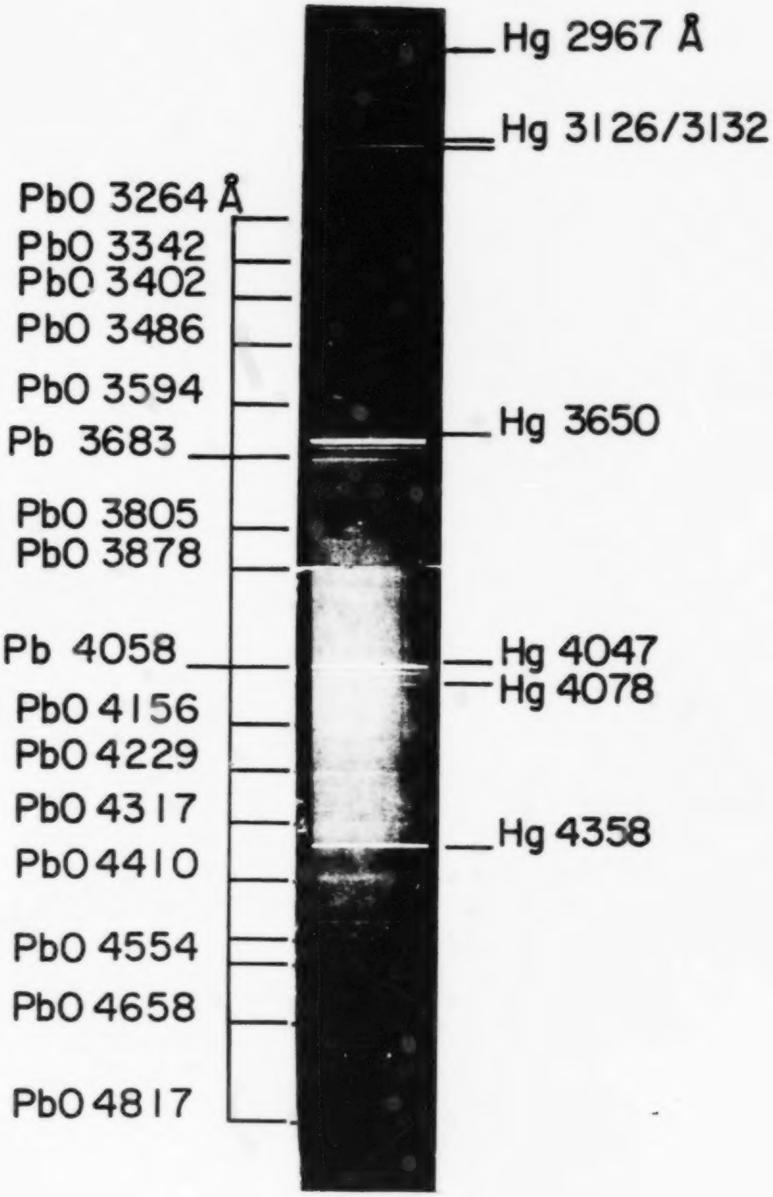

Figure 26. Spectrogram of luminous blue flame appearing in exhaust gas reactor. Chevrolet 350 in.^{3} engine, leaded fuel, 1200 rpm, 30 hp, 12.5:1 air fuel ratio, air injection fraction approximately 0.3.

(4) Summary

The following observations have been made regarding light emission:

(a) Illumination varies directly with the rate of gas input to the reactor.

(b) There are marked cycle-to-cycle and cylinder-to-cylinder differences in light emission.

(c) To an extent cylinder-to-cylinder differences repeat.

(d) During warm up illumination rises slowly and in an intermittent manner.

(e) Spectral lines observed were those of lead and lead oxide.

(f) Maximum intensity was near 4000 angstroms.

B. SINGLE CYLINDER EXPERIMENTAL REACTOR STUDY

1. Objectives

The objectives of the experimental reactor study were: (1) to obtain data on the chemical kinetics of the oxidation of carbon monoxide, hydrogen, and hydrocarbons in internal combustion engine exhaust; and (2) to determine from this data gross kinetic rate equations which can be used in modeling thermal exhaust reactors.

2. Experimental Apparatus

The experimental reactor system is sketched in Figure 27. The exhaust gas inlet was attached directly to the exhaust port of a propane fueled single cylinder CFR variable compression ratio engine. Hot exhaust gas passed from the exhaust port through a perforated exhaust inlet tube and into a 1350 in.^{3} surge and mixing tank and then through a sparger tube and into the 59.5 in.^{3} reactor. The high-velocity jets generated by the sparger tube kept the reactor well stirred. Reactor mixing was discussed in detail in the Second Annual Progress Report. Air was injected into the reactor inlet tube after passing through a bank of heaters. A bypass loop was incorporated to permit the reactor residence time to be varied without changing engine conditions. The two tanks and connecting piping were made of Hastelloy-X and similar high-temperature alloys and the reactor was operated at temperatures up to about 1800°F.

Gas samples were withdrawn at the reactor inlet and outlet through water cooled sampling probes. Gas temperatures were measured with shielded thermocouples in the surge tank, at the reactor inlet, at three locations inside the reactor, and at the bypass flowmeter. One of the thermocouples inside the reactor was movable and was used to obtain temperature profiles along the length of the reactor. The reactor wall temperature was measured at one location on the outside of the cylindrical surface. Temperature nonuniformities and wall effects were discussed in the Second Annual Progress Report. Surge tank and reactor pressures were measured with mercury manometers. Propane and air flowrates to the engine and injection air flowrate were measured with critical flow orifices, and injection air temperature with a shielded thermocouple. Flowrate through the reactor was measured by using the calibrated sparger tubes as square-edged orifices.

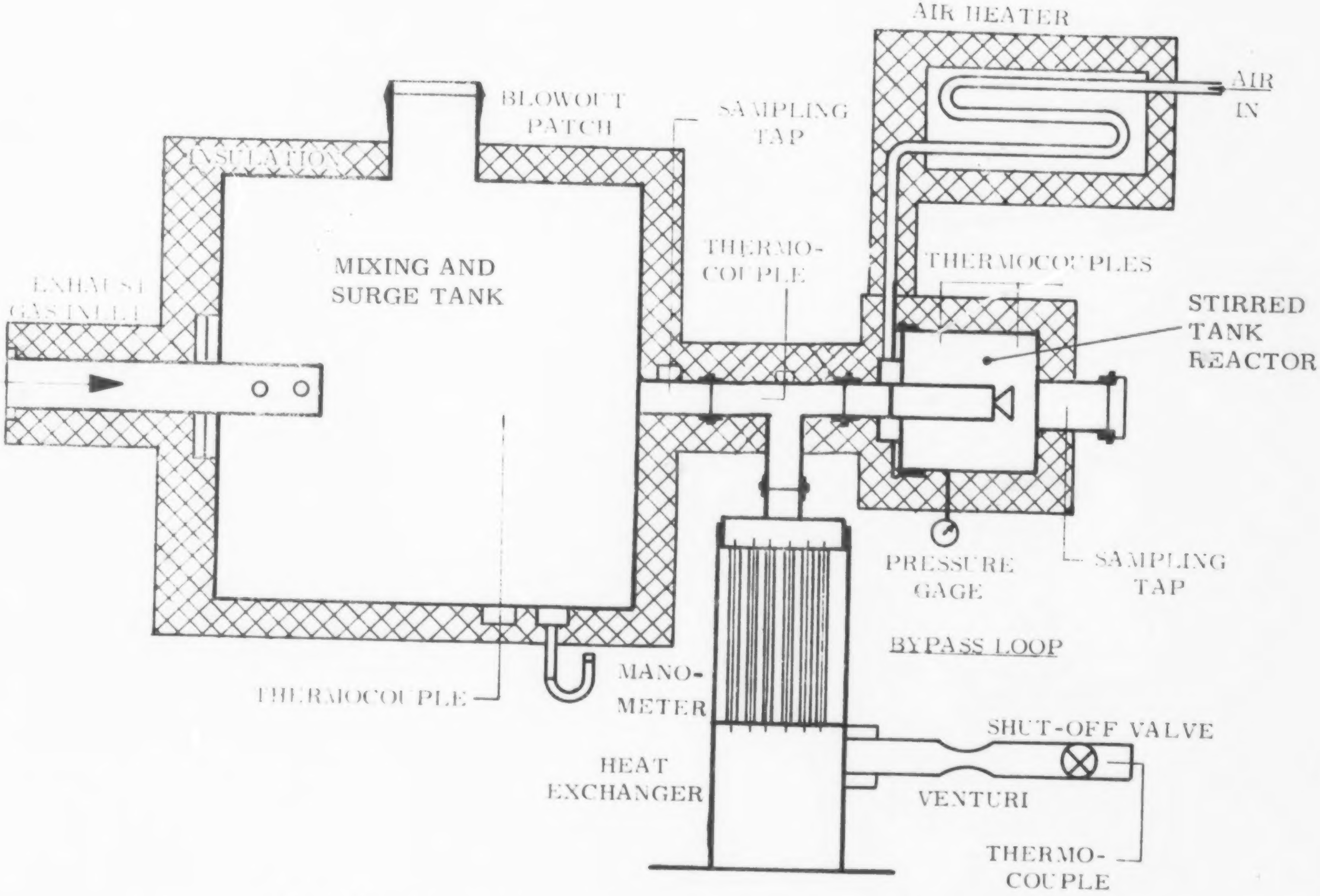
AIR HEATER
AIR IN
BLOWOUT PATCH
SAMPLING TAP
INSULATION
EXHAUST GAS INLET
MIXING AND SURGE TANK
THERMO- COUPLE
THERMOCOUPLES
STIRRED TANK REACTOR
PRESSURE GAGE
SAMPLING TAP
BYPASS LOOP
THERMOCOUPLE
MANO- METER
HEAT EXCHANGER
SHUT-OFF VALVE
VENTURI
THERMO- COUPLE

Figure 27. Two-tank experimental reactor system schematic.

Exhaust gas composition was controlled mainly by adjusting fuel/air ratio and spark timing, while temperature was controlled by adjusting spark timing and compression ratio, and by passing cooling air through the heat exchanger at the surge tank entrance. Injection air flowrate was controlled by adjusting the pressure upstream of the critical flow orifice, and its temperature was controlled by adjusting the power to the air heaters with a variable transformer.

3. Experimental Results

a. SUMMARY OF CO OXIDATION RATE RESULTS

(1) Range of Parameters

The range of parameters for which CO oxidation has been studied in the two-tank reactor system is given in Table VI. Output values of 0.1 to 5% CO and .2 to 8% O_2 were observed in the multicylinder reactor study, Phase I.

TABLE VI

RANGE OF PARAMETERS

(Carbon Monoxide Oxidation)

CO Conversion	20 to 60%
Temperature	1130 to 1525°F
Mean residence time	74 to 240 msec
Volume fraction CO	
- in	0.5 to 2.3%
- out	0.[illegible] to 1.0%
Volume fraction O_2	0.6 to 4.5%
Wall materials	Hastelloy-X Copper

(2) Regression Results

A linear regression was used to find the best fit values for the constants in the equations

$$\ln r_{CO} = \ln K - \frac{E}{RT} + A \ln P_{CO} + B \ln P_{O_2} \qquad (1)$$

$$\ln r_{CO} = \ln K - \frac{E}{RT} + A \ln P_{CO} + B \ln P_{O_2} + C \ln P_{NO} \qquad (2)$$

where r_{CO} = rate of disappearance of CO in lb-moles/sec-in.^{3},

R = gas constant in cal/gm-mole°K,

T = temperature in °K, and

P_x = partial pressure of species x in psia.

Regressions for each equation have been performed over the entire range of temperatures and over two ranges, above and below 1000°K, respectively, resulting in six separate correlations. Inclusion of all data in the regression for the parameters in Eq. (1) and all data where the NO concentration was measured in the regression for Eq. (2) result in the best fit values given in Table VII. Tolerances represent one unit of standard error. The apparent activation energy and reaction order with respect to CO are seen to be highest in the higher temperature range. To illustrate the variation of the predicted rate with temperature, the different expressions are plotted in Figure 28 for a mixture containing 1% CO, 1% O_2, and 500 ppm NO by volume.

Using the best fit values of E, A, B, and C determined by the regression program, an experimental value of the logarithm of the preexponential constant K was determined for each data point, and a comparison of rates with the different sparger tubes and with and without a copper sleeve in the reactor was made by comparing mean values and standard deviations of the distributions of ln K for the different subsets of data. The characteristics of the sparger tubes as well as the copper sleeve experiment are detailed in the Second Annual Progress Report.[12]

Table VIII contains a summary of the data analyzed in this way. (Sparger tube [illegible] was the one having the smaller holes.) Since K, rather than ln K, is directly used in the rate calculation, the results have also been tabulated in terms of K. The items denoted "mean, K" "std. dev., K" do not represent true means and standard deviations of the distribution of values for K, but are simply antilogarithms of values determined from the logarithmic distribution. The Second Annual Progress Report also includes a detailed comparison of these correlation results with others in published literature.

The equations in Table VII may be used to predict carbon monoxide oxidation rates in thermal reactors. Where NO concentration is known its addition improves the correlation.

TABLE VII

REGRESSION PROGRAM RESULTS, CO OXIDATION RATES

$\ln r_{CO} = \ln K - E/RT + A \ln P_{CO} + B \ln P_{O_2}$

Temperature Range (F°)	No. of Runs	ln K	E cal/gm-mole	A	B	Multiple Correlation Coef.
1130 to 1340	70	-8.23	28,770 ± 2,441	.710 ± .073	-.006 ± .084	0.851
1340 to 1525	87	4.55	42,310 ± [illegible]	.326 ± .064	-.058 ± .062	0.857
1130 to 1525	157	-2.68	28,198 ± 1,111	.269 ± .050	-.051 ± .057	0.913

$\ln r_{CO} = \ln K - E/RT + A \ln P_{CO} + B \ln P_{O_2} + C \ln P_{H_2O}$

Temperature Range (F°)	No. of Runs	ln K	E cal/gm-mole	A	B	C	Multiple Correlation Coef.
1130 to 1340	50	-3.69	26,087 ± 2,765	.108 ± .105	.027 ± .085	.048 ± .065	0.849
1340 to 1525	87	7.56	45,841 ± [illegible]	.386 ± .068	-.031 ± .064	.145 ± .060	0.838
1130 to 1525	137	-1.43	[illegible],137 ± 1,044	.148 ± .047	-.003 ± .050	.144 ± .044	0.897

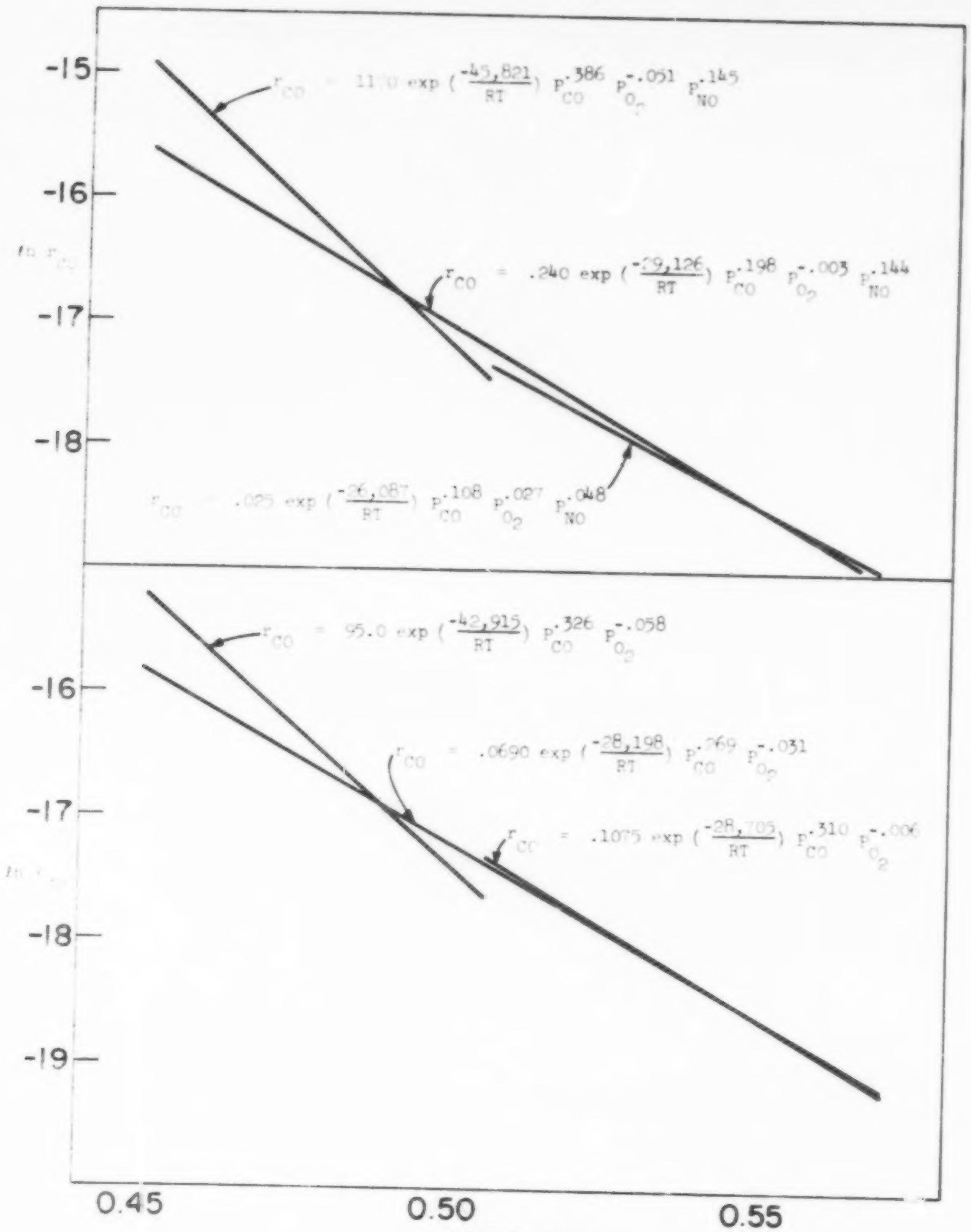

Figure 28. Predicted rates for CO oxidation for a mixture containing 1% CO, 1% O_2, and 500 ppm NO.

TABLE VIII

COMPARISON OF EXPERIMENTAL CO OXIDATION RATES WITH TWO WALL MATERIALS AND TWO SPARGER TUBES

$$\ln K = \ln r_{CO} + E/RT - A \ln P_{CO} - B \ln P_{O_2}$$

Temperatures below 1000°K

E = 28,705 A = .310 B = -.006

Data Set	No. of Runs	min. ln K	max. ln K	mean ln K	std. dev. ln K	min. K	max. K	mean* K	std. dev.* K
Sparger Tube #1 (Without Cu insert)	48	-2.96	-1.73	-2.218	.266	.0520	.1773	.1094	[illegible]
Sparger Tube #1 with Cu insert	13	-2.75	-1.57	-2.194	.289	.0642	.208	.1120	[illegible]
Sparger Tube #2 (Without Cu insert)	9	-2.85	-1.78	-2.364	.330	.0579	.169	.0945	[illegible]
All runs	70	-2.96	-1.57	-2.252	.262	.0520	.208	.107	[illegible]

Temperatures above 1000°K

E = 42,915 A = .326 B = -.058

Data Set	No. of Runs	min. ln K	max. ln K	mean ln K	std. dev. ln K	min. K	max. K	mean* K	std. dev.* K
Sparger Tube #1 (without Cu insert)	57	3.93	5.05	4.537	.278	51.0	166	95.5	26.2
Sparger Tube #1 with Cu insert	19	4.18	5.30	4.707	.245	65.5	201	111.	27.5
Sparger Tube #2 (without Cu insert)	11	4.00	4.71	4.376	.320	54.6	111	80.6	20.7
All runs	87	3.93	5.30	4.554	.250	51.0	201	95.0	24.5

All Temperatures

E = 28,198 A = .269 B = -.031

Data Set	No. of Runs	min. ln K	max. ln K	mean ln K	std. dev. ln K	min. K	max. K	mean* K	std. dev.* K
Sparger Tube #1 (without Cu insert)	105	-3.37	-2.11	-2.671	.280	.0344	.1212	.0695	.0197
Sparger Tube #1 with Cu insert	32	-3.38	-1.97	-2.578	.326	.0575	.140	.0762	.0259
Sparger Tube #2 (without Cu insert)	20	-3.34	-2.17	-2.858	.324	.0355	.1145	.0577	.0240
All runs	157	-3.34	-1.97	-2.676	.306	.0355	.140	.0690	.0234

TABLE VIII (Concluded)

$$\ell n\, K = \ell n\, r_{CO} + E/RT - A\, \ell n\, P_{CO} - B\, \ell n\, P_{O_2} - C\, \ell n\, P_{NO}$$

Temperatures below 1000°K

E = 26,087   A = .108   B = .027   C = .048

Data Set	No. of Runs	min. *ℓn* K	max. *ℓn* K	mean *ℓn* K	std. dev. *ℓn* K	min. K	max. K	mean* K	std. dev.* K
Sparger Tube #1 (without Cu insert)	28	-4.00	-3.34	-3.649	.181	.0184	.0356	.0261	.0047
Sparger Tube #1 with Cu insert	13	-4.13	-3.13	-3.708	.350	.0161	.0439	.0247	.0088
Sparger Tube #2 (without Cu insert)	9	-4.27	-3.23	-3.763	.306	.0140	.0397	.0232	.0073
All runs	50	-4.27	-3.13	-3.685	.255	.0140	.0439	.0252	.0064

Temperatures above 1000°K

E = 45,821   A = .366   B = -.051   C = .145

Data Set	No. of Runs	min. *ℓn* K	max. *ℓn* K	mean *ℓn* K	std. dev. *ℓn* K	min. K	max. K	mean* K	std. dev.* K
Sparger Tube #1 (without Cu insert)	50	6.46	7.50	7.011	.249	640	1810	1110	282
Sparger Tube #1 with Cu insert	19	6.79	7.80	7.239	.300	890	2440	1390	425
Sparger Tube #2 (without Cu insert)	11	6.68	7.25	6.957	.222	800	1410	1060	235
All runs	80	6.46	7.80	7.058	.275	640	2440	1170	320

All Temperatures

E = 29,126   A = .198   B = -.003   C = .144

Data Set	No. of Runs	min. *ℓn* K	max. *ℓn* K	mean *ℓn* K	std. dev. *ℓn* K	min. K	max. K	mean* K	std. dev.* K
Sparger Tube #1 (without Cu insert)	[illegible]	-2.03	-0.93	-1.447	.252	.1315	.395	.238	.0605
Sparger Tube #1 with Cu insert	32	-2.12	-0.81	-1.339	.366	.120	.445	.262	.098
Sparger Tube #2 (without Cu insert)	20	-2.04	-0.90	-1.540	.309	.1305	.407	.215	.067
All runs	130	-2.12	-0.81	-1.429	.297	.120	.445	.240	.067

b. SUMMARY OF HC OXIDATION RATE RESULTS

(1) Range of Parameters

The range of parameters for which HC oxidation has been studied is given in Table IX. During normal operation output values of 0 to 800 parts per million C_6 were observed in the multicylinder reactor study of Phase I.

TABLE IX

RANGE OF PARAMETERS

(Hydrocarbon Oxidation)

Hydrocarbon conversion		20 to 80%
Temperature		1040 to 1408°F
Mean residence time		110 to 750 millisec
Hydrocarbon concentration	-in	40 to 400
	-out	8 to 150
(Total hydrocarbons as n-hexane, measured by flame ionization detector)		
Fraction paraffins	-in	.42 to .60
	-out	.23 to .85
Fraction olefins	-in	.34 to .58
	-out	.15 to .77
Fraction aromatics	-in	~ 0
	-out	~ 0
Oxygen concentration		0.3 to 4.3%
NO concentration		3 to 850 ppm
Sparger tubes		#2 only
Wall materials		Hastelloy X only

(3) Regression Results

A linear regression was used to find the best fit values for the constants in the equations

$$\ln r_{HC} = \ln K - \frac{E}{RT} + A \ln P_{HC} + B \ln P_{O_2} + C \ln P_{NO} \quad (3)$$

$$\ln r_{HC} = \ln K - \frac{E}{RT} + A \ln P_{HC} + B \ln P_{O_2} + C \ln P_{NO} + D \ln P_{CO} \quad (4)$$

where r_{HC} = rate of disappearance of HC in lb-moles/sec-in.^{3}. The other parameters are the same as in the CO oxidation equations.

Regression for each equation was performed over the range of temperature 1090°-1350°F. The regression result for Eq. (3) is shown in Table X. Tolerances are one unit of standard error. The scatter is clearly greater than that for the CO data. The regression results for Eq. (4) are shown also in Table X. A significant improvement was made by including CO concentration. The multiple regression coefficient was 0.893 for Eq. (4) compared to 0.763 for Eq. (3). Equation (4) results reflect an additional 29 runs in which CO was added (13 runs) and H_2 added (16 runs) to the exhaust gas. The objective was to change the ratio of H_2 to CO in the reactor feed. This ratio tends to be fixed in engine exhaust for a particular fuel. In so far as Eq. (3) is concerned, these 29 runs yielded data which fell within the range of parameters given in Table X. As a point of interest the reaction order for CO in Eq. (4) was .576 for just the 29 runs as opposed to .512 for all 105 runs. Equation (4) is believed to reasonably represent the trends in the hydrocarbon oxidation data and is recommended for use in estimating oxidation in thermal reactors.

c. SUMMARY OF H_2 OXIDATION RATE RESULTS

(1) Range of Parameters

The range of parameters for which H_2 oxidation has been studied is given in Table XI. During normal operation output values of 0 to 2% H_2 were observed in the multicylinder reactor study of Phase I.

TABLE X

HYDROCARBON OXIDATION REGRESSION RESULTS

$$\ln r_{HC} = \ln K - \frac{E}{RT} + A \ln P_{HC} + B \ln P_{O_2} + C \ln P_{NO} \quad \text{(76 runs)}$$

Multiple correlation coefficient = .763

$\ln K$ = .536
E = 30,533 ± 4,171

A = .488 ± .106
B = .357 ± .068
C = .392 ± .038

min $\ln K$ = -1.242
max $\ln K$ = +1.245
mean $\ln K$ = 0.536
std dev $\ln K$ = .410

min K = .289
max K = 3.48
mean* K = 1.40
std dev* K = .591

$$\ln r_{HC} = \ln K - \frac{E}{RT} + A \ln P_{HC} + B \ln P_{O_2} + C \ln P_{NO} + D \ln CO \quad \text{(105 runs)}$$

Multiple correlation coefficient = .893

$\ln K$ = .175
E = 29,836 ± 3,046

A = .338 ± .064
B = .537 ± .082
C = .415 ± .040
D = .512 ± .123

TABLE XI

RANGE OF PARAMETERS

(Hydrogen Oxidation)

No. of data points		53
Hydrogen conversion		20 to 80%
Temperature		1090 to 1380°F
Mean residence time		110 to 250 millisec
Hydrogen concentration	-in	0.2 to 1.5%
	-out	0.1 to 1.0%
Oxygen concentration		0.3 to 4.3%
NO concentration		3 to 840 ppm
Sparger tubes		#2 only
Wall materials		Hastelloy X only

(2) Regression Results

A linear regression was used to find the best fit values for the constants in the equations

$$\ln r_{H_2} = \ln K - E/RT + A \ln P_{H_2} + B \ln P_{O_2} \qquad (5)$$

$$\ln r_{H_2} = \ln K - E/RT + A \ln_{P_{H_2}} + B \ln P_{O_2} + C \ln P_{NO} \qquad (6)$$

$$\ln r_{H_2} = \ln K - E/RT + A \ln P_{H_2} + B \ln P_{O_2} + D \ln P_{CO} \qquad (7)$$

where r_{H_2} = rate of disappearance of H_2 in lb-moles/sec-in.^{3}. Other parameters are as defined previously.

Regression for each equation was performed over the range of temperature 1090-1380°F. The regression results are shown in Table XII. In general none of the equations correlate the data particularly well, the multiple correlation coefficient being about 0.39 for the first two and 0.49 for the third. Moreover the reaction orders are close to zero in every case except for CO. The doped data gave approximately a zero order with respect to CO, while all data taken together indicated an order of about 1/2, but in both cases the overall correlation coefficient was very low. Thus within the temperature range in which intermediate conversion was observed, little success was experienced in correlating observed rates with an equation of the desired form. It was observed that below about 1100°F appreciable H_2 conversion (20% or more) almost never occurred, while above about 1300°F fairly complete conversion (80% or more) almost always occurred. It was also observed that whenever appreciable CO conversion occurred (above [illegible]%) the hydrogen was nearly completely oxidized (above 80% conversion with very few exceptions), but nearly complete H_2 conversion also occurred in many cases with very little CO conversion.

The equations in Table XII not only failed to correlate the data very well within the 1100°F to 1300°F temperature range, but in conflict with the observations above did not indicate substantially different rates at (for example) 1000°F and 1350°F (runs in which conversion of H_2 was less than 20% or more than 80% were not included in the data regressed). Thus this equation very definitely should not be used in predicting rates outside the 1100°F to 1300°F temperature range, and is of little value even in this range. It is therefore not recommended for use in modeling thermal exhaust reactors.

TABLE XII

HYDROGEN OXIDATION REGRESSION RESULTS

$$\ell n\, r_{H_2} = \ell n\, K - \frac{E}{RT} + A\, \ell n\, P_{H_2} + B\, \ell n\, P_{O_2}$$

Multiple Correlation Coefficient = .583

ℓn K = -8.688

E = 17,804 ± 4433

A = .0258 ± .1343

B = -.0609 ± .1505

min ℓn K = -9.905

max ℓn K = -7.694

mean ℓn K = -8.688

std. dev. ℓn K = .505

min K = .0000499

max K = .000462

mean* K = .000172

std. dev.* K = .000088

$$\ell n\, r_{H_2} = \ell n\, K - \frac{E}{RT} + A\, \ell n\, P_{H_2} + B\, \ell n\, P_{O_2} + C\, \ell n\, P_{NO}$$

Multiple Correlation Coefficient = .594

ℓn K = -5.236

E = 22,299 ± 6393

A = .118 ± .164

B = .0375 ± .1812

C = .0861 ± 0882

min ℓn K = -6.534

max ℓn K = -4.258

mean ℓn K = -5.236

std. dev. ℓn K = .500

min K = .00147

max K = .0142

mean* K = .00540

std. dev.* K = .00279

$$\ell n\, r_{H_2} = \ell n\, K - \frac{E}{RT} + A\, \ell n\, P_{H_2} + B\, \ell n\, P_{O_2} + D\, \ell n\, P_{CO}$$

Multiple Correlation Coefficient = .480

ℓn K = -15.6

E = 6330 ± 2497

A = -.333 ± .160

B = -.154 ± .122

D = +.526 ± .216

In consequence of the failure of the above equations to predict hydrogen oxidation results, a zero-order reaction was assumed (in line with the regression results) with activation energy and preexponential term adjusted to predict virtually zero conversion below 1100°F and virtually complete conversion above 1300°F, behavior in line with the observed effect of temperature.

For a reaction, in which temperature alone determines the rate, the extent of conversion is:

$$\text{Conversion} \;=\; X \;=\; \frac{kV}{\dot{m}C_o}\, e^{-E/RT};$$

where $r = ke^{-E/RT}$ is rate of reaction, lb moles/cu in. sec;

V is reactor volume, cu in.,

$\dot{m}$ is flowrate, lb moles/sec,

and C_o is entering concentration, mole fraction.

Using this expression, experimental data in X versus T can be corrected to the same flowrate $\dot{m}$ and entering concentration C_o by a simple ratioing procedure. In Figure 29 the data for hydrogen are shown corrected to 20 lb mass/hr and C_o = 0.6% H_2.

The correction of conversions does not alter the scatter in relation to temperature, however, it does redistribute the conversions so that a slope for conversion versus temperature can be identified. This slope, discounting the scatter, suggests that conversion would proceed from 0 to 1 in approximately 1[illegible]°F. To reduce this observation to an analytical expression, the points (X,T) = (.2,1195) and (.8,1280) were fit to the zero-order conversion equation. This gave k = 12,660 and an activation energy E = 52,000 cal/g-mole. The final equation is:

$$r_{H_2} \;=\; 12,660\; e^{-52,000/RT}, \text{ lb moles/cu in. sec} \qquad (8)$$

In the absence of better data, Eq. (8) may be used to predict hydrogen oxidation in thermal reactors.

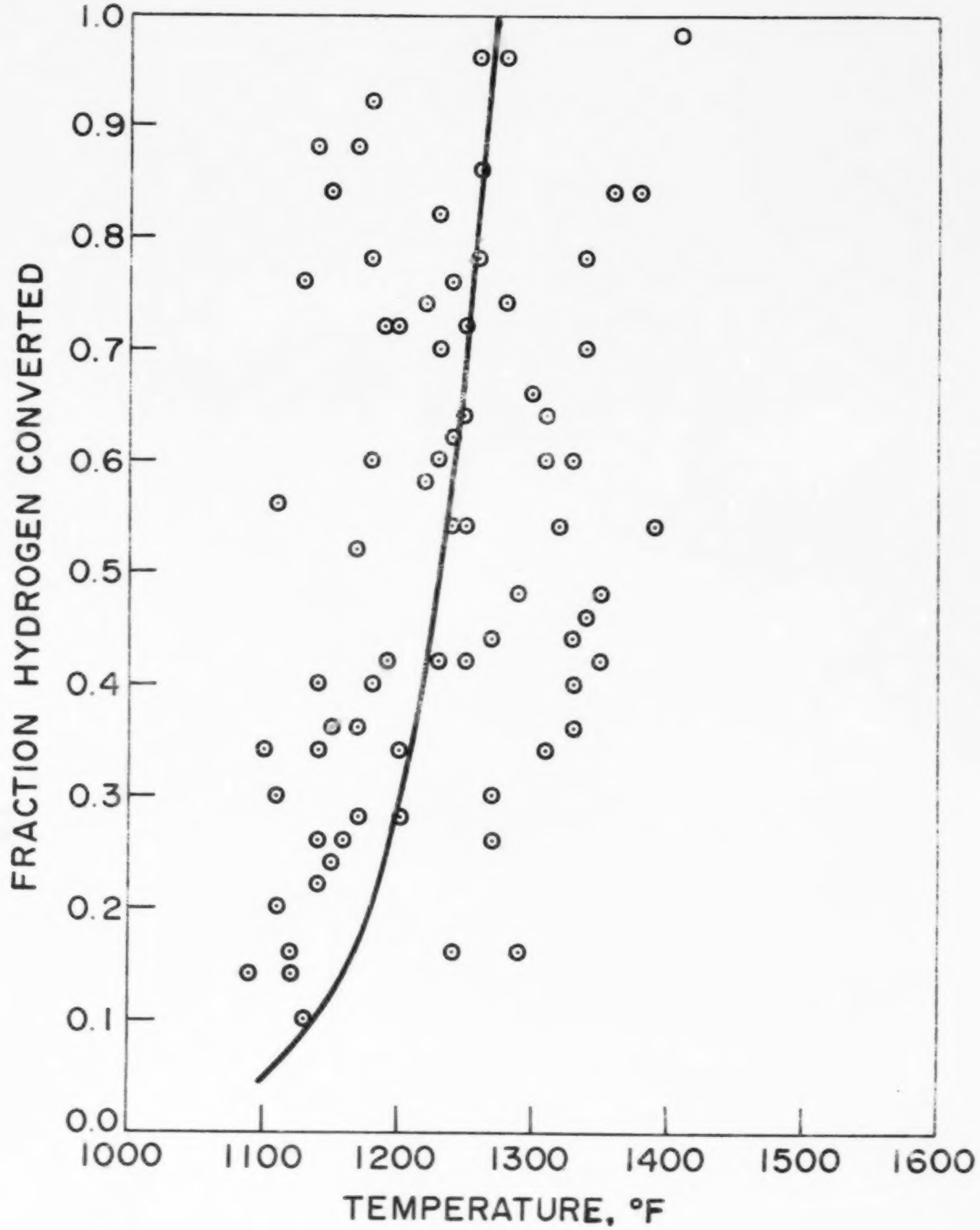

Figure 29. Conversions of hydrogen corrected to 20 lb exhaust/hr and .006 mole fraction hydrogen entering, $r_{H_2} = 12,660e^{-52,000/RT}$.

C. REFERENCES FOR PHASE I

1. Cantwell, E. N., *et al.*, "A Progress Report on the Development of Exhaust Manifold Reactors," *SAE paper 690139*, January 1969.

2. Cantwell, E. N., *et al.*, "Recent Development in Exhaust Manifold Reactor Systems," *Inst. of Mech. Eng. Preprint* ADP13 (B)/70, May 1970.

3. Cantwell, E. N., and J. J. Mikita, "Exhaust Manifold Thermal Reactors—A Solution to the Automotive Emission Problem," *68th Annual Nat. Pet. Ref. Assoc.*, April 1970.

4. Cantwell, E. N., and A. J. Pahnke (DuPont), "Design Factors Affecting the Performance of Exhaust Manifold Reactors," *SAE paper 650527*, 1965.

5. Blenk, M. H. and R. G. E. Franks, "Math Modeling of an Exhaust Reactor," *SAE paper 710607*, 1971.

6. Klosterman, D. L. and J. E. Sigsby, "Application of Subtractive Techniques to the Analysis of Automotive Exhaust," *Env. Sci. Tech.*, *1*, No. 4, April 1967, p. 309.

7. Oberdorfer, P. E., "Determination of Aldehydes in Automobile Exhaust Gas," *SAE paper 670123*, January 1967.

8. U. S. Bureau of Mines, "Procedures for Determining Exhaust Carbonyls as 2, 4-Dinitrophenylhydrazones," APRAC Project CAPE-11-68, Final Report, 1968.

9. Papa, L. J., "Colorimetric Determination of Carbonyl Compounds in Automotive Exhaust as 2, 4-Dinitrophenylhydrozones," *Env. Sci. Tech.*, *3*, No. 4, April 1969, p. 397.

10. Saltzman, B. E., *Analytical Chemistry*, *32*, p. 135, 1960.

11. Patterson, D. J., *et al.*, "Kinetics of Oxidation and Quenching of Combustibles in Exhaust Systems of Gasoline Engines," Annual Progress Report No. 1 to CRC, 1969-70.

12. Patterson, D. J., *et al.*, "Kinetics of Oxidation and Quenching of Combustibles in Exhaust Systems of Gasoline Engines," Annual Progress Report No. 2 to CRC, 1970-71.

13. Levenspiel, O., *Chemical Reactor Engineering*, Wiley & Sons, New York, 1962.

C. REFERENCES FOR PHASE I (Concluded)

14. Schwing, R. C., "An Analytical Framework for the Study of Exhaust Manifold Reactor Oxidation," SAE Preprint 700109, January 1970.

15. Glass, W., et al., "Synchrothermal Reactor System for Control of Automotive Exhaust Emissions," SAE paper 700147, 1970.

DETAILED PROGRESS - PHASE II

COMPUTER MODEL DEVELOPMENT

Preceding page blank

FOREWORD

Contents of This Chapter

A theoretical framework for the design of thermal reactors has been synthesized taking into account both the full extent of chemical reactor design theory and the high frequency cyclic operating characteristics of automotive exhaust reactors. An array of analytical design tools in the form of highly adaptive computer simulation programs has been developed to aid design efforts on exhaust reactors where thermal quenching and turbulent mixing are determining factors.

After a general introduction to the thermal reactor problem, the discussion in this phase is divided into ten subsections. Parts I and II describe the theory and development of the generalized patterns of flow reactor simulation used for predicting performance of partially mixed reactors under warmed-up steady state conditions. Part III discusses a method for estimating the coalescence parameter in a new design. This parameter is a measure of the micromixing intensity within the various sections of the reactor. Part IV describes calculated results which verify that the performance of the single cylinder engine experimental kinetics test reactor discussed in Phase I-B was not mixing limited.

An understanding of Parts I, II, III, and IV is not essential for interpreting the comparisons between warmed-up steady state experimental and computed performance of the multicylinder engine DuPont Model V reactor. These comparisons are included in Part V.

Part VI describes the development of the computer model for unsteady state warm-up of an initially cold reactor. An understanding of this section is not essential for interpreting the comparisons between experimental and computed warm-up performance for the DuPont Model V reactor which are included in Part VII or the warm-up computer projections in Part VIII. These projections include the effects of specific reactor configurations, inlet combustible concentrations, and ignition sources on time to lightoff. Finally, Parts IX and X discuss conclusions and use of the results.

As an aid to the reader, a detailed overview of the modeling efforts follows.

Preceding page blank

Overview of Modeling Efforts

Previous work on flow patterns and micromixing in chemical reactor design are critically reviewed herein. Cell-wise mixing models and Monte Carlo type solutions were selected as the best means to treat the coupled mixing and multiple reactions of separate streams of air and exhaust entering in cyclic flows and with cyclic temperature and composition. In the most general model, different reactor configurations are simulated by a forward flow of cells through a user-designated network of parallel and series modules. These are either cell-wise mixed stirred tanks or cell-wise mixed plug flow reactors. "Micromixing" is simulated by coalescence and redispersal of cells. Subordinate models wherein particular assumptions are relaxed were investigated, with particular attention given to mixing with instantaneous reaction.

An experimental single cylinder stirred tank reactor was described in Phase I. It was built to obtain mixing-independent kinetics required for modeling. This reactor was designed to operate under conditions of intense turbulent mixing generated by high velocity entrance jets; both theoretical and experimental results indicated no significant limitation due to segregation of air and exhaust. A near-zero reaction order for oxidation of carbon monoxide was established.

An unsteady state thermal model was developed to simulate warm-up of an arbitrary number of metal surfaces or insulating components in a reactor, subject to user-specified heat exchange by radiation, convection, and/or conduction. The computed temperatures of designated surfaces and the computed values of heat transfer coefficients for exhaust side convection were used to establish heat losses for an ideal backmix simulation of all or part of the reactor volume. Exhaust temperature and conversions of several species are obtained using a search strategy. Computations make use of the difference in time scale for changes in metal temperatures (minutes) and adjustments in gas temperature relative to given values of heat generation and heat loss terms (tenths of a second). Good correspondence was established with experimental results for unchoked engine start up. Sensitivity of reactor ignition to selected parameters was investigated.

It is concluded for modeling, based on mixing independent kinetics, that the high temperature conversions substantially below 100% that are observed in reactors are mixing limited rather than temperature-kinetics limited. The work of Corrsin on idealized turbulent mixers was found to predict reasonable mixing intensities from flow and geometry. Mixing intensity is discussed in relation to entrance geometry and air inlet timing, with the conclusion that the intensity could perhaps be doubled by changing the timing and location of air injection.

INTRODUCTION TO THE THERMAL REACTOR PROBLEM

In recent years groups within the petroleum and automotive industries have expended considerable efforts to develop effective spark-ignition engine exhaust treatment systems. Such systems have included catalytic or noncatalytic thermal reactors or combinations of the two. Brownson (4), Chandler (7), Cantwell (5,6), and Schwing ([illegible]), have reported on the success with using noncatalytic thermal reactors to oxidize the exhaust carbon monoxide and hydrocarbon constituents.

The goals of thermal reactor design are clear: to complete the combustion of unburned and partially burned exhaust components. The operation of thermal reactors is at first view qualitatively simple: Air and exhaust mix, oxidation proceeds, and heat is liberated. Carbon monoxide, hydrogen, and hydrocarbons are thereby reduced, but nitrogen oxides are not significantly altered.

When air is injected into combustible rich exhaust gases in a conventional exhaust system, some reaction will occur in the manifold, exhaust pipe, and muffler without the use of a specially designed reactor. As a means to achieve higher conversions, thermal reactors are designed to extend the residence time of the exhaust gases in a high temperature zone to provide greater opportunity for mixing and reaction before reactions are quenched by cooling. Typical flow through a thermal reactor exhaust system is shown in Figure 1. Exhaust proceeds through the reactor in three passes so that hot reacted gases in the outer annulus tends to thermally isolate the inner core.

The simulations run in this study have been limited to the thermal reactor itself and the engine exhaust ports which lead to it; no attempt has been made to model the exhaust pipe and muffler. The methods of analysis developed would however apply, if sufficient information were available on this high quench region to form a valid basis for simulation.

Operation of a thermal reaction from a cold start has been characterized in the University of Michigan CRC study and others by a latent period of slight conversion during which oxidation of combustibles is partially quenched due to heat loss, followed by an approach to a steady-state mode where conversions are high but do not reach 100% except for hydrogen (approximately [illegible] to 94% for carbon monoxide and 93 to 98% for hydrocarbon for low pressure air injection and high temperature operation).

The various rate processes associated with an analysis of thermal reactor design can be readily identified as heat transfer, mixing, chemical reaction, and flow. Design information required thus consists of heat transfer coefficients, heat capacities, and heats of reaction; mixing parameters, reaction

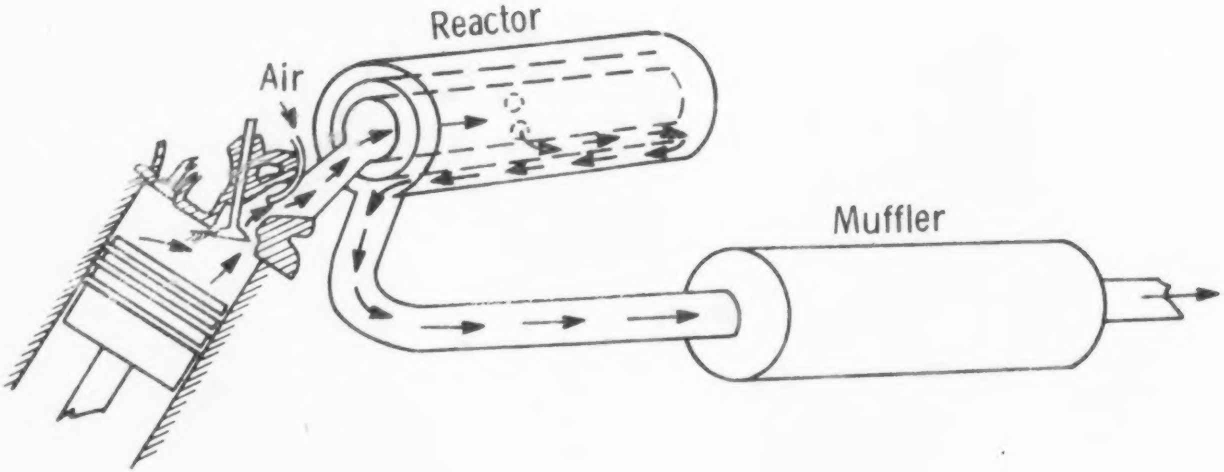
Air
Reactor
Muffler

Figure 1. Schematic of exhaust flow from one cylinder through a thermal reactor exhaust system.

rate constants, and associated rate laws; and stoichiometry. Design constraints exist for the size of the reactor, operating temperature, the energy available for mixing, the heat losses from the reactor, and the time-distributed composition, temperature, and flowrate entering the reactor.

The goal of reactor modeling has been to develop basic tools in the form of highly flexible computer simulations to obtain insights concerning these interactive processes. Our goal is to divorce our approach from any specific reactor geometry so as to provide a general design basis that is widely applicable. Given the constraints on thermal exhaust reactors, we wish to predict the performance of given reactor designs, including correspondence with experimental results for the DuPont Model V reactor and the kinetics test reactor employed in the CRC study. From these fixed points, it is our intent to interpolate in an approximate manner to judge the limits of performance for practical exhaust reactors as a class.

Modeling effort has been divided between the problems of warm-up and conversion at stationary state. The a priori assumption made to establish this division was that warm-up to the point of lit-off operation depended primarily on change in heat loss and reactor gas temperature occurring on a time scale of minutes and only negligibly on extent of incomplete mixing. On the other hand, incomplete conversion during "steady state" operation at elevated temperature was assumed to depend on a coupling of mixing with kinetic and thermal effects.

Constraints on Design and Operation

Residence times in existing devices are dictated by exhaust flows in the range of 100 to 300 lb/hr through a reactor volume of approximately [illegible] cu in. Corresponding mean residence times are .084 to .028 sec at 1500°F. We will assume that a doubling of reactor volume is permissible, so that residence times are restricted to approximately 0.15 sec. Optimum volume is not necessarily the largest possible, since a slower warm-up tends to offset the advantage of a longer residence time.

For the DuPont Model V reactor, the maximum recommended core temperature is 1700°F. Since conversion of carbon monoxide as the specie most resistant to oxidation is observed to approach its limiting upper value at approximately 1400°F, this is not a serious constraint on conversion. It is of course an important consideration in determining reactor durability (7).

Low exhaust temperature resulting from heat loss is a serious limitation during warm-up when temperature primarily governs conversion. Cold-start tests run in the CRC studies were particularly affected because of a necessity to run at a predetermined air/fuel ratio from time zero. Choking to produce a high level of combustible in the exhaust at start-up has been used in practice to greatly reduce the time to lightoff.

Limits on mixing are posed by the energy available and the dimensions of the inlets to the reactor. A very large amount of energy is available at the time of exhaust blowdown through the exhaust valve, however this may not be effectively utilized. Pressure drops that are tolerable in a reactor are comparatively low, perhaps 1 or 2 psi. This important class of constraints will be discussed later in detail.

Inlet Flow, Composition, and Temperature

Inlet properties represent a special class of constraint on reactor design because of their cyclic character. The implications of periodic flow and temperature variation are readily visualized by considering the adverse effect of a high flow of exhaust entering coincidentally with a low flow of air or the persistence of a low-temperature fraction within a reactor lacking a sufficient backmixing effect.

Instantaneous exhaust velocities were measured by Yun and Mirsky on a one-cylinder engine by a laser-schlieren technique in Phase III. The measured velocities have been corrected for an assumed temperature span of 800° between peak blowdown temperature and a 1200°F tailing flow to produce the piecewise linear mass flow curve shown in Figure 2. This "normalized" curve was used for all simulations that involve periodic flow. Neither the measurements as applied to multicylinder engines nor the models are felt to possess an exactness warranting refinement for various operating conditions.

Periodicity in exhaust flow is also influenced by the timing of cylinder firings into the reactor. Simulations are run for cylinders 1, 3, 5, and 7 of a V-8 engine discharging at 474°, 24°, 204°, and 294° on a 720° engine cycle. The span of flow for each cylinder is 278°, corresponding to the duration of exhaust value opening. Cylinders 1 and 3 tend to fire individually with a minor amount of overlap, but cylinders 5 and 7 overlap appreciably. Total "normalized" exhaust flow for the four combined cylinders is shown in Figure 3.

The normalized air flow shown in Figure 4 is based on hotwire velocity measurements. Flow to each cylinder port is reasonably constant except for dips coinciding with exhaust pulses occurring during blowdown and again at the time of maximum piston velocity. The other fluctuations in measured air flow, which coincide with pulses from the other three cylinders attached to the reactor, amount to only about ±10% of average flow and are neglected in the present simulations.

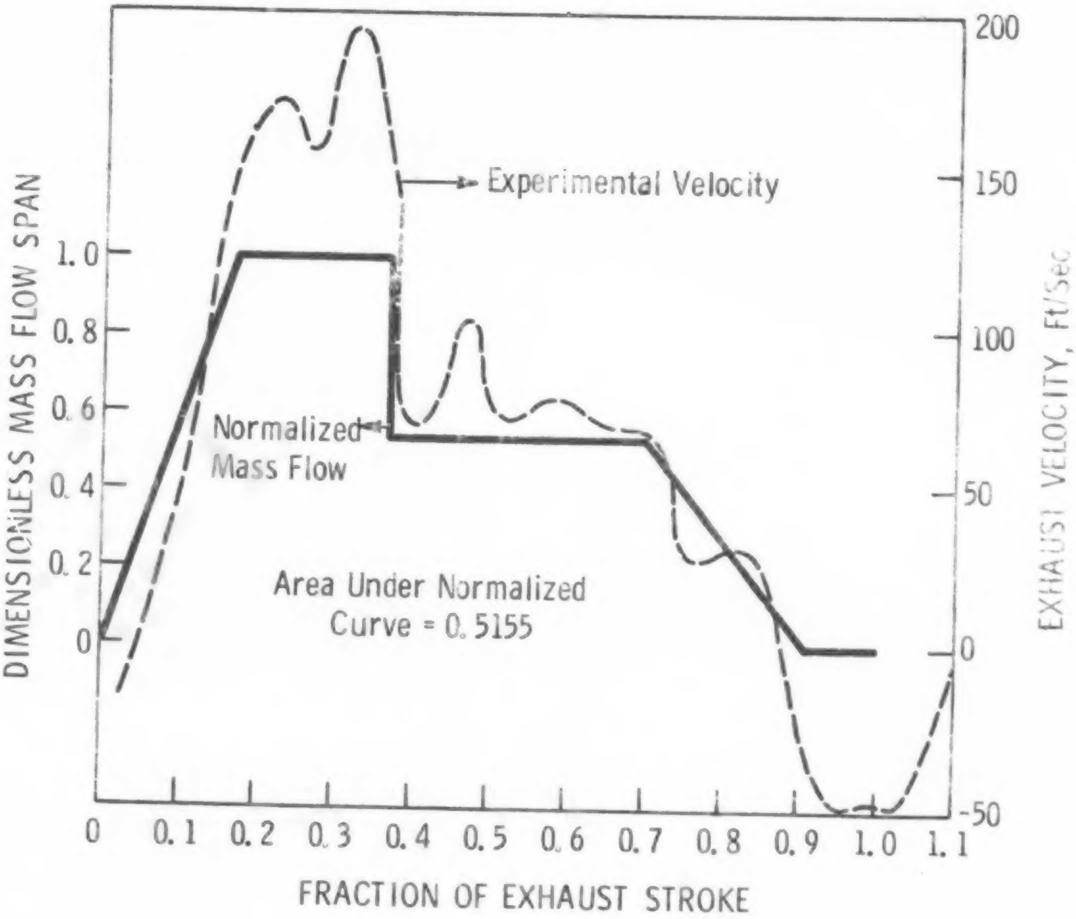

Figure 2. Characteristic variation in cyclic exhaust flow from a single cylinder spark ignition engine. Velocities measured by laser-schlieren methods, Yun and Mirsky, CRC program.

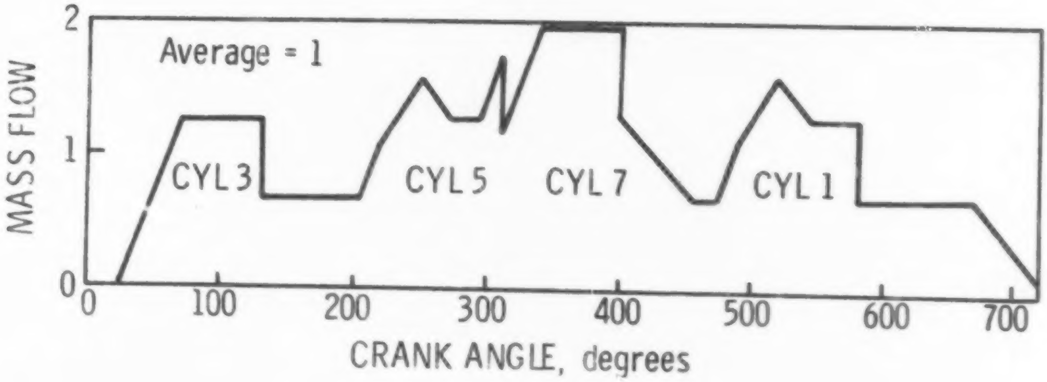

Figure 3. Combined normalized flow for cylinders 1,3,5, and 7 of a V-8 engine.

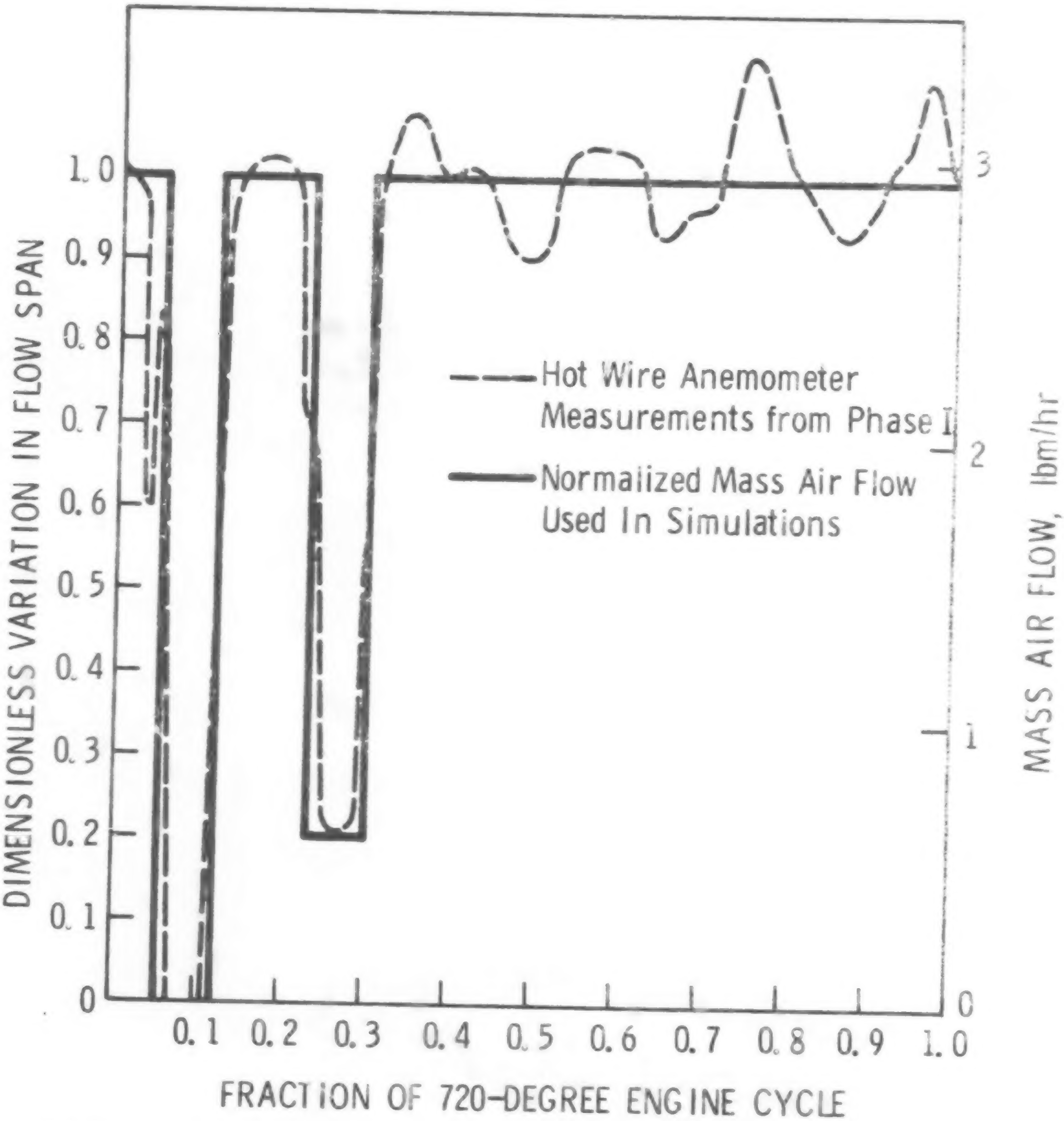

Figure 4. Characteristic variation in cyclic mass flow through air injection tube during a 720° engine cycle. Fraction zero coincides with opening of the exhaust valve. Area under the normalized curve = .874.

In the absence of experimental data on variation in exhaust temperature, it was assumed that peak temperature occurred coincidentally with peak exhaust flow, as shown by the solid curve in Figure 5. All simulations involving periodic temperature variation were performed on this temperature pattern shown by the dotted curve in Figure 5. This curve has been placed in a position which averages out the tailing temperature drop, which is felt to be partially due to greater heat loss specific to exhaust flow as flow drops to zero. Temperature span for these data as plotted, between 0 and 1 on the dimensionless scale, is approximately 900°F.

In Tabaczynski's (35) study, engine speed between 1300 and 1800 rpm was shown to have little affect on temperature span. However, departures in air fuel ratio from stoichiometric did lower the span by up to 200°F.

Since the temperature drop during blowdown is associated with expansion of the exhaust gas within the cylinder, we can estimate temperature span solely by the change in pressure within the cylinder. Pressure at the time the exhaust valve opens is approximately 75 psia at full load and 20 psia at no load, based on unpublished engine test data, Automotive Laboratory, The University of Michigan. If we assume that the gas within the cylinder expands isentropically and that the discharge through the valve is a constant temperature throttling process, we can then estimate temperature span from the expansion properties of an ideal gas.

i.e.,

$$\frac{T_{high}}{T_{low}} = \left[\frac{P_{high}}{P_{low}}\right]^{\frac{1-\gamma_c}{\gamma_c}} \quad ; \quad \gamma_c = 1.3$$

Applied to an expansion from 75 to 15 psia for T_{low} = 1200°F (1660°R), we obtain a temperature span of 325°F. At 20 psia, the span is 114°F. This calculation indicates that the span of temperature variation may change greatly depending on engine load.

The time variation in concentration of total hydrocarbon shown in Figure 6 was obtained by summing species concentrations published by W. A. Daniels (10). Carbon monoxide and hydrogen were assumed to be uniformly distributed in the exhaust.

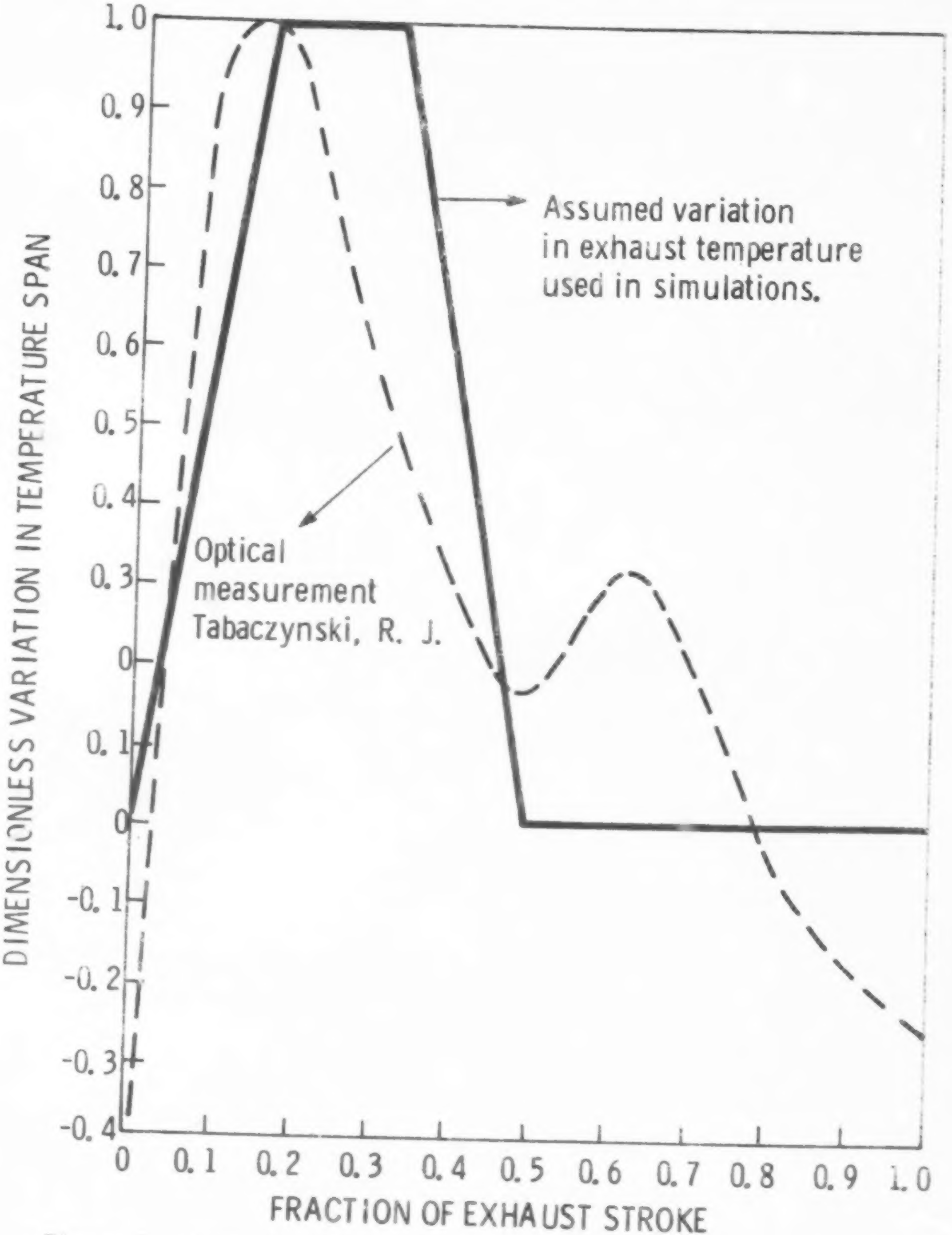

Figure 5. Assumed variation in cyclic exhaust temperature based on coincidence with measured peak flow, compared with optical measurements by Tabaczynski (35).

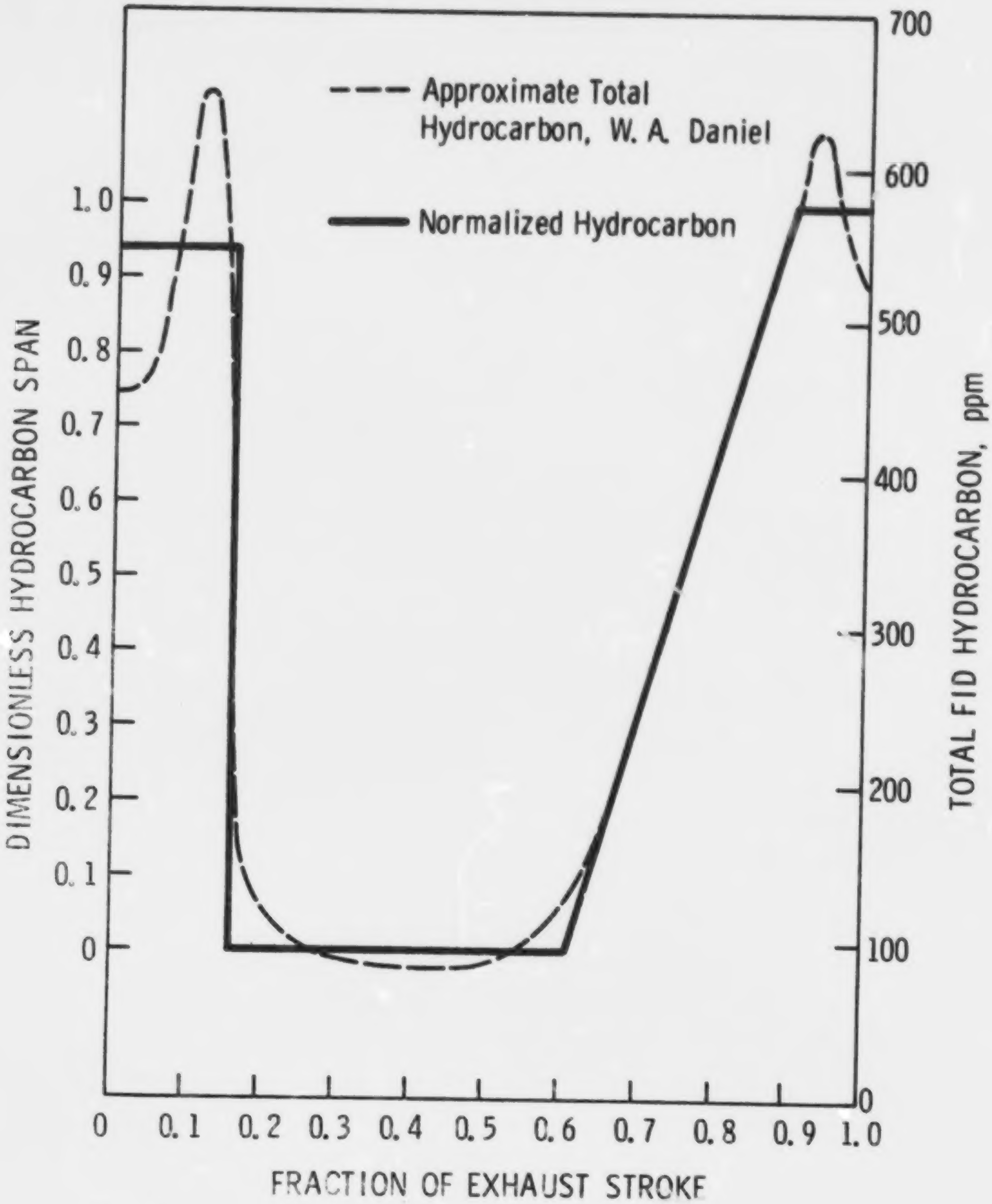

Figure 6. Characteristic variation in cyclic hydrocarbon concentration. Area under normalized curve = .3954.

MODEL BUILDING AND PARAMETER EVALUATION FOR STATIONARY STATE OPERATION

I. Mixing Coupled with Reaction

Failure to reach complete conversion of combustibles at high exhaust temperatures is a strong indication that conversions are mixing limited. Only a high-order rate dependence on one of the vanishing species could otherwise account for this failure, and this is not consistent with the kinetics and their use in the analysis which follows later. Therefore, the simulations undertaken for steady state reactor operation have been designed to permit a very general treatment of coupled mixing and reaction. It seems evident that many problems associated with combustion and pollution control should benefit from application of the resulting simulation programs.

By virtue of a number of the features of the exhaust problem already given, it is easy to visualize reasons why a portion of the exhaust combustibles might escape from the reactor unmixed with air and therefore unreacted. To enumerate: input of separate streams of air and exhaust into a reactor immediately implies that some nonzero fraction of the reactor volume must contain partially segregated air and exhaust; a very "short" residence time tends to insure that some appreciable segregation persists throughout the reactor; the virtual exclusion of air flow during peak input of exhaust (low pressure air injection) further promotes this segregation; the wide distribution of inlet temperatures related both to temperature difference between air and exhaust and distribution within exhaust potentially allows reaction to be quenched in a low-temperature fraction of flow in spite of adequate local mixing; and finally the restriction of hydrocarbon combustible primarily to a small fraction of entering exhaust volume reduces the probability that a stoichiometrically sufficient amount of air will mix with it.

Quantitative treatment of these phenomena is guided by the classical concepts of chemical reactor design, starting with the elementary design equations for stirred tank and plug flow reactors and extending to constructs for treating locally segregated reactants. While no ready-made method of solution existed which would treat the full gambit of features characterizing this problem, the basic concepts needed had been established. Thus, model building became the task of fitting the concepts into a suitable computational framework. To establish the motivation that guided the development of simulations, key literature concepts will be reviewed.

A. REVIEW ON MIXING IN CHEMICAL REACTOR DESIGN

A frequent problem in reactor design is the computation of conversions for "nonideal" mixing from kinetic data obtained for "ideal" mixing, as for instance in applying the data obtained from the single cylinder reactor system to predicting the performance of the DuPont Model V reactor. If we were only interested in a single device, we could lump all mixing effects with an empirical correlation of "kinetics" and the problem would be at an end. However, to perform a nontrivial service to design it is necessary to start with kinetics which are essentially nonmixing limited and to apply these kinetics in a well motivated manner to a range of mixing conditions. Mixing must therefore be considered both in obtaining kinetic data and in subsequently applying these data to design.

It is useful to reflect on mixing in descriptive terms before we attempt a more precise treatment with the aid of literature design concepts. First, "mixing" involves several distinct, though not mutually exclusive, physical circumstances: mixing is the blending of two or more separate streams; the backmixing of flow within a stirred tank as opposed to "segregation" in a narrow pipe: the exchange of material between separate droplets in a dispersed phase or between separate eddies in the structure of a turbulent flow. In turbulent mixing of miscible fluids having different properties, mixing can be thought of as a continual reduction in the length scale of property variation until the property gradients are eliminated by thermal conduction or molecular diffusion. Mixing must proceed down to this point of intimate molecular interspersal before chemical reaction can occur. However, mixing may be partially restricted on a length scale far larger than this, depending on the pattern of flow. Consideration of a specific length scale is conveniently avoided in most of the literature on reactor design.

The most elementary aspect of mixing in reactors is concerned with pattern of flow on a length scale determined by overall reactor dimensions, which uses as its starting point the difference in performance between ideal plug flow and ideal stirred tank reactors. Design equations for these, which are available in several texts, e.g., Levenspiel (22), indicate lower conversions in a stirred tank for all reaction orders greater than zero but no difference for zero order (neglecting thermal effects). The disadvantage of stirred tank flow is that entering material is immediately dispersed equally throughout the reactor and is therefore subject to early departure; indeed the distribution of residence times, represented by an exponential decay curve, indicates that a larger fraction of material departs in the time interval immediately following entry than in any similar time interval thereafter.

The first step beyond the treatment of the idealized flow extremes is the building of models for intermediate flow patterns. In this area there has been collected a very large body of literature dealing with numerous models and their mathematical descriptions; much of this work has been summarized by

Levenspiel and Bischoff (23) and Levenspiel (22). Three model types serve to categorize this work: dispersion models, recycle models, and stirred tanks in series models.

The axial dispersion model treats axial mixing for flow through an empty tube as a diffusional process, wherein all mixing effects of molecular and turbulent diffusion, and holdback due to velocity profile are lumped together into an apparent diffusivity in a partial differential equation of the standard diffusion type.

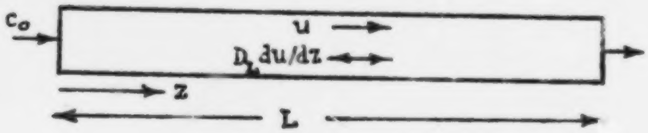

$$\frac{d^2c}{dy^2} - Pe\frac{dc}{dy} + \frac{L^2}{D_L}c = 0; \qquad y = z/L \qquad (I\text{-}1)$$
$$Pe = Lu/D_L$$

$$c_o + = c_o + \frac{1}{Pe}\frac{dc}{dy}\bigg|_{0^+} \qquad (I\text{-}2)$$

$$\frac{dc}{dy}\bigg|_{L^-} = 0 \qquad (I\text{-}3)$$

The axial dispersion model approximates behavior ranging from ideal plug flow to ideal stirred tank as the axial diffusivity D_L ranges from 0 to ∞ for L ≠ 0, as length L ranges from ∞ to 0 for $D_1 \neq 0$, or more generally as the Peclet number, Pe, representing the ratio of bulk transport to dispersion ranges from ∞ to 0. The model has been extended to cover radial dispersion also (14).

The recycle model (17,28) consists of a plug flow reactor with recycle from the exit back to the inlet.

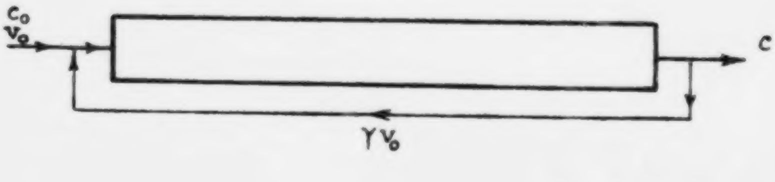

Design equation:

$$\tau = (1 + \gamma)\, c_o \int_{\frac{\gamma}{1+\gamma} X(\tau)}^{X(\tau)} \frac{1}{-r(X)}\, dX \qquad \text{(I-4)}$$

The recycle model represents ideal plug flow for a recycle ratio γ equal to zero and approaches an ideal stirred tank as $\gamma \to \infty$.

The ideal stirred tanks in series model represents degrees of backmix by means of a series of perfectly mixed tanks, wherein feed to each tank is immediately dispersed uniformly throughout that tank. The condition within one tank becomes the inlet condition to the next.

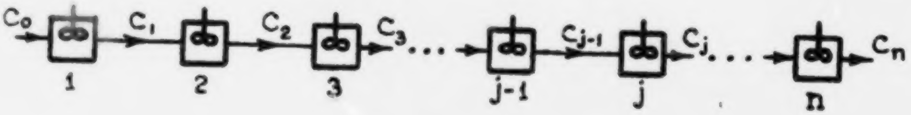

Conversion in a one-dimensional array of n equal size tanks for a one step reaction of order n, $n \neq 0$, or 1, is shown from the material balance on the jth tank to be the solution to the set of equations:

$$\frac{k\, \tau_T\, c_o^{\,n-1}}{n} \left(\frac{c_j}{c_o}\right)^n + \frac{c_j}{c_o} - \frac{c_{j-1}}{c_o} = 0 \qquad \text{(I-5)}$$

$$j = 1, 2, \ldots, n.$$

For a first order reaction, this reduces to an explicit expression:

$$\frac{c_n}{c_o} = \frac{1}{\left(1 + \frac{k \tau_T}{n}\right)^n}\ ; \qquad \text{(I-6)}$$

and for zero-order reaction, the conversion becomes independent of number of tanks n:

$$\frac{c_n}{c_o} = 1 - \frac{k\tau_T}{c_o} \quad ; \quad k\tau_T < c_o \,. \tag{I-7}$$

The model is precisely an ideal stirred tank for $n = 1$ and approaches plug flow as $n \to \infty$. For large n, n has been shown to be directly proportional to the Peclet number Pe in the axial dispersion model (22). At low values of n, the ideal tanks in series models represent degree of backmixing in a very discretized fashion, as they progress from a single CSTR to 2,3,4 ... tanks. This can be offset by using tanks of different sizes; however, this destroys the simplicity and computational convenience of the model. Besides different size tanks, the model has been variously generalized to include nonuniform flow rates between tanks, backflow, and multiple dimensioned arrays of tanks (1,13,30,34,36).

Having established certain models to represent pattern of flow, it is of course permissible to combine them to suit specific purposes. A simple example is a combination of one or more stirred tanks with a plug flow reactor. Combinations of this type will be discussed in the next section.

Further details of theory are presented in the Appendices.

B. THE PATTERN OF FLOW MICROMIXING SIMULATION

A general quasi steady-state (cyclic) simulation program, denoted as "MICROMIX PATTERN OF FLOW" (MMPOF), was written to investigate the coupled effects of mixing with reaction and heat loss by providing for forward movement of a train of cells through a user-specified network of (nonideal) reactor modules. This program and subordinate programs which perform more restricted calculations are described here with reference to the assumptions that guide the calculations. More detailed descriptions of the structure and use of simulations are given in the computer programs that are on file with sponsoring agencies and enclosed on microfiche (see Reference 32).

Solutions for the cyclic stationary state are obtained by performing an unsteady-state approach from a specified initial condition using Monte Carlo type methods.

Flow leaving an engine or an air jet is assumed to be divided into equal sized cells, each containing the same number of moles. Cell input is distributed with respect to time to reflect cyclic variations in flow associated with the firing of individual cylinders and flow variation therein. Mixing between the segregated inlet streams of air and exhaust is accomplished by coalescences and redispersals of pairs of cells. The pattern of flow for cells passing through the reactor system is determined by the design of the module network and the inter-module flow streams. By changing the arrangement and type of modules, a large variety of cell residence time distributions can be simulated. Each module and flow stream arrangement also fixes the availability of cells to collide with other cells present in the reactor system.

Modules within the reactor system can be designated to have either a nonideal stirred-tank or a nonideal plug-flow pattern of cell flow. In a stirred tank module, cells are chosen at random to either coalesce or depart from the module. In a plug flow module, cells proceed through the reactor in the same order in which they entered; the cells are grouped into sets, called "slugs," and only cells within the same slug are allowed to experience coalescence. By considering a large number of slugs, each containing a number of cells, it is possible to approach the condition of mixing and reacting only those materials which enter at the same time. Some longitudinal dispersion is, however, inevitable.

Reactions within individual cells proceed as though each cell were a separate batch reactor. The changing temperature and composition of a cell is updated for reaction and heat loss each time that that cell is chosen to experience coalescence or to leave the reactor module. The updating procedure is based on a one-step integration followed by an optional corrector step at a mean temperature and composition.

Operation of a simulation is conducted for one module at a time, where this is permitted by the assumption that cells are allowed only forward movement to modules occupying a more advanced serial position. All parameters for the module: volume, pressure, heat loss, flow, and mixing are supplied independently for each module. The output from a particular module can be saved in one of several parallel property rosters for as long as it is required as input to a subsequent module in the network. Several output streams can be combined to represent a convergence of internal flow streams; or flow can be divided to proceed from one module to two or more forward positioned modules.

Inlet cell trains can be generated within the simulation, or a roster of cell properties can be read as data. All parameters that are necessary for trial operation of the simulation have been given default values which can be overridden by reading data.

Simulation output consists of a listing of all input parameters, averaged outputs for individual modules, and average final outputs. No variances are computed in "MMPOF," however, if desired, the complete roster of outlet cell properties can be printed binary form for any or all of the reactor modules. Variances can be computed for these dumped properties, and in addition auxiliary programs have been written to compute and graph histograms for all distributed properties. All printing is under control of logical variables within the program, and can be suppressed if desired.

Data for simulations are categorized as follows:

Chemical properties -

- species
- thermodynamic constants
- chemical reactions and stoichiometry
- chemical rate equations
  - activation energies
  - reaction orders

Inlet conditions -

- number of inlet streams
- cyclic flow rates
- cyclic temperatures
- cyclic concentrations

Reactor configuration (macromixing) -

- module network
- module types, nonideal stirred tank or nonideal plug flow
- internal flow fractions
- replicate flow streams and their phasing
- module volumes

Micromixing parameters -

- number of cells per inlet cycle
- number of cells per plug-flow slug
- the "mixing parameter," I_m for each module

Heat losses -

- a constant value of module heat loss
- a heat transfer coefficient for distributing heat loss among cells

Timing parameters -

- length of simulation
- cycles discarded for washout
- cycle timing, engine rpm

Printing control -

- input parameters
- averaged results
- cell properties

All cyclic input flows, temperatures, and compositions are computed in FORTRAN FUNCTION SUBPROGRAMS, named FNF, FNT, and FNX, respectively. These functions are written to allow the user to specify completely arbitrary amplitudes for cyclic property variations during the active period of a particular input stream. Both the amplitude and the active time span are normalized to a range of 0 to 1. Scaling for the normalized amplitude is supplied by input data, and the scaled variations are then added to a data-specified low value for the property concerned to obtain the correct instantaneous value.

1. Organization of Modules and Flows

In Figure 7, the organization of the pattern of flow simulation is illustrated by means of a hypothetical network of modules and internal flow streams. Inlets, outlets, and reactor modules are positioned on a grid given by the intersections of "module streams" and "serial positions." The number of module streams is chosen to equal the largest number of cell property rosters that are to be saved at any one given time. If a property roster is no longer needed either to supply inlet properties to another module or to contribute to the final outputs, another module can be positioned ahead of it on the same stream causing output from the new module to replace the old.

The first and last serial positions in a simulation are reserved for the inlets and outlets, respectively. A simulation may have both multiple inlets and outlets if desired. The intermediate serial positions are occupied by either nonideal stirred tank or plug flow modules, with the possibility of two or more occupying parallel positions at a given serial position.

Internal flow streams must proceed from the last module on a stream to a serial position that is further advanced by one or more positions. Calculations are done in order of serial position, which in the absence of backflow between modules guarantees that calculations can be performed consecutively. The flow network may include both division and confluence of flows. In either case, the cell size in moles can be adjusted by integer cell division. Noninteger divisions are disallowed because of the mixing that is implied by the consolidation of cell fragments.

Flow streams can be replicated to represent parallel streams which contain similar flows except for a shift in phase or position within an engine cycle. In Figure 7, an original flow stream plus three replicates are shown between modules [NS,NP] = [2,2,] and [3,4] to represent flow out of four exhaust ports into a single reactor core. Flow from each port can be phased independently to reflect the timing of cylinder firings. This phasing feature eliminates the need to perform separate simulations on all four ports.

The illustrative simulation network represented in Figure 7 includes the following features:

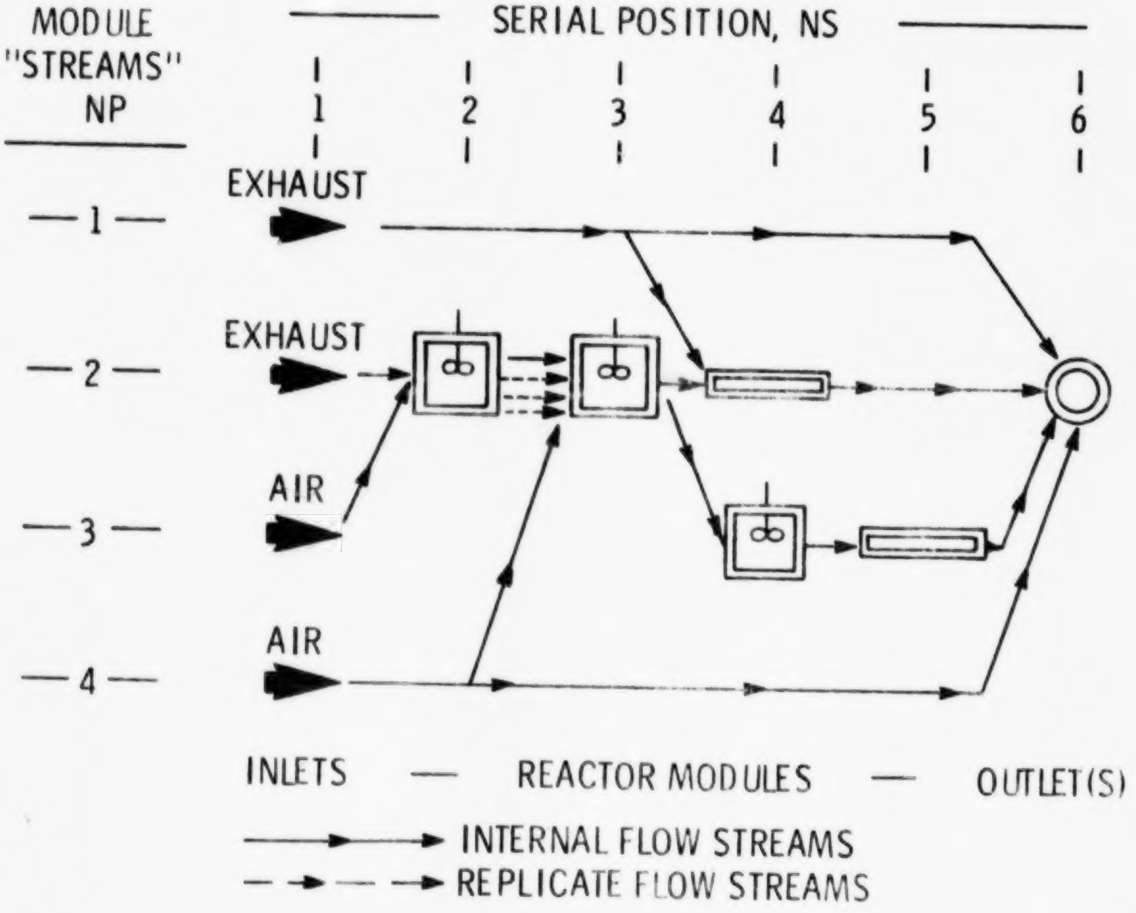
MODULE "STREAMS" NP
SERIAL POSITION, NS
1
2
3
4
5
6
EXHAUST
EXHAUST
AIR
AIR
1
2
3
4
INLETS — REACTOR MODULES — OUTLET(S)
INTERNAL FLOW STREAMS
REPLICATE FLOW STREAMS

Figure 7. Illustrative module network for simulation "MMFOF".

Separate streams of air and exhaust are directed into a stirred tank port, [NS,NP] = [2,2], where they mix and partially react. Outlet properties from the single port simulatuion are replicated three times and phased to represent four ports firing into a stirred tank reactor core [3,2]. An auxilliary flow of air is directed into the core. Output from the core is divided between a plug flow module [4,2] representing an existing annulus, which also receives a bypassed fraction of exhaust, and a sequence of a stirred tank and a plug flow module. A single outlet receives flow from two plug flow annuli and from both bypassed air and exhaust. This particular simulation has never been run and is used only as an illustration.

2. Inputs to Simulation Modules

The first set of inputs in serial position NS = 1 can be specified either by reading rosters of cell properties, which may have been generated by a previous simulation, or by invoking a property generating subprogram, "ENGINE," which supplies cell properties based on the flow and property distributions described previously (Figures 2 through 6). All simulation parameters controlling input are defined in the computer program documentation (32); input parameters can be separately identified from the FORTRAN NAMELIST and DATA declarations, where the latter are used to preassign default values to all input variables.

The division of integrated flow from subprogram "ENGINE" to generate cells containing equal moles and the assignment of corresponding temperatures and mole fractions is shown schematically in Figure 8. The cell roster includes storage for values of inlet time, temperature, mole fractions, and age for one engine cycle comprising four cylinder firings. Compilation of rosters from internal flow streams proceeds similarly. In general, separate rosters are maintained for outputs from several modules, assuming that their values will be needed subsequently; only one inlet roster is needed since module simulations are performed sequentially. Rosters will in general include input or output for several engine cycles to reduce the effect of random error.

Outlet times from one module generally become inlet times for the next, except when they are adjusted for cycles that are discarded to accomplish washout of initial cells in a stirred tank module. Phasing of replicate flows may also change inlet times.

"Age" is the accumulated time spent in as many reactors as a cell has traversed; these are never adjusted. Their values are used to determine residence time distribution, both at the terminal exit and at intermediate points.

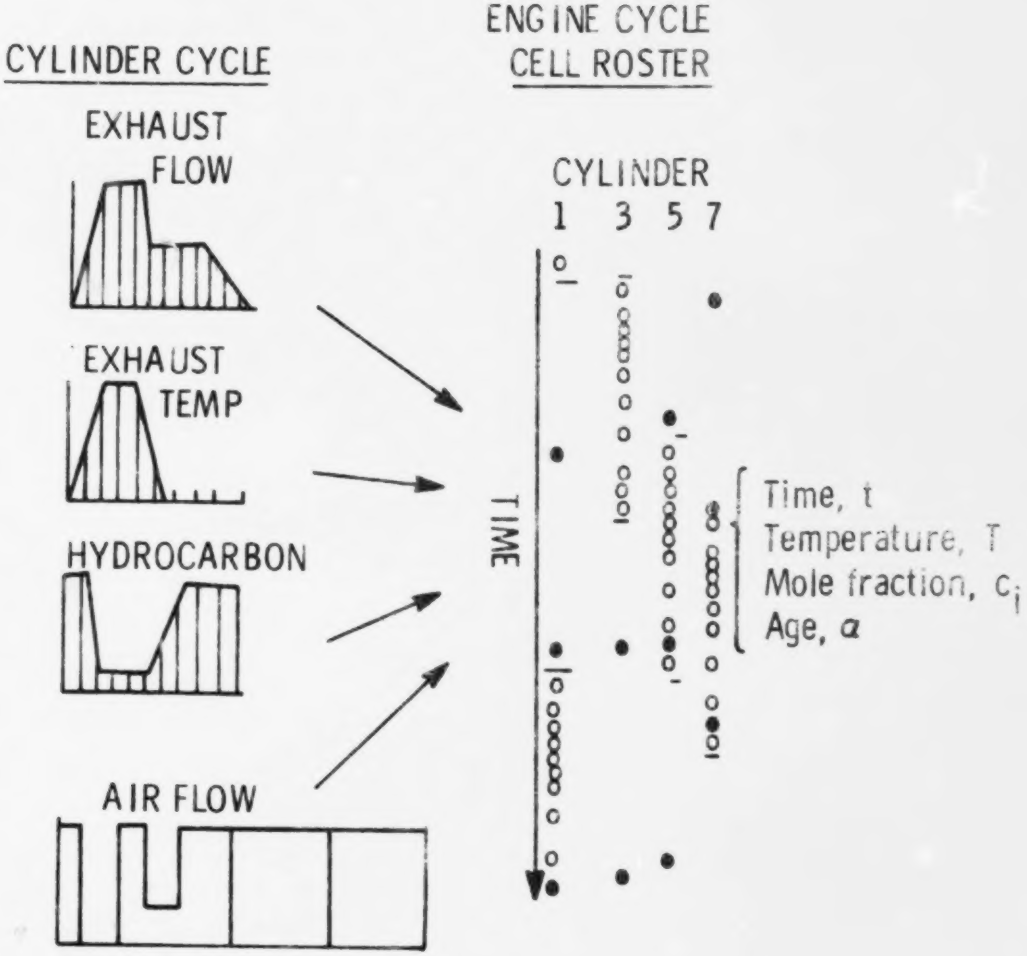
CYLINDER CYCLE
EXHAUST FLOW
EXHAUST TEMP
HYDROCARBON
AIR FLOW
ENGINE CYCLE CELL ROSTER
CYLINDER
1 3 5 7
TIME
Time, t
Temperature, T
Mole fraction, c_i
Age, α

Figure 8. Schematic on the compiling of the inlet cell roster.

5. Flow and Mixing in "POF"

Macromixing in the sense of cell flow pattern is determined entirely by the module network and the internal flow streams.

a. Stirred Tank Modules

Micromixing within a stirred tank module is governed by assumptions stated in Figure 9. Three rosters are required: inlet, reactor, and outlet. The reactor roster is initialized with unreached but mixed feed, averaged over one cycle, with the temperature adjusted by adding T_o^+ to lower or raise the starting temperature for the purpose of studying ignition. Cells are entered sequentially from the input roster and displaced randomly selected cells out of the reactor into the outlet roster. The simulation is first operated for a specified number of cycles without saving output to wash out the initial cells. Total duration of each stirred tank simulation is specified as a maximum number of engine cycles. If operation proceeds past the end of the inlet roster, input is resumed from the start.

Mole compression is neglected in cell calculations causing intermediate mole fractions to be in error by up to approximately 3% of their correct value for normal exhaust concentrations. Mole fractions are corrected to a sum of "1" at the end of the simulation. This error would be more serious in other applications of the simulation if reactants in unequal molar reactions were less dilute. The error does not affect the mass balance for individual species within cells, the low mole fractions times the entering number of moles give the correct specie mole content. However, use of the uncorrected total moles per cell causes both individual cell and aggregate cell volumes to be high, producing small errors in cell population and in specie conversion rates, $\bar{F}_i \cdot V_c$. Error in mole fraction changes relating to reaction rates results only from the contribution of partial pressures appearing in the rate equations, since the contribution of high cell volume is cancelled out when the rate is divided by the uncorrected high mole content. The reason for neglecting mole compression was to reduce the running time of the simulation.

Adjustment of the cell population in a stirred tank takes place at the start of each cycle, to fit the total number of moles in the reactor to the module volume, using the perfect gas law and the average temperature for cells exited during the previous cycle. This allows a change in cell population to correct for the unsteady approach of average cell temperature to the limiting value experienced at stationary state cyclic operation, but it ignores changes in aggregate cell volume due to fluctuations in average temperature within a cycle. For stirred tank simulations performed on an entire reactor volume containing most of one cycle of flow, preliminary work with an ideal stirred tank simulation indicated fluctuations of approximately ±4% in reactor mole contents. When the simulation is used for small volumes such as the exhaust ports, the within cycle temperature fluctuation will be much higher, with

Figure 9. Flow and mixing in non-ideal stirred tank modules within "MICROMIX PATTERN OF FLOW"

STIRRED TANK MODULE

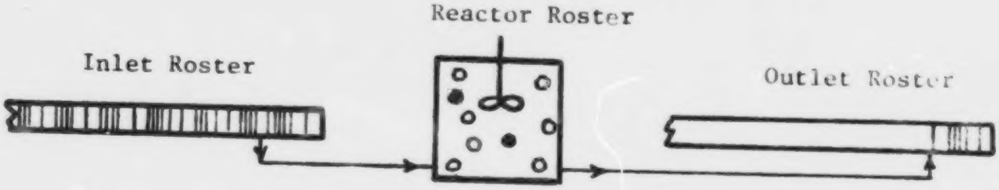

Major Assumptions:

1. Cells contain equal moles.
2. The slight effect of mole compression due to reaction of dilute species is neglected until the end of the simulation, when mole fractions are corrected.
3. Cell population is adjusted once each cycle to compensate for the solution's approach to an average temperature.
4. Coalescences of cells are random independent.
5. The micromixing parameter "I_m", representing coalescences per cell entry, is constant so that coalescence frequency ω_i varies in proportion to cyclic changes in input frequency ω_r.
6. Two cells mix perfectly at coalescence.
7. Redispersal is immediate.
8. Cells departing from the reactor are chosen randomly.
9. Cells between events are treated as homogeneous batch reactors.
10. Heat losses are distributed according to cell temperature.

fluctuation on reactor mole contents being perhaps ±15%. However, this is partially offset by also neglecting fluctuations of approximately ±5% in port pressure, where peak pressure coincides with peak exhaust flow and peak exhaust temperature. Considering the low conversions that are indicated for the ports, there is little practical reason to change the simulation in favor of more frequent updates of cell population; however an option has been developed for checking cell population as often as cells are entered.

b. Plug Flow Modules

For a plug flow module, operation is simplified by the fact that changes in cell properties can be computed in place on the inlet roster. Two indices shown by the vertical arrows in Figure 10 indicate the first and last cells present in the reactor. The cell population is adjusted by controlling exits to fit an average temperature for cells in the reactor at the time of exit of each slug from the reactor. Working with 16 to 44 slugs per cycle, the temperature variation between slug exits was small.

The important features of the plug flow simulation are that cells enter and leave in unchanged order and that coalescences occur only between cells in the same slug. Since slugs need not represent negligible time slices, the size of a slug is a parameter which can be used to introduce more or less axial dispersion in the nominally plug flow reactor.

4. Heat Loss

Heat loss from the reactor is specified both as a total rate of heat loss, Q Btu/hr, and as a heat transfer coefficient HA_c Btu/hr°F. These two parameters are used to distribute heat loss among cells in relation to their temperature as follows:

Assuming that each cell sees a fraction of wall represented by $1/N_c$, where N_c is the number of cells,

$$Q_{cell} = \frac{1}{N_c} HA_c \, (T_{cell} - T_{wall}) \qquad \text{(I-8)}$$

$$Q = HA_c \, (T_{avg} - T_{wall}) \qquad \text{(I-9)}$$

$$\text{or } T_{wall} = T_{avg} - \frac{Q}{HA_c} \qquad \text{(I-10)}$$

$$Q_{cell} = \frac{Q}{N_c} + \frac{HA_c}{N_c}(T_{cell} - T_{avg}) \qquad \text{(I-11)}$$

Figure 10. Flow and mixing in non-ideal plug flow modules within "MICROMIX PATTERN OF FLOW"

PLUG FLOW MODULE

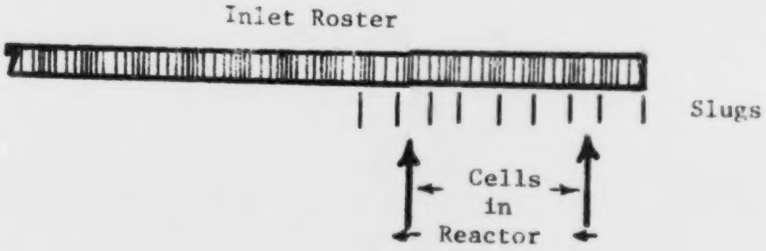

Major assumptions:

1. Cells contain equal moles.
2. The slight effect of mole compression due to reaction of dilute species is neglected until the end of the simulation, when mole fractions are corrected.
3. Cell population in the reactor is adjusted after each slug exit.
4. Coalescences occur only within slugs.
5. The first cell in a coalescence is chosen randomly from among all cells in the reactor. The second is chosen randomly from the same slug as the first.
6. The micromixing parameter, I_m, is constant.
7. Two cells mix perfectly at coalescence.
8. Redispersal is immediate.
9. Cells leave in the order they entered.
10. Cells between events are treated as homogeneous batch reactors.
11. Heat losses are distributed according to cell temperature.

5. Kinetics, Material and Energy Balances

Cell properties, temperature and mole fractions, are updated for batch reaction before each coalescence or departure from the reactor. All computations concerned with updating (reaction rates, material and energy balances) are assigned to a FORTRAN SUBROUTINE, "UPDATE."

The method of updating computes a rate of cell heat loss and rates of reaction for "q" combustible species at the beginning of the update, and performs one-step integrations of temperature and reactant mole fractions based on these initial rates. An option is provided for a corrector step based on midvalue mole fractions and temperature.

Reaction stoichiometry for reaction "k" and species "i," given by $\nu_{i,k}$, is written for one mole of the combustible specie. A total of "m" species are assumed to be ordered with "q" combustibles appearing first, followed by oxygen, then products, and finally inerts:

e.g., if CO is the first combustible:

$$\nu_{1,1}\,\mathrm{CO} + \nu_{q+1,k}\,\mathrm{O_2} \rightarrow \nu_{q+2,1}\,\mathrm{CO_2} \tag{I-12}$$

with

$$\nu_{1,1} = -1,\ \nu_{q+1,1} = -1/2,\ \nu_{q+2,1} = 1$$

Reaction rates are expressed in Arrhenius form:

$$r_k = A_k e^{-E_k/RT} \prod_{i=1}^{m} (PC_{j,i})^{\eta_{i,k}} \tag{I-13}$$

A complication in update calculations is the necessity for checking for specie disappearance during the update period between the time of the last update t_1 and current simulation time t. If a combustible is depleted, as shown in Figure 11, its mole fraction becomes zero and its contributions to the rate of oxygen depletion and to the energy balance are ended. Oxygen mole fraction $C_{j,q+1}$ must be updated in a piecewise fashion where combustible depletions occur. If oxygen itself is depleted, all reaction ceases and only heat loss is continued to time t.

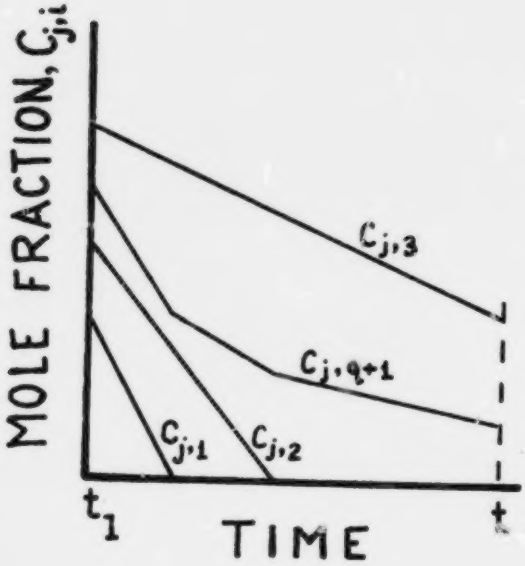

Figure 11. Mole fraction integration showing disappearance of species.

Material and energy balance equations for linear updating of mole fractions $C_{j,i}$ and temperature T_j are as follows:

$$C_{j,i}(t) = C_{j,i}(t_1) + \frac{\overline{r}_i(t^*) \cdot \Delta t^* \cdot V_c(t^*)}{Mc}, \quad i = 1,\ldots,q+1; \tag{I-14}$$

$\overline{r}_{q+1}$(oxygen) is corrected whenever a combustible species disappears.

$$r_i(t^*) = \sum_{k=1}^{q} \nu_{i,k}\, r_k(t^*) \qquad i = 1,2,\ldots,q+1 \tag{I-15}$$

$$\nu_{i,i} = 1; \qquad \nu_{i,k} = 0; \qquad i = 1,\ldots,q; \qquad i \neq k$$

$$V_c(t^*) = M_c RT(t^*)/P \tag{I-16}$$

$$\Delta t_i^* = \begin{Bmatrix} \text{disappearance time } \Delta t_{di}\text{, if species disappears} \\ t-t_1 \text{ if species does not disappear} \end{Bmatrix}$$

$$T_j(t) = T_j(t_1) + \frac{\left\{ \sum_{k=1}^{q} r_k(t^*)\, V_c(t^*)\, \Delta H_{r_k}(t_1) - Q_c \right\} \left\{ t-t_1 \right\}}{N_c \overline{C}_p(t_1)} \qquad \text{(I-17)}$$

$$\Delta H_{r_k} = H_k + \sum_{i=q+1}^{m} \nu_{i,k} H_i \qquad \text{(I-18)}$$

$$C_{p_i}(T) = a_i + b_i T + c_i T^2 + \frac{d_i}{T^2} \qquad \text{(I-19)}$$

$$H_i = \int_{298}^{T} C_{p_i}(T)\, dT \qquad \text{(I-20)}$$

$t^* = t_1$ for the predictor step
t^* = times corresponding to midvalue properties for the corrector step

For products, $C_{j,i}$ is determined from stoichiometry

$$C_{j,k}(t) = C_{j,i}(t_1) + \nu_{i,k}(t_1)\,[C_{j,k}(t_1) - C_{j,k}(t)] \qquad \text{(I-21)}$$

It should be understood that where rates $\overline{r}_i$, cell volume V_c, and heats of reaction ΔH_{r_k} are shown as functions of time t^*, they are in fact functions of mole fractions $C_{j,i}(t^*)$ and/or temperature $T_m(t^*)$.

The advisability of using a corrector step depends on temperature, residence time, and mixing intensity as they affect the amount of reaction occurring between t_1 and t. If the update periods are sufficiently short to involve only a slight amount of reaction, the midpoint correction is not needed. Likewise, if reactions are so rapid as to be nearly instantaneous, correction is unnecessary. However, all current calculations using "POF" did use the correction.

C. SIMPLIFIED MIXING SIMULATIONS

A number of simplified computer programs were developed to perform particular simulations more efficiently on the computer than they could be performed using "MMPOF." In order of decreasing complexity, these are:

1. "MICROMIX I" - stirred tank RTD only;
2. "MICROMIX II" - stirred tank RTD only.
3. "MICROMIX PF" - plug flow RTD only;
4. "EXHAUST" - ideal stirred tank at $I_m = \infty$ but with provision for cyclic input.
5. "MIXONLY" - cell mixing with instantaneous reaction for single stirred tank or plug flow modules;
6. "MIXONLY POF" - cell mixing with instantaneous reaction for series combinations of stirred tanks and plug flow modules.

All of the foregoing except "EXHAUST" are cell coalescence models which are essentially similar to "MMPOF" in those calculations which they are designed to perform. Descriptions which follow will be limited to the distinguishing features.

1. "MICROMIX I"

"MICROMIX I" computes a Monte Carlo solution for the stirred tank cell mixing model only, based on assumptions that differ from provisions found in "MMPOF" in the following respects:

(1) Cell population is constant.

(2) The cell inlet frequency ω_r is assumed to be constant. Cell properties are however allowed to fluctuate cyclically.

(3) Heat losses from cells are computed by wall collisions, assuming that a cell assumes the wall temperature at the time of collision. The wall collision frequency is computed from a heat transfer coefficient HA_c.

$$Q = HA_c(T_{avg} - T_{wall}) = \sum_{i=1}^{\omega_w} M_c C_P (T_{cell_i} - T_{wall}) \qquad (I-22)$$

If M_c and C_p are constant,

$$\omega_w = HA_c/M_cC_P. \qquad (I-23)$$

(4) Updating of cell temperature and composition is performed by the modified Euler method (2 function evaluations on the first step and 1 evaluation per step thereafter). Step size is computed to limit conversions for all species to less than a specified fraction during one time step.

(5) Reaction stoichiometry is unrestricted and the kth reaction may include any of "m" species as reactants or products:

$$\sum_{i=1}^{m} \nu_{i,k} \ A_i = 0 \qquad (I-24)$$

ν is positive for products and negative for reactants.

(6) Variances are computed for distributed properties.

2. "MICROMIX II"

"MICROMIX II" is similar to "MICROMIX I" except for the following:

(1) Heat loss from individual cells is a constant; i.e., it is not distributed in relation to temperature.

(2) Stoichiometry is restricted to oxidations written for one mole of a combustible, as in "MICROMIX POF."

(3) Kinetic integration proceeds in a single step with a corrector step option, as in "MICROMIX POF."

3. "MICROMIX PF"

"MICROMIX PF" computes a Monte Carlo solution for the plug flow cell model only, based on assumptions that differ from "MMPOF" as follows:

(1) A slug of cells enters the reactor at the time it is filled with a specified number of cells from the integration of inlet stream. All cells in the slug leave together at the time that the volume entering behind it equals the volume of the reactor.

(2) Coalescence frequency is specified as $\omega_i/2$.

(3) $I_m = \omega_i/2\omega_r$ is calculated when a slug leaves the reactor. If desired, the time of flight for the slug can be continued to satisfy a specified value of I_m.

(4) Heat losses are treated as cell wall collisions (see MICROMIX I), with provision for making the local wall temperature and the convective coefficient functions of position in the reactor.

(5) A frequency can be specified for updating properties for all cells in the reactor and computing slug average properties.

(6) The simulation is designed to perform an integer number of coalescences between the times that all cells are updated. Furthermore, integration of inlet flows proceeds on a time step which is an integer fraction of coalescence period or vise versa.

4. "EXHAUST"

"EXHAUST" is an ideal stirred tank simulation ($I_m = \infty$) which utilizes the cyclic inlet flows and properties that have been described for "MMPOF." No cells are involved, since input is assumed to be perfectly mixed with reactor contents at the time of entry.

"EXHAUST" computes an unsteady state approach to repeated cyclic operation by integrating rates of change in enthalpy and moles of individual species within the reactor obtained from material and energy balances. Integration is by means of a fourth order Runge-Kutta method. The integration of change in enthalpy leaves temperature to be computed by a half-interval root finding method.

Flow out of the reactor is computed from gage pressure in the reactor; absolute pressure in the reactor is computed by the perfect gas law.

5. "MIXONLY"

The most highly simplified version of the cell coalescence models considers only instantaneous reactions for two steady reactant streams entering a single stirred tank or plug flow reactor. Chemical kinetics are not considered. This program allows two reactants to enter the reactor in a train of cells, some of which contain reactant "A," and the remainder containing reactant "B." The average entering concentrations, stoichiometry, and proportion of the entering cells containing "A" are variable. The reactor contains a preset number of cells, and coalescences occur at a specified frequency of I_m per cell input.

During coalescence, the limiting reactant is annihilated (instantaneous reaction), and the cells redisperse containing products and one excess reactant (equal in each cell). Mixing only occurs if both reactants are not present.

The variables of interest are as follows:

$$A + \nu_B B \rightarrow \nu_C C$$

(1) Stoichiometric coefficients for the reactions, ν_B, ν_C.

(2) The concentrations of reactants in input cells (C_{AO}, C_{BO}).

(3) The feed stoichiometric ratio of A:B, "SR."

(4) The dilution ratio, "DR" = no. of "B" cells/no. of "A" cells entering.

(5) Number of cells in the reactor (N_c).

(6) Number of coalescences per input cell, I_m.

(7) Average fractions of A and B converted (during several cycles of feed).

Mean residence time is not a parameter of MIXONLY because of the assumption that reaction occurs instantaneously upon mixing.

For the plug flow option in "MIXONLY," conversion is determined by initializing the contents of a batch of cells with a desired segregated feed and following the average conversion as a function of cumulative coalescences for the batch. Conversions are averaged over several batches for the purpose of eliminating random error.

a. "MIXONLY" Reproducibility and Cell-Population Bias

For N_c = 100 cells in a stirred tank reactor, "MIXONLY" checks the results of Spielman and Levenspiel (33) for N_c = 500 as shown in Figure 12.

A check on the reproducibility of "MIXONLY" stirred tank simulations yielded the σ limits for 1τ and 9τ (N_c = 110 cells) shown by the shaded areas in Figures 13 and 14. For given values of dilution ratio DR and stoichiometric ratio SR, reproducibility is governed by the number of cells passing through the reactor rather than by cell population. However, a bias is introduced as the cell population is reduced. With regard to reproducibility alone, the 9τ limits which decline from approximately .02 to less than .01 as conversions increase from .10 to .90 are representative of subsequent MIXONLY simulations that are reported.

To obtain an estimate of low-population bias, simulations for a stirred tank were run at N_c = 2, 5, 10, and, 110 cells in the reactor. The reference case of 110 cells was run for 25τ; tests at lower cell counts were run for 9τ.

The results of Figure 13 for an air dilution ratio DR of 0.1 and a stoichiometric ratio SR of 1.5 indicates that the biases introduced by 10 and even 5 cell populations are less than the one σ statistical uncertainty for one mean residence time at N_c = 110 and for mixing parameter I_m out to 5. Beyond I_m = 5, 5 cells produce conversions which are decidedly low.

In Figure 14, results for DR = 0.5 and SR = 1.5 indicate greater bias for both the 5 and 10 cell populations; however, even here N_c = 10 results fall close to the one σ limits for 1τ at N_c = 111 cells.

In Figures 13 and 14, the extreme condition of having only 2 cells in a reactor is presented to help visualize the sources of error due to a low cell population. First, any increase in I_m above the value of 1 has no effect on conversion since coalescing the same two cells more than one time produces no additional mixing. The large number of unproductive coalescences that are thus produced tends to limit conversions to values lower than would be experienced if a large number of cells were present. Conversely, at lower levels of mixing and conversion, products are lost in greater proportion than their mole fraction would warrant. Their replacement by fresh reactant tends to make coalescences erroneously productive. As cell population increases above 2, these effects are reduced but are not entirely eliminated for any finite population.

Comparison of conversions in Figures 13 and 14 at N_c = 5 illustrates the influence that dilution ratio, DR, has on population bias. Where exhaust cells predominate by 10 to 1 (DR = 0.1), the tendency toward unproductive coalescences between exhaust and exhaust controls and conversions are low out to I_m = 10. However at DR = .5, coalescences are more effective than they should be due to excess replenishment of reactant.

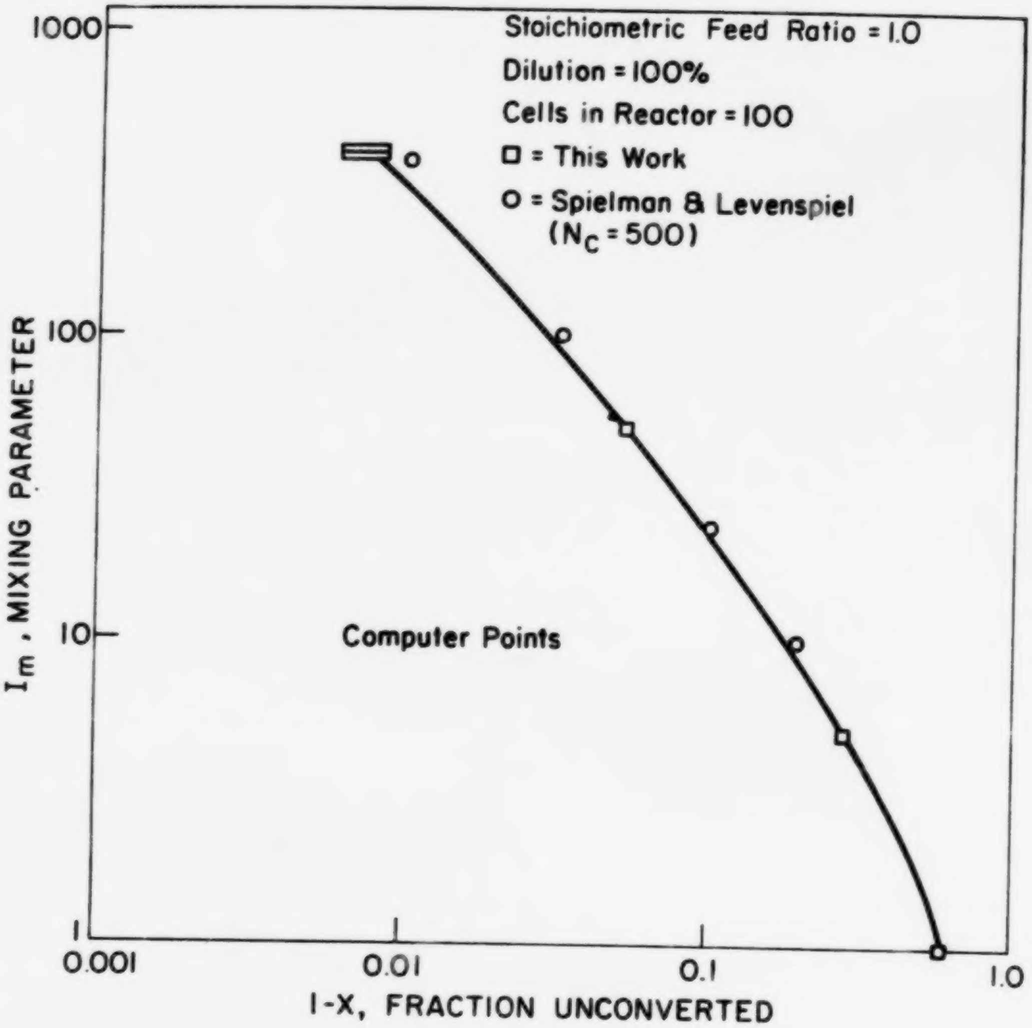

Figure 12. Mixing with instantaneous reaction, A+B → 2C. Check with Spielman and Levenspiel (33).

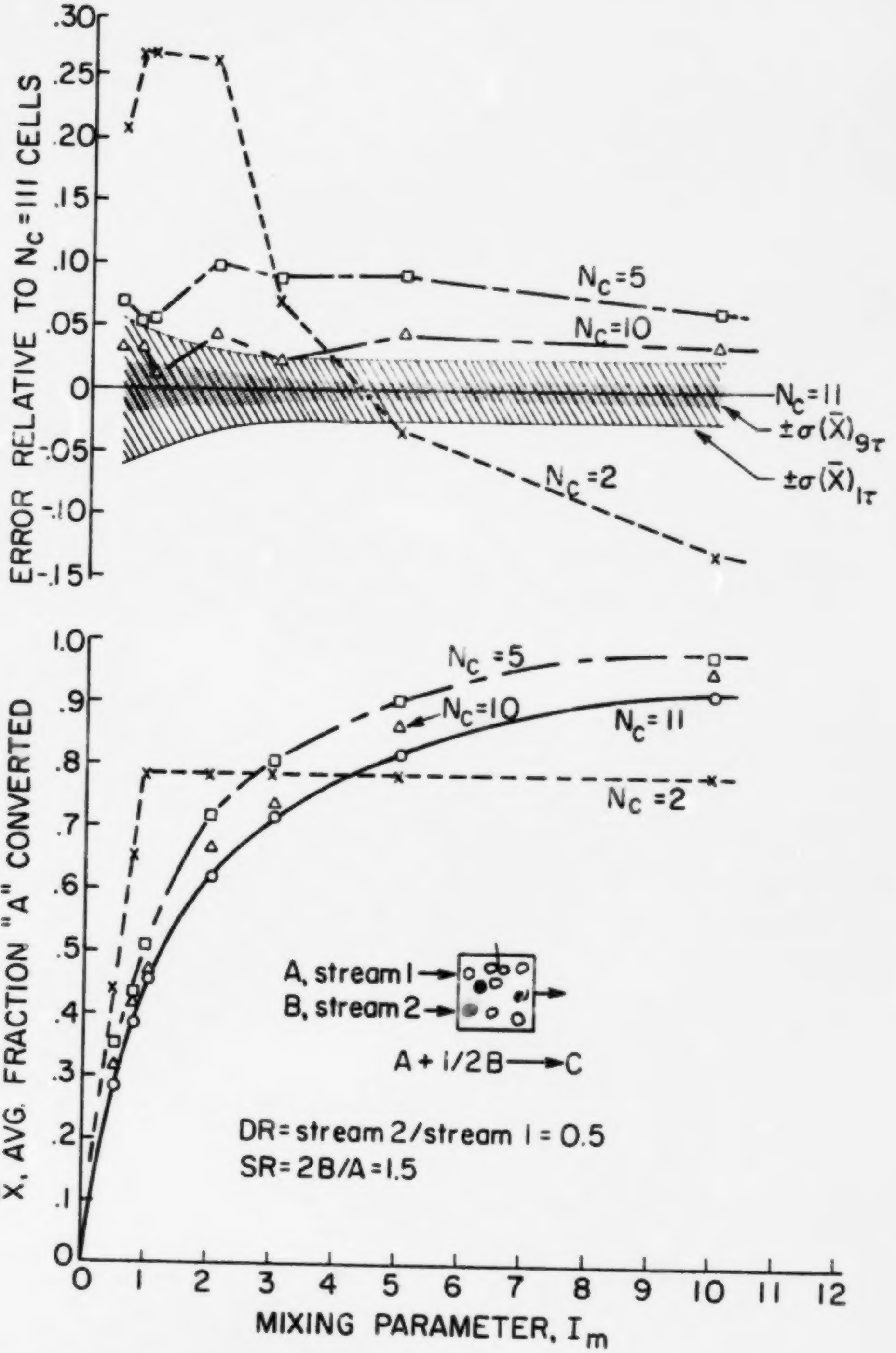

Figure 13. The effect of a small number of cells in the reactor, N_c, on conversion for a stirred-tank simulation of mixing with instantaneous reaction, A + 1/2 B → C. Dilution ratio, DR = 0.5; stoichiometric ratio, SR = 1.5.

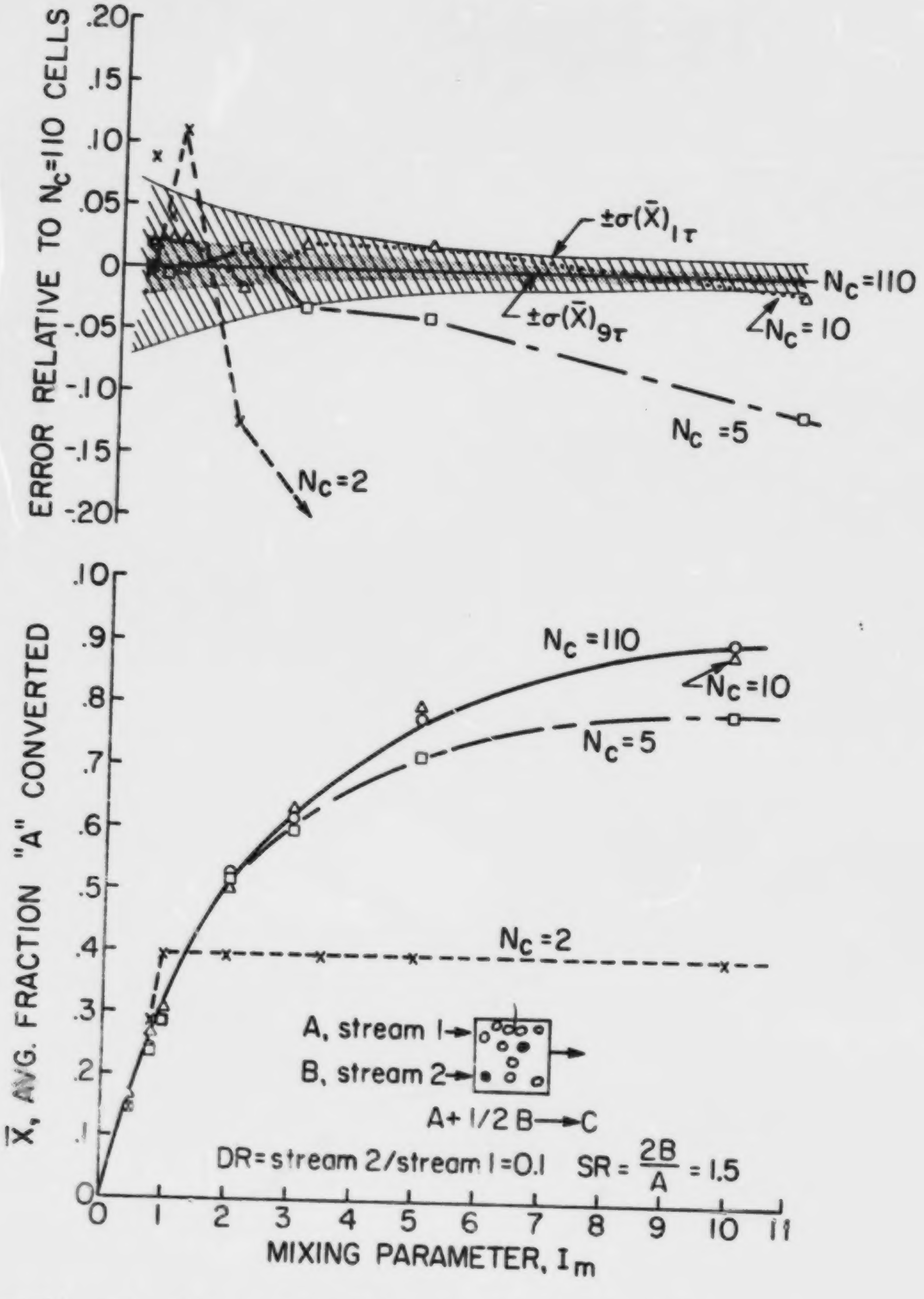

Figure 14. The effect of a small number of cells in the reactor, N_c, on the conversion for a stirred-tank simulation of mixing with instantaneous reaction, A + 1/2 B → C. Dilution ratio, DR = 0.1; stoichiometric ratio, SR = 1.5.

6. "MIXONLY POF"

The "MIXONLY POF" simulation extends calculations for cell-wise mixing with instant reaction to series combinations of stirred tanks and/or plug flow reactors. No parallel combinations are allowed. As before, calculations are for two steady reactant streams containing separate reactants.

An optional calculation of "MIXONLY POF" determines the internal distributions of both the cell ages and the Danckwerts' (11) point ages for cell-wise mixed stirred tanks in series. Cell ages, which are determined by accumulating the time spent in all tanks to any given point without averaging at times of coalescence, have the same distribution as molecular ages and can be used for estimating the molecular age distribution, $\Phi(\alpha)$. If accumulated ages are averaged at time of coalescences, the values obtained are the average ages of material within cells, which from Danckwerts' (11) definition are point ages, α_p. Distributions within any tank can be obtained at the exit, since the exiting cells are a random sampling of the tank contents. The distribution over the system is obtained by combining separate distributions for all tanks, System variances are computed, so that Danckwerts' "J" = $\mathrm{var}(\alpha_p)/\mathrm{var}(\alpha)$ can be evaluated for various numbers of tanks, n, and values of mixing parameter, I_m.

II. General Parameter Evaluation

A. SIMULATIONS RUN ON MIXING WITH INSTANTANEOUS REACTION

The sensitivities of the "MIXONLY" simulations to the parameter for mixing, I_m, for stoichiometry, SR, and for stream dilution, DR, were mapped over ranges to be employed later for mixing coupled with kinetics using "MICROMIX II." The base case is SR = 1.5, DR = .25. Conversions of "A" apply to CO in general, but could apply to HC or H_2 as well.

1. Stirred Tank Simulations

The effect of increasing the coalescence parameter, I_m, in a stirred tank simulation (Figures 15 and 16) is first to reduce the fraction of "A" unconverted sharply after which further decline proceeds more gradually so that curves (stoichiometric ration, SR, being greater than 1) become asymptotic to zero unreacted only as $I_m \to \infty$. To achieve 99% conversion requires $I_m \simeq 55$ for the base case.

Sensitivity to stoichiometric ratio "SR" and dilution ratio "DR" (Figures 17 and 18) is a lower stoichiometric ratio and dilution ratio (SR < 1.5 and DR < .25), but much less change results at higher values. The region of high sensitivity thus corresponds to the customary operating conditions for exhaust reactors; hence these two parameters must be considered important. Their importance is reduced as I_m becomes large, and would disappear as $I_m \to \infty$, except for values of SR less than 1.

2. Plug Flow Simulations

For plug flow (Figures 19, 20, and 21), the fraction of "A" unconverted drops more sharply with increases in I_m due to the elimination of the early cell departures which can occur in a stirred tank. At the base case (DR = .25, SR = 1.5), conversion goes to completion between $I_m = 5$ and 6 for N_c = 100.

To obtain an estimate of repeatability for the plug-flow MIXONLY simulation, two series of five 100-cell batches were run (Figure 19). The vertical lines at each point represent the maximum spread in conversion for all 10 batches. The difference between averages for the two five-batch series was approximately .01 fraction conversion.

Statistical variance (Figure 19) in the concentration of the limiting reactant "A" during plug flow mixing first increases due to reaction and then

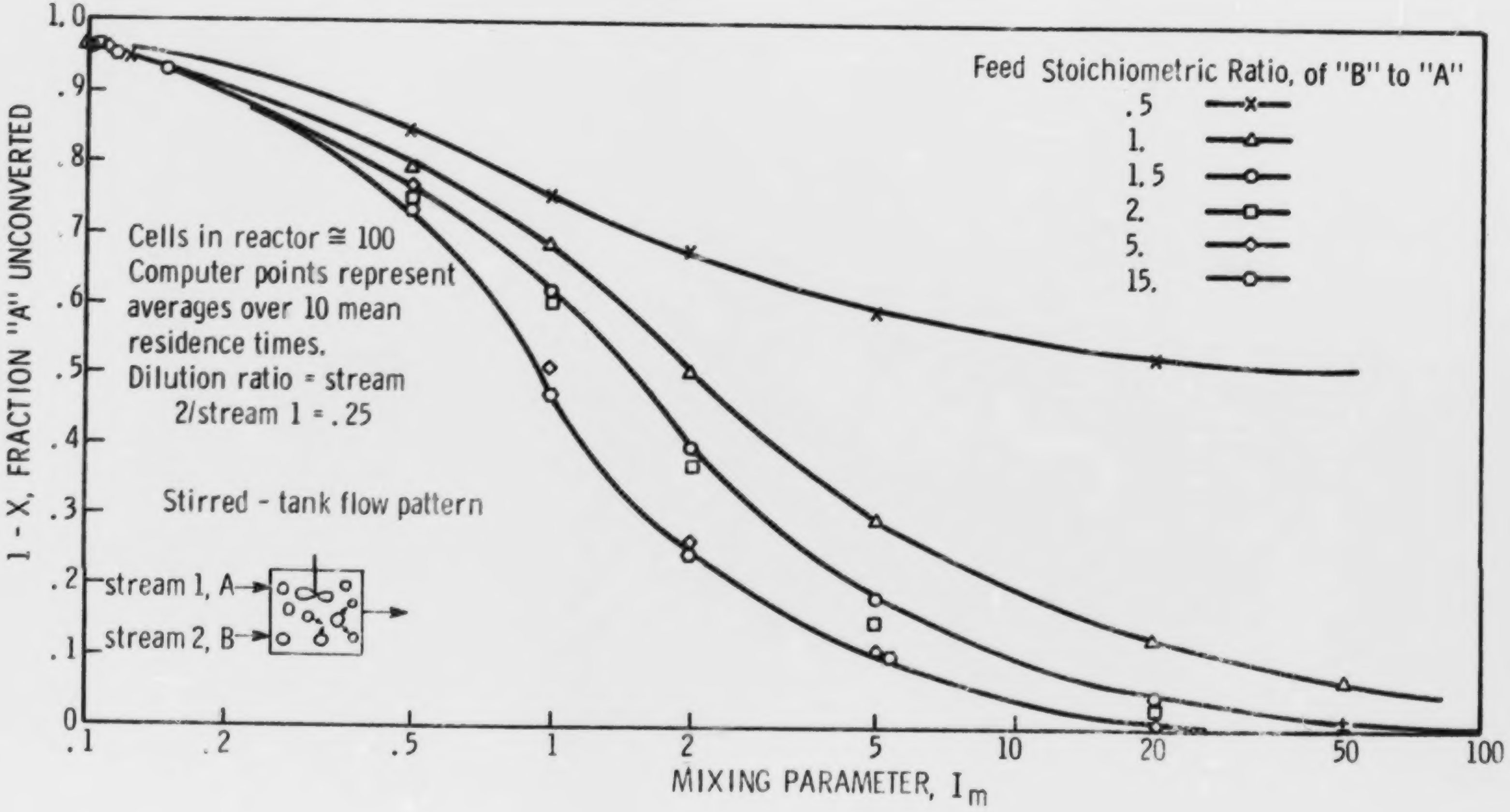

Figure 15. Stirred-tank mixing with instantaneous reaction, A + 1/2 B → C. All "A" enters in stream 1 and all "B" enters in stream 2. Various curves represent different values of the feed stoichiometric ratio, SR.

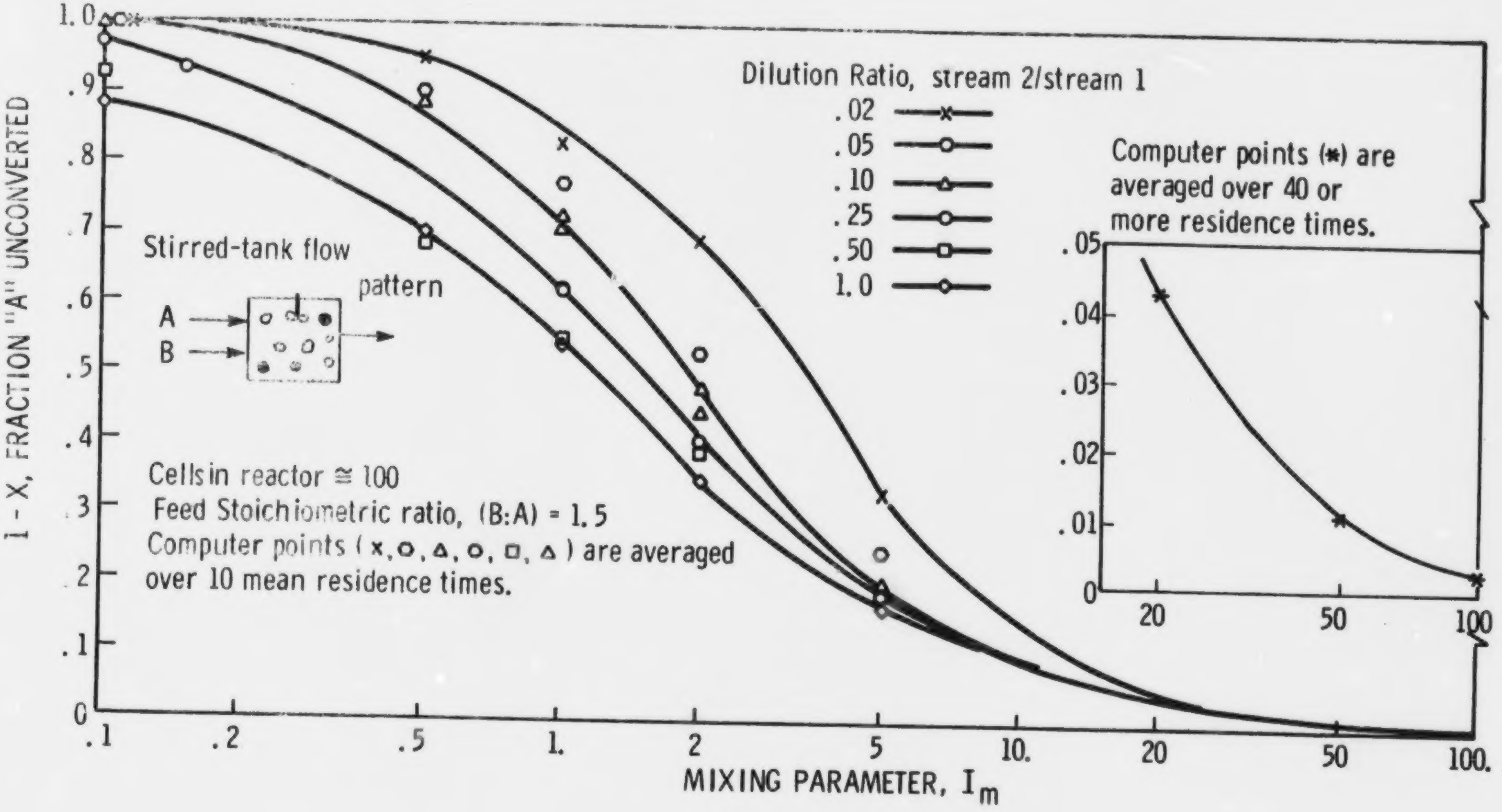

Figure 16. Stirred-tank mixing with instantaneous reaction, A + 1/2 B → C. All "A" enters in stream 1 and all "B" enters in stream 2. Various curves represent different values of the dilution ratio parameter, DR.

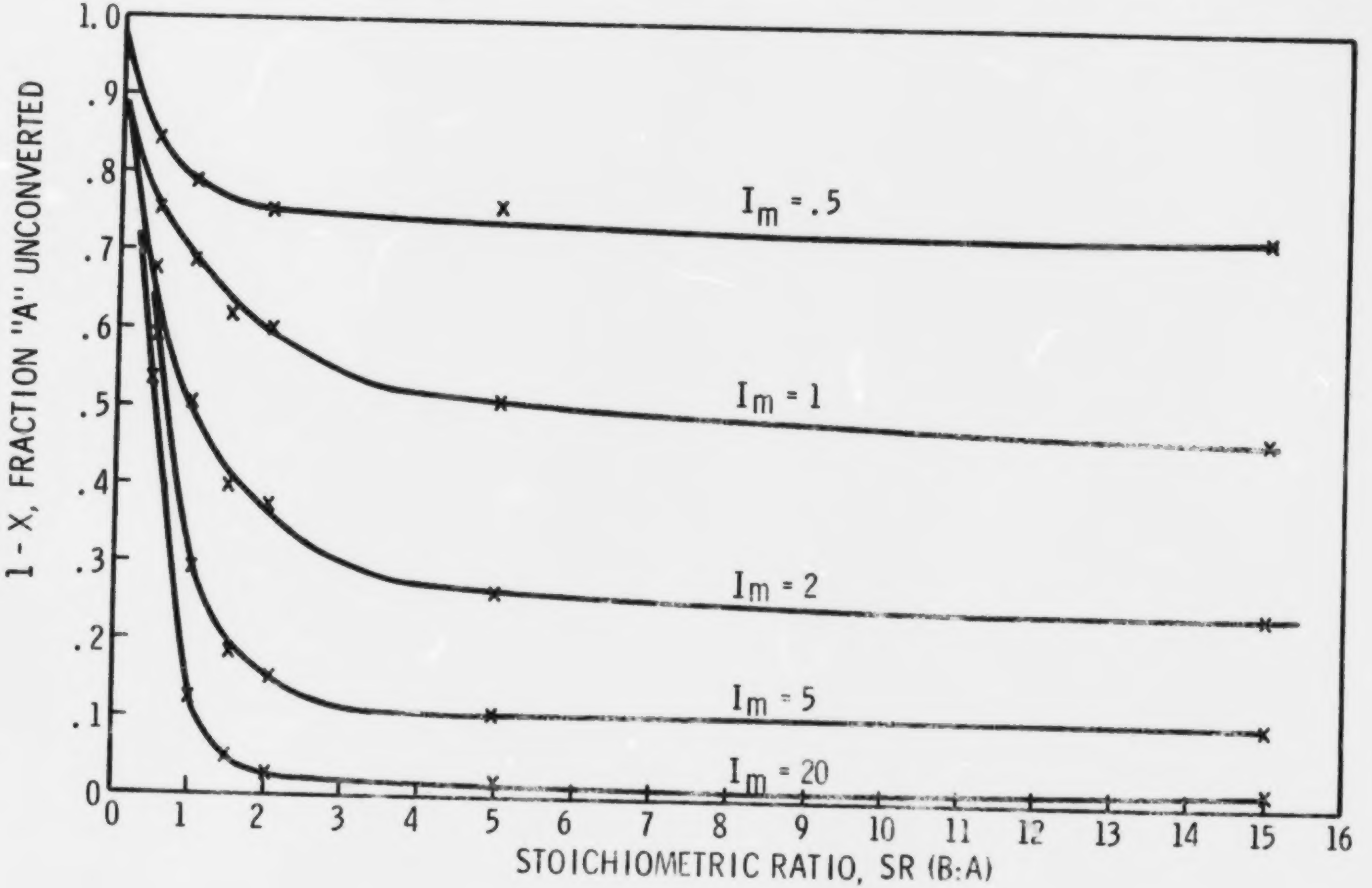

Figure 17. Effect of feed stoichiometric ratio, SR, on stirred-tank cell mixing with instantaneous reaction, A + 1/2 B → C. All "A" enters in stream 1 and all "B" enters in stream 2.

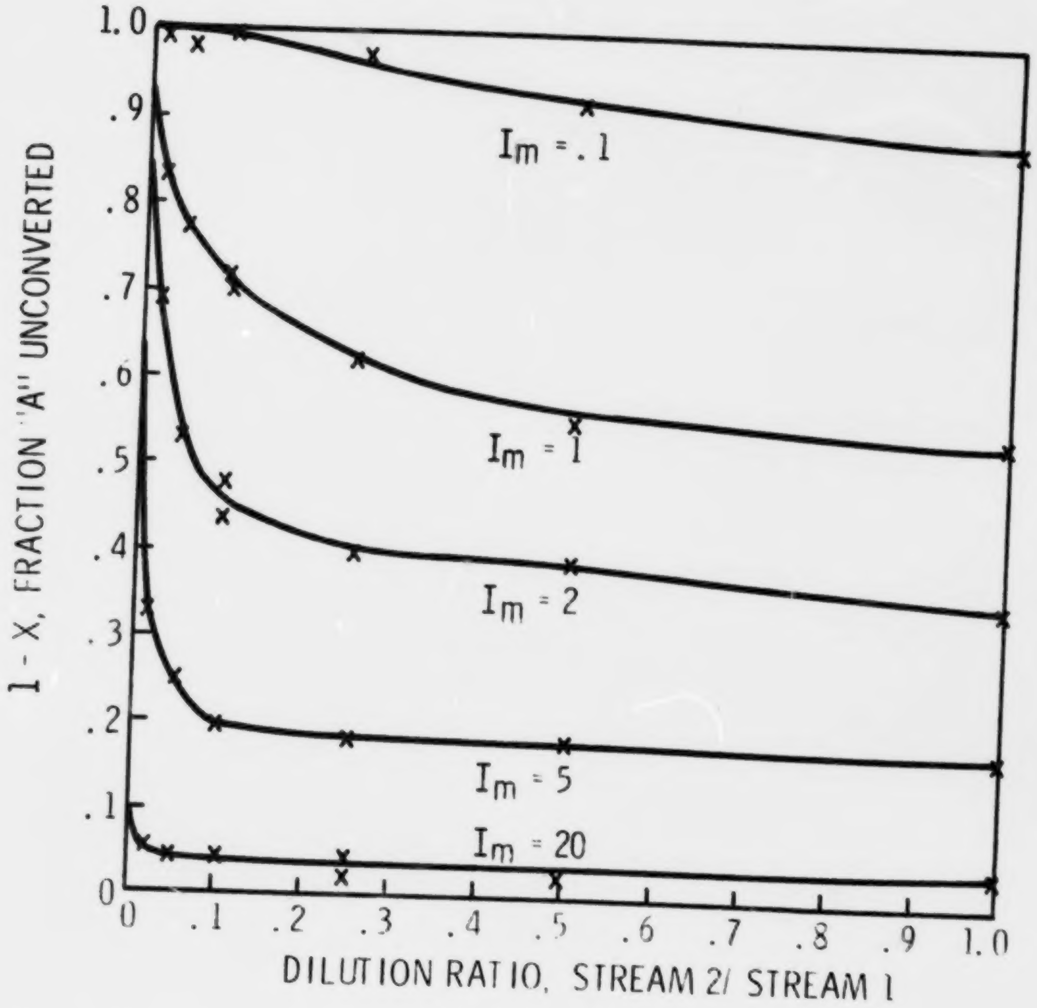

Figure 18. Effect of dilution ratio (stream 2/stream1) on stirred-tank cell mixing with instantaneous reaction, A + 1/2 B → C. All "A" enters in stream 1 and all "B" enters in stream 2.

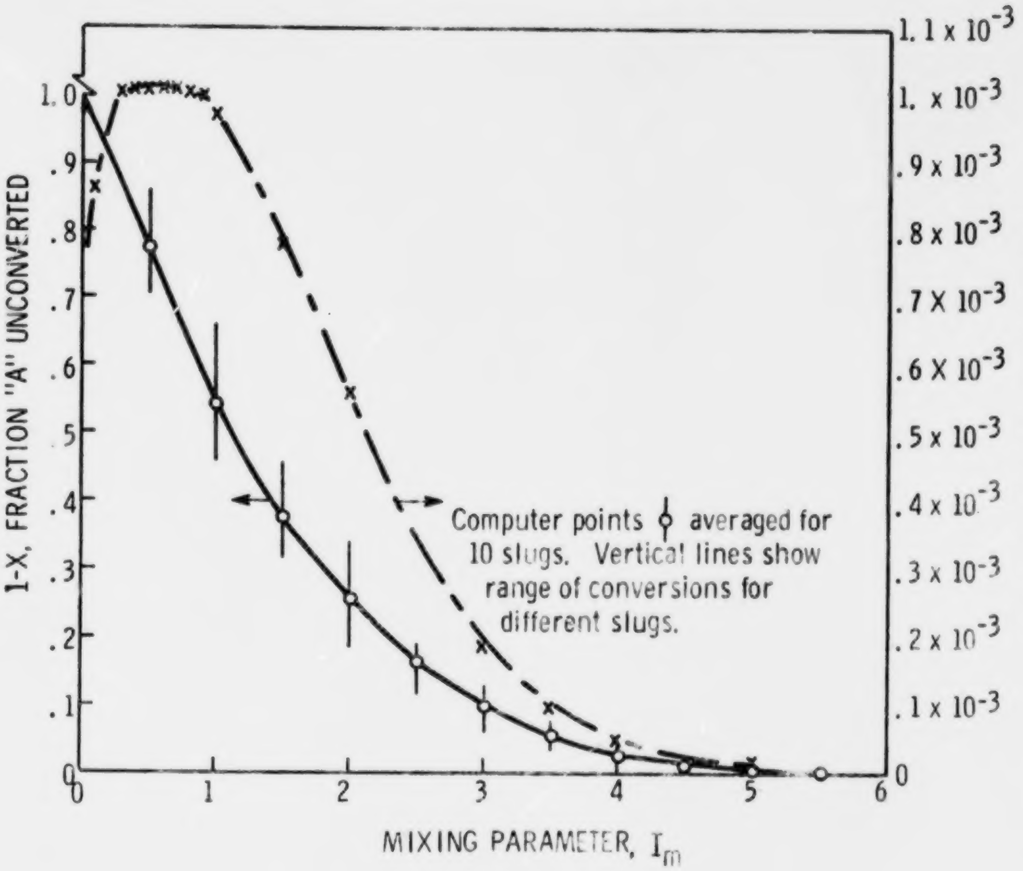

Figure 19. Plug-flow cell mixing with instantaneous reaction, A + 1/2 B → C. All "A" enters in stream 1 and all "B" enters in stream 2. Feed stoichiometric ratio SR = 1.5; dilution ratio, DR = .25. Number of cells per slug, N_{cs} = 100. C_A in stream 1 = .07; C_B in stream 2 = .21.

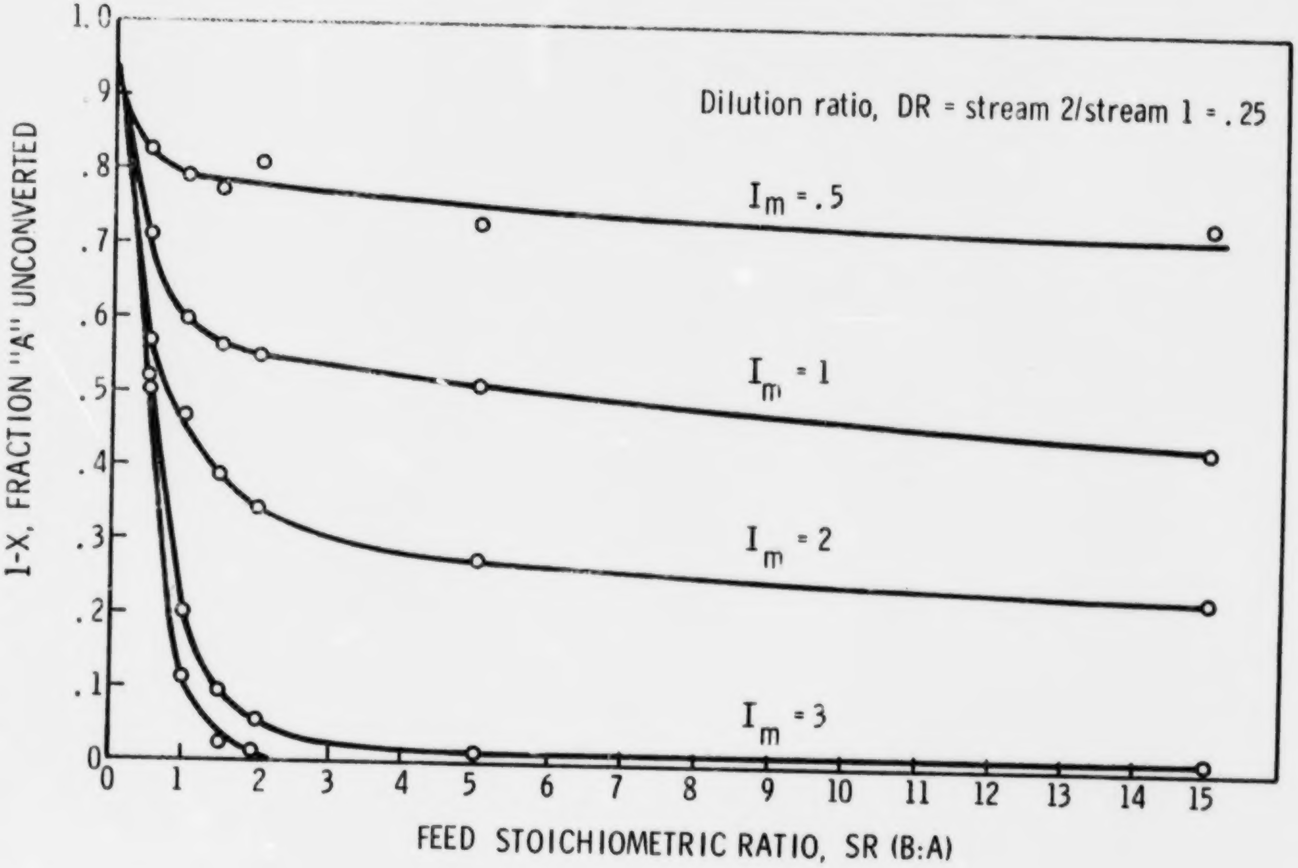

Figure 20. Effect of feed stoichiometric ratio on plug flow cell mixing with instantaneous reaction, A + 1/2 B → C. All "A" enters in stream 1 and all "B" enters in stream 2.

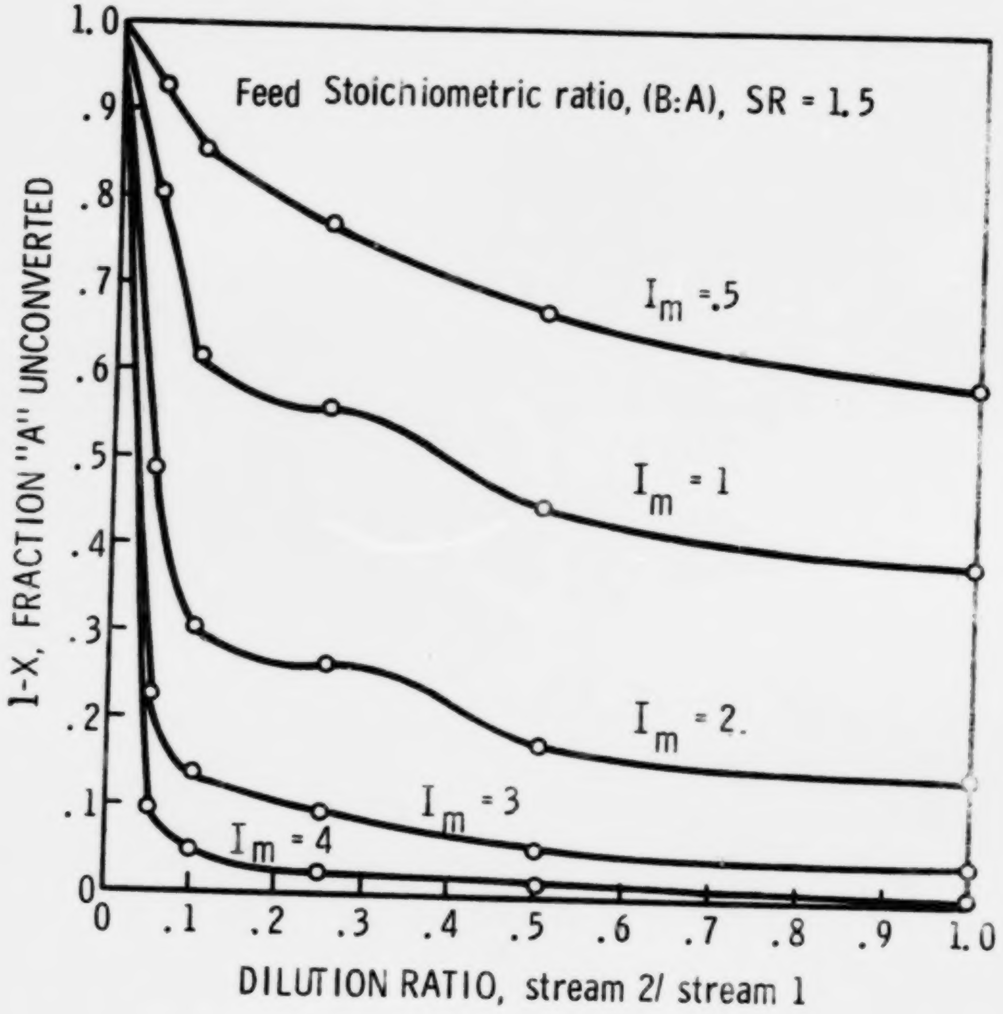

Figure 21. Effect of dilution ratio, DR, on plug-flow mixing with instantaneous reaction, A + 1/2 B → C. All "A" enters in stream 1 and all "B" enters in stream 2.

decays as mixing removes variance faster than it is produced by reaction. As has been shown, variance in batch mixing without reaction decays exponentially with time, or with cumulative coalescences in the case of the "MIXONLY" model.

3. Tanks in Series Simulations

The effects of dilution ratio "DR" and stoichiometric ratio "SR" for plug flow mixing, (Figures 20 and 21) once more depend on the value of the mixing parameters; and, values of either parameter less than the base values (DR = .25, SR = 1.5) again represent the region of high sensitivity.

In order to bridge the difference in response to I_m indicated for stirred tank and plug flow cases, a series of runs were performed on a "MIXONLY POF" tanks-in-series model for 2, 5, and 10 equal size tanks. The equal size is of importance only as a basis for assuming an equal distribution of coalescences among tanks, since residence time per se is not important in the case of instant reaction. Results, shown in Table I, indicate as expected that at high values of I_m, conversion increases with an increase in number of tanks— the largest difference being between 1 and 2 tanks. What was not expected but is indicated is that conversions are slightly higher for the stirred tank at very low values of I_m (see Figure 22 and Table I). This effect can reasonably be attributed to the fact that a stirred tank allows early departure of products as well as reactants and that the removal of more product reduces the incidence of unproductive duplicate coalescences.

Using the provision for computing internal distributions of molecular and point ages described earlier, values of Danckwerts' (11) "J" factor were computed as a function of the number of tanks "n" and the mixing parameter "I_m" (Figure 23). The bound at $I_m = \infty$ was computed from the following formula, which is developed in Appendix C.

$$J = \frac{\sum_{i=1}^{n} i^2 - \frac{1}{n}\left[\sum_{i=1}^{n} i\right]^2}{\sum_{i=1}^{n} (n-i+2)(n-i+1) - \frac{1}{n}\left[\sum_{i=1}^{n} (n-i+1)\right]^2} \qquad \text{(II-1)}$$

To illustrate the effect of "J" on conversion, the base case conversion (DR = .25, SR = 1.5) were plotted versus "J" with "n" and I_m as parameters (Figure 24). Since a change in "J" at fixed I_m is determined by the number of tanks in series, results are similar to those already shown for "n" as the independent variable; that is, conversion increases as either "n' or "J" increases for large I_m and decreases slightly for small I_m. This figure indicates an overwhelming dependence of conversion of the mixing parameter I_m as compared to "mixedness" defined by "J."

TABLE I

CONVERSIONS OF "A" FOR MIXING WITH INSTANTANEOUS REACTION OF SEPARATE REACTANT STREAMS IN "n" EQUAL SIZE CELL-WISE STIRRED TANKS IN SERIES

Reaction: $A + \frac{1}{2} B \rightarrow C$

Stoichiometric ratio, SR, is for "B" in stream 2 to "A" in stream 1.
Dilution ratio, DR = stream 2/stream 1.

Stoichiometric Ratio, SR	I_m	DILUTION RATIO, DR												
		0.10				0.25					1.00			
		n				n					n			
		1	2	5	∞	1	2	5	10	∞	1	2	5	∞
1.0	.2	.059	.046	.039	.039	.092	.093	.065		.104	.154	.174	.129	.175
	1.	.267	.267	.291	.288	.344	.351	.359		.386	.383	.430	.502	.494
	5.	.610	.771	.798	.903	.684	.766	.860		.925	.699	.784	.863	.941
1.5	.1					.050	.056	.029	.044	.039				
	.2	.063	.047	.039	.030	.095	.081	.077	.073	.078	.166	.189	.136	.173
	1.	.294	.307	.338	.337	.398	.409	.446	.447	.434	.450	.505	.578	.577
	5.	.802	.884	.932	.988	.815	.921	.961	.983	.995	.828	.906	.961	.997
	10.	.906	.968	.9968	1.000	.917	.977	.9974	.9997	1.000				
5.0	.2	.060	.050	.039	.043	.102	.103	.066		.091	.163	.217	.150	.197
	1.	.412	.396	.412	.359	.510	.507	.538		.545	.570	.620	.732	.734
	5.	.902	.958	.985	.9982	.903	.956	.987		1.000	.909	.975	.989	1.000

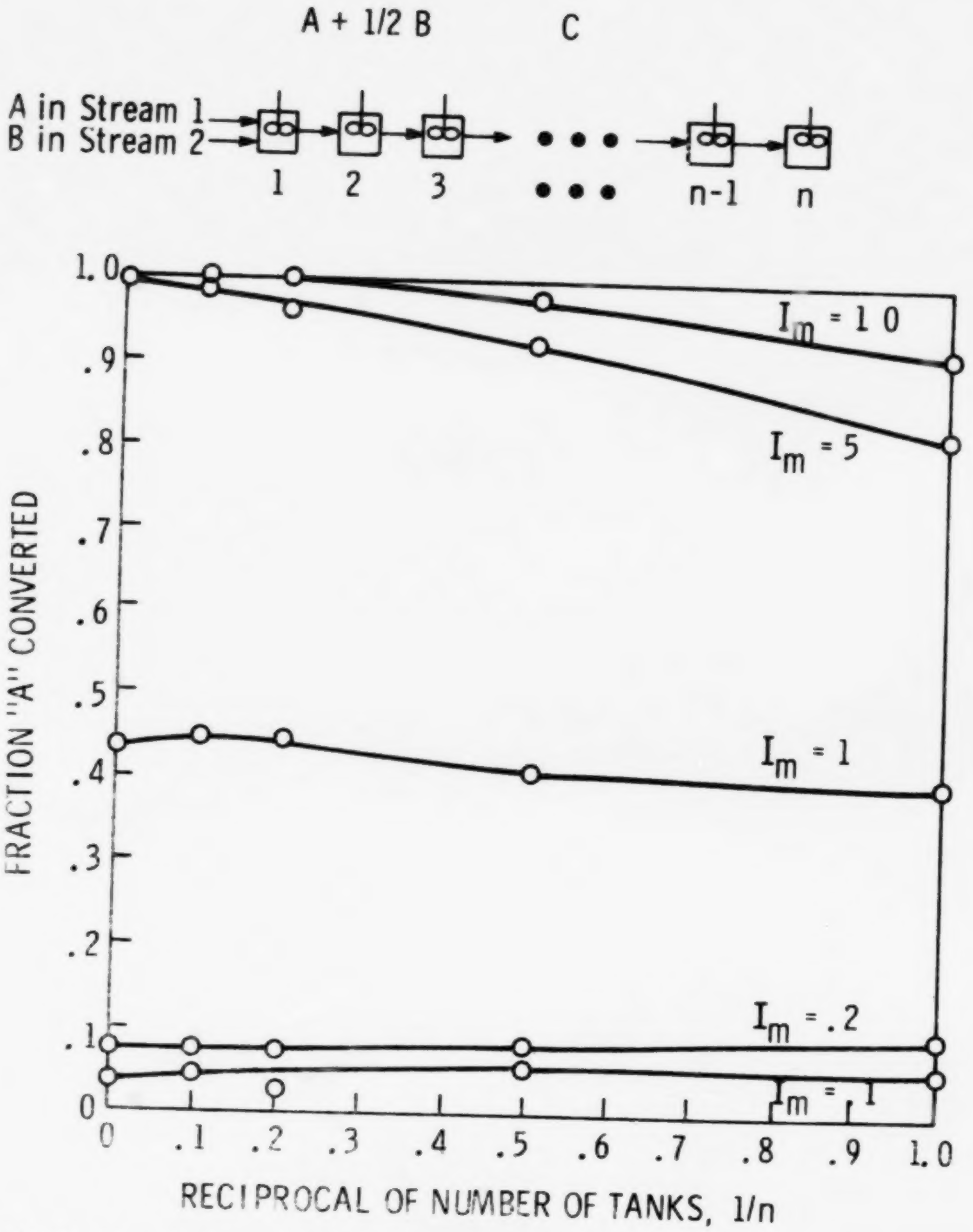

Figure 22. Mixing with instantaneous reaction for "n" equal size cellwise stirred tanks. The mixing parameter, I_m, is equally distributed among the tanks; stoichiometric ratio (B:A), SR = 1.5; dilution ratio, stream 2/stream 1 = 0.25.

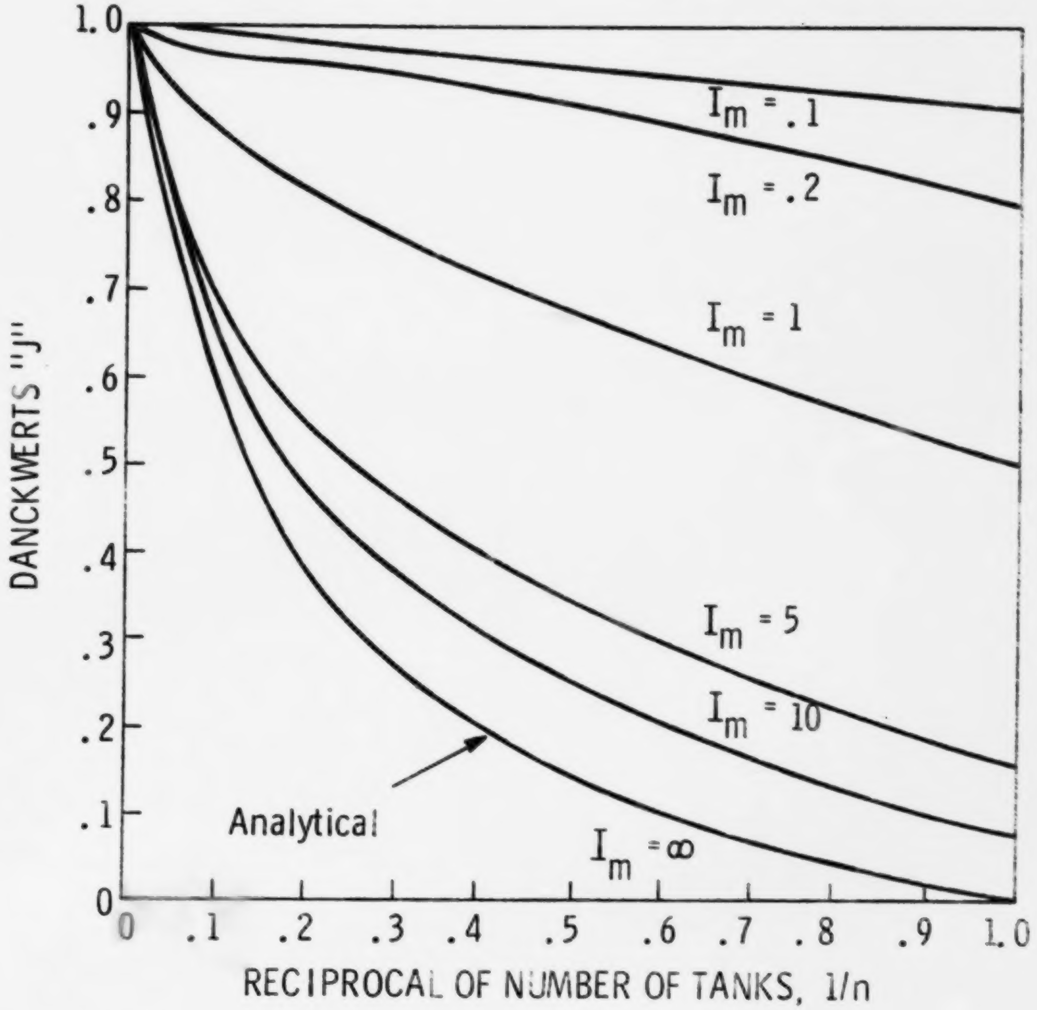

Figure 23. Danckwerts'(11) "J" factor for cell-wise mixed stirred tanks in series. Curves for I_m = .1 to 10 are computer derived. The curve for $I_m = \infty$ is analytical.

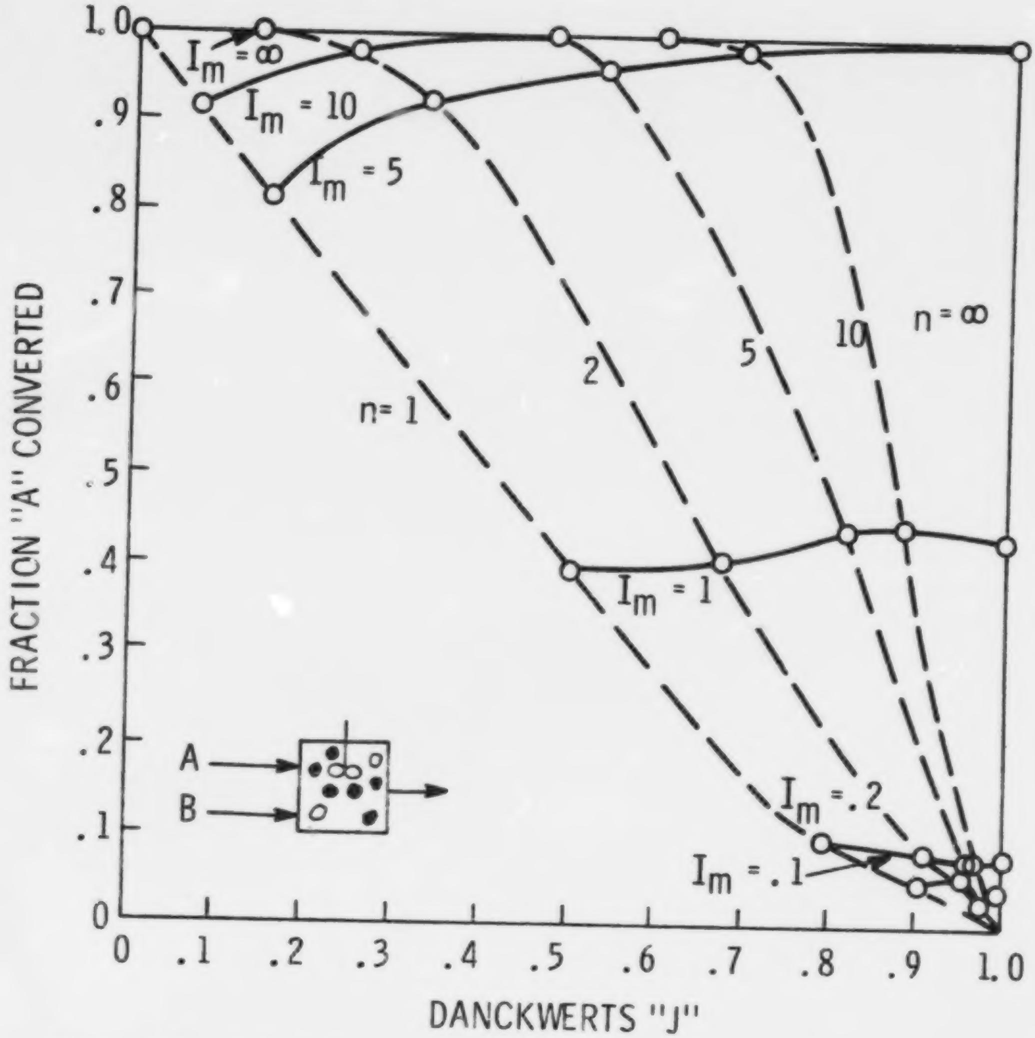

Figure 24. Influence of Danckwerts' "J" on fraction "A" converted for instantaneous reaction of "A" in cell-wise mixed tanks in series. A + 1/2 B → C; Feed stoichiometric ratio (B:A), SR = 1.5; stream dilution ratio (stream B: stream A), DR = 0.25.

B. COUPLED MIXING AND KINETICS AT STEADY FLOW: PARAMETER STUDY ON "MICROMIX II"

In order to obtain an overview of sensitivities to important parameters, including kinetics, a large number of steady flow simulations were run on the stirred tank cell mixing program MICROMIX II. The parameters added to I_m, DR, and SR (which were investigated already in MIXONLY) were cell temperature "T_j," mean residence time "τ," reaction orders "$\eta_{i,k}$" and activation energy "E_k." Simulations were again conducted about a base condition (Table II), which here included the assumption that air was preheated to enter at the same temperature as the exhaust. Cold air was tested as a variation on the base case.

Simulations were run for approximately 50 cells in the reactor (depending on dilution ratio and temperature) and 10 mean residence times, resulting in a statistical uncertainty of about $\sigma = 0.035$ or less depending on conversion level. The statistical limits for the high temperature asymptotes from "MIXONLY" are $\sigma = 0.02$ or less.

The reaction treated in these simulations is intended to represent oxidation of carbon monoxide. Base case reaction kinetics are zero order and represent a rounding of constants in the rate equation determined for carbon monoxide in the CRC study.

$$CO + \frac{1}{2} O_2 \rightarrow CO_2$$

$$\text{"CRC" Rate equation:} \quad r_{CO} = .0721\ e^{-28,200/RT} P_{CO}^{0.269} \qquad \text{(II-2)}$$

Corresponding zero order rate equation:

$$r_{CO} = .1035\ e^{-30,000/RT} \qquad \text{(II-3)}$$

The leading coefficient in the zero-order equation was chosen so that conversion for the two equations would match at 1420°F and 50% conversion for a feed of 2% CO, P = 15 psia, and $\tau = .05$ see mean residence time at 1500°F (Figure 25).

1. Stream Dilution Ratio

Figures 26, 27, 28, and 29 are for dilution ratios, DR, of .1, .25, .50, and 1. These tests were run at a constant stoichiometric ratio, SR, by

TABLE II

CONDITIONS FOR TESTING PARAMETERS OF MICROMIX II

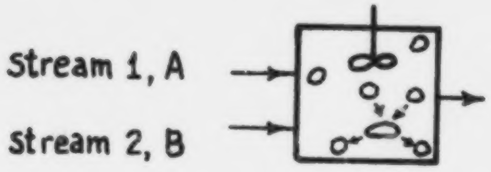

$$A + 1/2\,B \rightarrow C$$

$$r_A = k e^{-E/RT} P_A^{\eta_A} P_B^{\eta_B}$$

Test simulations were run for a base condition representative of oxidation of carbon monoxide in a thermal exhaust reactor and for departures from the base condition for each of the designated parameters. The particular inlet concentrations and rate equations are given with the results in Figures 26 to 39.

Parameter	Base Condition (Figure 27)	Alternate Parameter Values
Dilution ratio, DR = stream2/stream 1	.25	.1 (Fig.26), .5 (Fig. 28) 1 (Fig. 29)
Feed stoichiometric ratio, SR = 2B/A	1.5	1 (Fig. 30), 2 (Fig. 31), 5 (Fig. 32), 15 (Fig. 33)
Mixing parameter, I_m	1,2,5,20	None
Activation energy, E, cal/g mole	30,000	10,000 (Fig. 34), 50,000 (Fig. 35)
Reaction order in "A", η_A	0	1 (Fig. 36)
Reaction order in "B", η_B	0	1 along with η_A = 1(Fig. 37)
Heat loss	None	None
Mean residence time at 1500°F, τ	.050 sec	.002 sec (Fig. 38), .150 sec (Fig. 39)
Temperature of stream 2	same temp. as stream 1	100°F, cold air

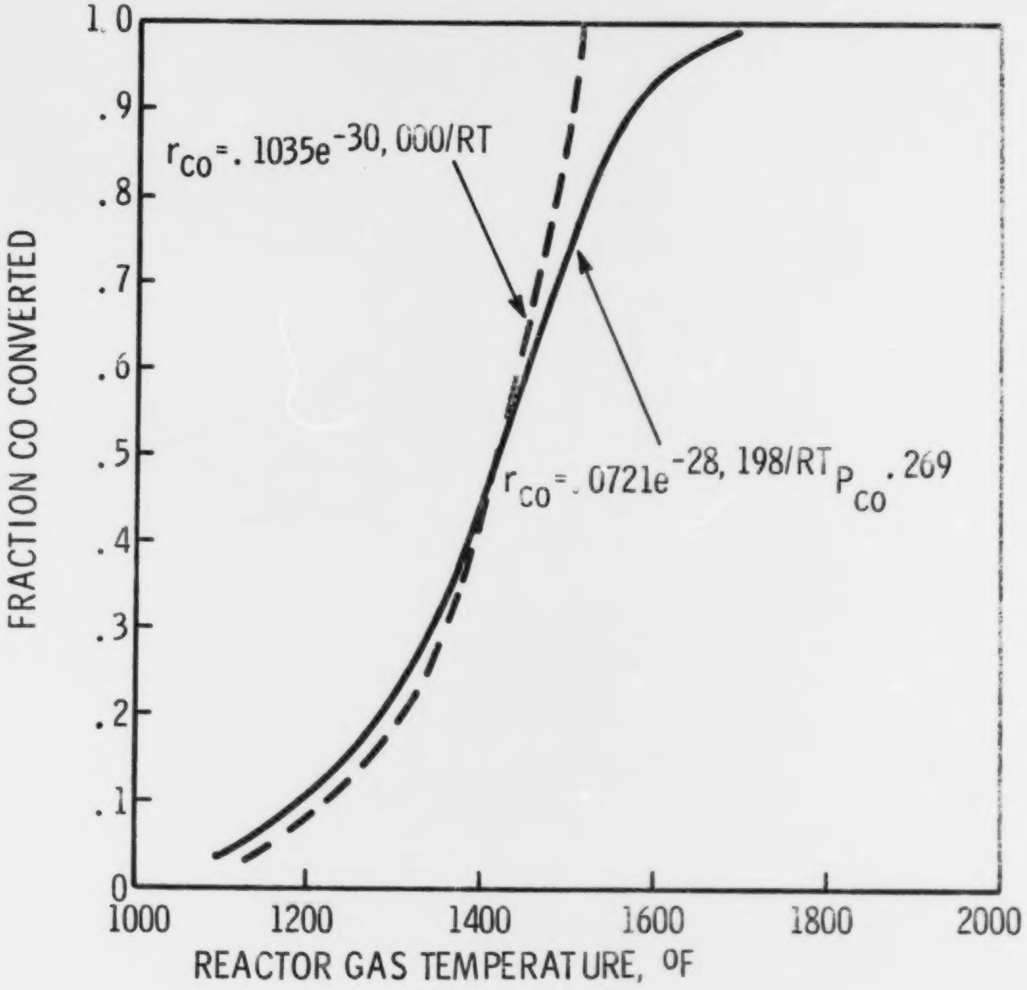

Figure 25. Comparison of stirred-tank conversion for zero order and .269 order CO kinetics at $I_m = \infty$. $CO_{in} = 2\%$, $P_{total} = 15$ psia, $\tau = .05$ sec mean residence time at 1500°F.

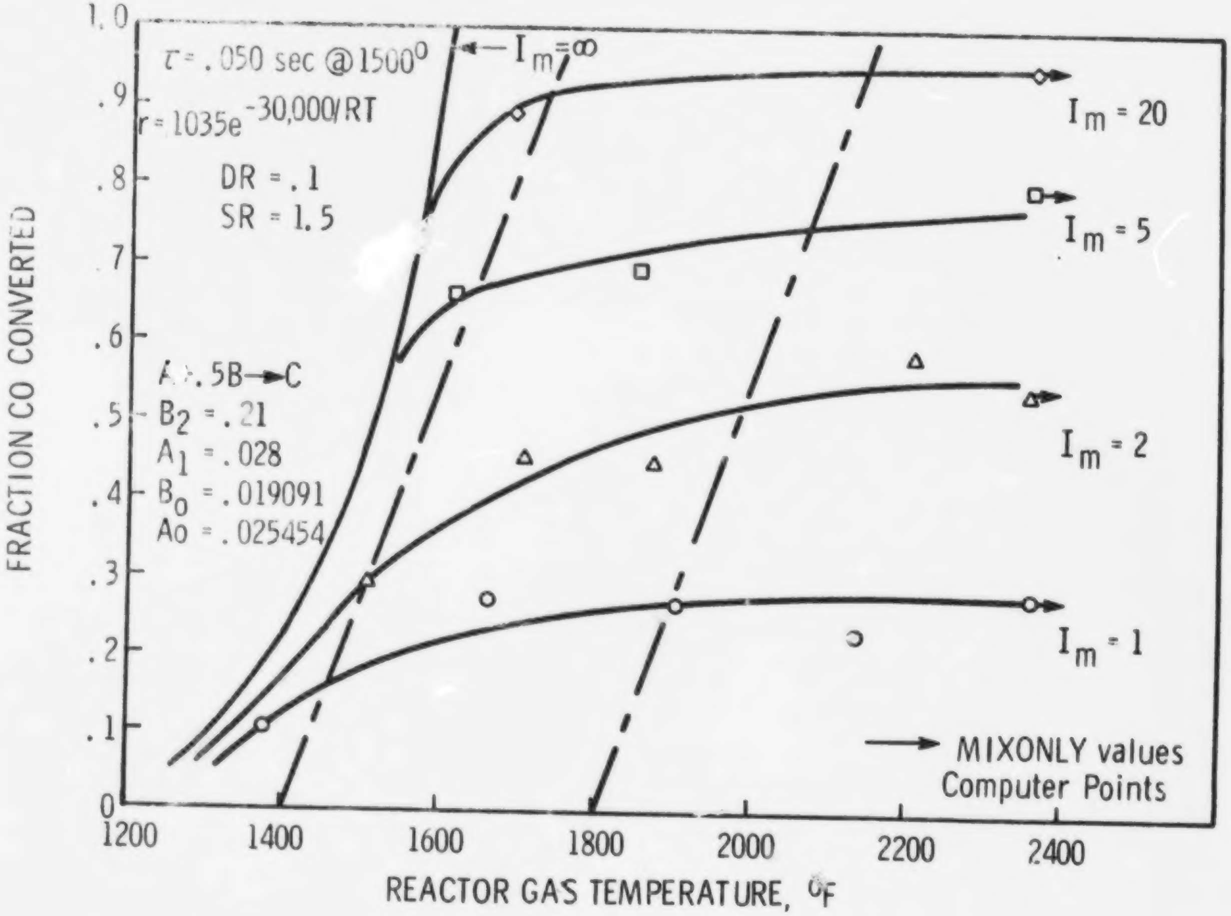

Figure 26. Material and energy balance curves for coupled reaction and mixing, $I_m = 1$ to ∞, in a cell-wise mixed stirred tank at dilution ratio, DR = .1.

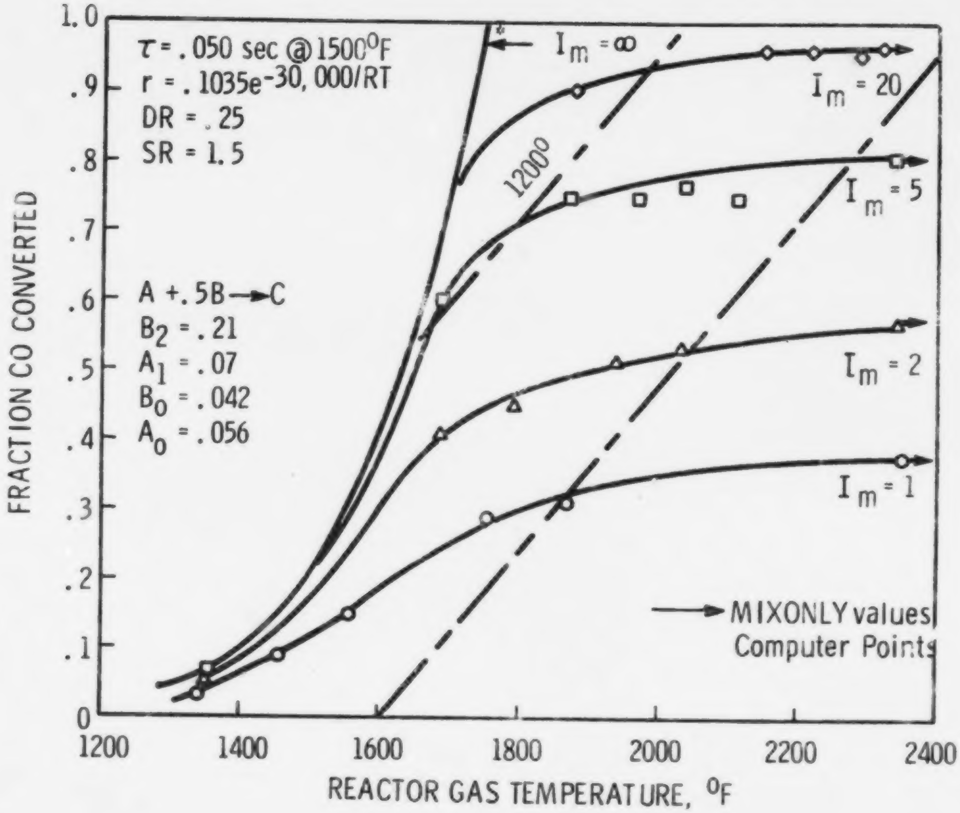

Figure 27. Material and energy balance curves for coupled reaction and mixing, I_m = 1 to ∞, in a cell-wise mixed stirred tank at dilution ratio, DR = .25. This is the base case simulation. Points ◇, □, △, ○ are from simulation "MICROMIX II". Point ✱ is experimental.

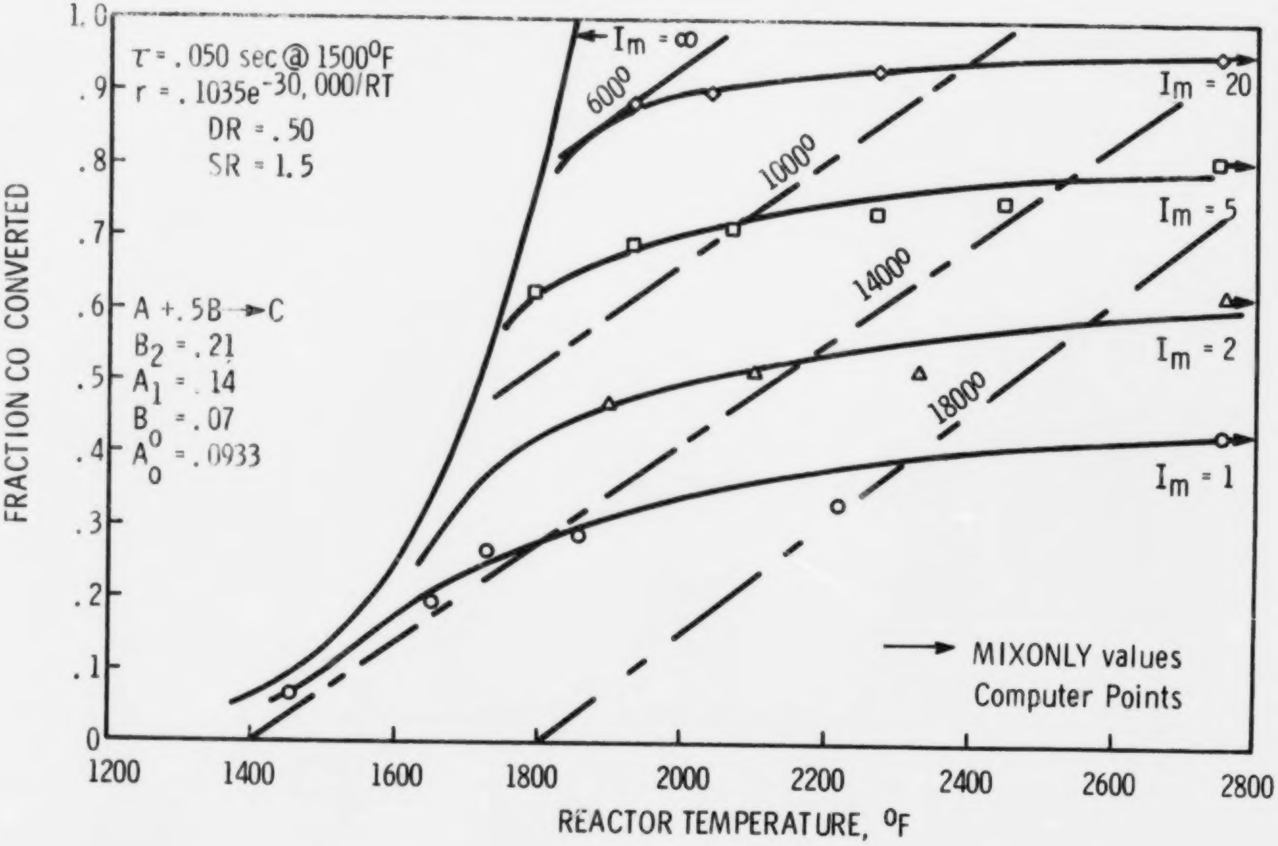

Figure 28. Material and energy balance curves for coupled reaction and mixing, I_m = 1 to ∞, in a cell-wise mixed stirred tank at dilution ratio, DR = .50.

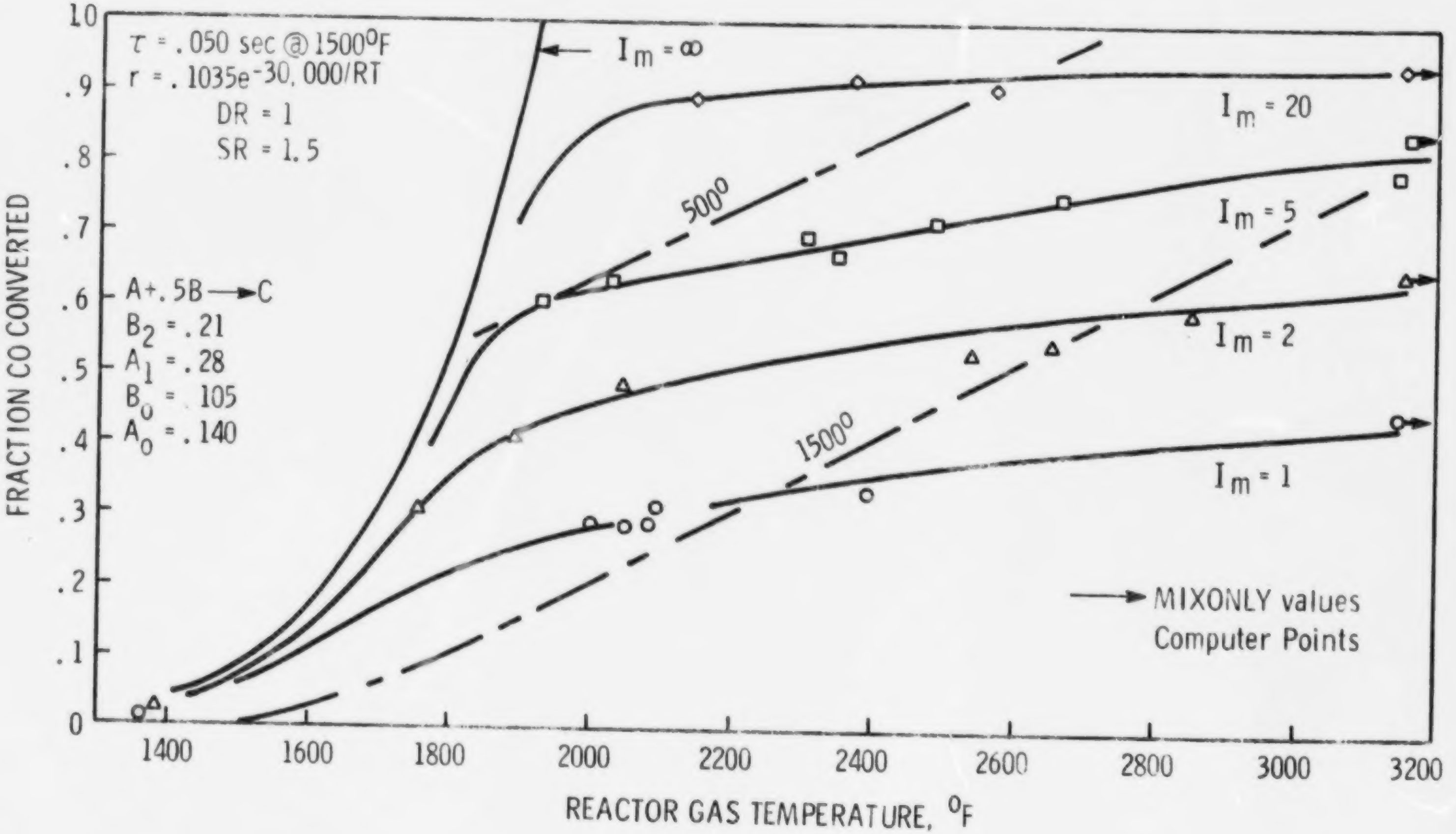

Figure 29. Material and energy balance curves for coupled reaction and mixing, I_m = 1 to ∞, in a cell-wise mixed stirred tank at dilution ratio, DR = 1.

maintaining the incoming concentration of "B" or air at 21% and increasing the concentration of "A" or carbon monoxide. The solid curves represent the material balances for different values of the mixing papameter I_m, and the dashed curves are energy balance lines for zero heat loss.

As the inlet CO concentration is increased, the slopes of the energy balance lines as drawn are reduced since given fractions of conversion produce a larger temperature increase. At the higher levels of carbon monoxide, low temperature energy balance curves intersect the material balance curves once at very low temperature and conversion off the left side of the graphs and again at high temperature and conversion appearing on the graphs. Reaching the high temperature solutions depends in these cases on specifying a high initial temperature for cells in the reactor at time zero. A low initial temperature results in virtually no reaction for these cases. Thus, a cell-wise mixed stirred tank is observed to exhibit an ignition phenomenon similar to that of an ideal stirred tank.

The behavior of all the material balance curves shown is similar, in that the ideal backmix result for $I_m = \infty$ represents a low-temperature bound from which curves depart and progress toward the "MIXONLY" asymptotes. The affect of increasing dilution ratio, DR, is to shift these asymptotes slightly toward higher conversion. The shift is greater at lower values of I_m, causing the spread in high temperature conversions associated with an increase in I_m to be smaller for a higher dilution ratio up to DR = 1.

2. Stoichiometric Ratio

In Figures 30, 31, 32, and 33, an increase in stoichiometric ratio for "B" (oxygen) to "A" (carbon monoxide) is accomplished by holding the dilution ratio DR at .25 and the inlet oxygen concentration at 21% while reducing the inlet carbon monoxide concentrations. This can be interpreted to represent either a change in total exhaust combustible or the earlier and later conversions of different exhaust species at effectively higher or lower stoichiometric ratios. An example of the latter is the effectively higher stoichiometric ratio associated with the early conversion of hydrocarbon compared to the effectively lower ratio for later conversion of carbon monoxide.

The shift in high temperature conversion between SR = 1 and SR = 15 is approximately 87% to 99% at I_m = 20 and 30% to 55% at Im = 1. At the low value SR = 1, representing the high inlet "A" concentration, achieving high conversion at the 1000°F inlet temperature depends again on specifying a high initial temperature.

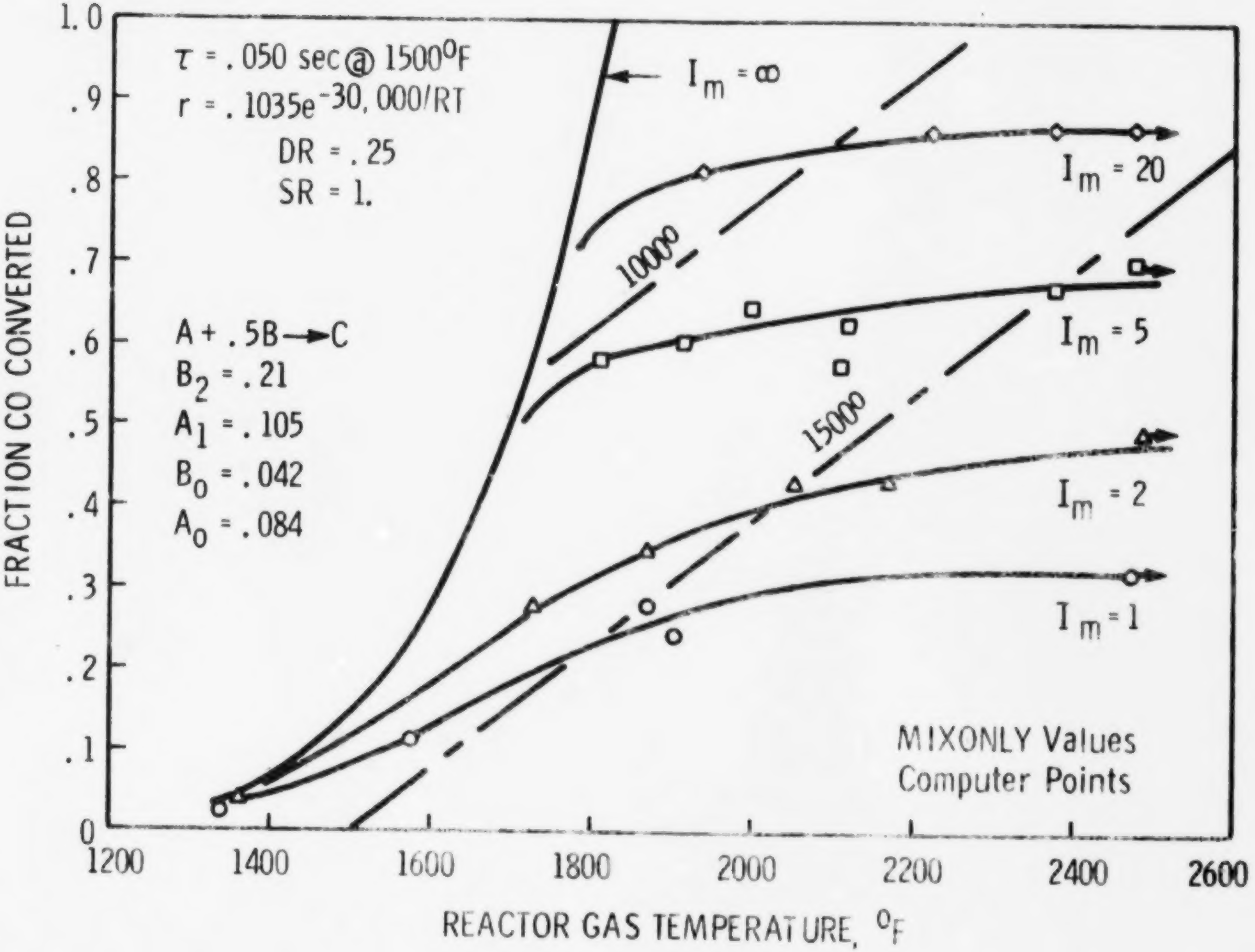

Figure 30. Material and energy balance curves for coupled reaction and mixing, $I_m = 1$ to ∞, in a cell-wise mixed stirred tank at a feed stoichiometric ratio (B:A), SR = 1.

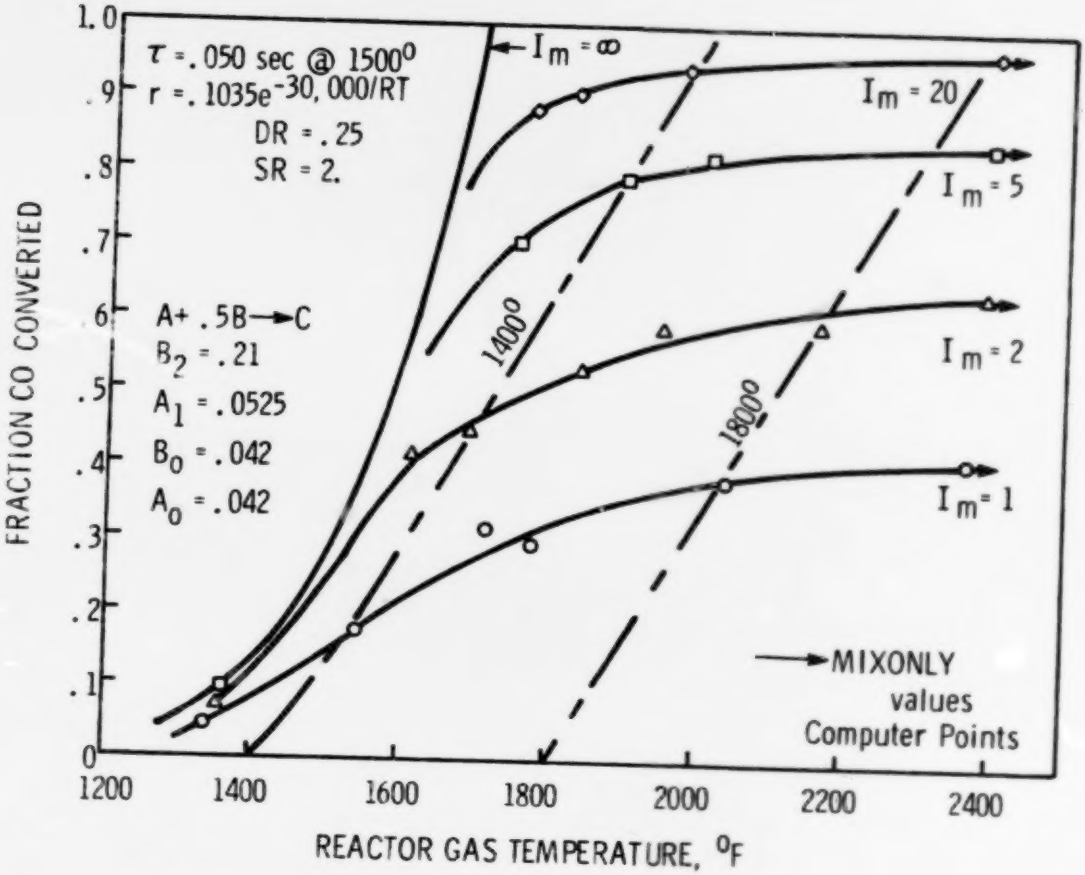

Figure 31. Material and energy balance curves for coupled reaction and mixing, I_m = 1 to ∞, in a cell-wise mixed stirred tank at a feed stoichiometric ratio (B:A), SR = 2.

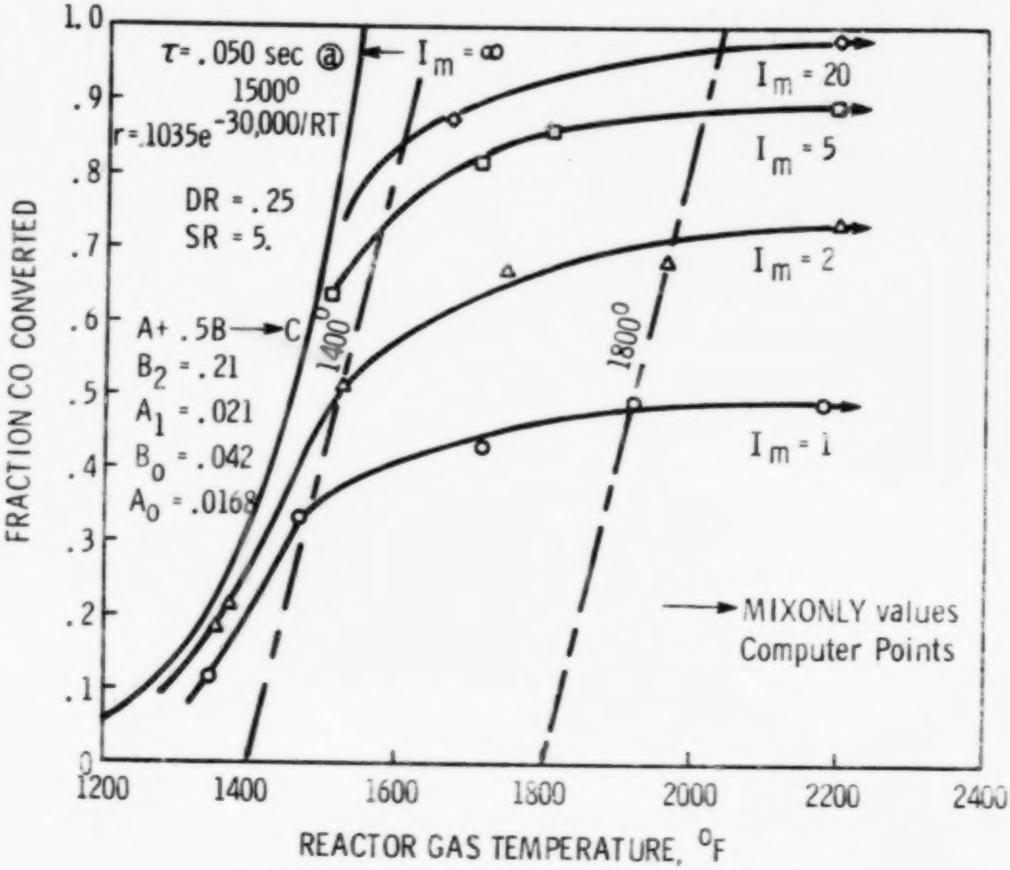

Figure 32. Material and energy balance curves for coupled reaction and mixing, $I_m = 1$ to ∞, in a cell-wise mixed stirred tank at a feed stoichiometric ratio (B:A), SR = 5.

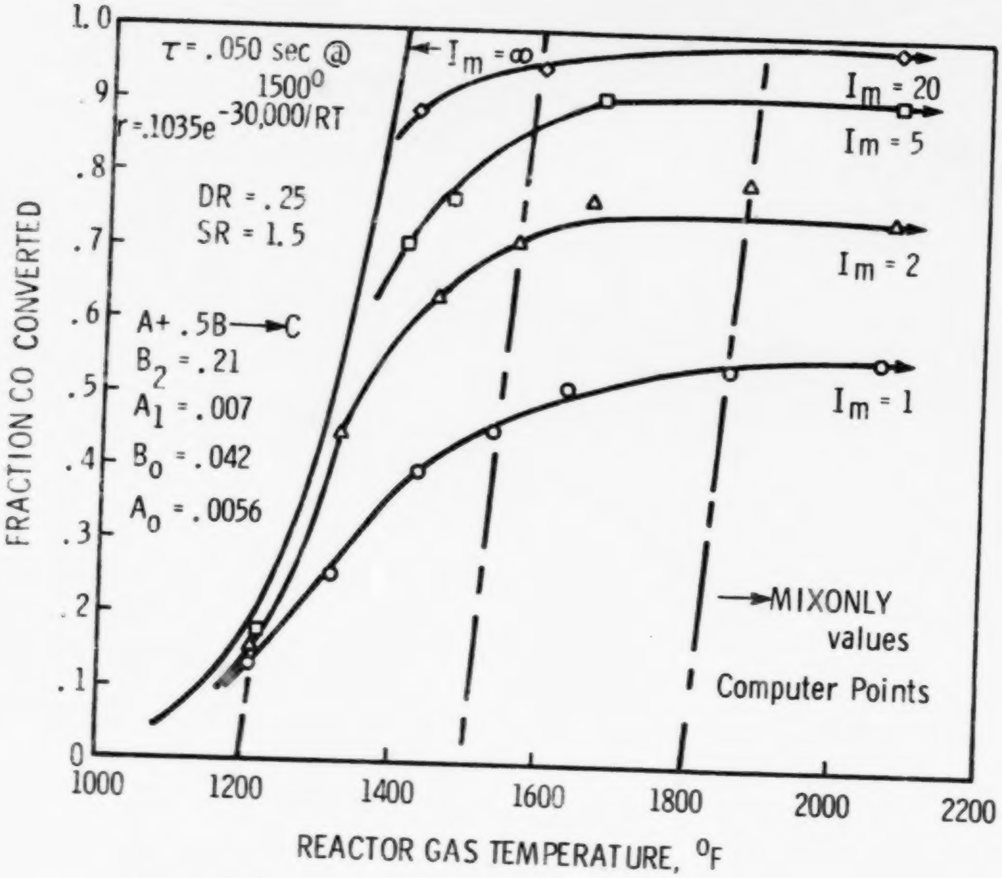

Figure 33. Material and energy balance curves for coupled reaction and mixing, I_m = 1 to ∞, in a cell-wise mixed stirred tank at a feed stoichiometric ratio (B:A), SR = 15.

3. Reaction Kinetics - Activation Energy and Order

Figures 34 and 35 demonstrate the change in the material balance curves when activation energy E is increased from 10,000 cal/g mole to 50,000 cal/g mole. A change was also made in the leading coefficient of the rate equation so that conversions match at 1615°F and 50% conversion. The change in slope is most evident in the material balance bound at $I_m = \infty$; however, at the lower activation energy, the approaches to the "MIXONLY" asymptotes for $I_m < \infty$ are also more gradual.

First order and second order kinetics (Figures 36 and 37) shift high conversions toward higher temperatures. When a high conversion must be obtained subject to an upper limit on temperature reaction order vies with mixing as a fundamental factor limiting conversion. Since mixing can be improved whereas kinetics are constant, it is a matter of the highest concern in reactor design to establish which of these effects govern. Further discussion of this matter will be offered later in reference to determination of exhaust reactor kinetics.

4. Mean Residence Time

Mean residence time (Figures 38 and 39) was changed from the base value of .050 sec to .002 and .150 sec, respectively, to indicate the relative conversions that would be obtained in an exhaust port volume and in a volume nominally twice that of the DuPont Model V reactor assuming operation as partially mixed stirred tanks.

At the .002-sec residence time, an appreciable level of conversion for CO is attainable only at high temperatures such as might be found in the hot fraction of a temperature distribution and not at an averaged exhaust temperature. The threefold increase in mean residence time to .150 sec has the effect of lowering the $I_m = \infty$ bound by approximately 150°F and moving it slightly more toward the vertical. For a zero-order reaction, as is being considered, the shift in temperature $T_2 - T_1$ is given by $R \cdot \ln(\tau_2/\tau_1) \cdot T_1T_2/E$, which for "small" changes in reactor volume makes the shift approximate proportional to the natural logarithm of the volume ratio.

5. Mixing Hot and Cold Streams

A simulation run at the base condition in all respects except for substitution of cold air for hot essentially reproduced the base case result shown previously in Figure 27. The only difference observed (which was not graphed) was a small upward shift in conversions at low temperatures, to place conversions for $I_m = 1$ and 2 about two percentage points above the $I_m = \infty$ curve rather than just below. It is important to recognize that these conversions were enhanced in reference to average reactor gas temperature, where entrance of cold air automatically implies a hotter exhaust to attain the same average.

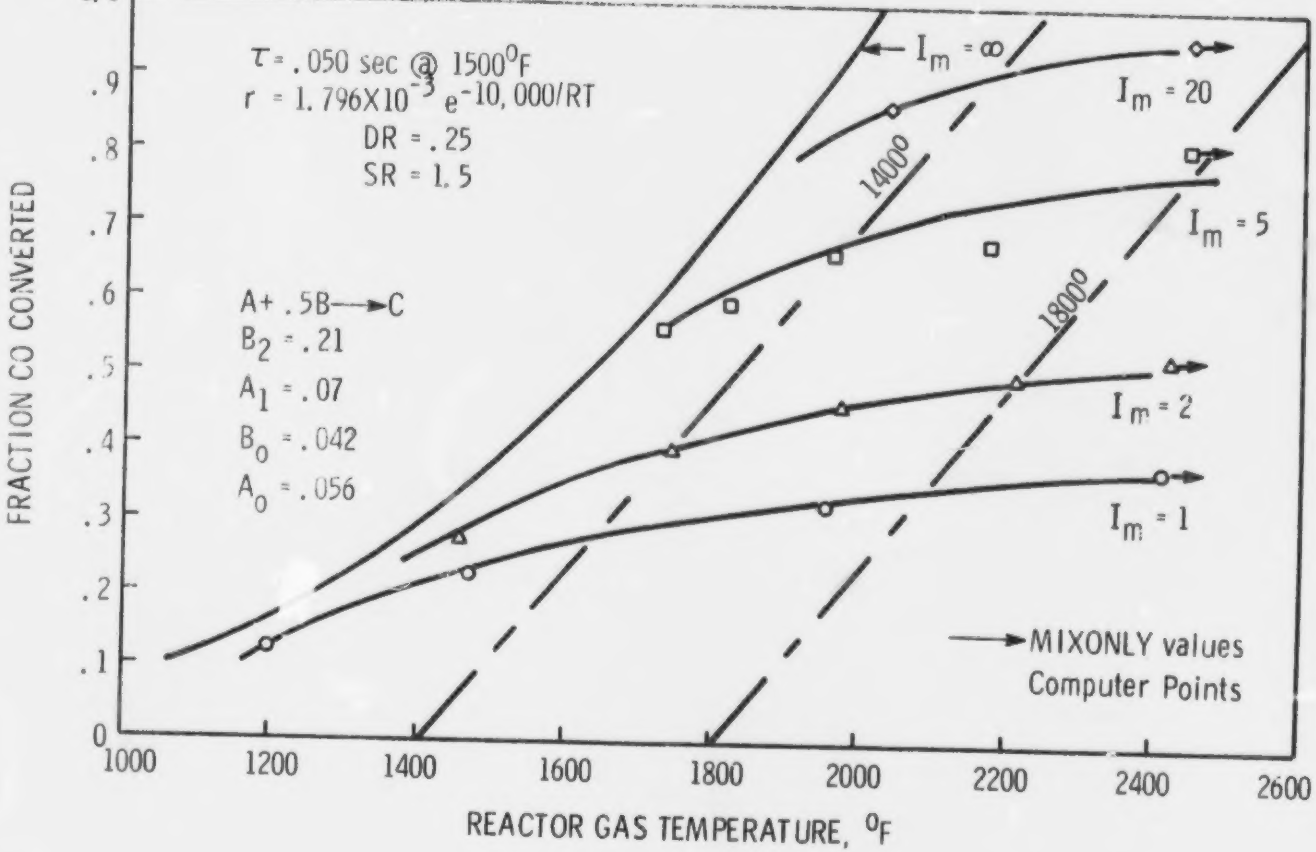

Figure 34. Material and energy balance curves for coupled reaction and mixing, I_m = 1 to ∞, in a cell-wise mixed stirred tank at activation energy, E = 10,000 cal/g mole.

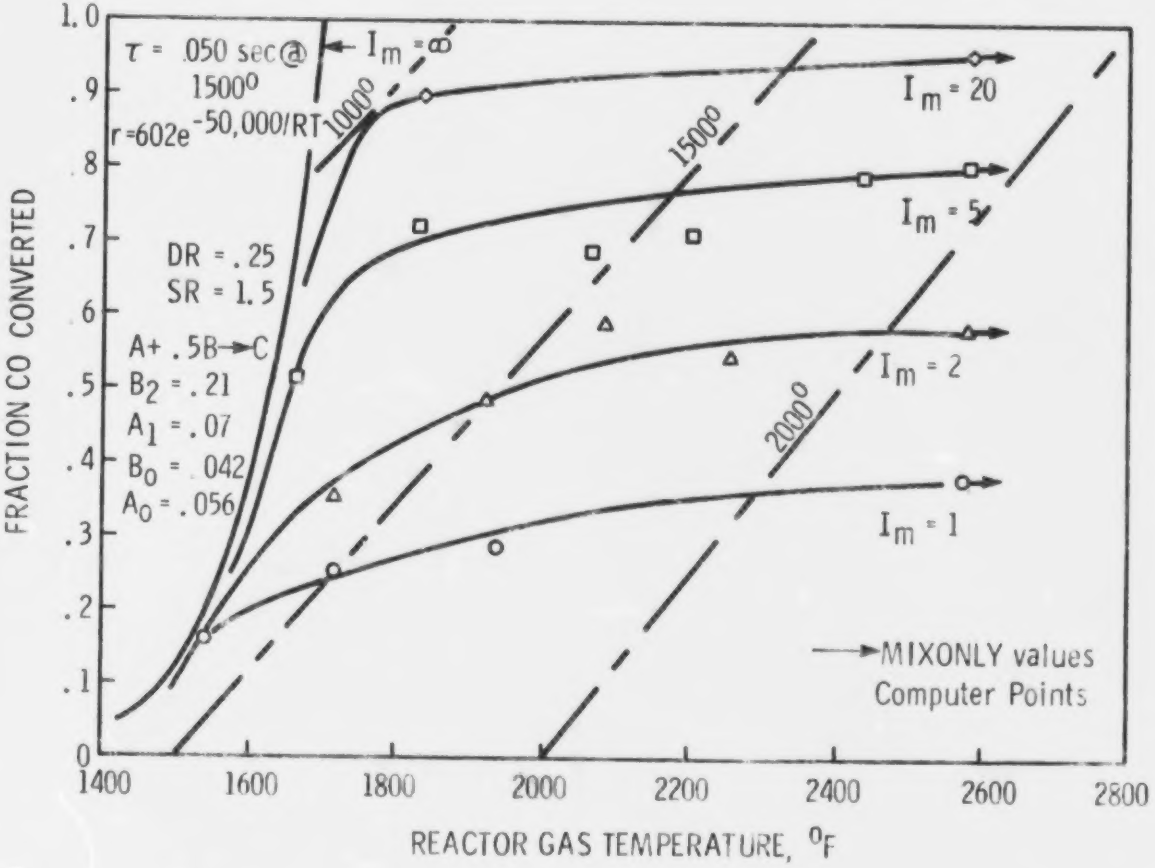

Figure 35. Material and energy balance curves for coupled reaction and mixing, $I_m = 1$ to ∞, in a cell-wise mixed stirred tank at activation energy, $E = 50,000$ cal/g mole.

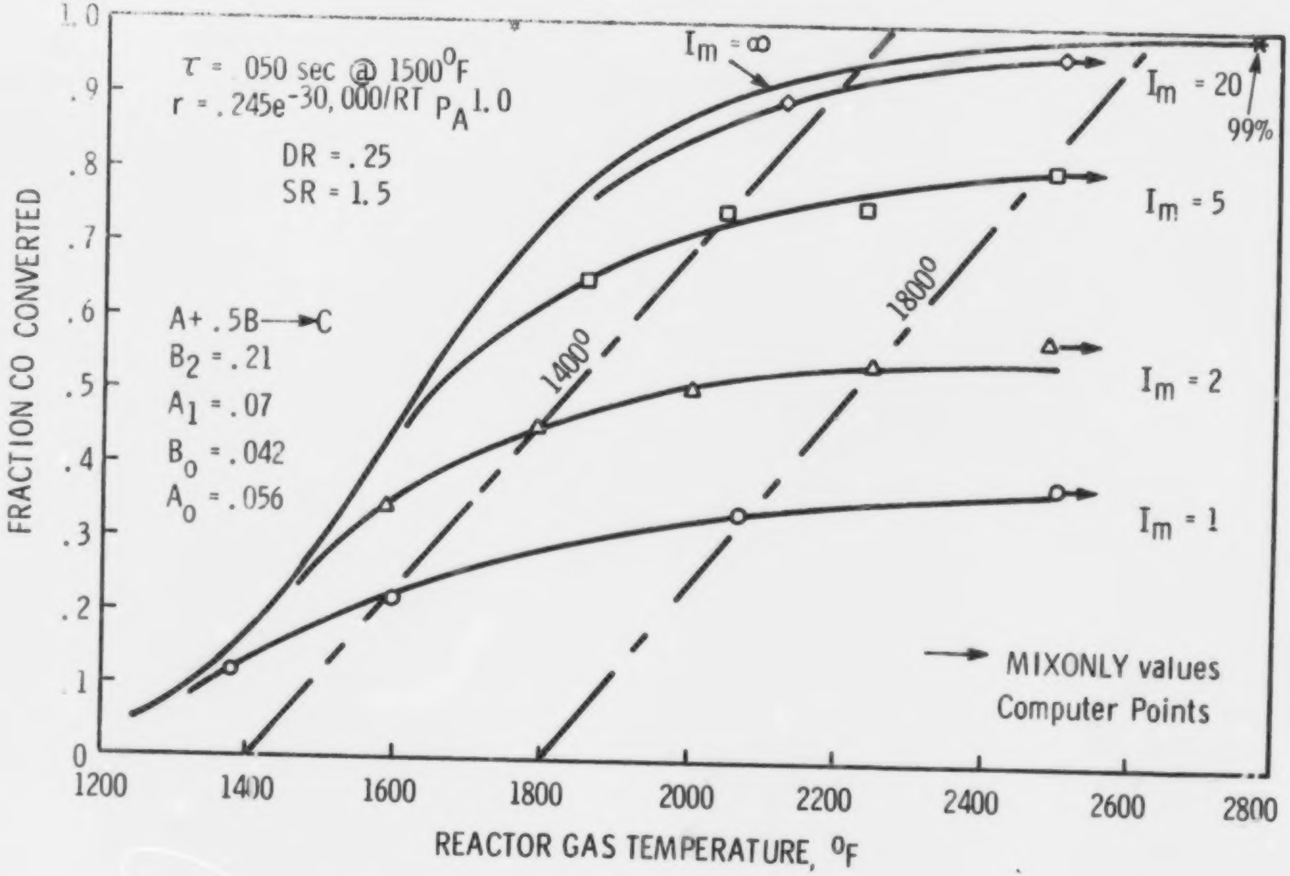

Figure 36. Material and energy balance curves for coupled reaction and mixing, $I_m = 1$ to ∞, in a cell-wise mixed stirred tank for first order reaction. Points ◇, □, △, ○ are from simulation "MICROMIX II". Point ✱ is experimental.

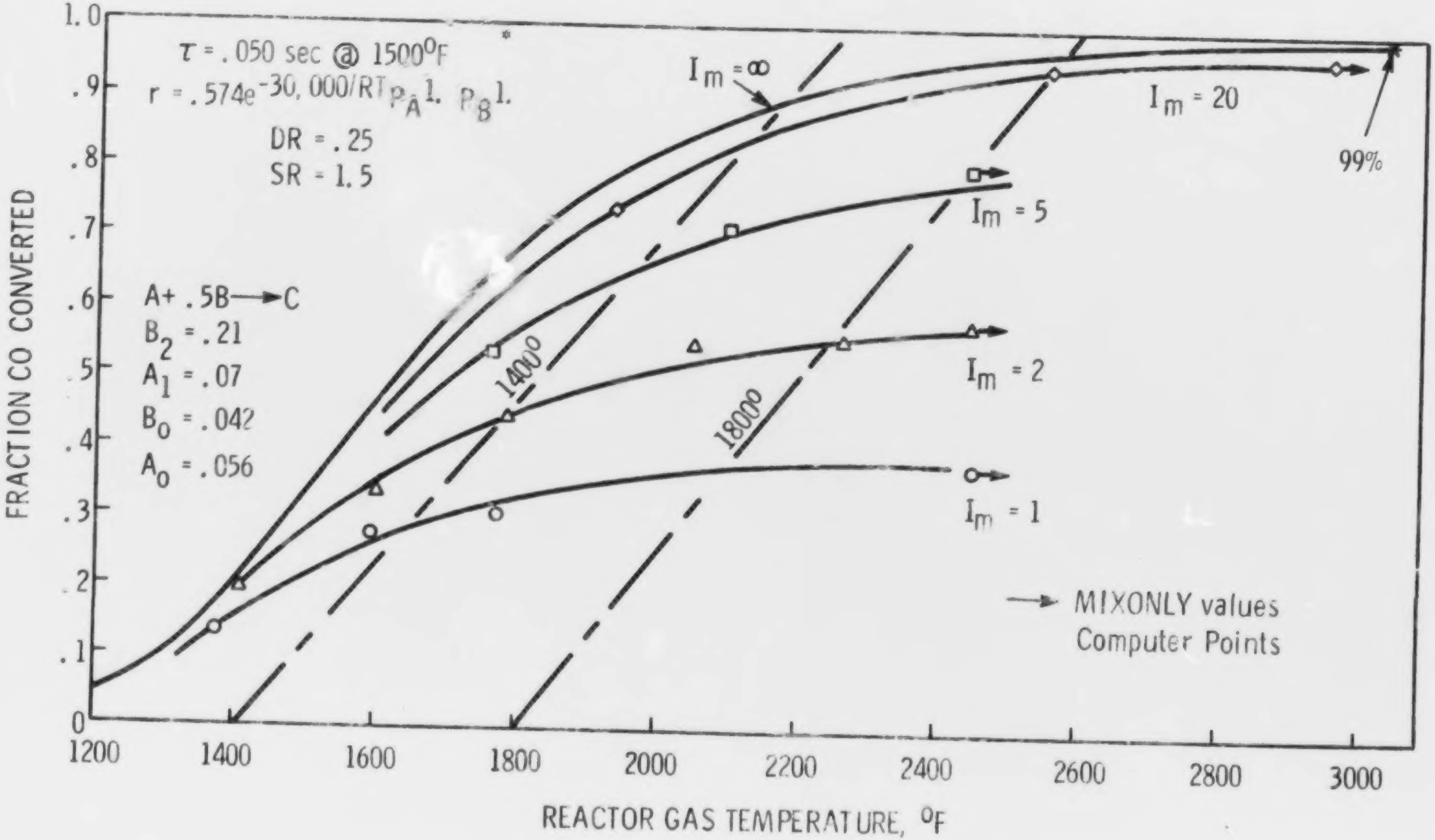

Figure 37. Material and energy balance curves for coupled reaction and mixing, $I_m = 1$ to ∞, in a cell-wise mixed stirred tank for second order reaction. Points ◇, □, △, ○ are from simulation "MICROMIX II". Point * is experimental.

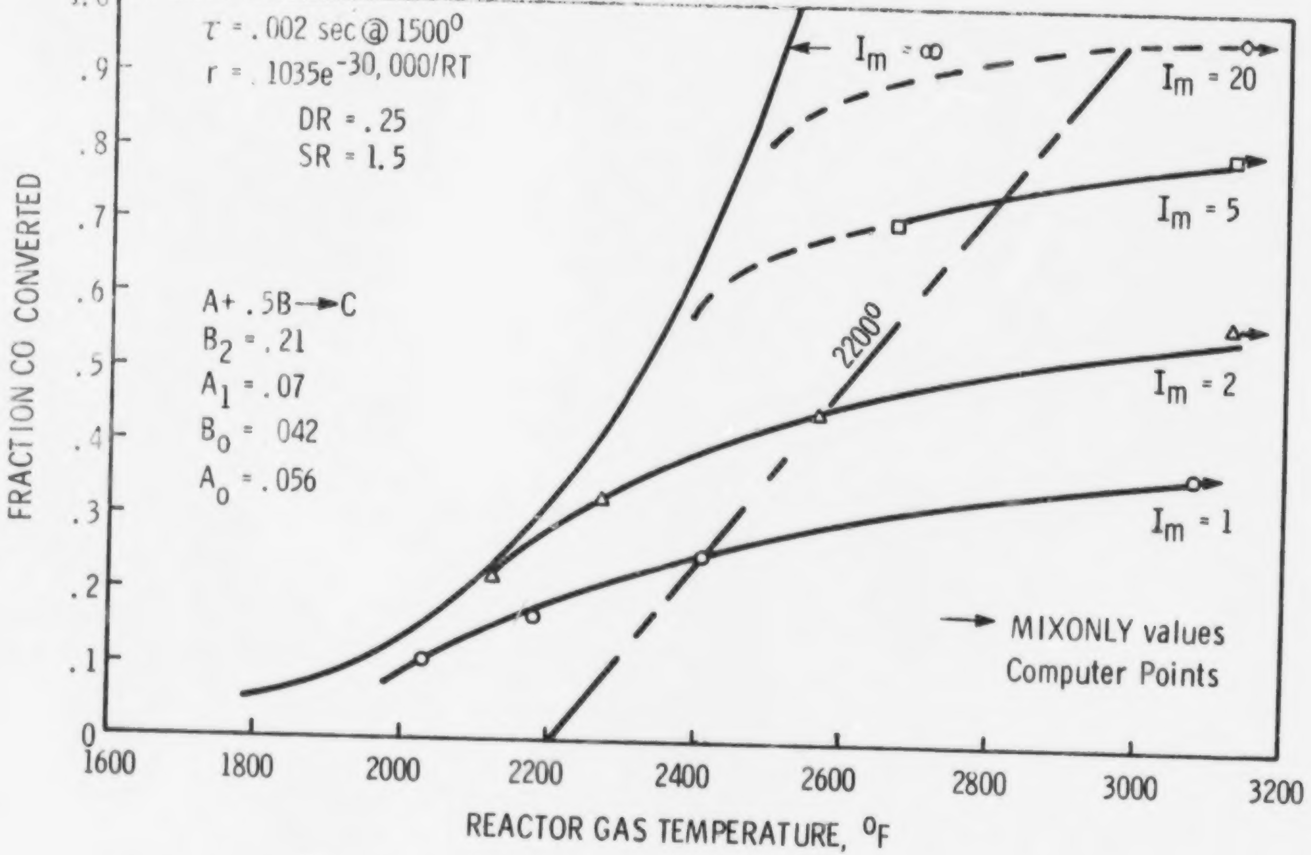

Figure 38. Material and energy balance curves for coupled reaction and mixing, I_m = 1 to ∞, in a cell-wise mixed stirred tank at a mean residence time, τ = .002 sec. at 1500°F.

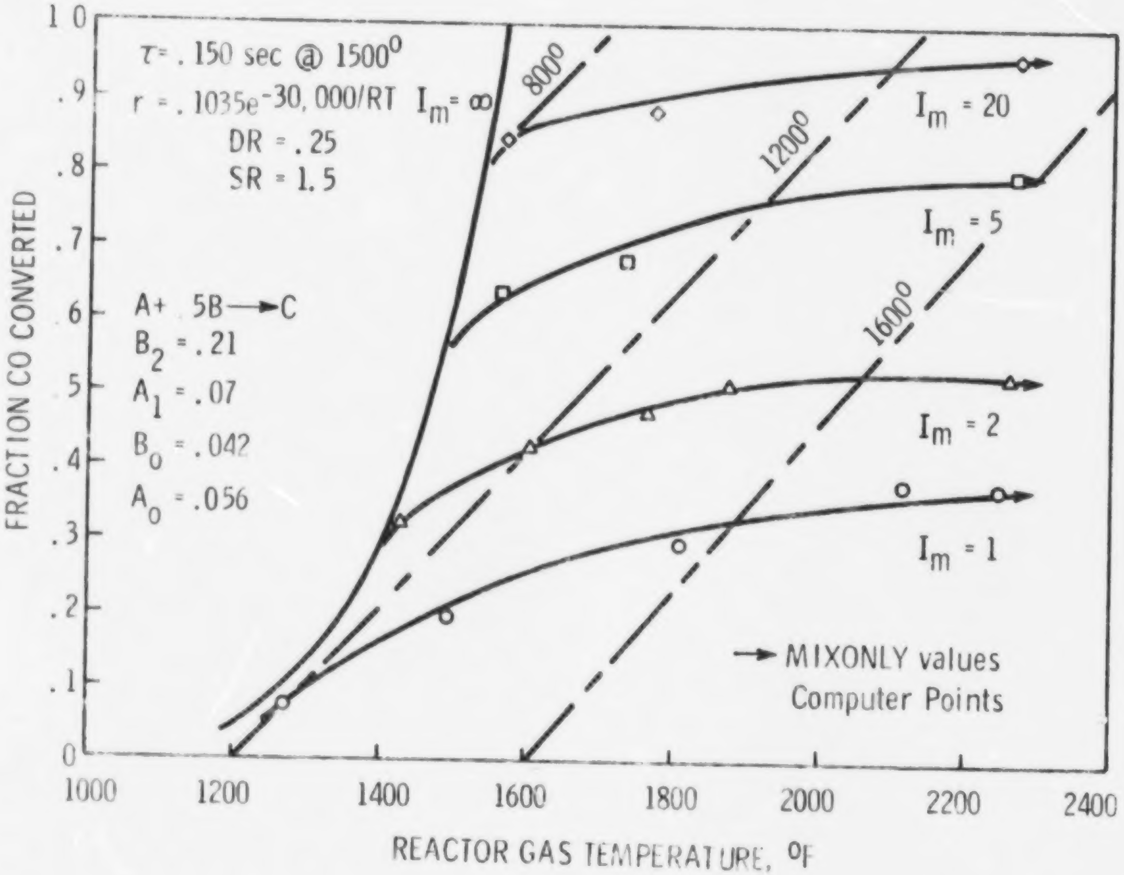

Figure 39. Material and energy balance curves for coupled reaction and mixing, I_m = 1 to ∞, in a cell-wise mixed stirred tank at a mean residence time, τ = .150 sec. at 1500°F.

SIMULATIONS ON STATIONARY STATE REACTOR OPERATION: COMPARISON WITH EXPERIMENTAL STUDIES

III. Estimates of the Coalescence Parameter, I_m

Starting with Corrsin's (8,9) correlation for the decay constant for variance in concentration, we proceed to compute values of I_m corresponding to the one-cylinder reactor and the DuPont Model V reactor.

We assume, as Evangelista (15,16) did for a spherical combustor, that mixing power "P_m" can be computed form the dinetic energy of the entering streams of jets. Initial consideration of the problem will neglect change in density for the entering gas.

For the ratio of mixing power P_m to mass in the reactor M we write

$$\frac{P_m}{M} = \frac{\left[(\rho\ v_j\ S)(1/2\ v_j^2/g_c)\right]}{\left[1/6\ \pi\ L_r^3\ \rho\right]} \tag{III-1}$$

where S is the total cross sectional area for all entering streams (or jets), v_j is jet velocity, and L_r is a sphere equivalent diameter for the reactor. We proceed by substitution to find I_m as a function of L_r, S and the integral scale of turbulent fluctuation L_c. Evangelista (16) further assumed that the

$$\tau = 1/6\ \pi\ L_r^3/S\ v_j \tag{III-2}$$

$$\beta \cong 1.07 \left(\frac{g_c\ P_m}{L_c^2\ M}\right)^{1/3} \tag{III-3}$$

$$I_m = \beta\ \tau \cong 1.07 \left(\frac{3\ S\ v_j^3}{\pi\ L_r^3\ L_c^2}\right)^{1/3} \left(\frac{\pi\ L_r^3}{6\ S\ v}\right) \tag{III-4}$$

$$I_m \sim 0.55 \left(\frac{L_r^3}{S\ L_c}\right)^{2/3} \tag{III-5}$$

integral scale of turbulent fluctuation L_c was equal to the sphere equivalent diameter L_r. Using the loading coefficient of [illegible]/2 that is obtained from

Corrsin's earlier publication (8) (rather than 1.07 as above) Evangelista obtained:

$$\beta_T = 1/4 \left(\frac{L_r^2}{S}\right)^{2/3} \qquad \text{(III-6)}$$

We first apply this analysis to the single cylinder reactor having a sphere equivalent diameter of L_r = 4.85 in. for a reactor volume of 59.5 cu in. and an inlet cross sectional area S of 0.0759 sq in. for 11 inlet holes of 3/32-in. diameter. Using Evangelista's assumption of $L_c = L_r$, we obtain I_m = 11.4, which limits covnversions S_{co} to approximately 92% for a dilution ratio DR = .25 and stoichiometric ratio SR = 1.5, based on results from "MIXONLY." Changing only the leading coefficient to 0.55 changes the prediction to I_m = 25 and $X_{co} \simeq .96$. Experimental conversions for all combustibles including carbon monoxide were observed to reach 99% or higher at sufficiently high temperature, indicationg that a mixing parameter value based on $L_c = L_r$ is low.

Evangelista's assumption, equating the scale of turbulent concentration fluctuation to the gross dimensions of flow, is quite obviously the most conservative estimate that can be offered. A calculation based on injection system dimensions yields a much higher estimate of I_m, which for L_c equal to the 3/32-in. jet orifices in the single cylinder reactor predicts I_m = 102 for the leading coefficient of 1/4 or I_m = 225 for the leading coefficient of .55.

"MIXONLY" simulations run at high values of I_m indicate that I_m = 100 corresponds to a conversion of 99.6% at DR = .25, SR = 1.5 and of 98.5% at DR = .1, SR = 1.5. At I_m = 200, the conversion is 99.4% at DR = .1 and SR = 1.5. The dilution ratio for the majority of experimental runs on the single cylinder reactor was in the vicinity of DR = .1; at this dilution ratio and at temperatures above approximately 1400°F hydrocarbons were converted by 99+%. Carbon monoxide which requires a higher exhaust temperature for its oxidation was converted by 99% only in an experiment conducted at 1687°F and DR ≃ .3, SR ≃ 2.

Thus, conversions computed from "MIXONLY" for values of I_m obtained by using a jet orfice diameter for L_c are in approximate agreement with experimental results. In view of uncertainties in the leading multiplier for Corrsin's equation (an efficiency factor) and in the percision of high experimental conversions, the extent of discrepancy between a simulation based on entrance dimensions and experiments cannot be judged. We would expect that values of I_m based on jet orifice diameter might be high due to neglect of jet expansion beyond the inlet.

Application of Corrsin's (8,9) equation to the DuPont Model V reactor is more difficult due to the complex flow and geometry. Exhaust enters through an exhaust valve of 1.5-in. diameter which opens to 0.41 in. and closes during a 278° interval on a 720° engine cycle. The peak flow of exhaust occurring during blowdown produces a high level of turbulence, but little or no air is added (with a low pressure air injection system) to the port during this period. Thus exhaust and air tend to enter the 1.36-in. diameter port sequentially and mix only after emptying into the core of the reactor.

If we proceed by neglecting change in density, we again compute $I_m = 0.55\,(L_r^3/SL_c)$. For a free volume of approximately 230 cu in. (which excludes the volume occupied by internal baffles and heat shields), the sphere equivalent diameter L_r is 7.6 in. S and L_c depend on what we assume for the scale of turbulent fluctuation: the worst assumption being that exhaust and air mix only after assuming the dimension of the port resulting in values of L_c = 1.36 in. and S = 5.80 sq in. This assumption results in I_m = 8.0, which corresponds to conversions in the range of 80 to 90% for a stirred tank MIXONLY simulation.

If air flow were coincident with exhaust flow, a good estimate of L_c would be the valve opening, L_c = 0.41 in., with corresponding S = 7.7 sq in. This assumption predicts I_m = 14.7.

In the case where exhaust blowdown is the effective means of mixing, the change in density for gas entering from the cylinder is large at the initial exhaust valve opening but is relatively smaller thereafter. Both the pressure drop and the orifice size are changing as the valve opens and the piston moves upward to displace exhaust out of the cylinder. Critical flow will be experienced during the initial period of blowdown, during which time the instantaneous valve opening will represent the throat of a critical flow nozzle beyond which velocity will continue to increase due to expansion of the gas. The effective entering jet diameter will in this case be the dimension of an expansion cross section of a nozzle at the downstream pressure rather than the throat dimension. Hence we are justified in using the constant density analysis for I_m within the reactor provided that S and L_c reflect mixing after expansion at the inlet. To illustrate, consider the instantaneous condition where exhaust is flowing from P_1 = 30 psia to P_2 = 15 psia, which is just over critical. For a well designed nozzle, the final velocity would approach that of an isentropic expansion: it would of course be lower for flow through an exhaust valve. However, to illustrate the effect in the limit, we compute final velocity for an isentropic expansion:

$$u_2 = 223.\sqrt{c_p\,T_1\left[1-(P_2/P_1)^{\frac{\gamma_c-1}{\gamma_c}}\right]} \qquad \text{(III-[illegible])}$$

where c_p is Btu/lb°R and T_1 is °R. The value of u_2 at 1800°R (1340°F) is then [illegible] ft/sec. For a mass flow rate F_m [illegible] lb/hr through an exhaust valve of diameter D, $A_2 = F_m/\rho_2 u_2$ = .[illegible] sq in. and [illegible] $A_2/\pi D$ = .[illegible] in. The corresponding coalescence rate I_m for mixing throughout the entire reactor volume is very large, $I_m \simeq 10,000$, which illustrates that air injected at the time of blowdown in immediate proximity to the exhaust valve would likely experience a very thorough mixing with exhaust as it passes through the reactor.

As the exhaust valve opens and pressure drops, the resulting noncritical flow can be treated as flow through a convergent nozzle where the throat dimension is the effective entering jet diameter. Thus, for the maximum valve opening of .410 in., we are brought back to the mixing parameter value given previously, $I_m = 14.7$.

To summarize, the opening of an exhaust valve involves a rapid transition in I_m from a value of several thousand to approximately 15. If air in sufficient quantity is injected near the exhaust valve during blowdown, this range of mixing intensities should be experienced. If however, air enters primarily in sequence with exhaust, both air and exhaust take on the dimension of the port and mixing will proceed with I_m equal to 8.

All foregoing estimates of I_m for the DuPont Model V reactor have assumed that turbulent mixing initiated at the inlet persists throughout the entire reactor. A more conservative view would allow for a decay of turbulence, and therefore a decay in the local value of I_m in relation to volume. If for example we assume that mixing persists unabated in the core but is damped to a negligible value thereafter in the annulus, I_m values corresponding to the core volume alone would be $I_m = 3.5$ for $L_c = 1.36$ in. (port diameter) and $I_m = 6.5$ for $L_c = 0.41$ in. (maximum valve opening).

The preceeding analysis has been based solely on the flow of exhaust since air injection at low pressure is a decidedly second-order effect. A high pressure air jet would, however, exercise a significant mixing effect depending on pressure drop and jet dimension. Multiple small jets would be more effective than a single larger jet. Calculation of I_m for particular designs would follow the course outlined in the foregoing discussion of exhaust blowdown.

IV. Simulations on the Kinetics Test Reactor

"MICROMIX II" was run on conditions corresponding to the kinetics test reactor to establish whether or not microsegregation of air and exhaust had influenced the conversion data from the system.

Simulations were performed for f_m = 33 lb/hr, reactor volume V = 59.5 cu in., and entering exhaust concentrations of .02 mole fraction CO and .008 mole fraction H_2. Inlet temperatures investigated ranged from 1240°F to 1600°F. Hydrocarbons were not included in the simulations.

Simulations were run at values of the mixing parameter, I_m, of 1, 5, 20, and 100 (Figure 40). The calculations presented based on the mixing theory of Corrsin (8,9) predict an I_m in the range of 100 to 200 for the experimental reactor. This is corroborated by the fact that experimental conversion ranged up to 99%, which is consistent with an I_m equal to 100.

At high temperatures, conversions as already noted approach the limiting upper bound representing the conversion for an infinitely rapid reaction limited only by mixing. The limiting values observed in Figure 40 for carbon monoxide agree well with those determined previously by the mixing simulation "MIXONLY" for a stoichiometric ratio of 1.5 to 1 for oxygen to combustibles.

In Figures 40, 41, and 42, the solid line represents conversion in a continuous ideal stirred tank reactor, CSTR, at $I_m = \infty$. The departure of the dashed curves, representing finite levels of micromixing, from the solid curve is a measure of the error introduced by neglecting micromixing. The departure of these curves increases as temperature and conversions increase, indicating as expected that mixing becomes relatively more critical compared to kinetics at higher temperatures where resistance due to chemical kinetics is small. The important fact to observe from the simulation is that departure from a CSTR conversion at I_m = 100 is negligible at 90% conversion. Since the data that were used for determination of kinetic parameters were truncated at 80% conversion, we can be sure that the effect of micromixing on these data was insignificant.

In order to obtain a measure of the correspondence between the simulation in Figure 40 and the kinetics test data, a subset of this data has been plotted on the same simulation, in Figure 41. The data points chosen are those for which the inlet concentration for CO and the flow rate are within ±10% of the simulation condition (2% CO, 30 lb/hr exhaust, 3 lb/hr air).

The data points in Figure 41 have been corrected slightly in temperature, based on an ideal CSTR material balance and the rate equation for oxidation of carbon monoxide. In the cases of CO, however, we have an order on partial

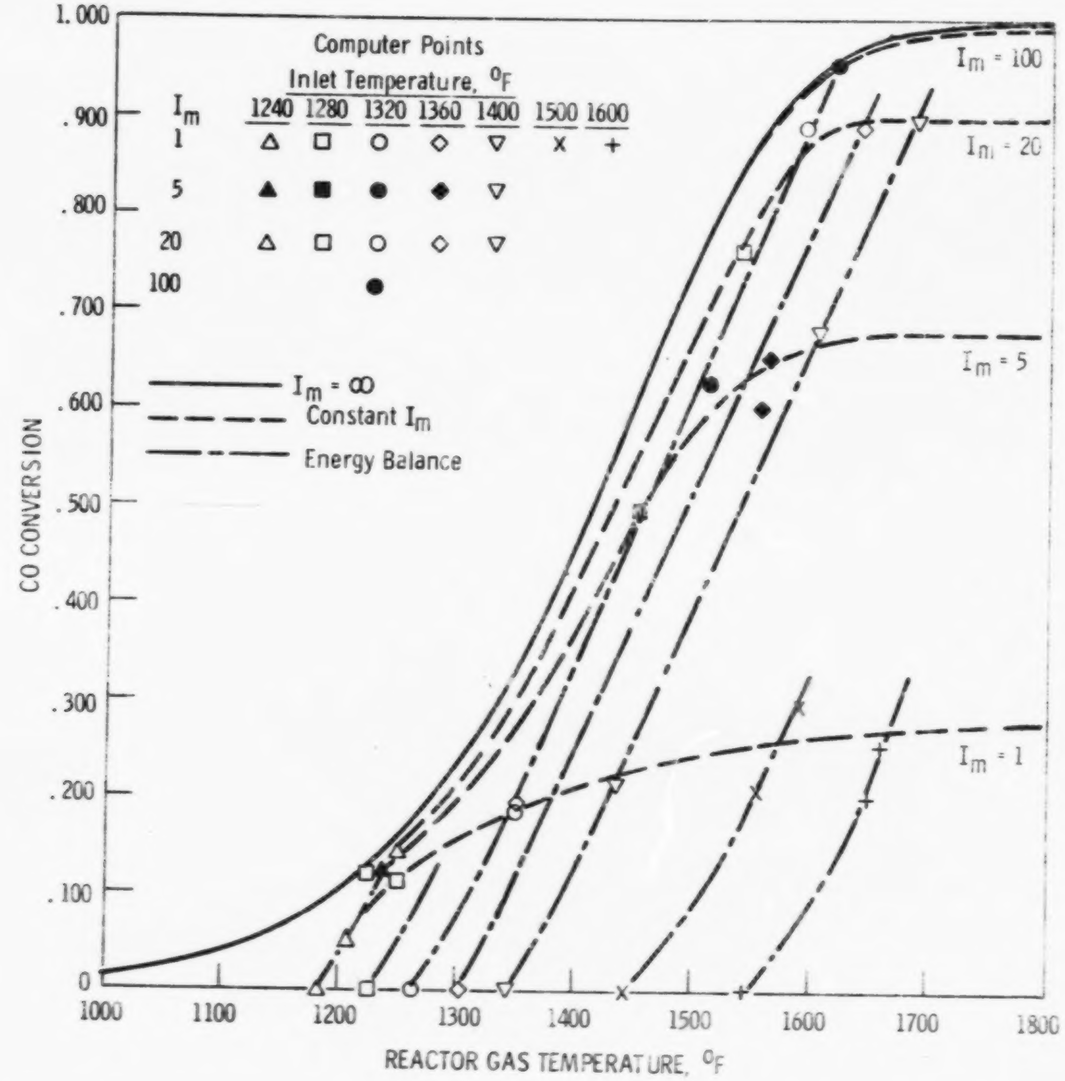

Figure 40. Simulation of CO conversions in the kinetic test reactor. Departure of cell-wise mixed conversions, I_m = 1 to 100, from the ideal CSTR, $I_m = \infty$. Points from simulation "MICROMIX II". Feed: 30 lb. exhaust/hr., CO = 2%, H_2 = .8%, air = 3 lb/hr.

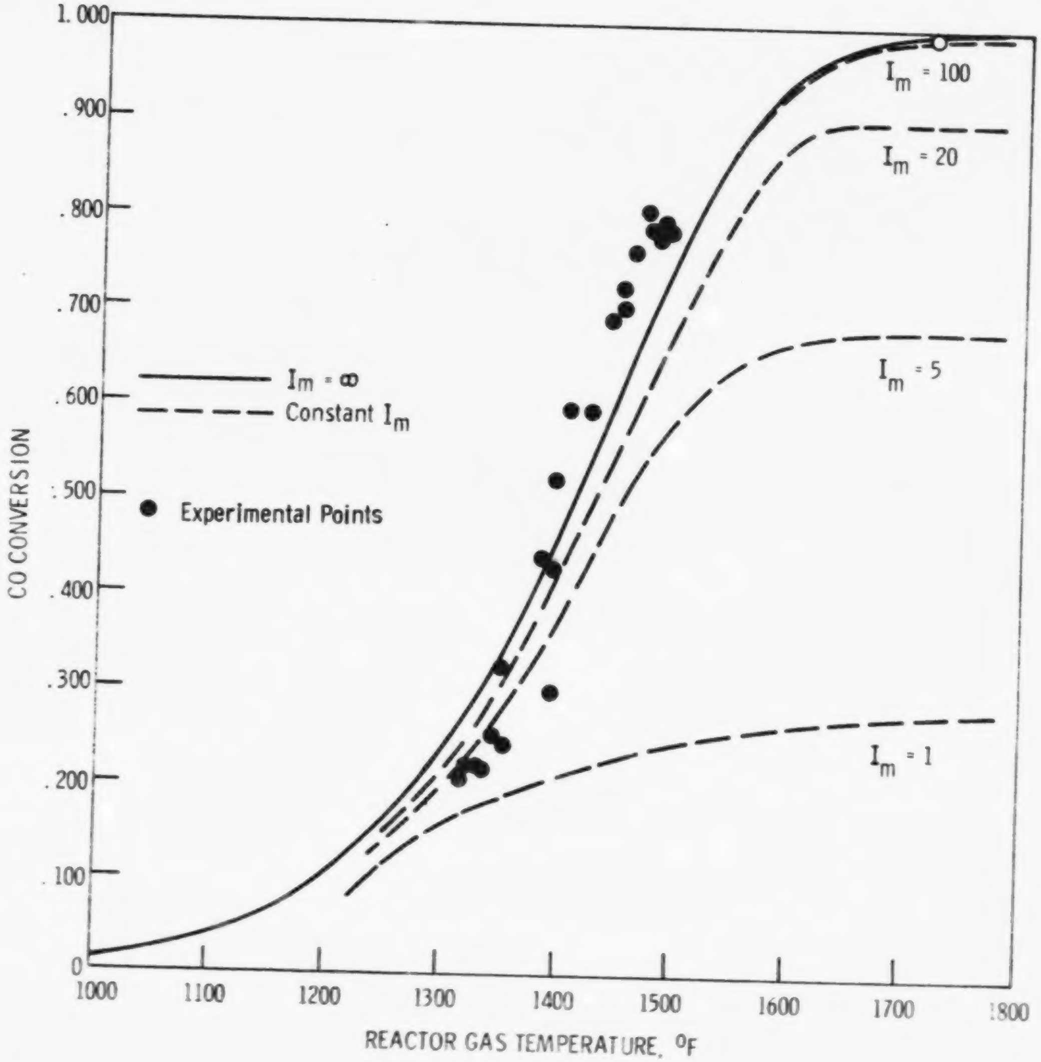

Figure 41. Experimental conversions from kinetics test data plotted on the cell-wise mixing simulation of Figure 40. Data points corrected to the simulation conditions of Figure 40.

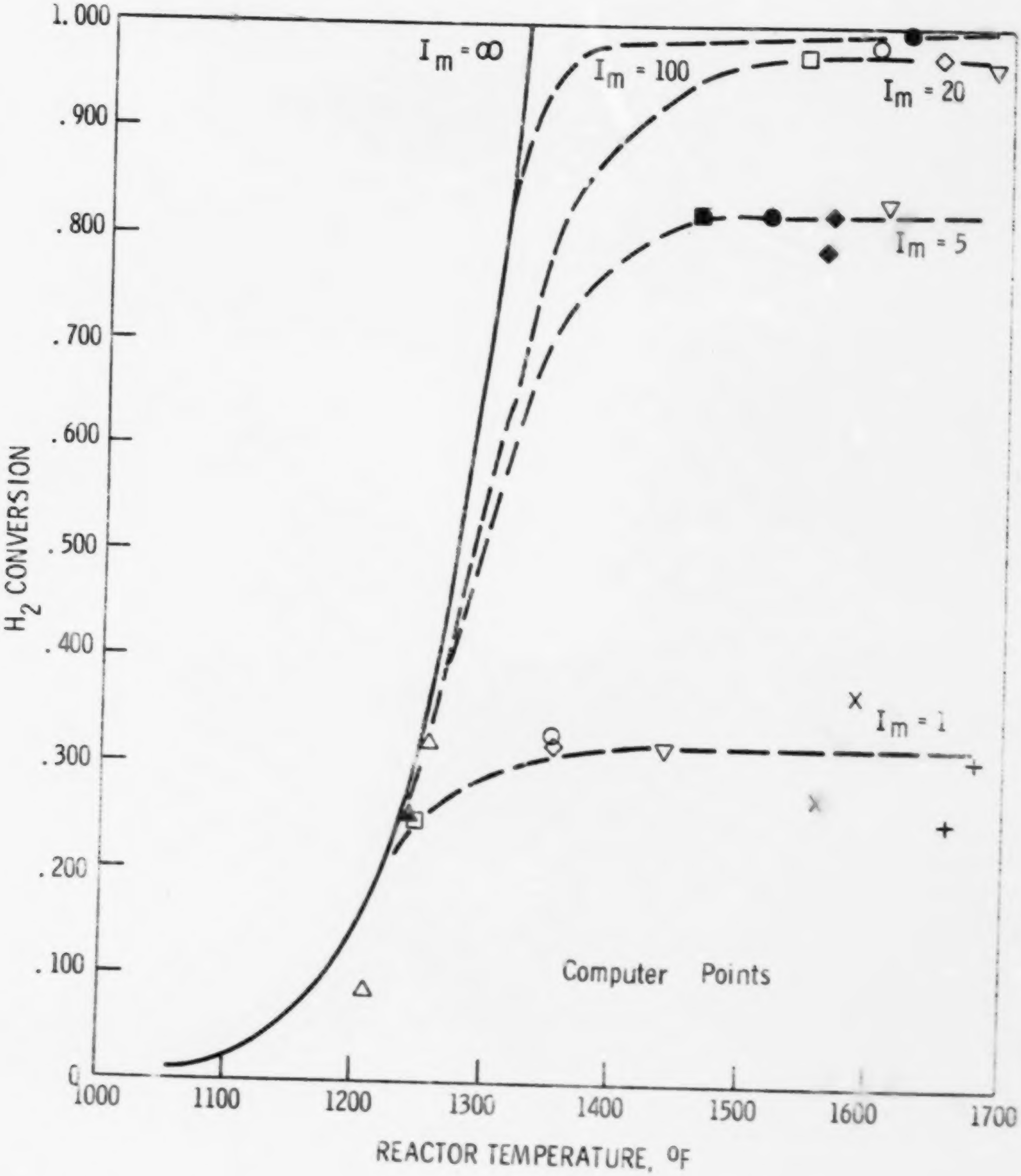

Figure 42. The effect of mixing parameter (I_m) on hydrogen conversion. Feed: 30 lb. exhaust/hr., CO = 2%, H_2 = .8%, air = 3 lb./hr.

pressure of carbon monoxide, which makes the correction easier if we correct temperature rather than conversions.

From the CSTR material balance on CO, with

$$X_{co} \triangleq (foC_{o\,co} - fC_{co})/foC_{o\,co} \quad , \tag{IV-1}$$

$$\frac{X_{co}}{(1-X_{co})^{n}} = \frac{A_{co}\ V\ P^{n}}{fo\ C_{o\,co}^{\ n-1}}\ (\frac{fo}{f})^{n}\ e^{-E_{co}/RT} \tag{IV-2}$$

For $C_{o\,co}$ = .02 mole fraction, we neglect departure of f_o/f from 1, and we define

$$A^{*} = \frac{A_{co}\ V\ P^{n}}{f^{*}\ C^{*}_{o\,co}} \quad , \tag{IV-3}$$

where f^* and $C^*_{o\,co}$ are condition on mole flow and inlet mole fraction to which we wish to correct a set of data. Then, taking the logarithm, we obtain

$$T^{*} = T + \frac{E}{R}\left[\frac{1}{\{\ln A^{*} - \ln X_{co} + n\ln(1-X_{co})\}} - \frac{1}{\{\ln\left(\frac{A_{co}VP^{n}}{f_{o}C_{o\,co}^{\ n-1}}\right) - \ln X_{co} + n\ln(1-X)\}}\right] \tag{IV-4}$$

The data in Figure 41 indicate a steeper rise in conversion along with temperature than is indicated by the simulation, even at $I_m = \infty$. This is a property of the subset of data that are plotted, since correcting all data produces a scatter diagram about the ideal CSTR line. However, we note that the experimental data most nearly represented by the simulation condition indicates less of the trailing off to high temperature (which is indicative of mixing limitedness, low activation energy, or high reaction order) than does the $I_m = \infty$ bound for the least-squares kinetics.

Besides the 22 kinetics data points in Figure 41 (which are truncated between 20 and 80% conversion), the high temperature test for CO run at $C_{o\,co}$ = .0525, EXHAUST = 30 lb/hr, AIR = 9 lb/hr, was corrected by the method indicated from 1087° to 1,107° for 99% conversion. Agreement with the simulation is good. Likewise, if we look back to the experimental point • in Figure 2 , which is the same high temperature run corrected by means of a zero order rate equation, we again observe quite good agreement. However, if we observe the point plotted on simulations for first or second order (Figures 36 and 37), we observe a very large discrepancy. Along the $I_m = \infty$ bounds, 90% conversion is reached at 2770°F for order 1, and 3000°F for order 2. This demonstrates both the difficulty in attaining high conversions for high order reactions and the necessity for near zero order to match the experimental observation for oxidation of carbon monoxide.

Results for hydrogen at single-cylinder reactor conditions (Figure [illegible]2) indicate that bounds on conversion set by the mixing parameters are higher than those observed for carbon monoxide. The explanation for this is that hydrogen reacts at lower temperatures, where the excess of oxygen is larger due to the slight oxidation of carbon monoxide. When compared with results from "MIXONLY," the limiting conversions for hydrogen lie between those for a stoichiometric ratio for oxygen to hydrogen alone and for oxygen to hydrogen plus carbon monoxide.

V. Simulations on the DuPont Model V Reactor

Simulations were run on "MIXONLY," "MICROMIX II," and "MICROMIX POF" programs using both steady and cyclic inlet flows for the purpose of identifying the mixing parameter values (for flow pattern and the mixing intensity I_m) which characterize this exhaust reactor. By bracketing the mixing performance of exhaust reactors as a class between the optimized mixing of the single cylinder reactor and that of the Model V, it is possible to interpolate with some degree of confidence to reach conclusions regarding the attainable performance of an improved practical device.

Two classes of experimental results were available from the Phase I study to form the basis for simulations: tests where air dilution fraction was varied for a constant exhaust feed; and tests where exhaust temperature was increased to achieve a level of maximum conversion by retarding the engine spark while holding other inlet properties essentially constant.

Patterns of flow for the Model V simulations are shown in Figure 45, along with values of the key parameters. Changes in these and other parameters are discussed in the text. In the patterns numbered 2, 4, and 5, the modules shown represent four engine exhaust ports, a reactor core, and an exit annulus. In pattern number 3, the annulus is divided and the parts assigned different rates of heat loss.

A. MAXIMUM CONVERSIONS FOR INSTANTANEOUS REACTION—"MIXONLY POF"

Simulations were run to parallel CRC experiments on the DuPont Model V reactor using "MIXONLY POF" (Table III). In these, the experiment which indicated a limiting high temperature conversion of 92% was used as a bench mark to establish values of the mixing parameter, I_m, subject to six conditions (plug flow, five tanks in series, and one stirred tank at assumptions 1 and 2 of Table III). These values of I_m were then used to predict conversions for two other sets of experimental conditions, which dictated the stoichiometric ratio SR and dilution ratio DR parameters used in the simulations.

The two assumptions of Table III differ in the amount of combustible which is considered to depend on mixing for reaction. The uncertainty is introduced because of a measurement showing [illegible] oxygen in the entering exhaust, which if actually present would have first claim on combustibles because of its premixed condition. The first calculation assumes that this oxygen measurement was spurious and should be zero, thereby causing all the combustibles to depend on injected air for oxidation. The conversions compared in this case are for the total combustible content. The second calculation assumes that the measurement is correct and that the combustible corresponding to it

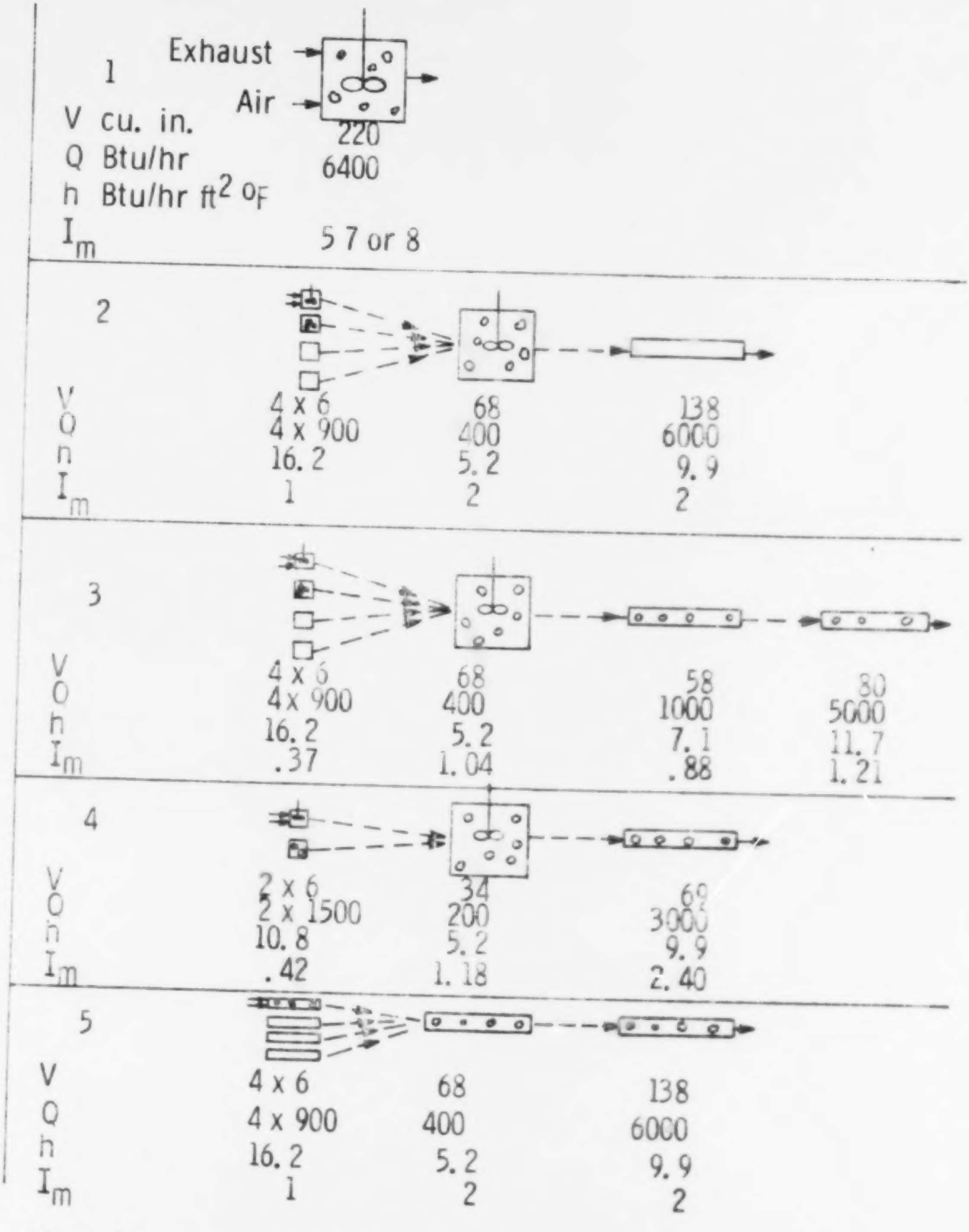
1
Exhaust
Air
V cu. in.
Q Btu/hr
h Btu/hr ft^2 °F
I_m
220
6400
5 7 or 8
2
V
Q
h
I_m
4 x 6
4 x 900
16. 2
1
68
400
5. 2
2
138
6000
9. 9
2
3
V
Q
h
I_m
4 x 6
4 x 900
16. 2
.37
68
400
5. 2
1. 04
58
1000
7. 1
.88
80
5000
11. 7
1. 21
4
V
Q
h
I_m
2 x 6
2 x 1500
10. 8
. 42
34
200
5. 2
1. 18
69
3000
9. 9
2. 40
5
V
Q
h
I_m
4 x 6
4 x 900
16. 2
1
68
400
5. 2
2
138
6000
9. 9
2

Figure 43. Patterns of flow run to simulate the DuPont Model V reactor.

TABLE III

COMPARISON OF HIGH TEMPERATURE EXPERIMENTAL CONVERSION WITH "MIXONLY POF" SIMULATIONS OF MIXING WITH INSTANTANEOUS REACTION

EXPERIMENTAL INLET CONDITIONS					EXPERIMENTAL CONVERSIONS, X			Assumption 1		Assumption 2	
CO %	H_2 %	HC ppm	O_2 %	AIR "DR"	Total Combustible	CO	Pattern of Flow	"SR"	I_m	"SR"	I_m
*** Test 308 used to establish mixing parameter values, I_m , ***											
1.91	0.52	820.	0.65	.097	.884	.82		1.20		1.93	
							pf		3.7		2.5
							5st		4.5		2.9
							1st		11.4		4.3
*** Simulations of conversions at [illegible] test conditions using the same I_m^s. ***											
									"X" TOTAL COMB.		"X" CO
2.84	0.83	770.	0.5	.093	.831	.75		.85		1.09	
							pf		.769		.734
							5st		.718		.700
							1st		.695		.671
3.08	1.20	790.	0.5	.192	.952	.93		1.55		1.92	
							pf		.970		.891
							5st		.950		.859
							1st		.932		.825

ASSUMPTIONS:

Under assumptions 1 and 2, stoichiometric ratio, SR, is computed in two different ways.

(1) Oxygen in injected air is ratioed to total combustible.

(2) Oxygen in injected air is ratioed to the combustible which exceeds oxygen in exhaust.

These alternatives are presented because of uncertainty for the validity of the reported oxygen concentration in exhaust. PATTERN OF FLOW: pf - plug flow; 5st -five stirred tanks; 1st - one stirred tank.

is removed from dependence on mixing. In this latter case, "MIXONLY POF" conversions are compared directly with experimental conversions for carbon monoxide, since the amount of hydrogen plus hydrocarbon is nearly equivalent to the oxygen measurement on the exhaust.

The results for either assumption indicate a proper trend but not a close agreement.

B. COMPARISON DILUTION RATIO ON CHANGES IN AIR

The experimental data on effect of dilution ratio DR, or air injection fraction, is shown by the solid lines in Figures 44 and 45. Starting at a combustible content of nominally 4.5% CO and 320 ppm hydrocarbon, carbon monoxide was reduced by approximately 95% to 1/4% and hydrocarbon by [illegible] to below 10 ppm. Maximum conversions were reached at dilution ratios of [illegible] to [illegible], where the increased probability of mixing and greater mass action from oxygen content (at least for hydrocarbon, which has a half order rate dependence on oxygen) produced their greatest beneficial effect before being counteracted by temperature drop associated with excess cold air.

The hysteresis shown by the experimental data in Figures 44 and 45 results from heating of a cold reactor versus cooling of a hot reactor. This behavior results from changes in heat loss and in the "initial" condition which establishes which of possibly several operating points will be assumed in relation to different combustible species and different regions of the reactor. For a single reactant in an ideal backmix reactor ($I_m = \infty$), ignition and hysteresis have been discussed in detail by Schwing (29). Further discussion on ignition is given in a later section of this report dealing with reactor warm-up. However, the more cumbersome mixing simulations treated here were not used to investigate ignition phenomena.

Hydrogen was not measured in the dilution ratio experiments, however it was included in the simulations because of its coupled thermal contribution. An inlet concentration of 1.8% H_2 was chosen based on a 4/10 ratio to inlet CO. This is approximately the average ratio observed for analyses performed on exhaust from the single cylinder test engine; it is equivalent to the equilibrium ratio for the water gas shift reaction at 2100°F assuming equal concentrations for CO_2 and H_2O.

The simulations on the effect of dilution ratio for the Model V were run both on the stirred tank cell mixing program "MICROMIX II" (Figure 44) and on the pattern-of-flow program "MICROMIX POF" (Figure 45) for the module network number 2 shown in Figure 43. The modules represent four ports of [illegible] cu in., a [illegible] cu in. stirred tank core, and a [illegible] cu in. plug flow annulus. Average exhaust flowrate matches the test rate of [illegible] lb/hr. Total reactor heat loss exclusive of ports, obtained from a typical "WARM-UP" simulations on the DuPont

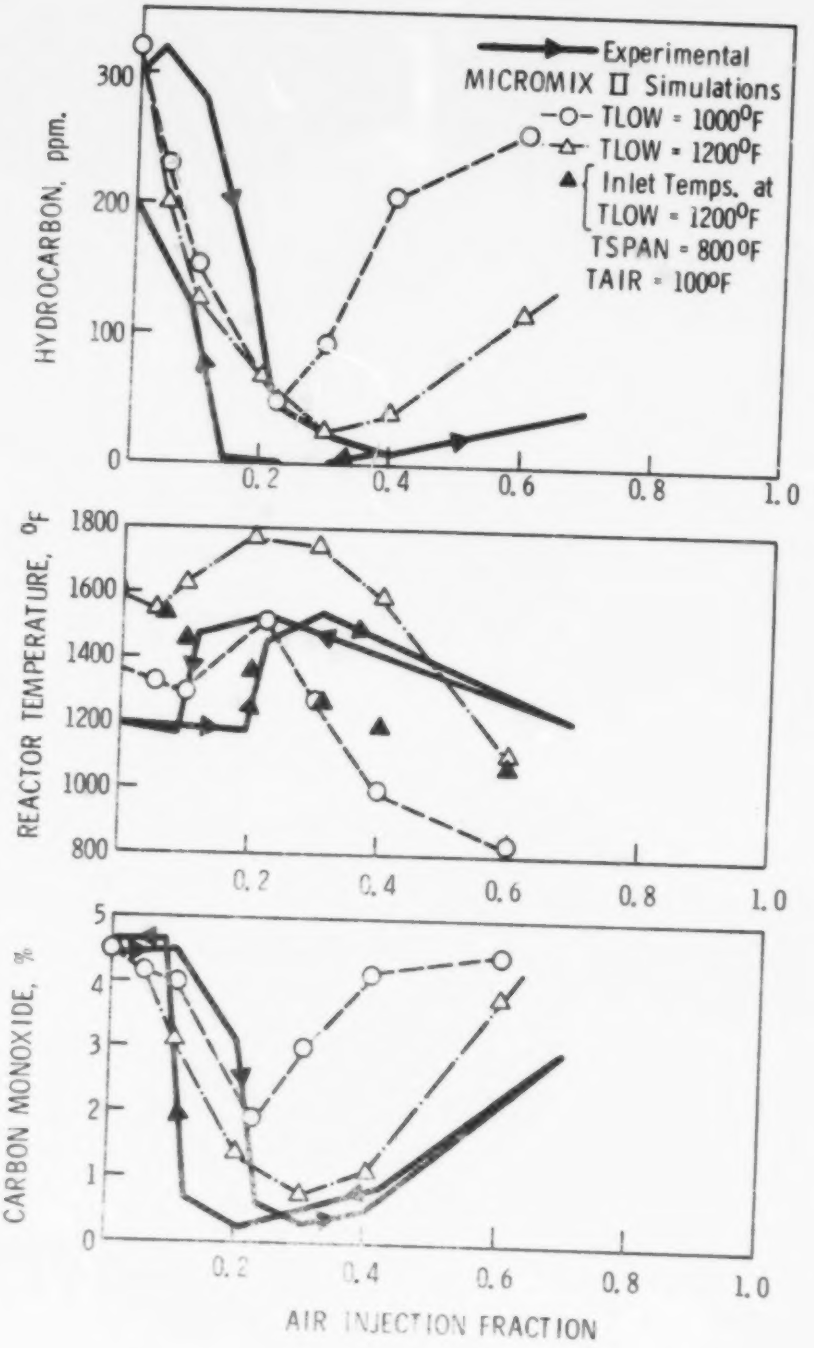

Figure 44. Stirred-tank simulation of the effect of air injection fraction at a mixing parameter value of $I_m = 8$. Experimental values are from the DuPont Model V reactor operated at 115 lb. exhaust per hour and at 12.3:1 air fuel ratio.

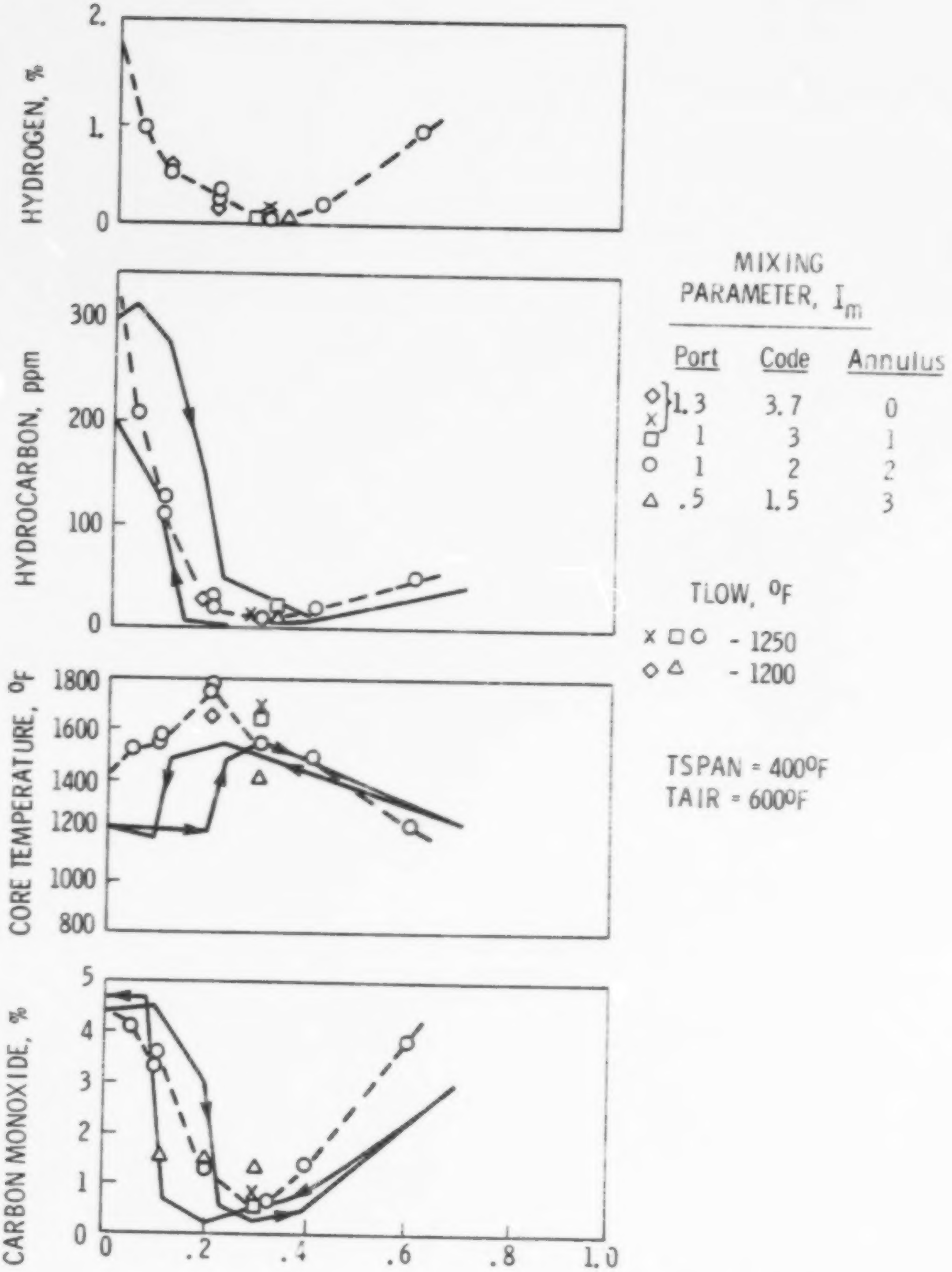

Figure 45. Simulation of the effect of air injection fraction using the pattern of cell flow shown in Figure 43, item 2.

Model V, was 6400 Btu/hr. In the POF simulation, heat loss was distributed: 900 Btu/hr for each port; 400 Btu/hr for the core; and 6000 Btu/hr for the annulus. Inlet properties were cyclically varied in accordance with the characteristic patterns described previously; temperature spans used were TSPAN = 800°F for "MICROMIX II," and TSPAN = 400°F for "MICROMIX POF."

The mixing parameter was set at $I_m = 8$ for the stirred tank simulations and $I_m = 5$ overall for the pattern of flow simulations. The mixing parameters for modules in POF were variously distributed as shown in Figure 45.

Trends in simulated conversions for increased air dilution ratio are in general agreement with the experimental results. The apparent lag in experimental conversions at low dilution ratio is, like hysteresis, an ignition phenomena which was not investigated in the simulation. The slope with which the combustible species disappear as the air fraction (DR) is increased indicates that blending of exhaust from successive firings of cylinders with air entering from all cylinder ports is quite complete. More specifically, under favorable lightoff conditions conversions tend to follow their stoichiometric limit leading to complete conversion at an air injection fraction of approximately .15, although leveling off prior to that point. Thus, even though air injection is maldistributed in time and in position (during the time that exhaust flows into the reactor from a given cylinder, air is flowing primarily from the three nonactive cylinders), no large amount of air is lost. This suggests that the core of the reactor, where blending must occur, is quite well mixed on a macro scale.

Poorer agreement is indicated between the simulations and experiments for the reactor gas temperature. This may be caused by a number of factors, all tied in with the fact that the single "time average" tempetature measurement at the core center line will bear a different relationship to either simulated or measured conversions depending on the distribution of temperatures and conversion throughout the reactor. First, the "time average" temperature measured by the thermocouple at the center line will tend to be low due to inadequate weighting of the high temperature-high flow exhaust pulses entering at blowdown and over weighting of air flow at low temperature entering over a longer period of time. The severity of this effect will depend on the placement of the thermocouple in relation to one of the entering exhaust ports. Then, when reaction begins only part of the resultant temperature rise will be evidenced in the port, the part depending on the amount of reaction in the port as opposed to the amount in the annulus that follows. Finally, at high dilution ratio, the decline in simulated temperature is greater than in the experimental due to a more rapid decline in conversions. This relates to the distribution of temperature, with persistence of a high temperature fraction favoring persistence of conversion as air injection increases. For hydrocarbon, persistence is evidenced in the "MICROMIX POF" simulation where backmixing is reduced below that of the stirred tank. Running the "POF" simulation at a higher temperature span for the entering exhaust would further prolong conversions toward higher air fractions.

The "POF" simulations were run at a lower temperature span and a lower average temperature for the entering exhaust. Average inlet exhaust temperature for "TLOW" = 1200°F is approximately 1600°F for the "MICROMIX II" simulation with TSPAN = 800°F, and is 1400°F for the "POF" simulation with "TSPAN" = 400°F. The larger temperature rise shown in Figure 45 for "POF" is the result of a low rate of heat loss from the core and use of a higher inlet air temperature (air was assumed to be preheated in the injection system to 600°F rather than entering at 100°F).

In the "POF" simulation shown in Figure 44, points are plotted for four different distributions of I_m among the reactor modules. The three points run at "TLOW" = 1250°F and DR = .5, (x, □, and o), represent a sequence from earlier to later mixing for flow through the reactor. Only the conversion of carbon monoxide is appreciably affected by this change, and it is found to be maximum (lowest CO concentration) at the middle distribution. This is a small indication of counterbalancing effects between an advantageous increase in residence time after mixing versus a disadvantageous coalescing of cells prior to adequate blending and backmixing of maldistributions. It should be recalled here that the "plug flow" section of the POF simulation does involve some backmixing of material depending on the size of the slugs (slugs in this instance represented 1/16 of an engine flow cycle and roughly 6 slugs were contained in the plug flow module at a given time).

The simulations that were run on dilution ratio do not attempt either to optimize the fit with the experimental data or to provide an extensive mapping of sensitivity to parameters. The two simulations run illustrate that higher conversions are obtained at lower dilution ratio and lower average inlet exhaust temperature for a POF representation of the Model V than for a "MIXONLY" representation. Since it is desirable to optimize such a trend, it would appear useful to run further simulations in this area. Considering the maldistribution of inputs, the principle of a blending volume as represented by the stirred tank core simulation followed by a "plug flow" exit section to eliminate early departure is a sound design feature (which is already incorporated in the Model V design to some extent). Simulations could be run on the relative size of these regions as one means of optimizing a design.

C. APPROACH TO A HIGH TEMPERATURE LIMIT ON CONVERSION OF CARBON MONOXIDE

Experiments in which the temperature of entering exhaust was increased by retarding the spark of the engine while at the same time holding other inlet properties essentially fixed, resulted in carbon monoxide conversions which increased from near zero to a maximum value of less than 100 in intervals of approximately 200°F increase. Conversions remained at an essentially constant maximum level even though temperature was further increased by as much as 250°F.

Inlet conditions for one such experiment were chosen as the basis for a series of simulations conducted for different patterns of flow using the

"MICROMIX POF" program. The purpose of these tests was to determine the effect that various combinations of mixing parameter I_m and flow pattern had on the approach to a high conversion, and to establish if possible a good correspondence between the experimental data and one particular pattern of flow.

The test chosen (test 3C8) was run for a mass flowrate of 117 lb/hr exhaust at 1.91% CO, 0.52% H_2, 0.65% O_2, and 820 ppm hydrocarbon; air dilution ratio was nominally DR = 0.10. Temperature was again measured at the reactor core centerline. As mentioned before, this temperature will not reflect the temperature rise associated with reaction occurring downstream from the core.

In order to portray the important differences between these simulations clearly without becoming lost in detail, we will first discuss only the highlights of each and return later to point out several of the interesting but less important features.

The five simulations in Figures 46, 47, 48, 49, and 50 were run on the respective flow patterns given in Figure 43. In Figure 46, results are shown for a stirred tank simulation (MICROMIX II) performed at values of I_m equal to 5, 7, and 8. The high temperature conversion at $I_m = 7$ best corresponds to the experimental conversion of 82% for carbon monoxide. A value of $I_m = 8$ was obtained based on Corrsin's equation with L_c equal to the port diameter.

Experimental conversions for hydrocarbon and hydrogen were 96% and 100%. The stirred tank simulation at $I_m = 7$ and a reactor temperature of 1720°F predicted [illegible] conversion for hydrocarbon and 97% for hydrogen (not graphed). The discrepancies in these values were felt to relate to allocation of the 0.65% oxygen that was reported to be contained in the entering exhaust. If this oxygen were consumed preferentially by hydrogen and then by hydrocarbon, all hydrogen would be consumed and hydrocarbon would be reduced to 270 ppm. Accordingly, a series of simulations were run on exhaust input containing 1.91% CO as before but at 0.% H_2, 0.% O_2, and only 270 ppm hydrocarbon. The high temperature conversion for the smaller amount of hydrocarbon was in this case 0.87, which amounts to 96% of the total hydrocarbon. The success of this strategy prompted the "preoxidized" inlet condition with 0.% H_c and 0.% O_2 to be used for the remaining simulations. Whether this is justifiable depends largely on the precision of the 0.65% O_2 exhaust measurement (which is in doubt). This points out the general difficulty that exists in predicting conversions for small amounts of reactive combustibles (hydrogen and hydrocarbons) where a small but uncertain amount of oxygen characteristically enters with the exhaust, and the distribution of this oxygen is unknown.

The simulation approach to the maximum conversion for CO in the stirred tank was decidedly more gradual than the experimental (Figure 46). Particularly when cyclic input was used, a considerable conversion persisted at low average temperature. The augmented conversion for the cyclic input over the steady input is due mainly to the persistence of a high temperature region in

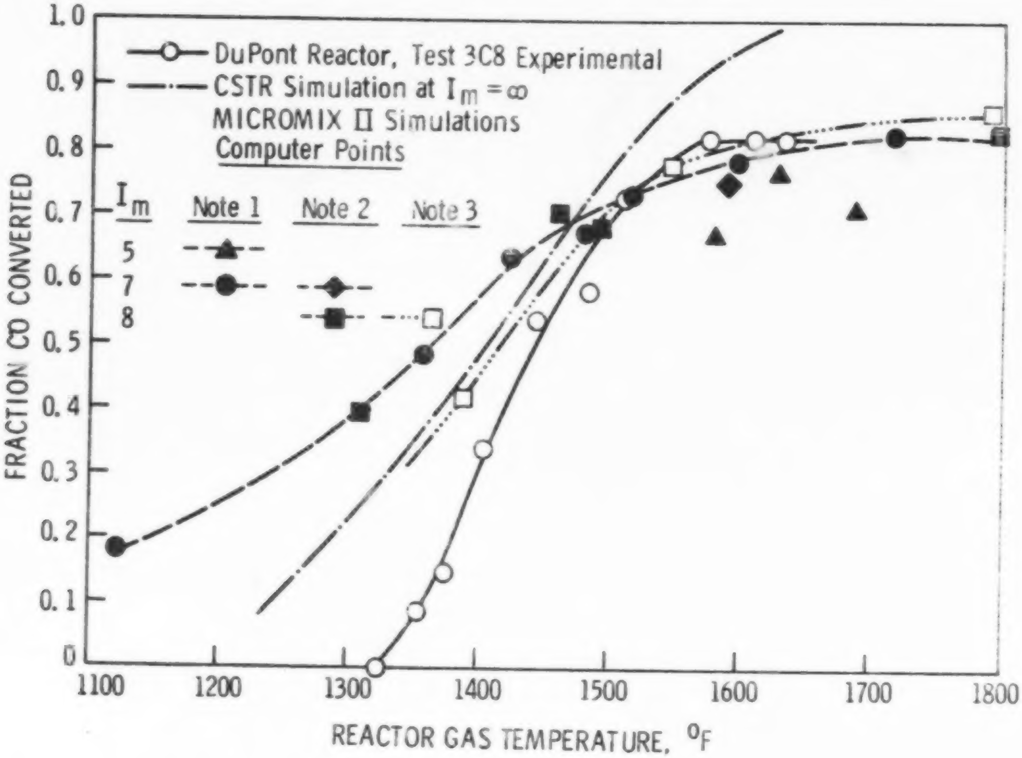

Figure 46. Simulation of the approach to high-temperature mixing-limited conversion for CO using a stirred tank cell mixing model. Input: exhaust - CO = 1.9%, H_2 = 0.52%, O_2 = 0.65%, HC = 820 ppm. Air dilution ratio, DR = .10 (air/exhaust).

Note 1: Cyclic inlet properties about the average values measured.

Note 2: Cyclic inlet properties at average inlet exhaust mole fractions of 1.91% CO, 0.0% H_2, 0.0% O_2, and 270 ppm HC.

Note 3. Steady mass-averaged inlet properties from each cylinder. Flow pulses due to timing of cylinders are retained.

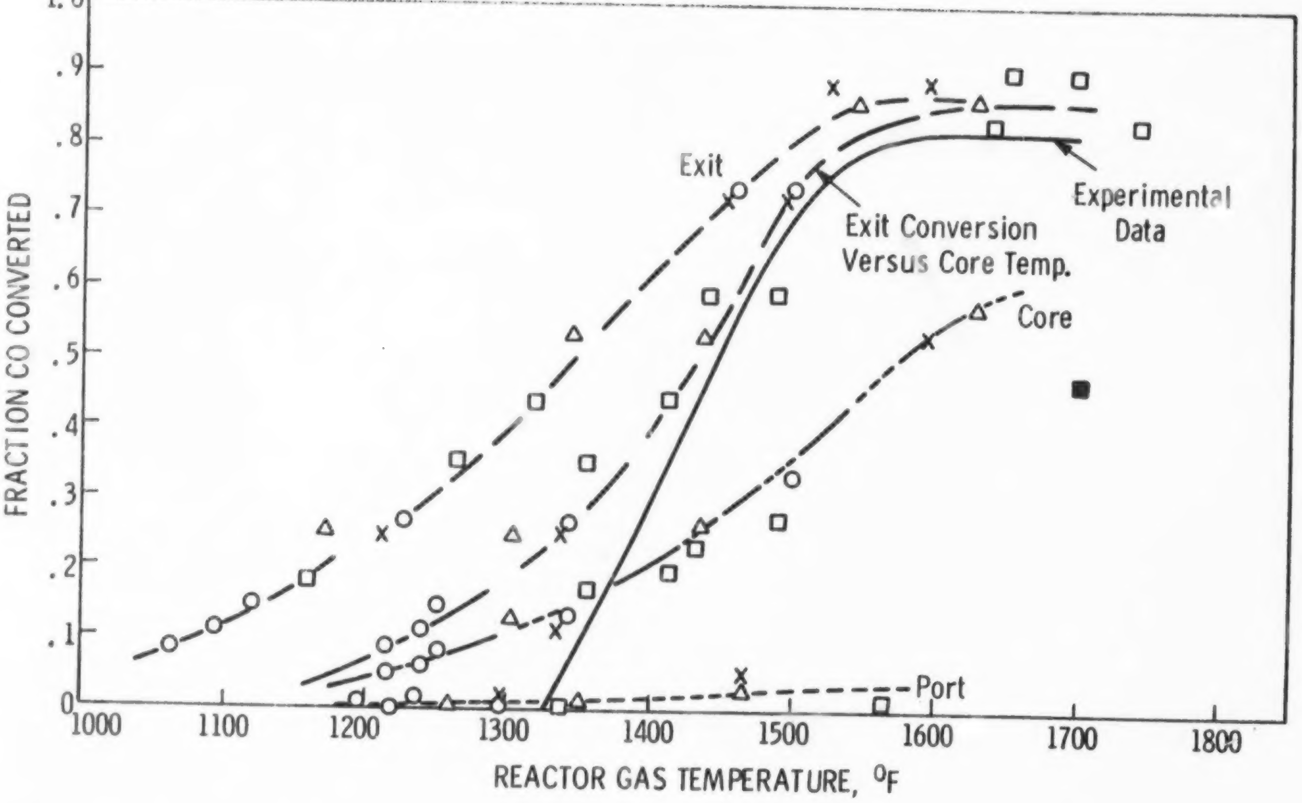

Figure 47. Simulation of the approach to high-temperature conversion for CO using the cell pattern of flow shown in Figure 43, item 2. Input: exhaust - CO = 1.9%, H_2 = 0.0%, O_2 = 0.0%, HC = 270 ppm.

Exhaust temperature span, "TSPAN": 800 °F - △ ; 4000 - □■ ; 0° - ○. 0° and $T_{EX} = T_{AIR}$ - ⊕
Distribution of the mixing parameter, I_m. [1.3, 3.7, 0.] - △□○⊞✱ [1., 2., 2] - ■●
Hydrogen in feed - ⊞

Points ✱ are for steady uniform feed.

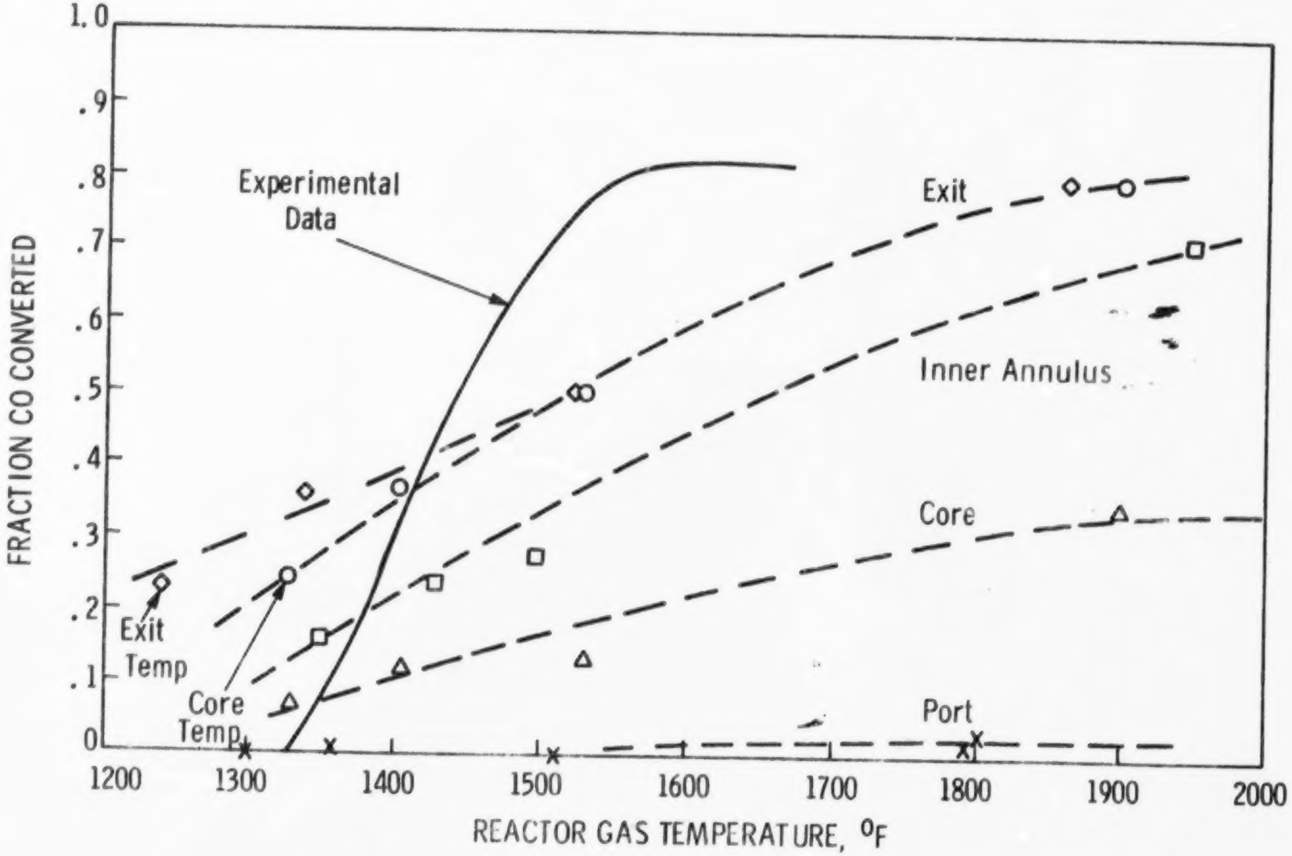

Figure 48. Simulation of the approach to high-temperature conversion for CO using the cell pattern of flow shown in Figure 43, item 3. Input: exhaust - CO = 1.9%, H_2 = 0.0%, O_2 = 0.0%, HC = 270 ppm.

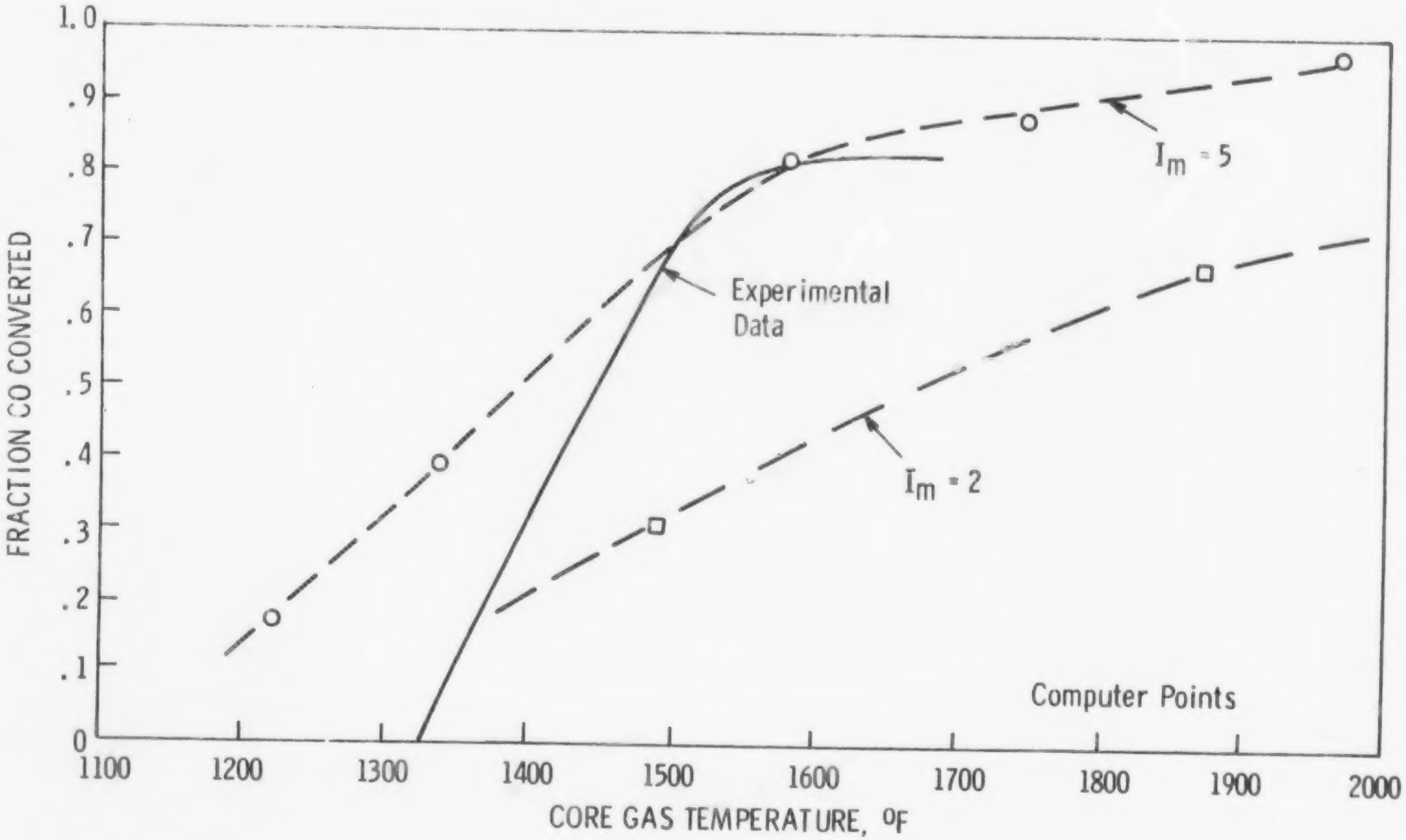

Figure 49. Cell mixed plug flow simulation (see Figure 43, item 5). Air flow ratioed to exhaust.

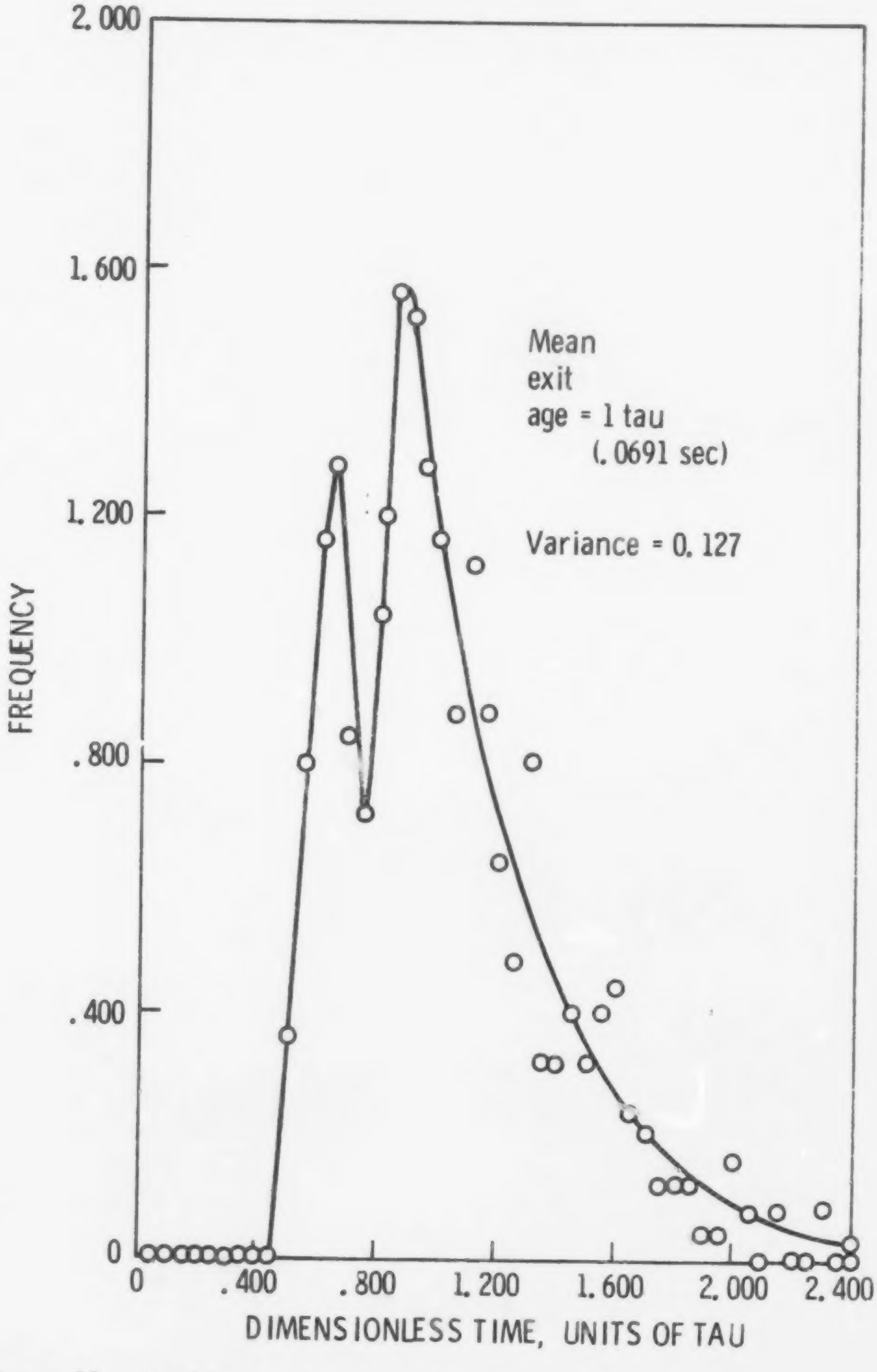

Figure 50. Residence time distribution for the simulation shown in Figure 47 and item 2, Figure 43.

the cell temperature distribution. However, even when inlet properties are steady a difference still exists which must be explained by the relationship that measured temperature bears to the distribution of reaction in the reactor. The behavior that we would most desire to explain is the transition in conversion from zero to maximum in 200°F: an offset in temperature can be more easily accepted if we consider the scatter in conversions observed about the least squares correlation of kinetics.

The simulations shown in Figures 46, 47, 48, and 49 represent a progressive shift from stirred tank to plug flow behavior. In Figure 47, the module network, the bias of I_m toward early mixing, and the high rate of heat loss that is exacted throughout the plug flow exit section cause approximately half the total reaction to occur in the stirred tank core. The combination of these factors causes the conversions for cyclic input to be shifted toward the experimental curve. Further change toward plug flow is represented in Figure 48, where a smaller heat loss in the leading section of the annulus and proration of I_m strictly by volume causes more reaction to occur in the plug flow sections. In this simulation and the one incorporating only plug flow elements (Figure 49), the increase in conversion with temperature is much more gradual, representing a distinctly different character than the experiment result. Hence on an overall view, the rapid increase in experimental conversions with temperature is best represented by the pattern-of-flow type simulation least removed from the stirred tank.

The "best" simulation (Figure 47, "POF" number 2 in Figure 45) still represents some departure from the experimental result; and the source of the discrepancy remains difficult to explain because of the larger number of factors bearing on the problem. The worst departure from the experimental observation is below 20% conversion, which it is interesting to note is a region that was truncated in developing the kinetics. However, to provide direction for future work we note that this "best" fit is given by a relatively small stirred tank core experiencing only negligible heat loss follows by an annulus which experiences a high rate of heat loss. In this arrangement, it can be argued that partial reaction in the core acts as a triggering mechanism to overcome the heat loss in the annulus. That is: partial conversion in the small core guarantees a rise in temperature since heat loss is small; temperature tends to decline in the annulus but reaction continues toward completion to some extent depending on the temperature extent upon entering and the extent to which heat of reaction forestalls quenching: thereby a partial conversion and modest temperature rise in the core may be amplified to a greater or lesser extent in the annulus depending on the influence that is exerted by the heat balance. The tendency for reaction in the core to influence CO oxidation in the annulus also depends on the amounts of hydrogen and hydrocarbon that are present to boost the temperature in the core without necessarily reacting the carbon monoxide, which depends on the operating point attained by the stirred tank core. A smaller stirred core volume would tend to raise the temperature at which triggering occurred; and a higher rate of heat loss from the annulus would increase the important of a triggering effect. Ignition in the stirred core would again depend on initial condition; this is not true of a plug flow section where an entering element of flow experiences no direct influence due to what entered earlier.

Balanced against the thermal triggering effect just described, we have the general tendency in moving from stirred tank plug flow behavior for reaction to be spread over a wider range of average temperature as the variance in entering temperature is allowed to persist due to lesser backmixing.

The residence time distribution for the "best" simulation is shown in Figure 50. The double peak is associated with the cyclically fluctuating inlet flow; specifically the high rate of flow during overlap of exhaust strokes for cylinders 3 and 5 causes early departure for a fraction of the cells in the reactor, thereby producing the early peak shown in the RTD. The variance for the RTD is 0.127, which corresponds to the variance for eight equal sized tanks in series. This is one measure of dispersion, which however will be low in this instance since the RTD for cells as computed ignores the axial dispersion that is implied by coalescence of cells within slugs in the plug flow module.

The distribution of reaction for carbon monoxide in the "best" simulation (Figure 47) indicates that less than 5% of total conversion occurs in the ports, something over 50% occurs in the core and the remainder occurs in the annulus. Hydrocarbons, subject to the assumption that oxygen in entering exhaust preferentially oxidizes H_2 and HC, was converted by approximately 90% in the core. High core conversions have been established by experimental measurements (25), which indicate 60% and higher conversions of CO in the core and 80% and higher conversion of hydrocarbon depending on dilution ratio.

The distribution of temperatures in Figure 47 indicates that the exit temperature is characteristically 100°F lower than the core temperature. This agrees with Blenk's (3) measurements for a low inlet CO concentration. At higher levels of entering CO, the experimental temperature difference increases to 250°F (3,25); which was not indicated by the POF simulations. However, temperature distribution becomes highly sensitive to the distribution of reaction through the reactor as combustible concentrations increase. Insufficient data were obtained to establish any detailed correspondence with reactor temperature distributions. However, considering that temperature rise may be the best available indication of local conversions within a reactor, more careful attention should be given to this facet of reactor studies in future coordination of POF-type simulations with experimental design. This would contrast with the prevailing philosophy in the current effort, which was to treat conversions primarily on an entrance to exit basis. Some caution should be exercised in heading too far in the other direction (of identifying physical parts with simulation modules), since the entire approach to modeling represents a very profound idealization as compared to the complexity of any real reactor.

Other changes which were made in running the POF simulation (see Figure 51 and keyed points in Figure 47) involved the exhaust temperature span and cyclic versus steady input. At low and intermediate temperature and conversion levels, conversion was enhanced by increasing the temperature span. At high temperature (1460°F entering exhaust), the conversion was slightly lower for TSPAN = 600°F than for an entirely uniform inlet flow, temperature and concentration. At both 74% and 25% conversion levels, the use of cyclic flow and concentration versus steady flow and concentration was shown to have a negligible effect when variance in entering temperature was zero (i.e., TSPAN = 0 and $T_{AIR} = T_{EXHAUST}$).

Distribution of the mixing parameter was changed in the simulations of Figure 47 from $I_m = (1.5,3.7,0)$ to $I_m = (1,2,2)$ for port, core, and annulus, respectively. Pairs of points (○,● and □,■) that are comparable except for this change exist at reactor gas temperatures of ~1100°F and ~1650°F, and in both cases a high conversion is predicted by the distribution (1,2,2). This is felt to be true primarily because of the unproductive coalescences which occur in the port, where the very small size of the module and essentially sequential entry of air and exhaust prevent any significant blending of air and exhaust cells.

Hydrogen reintroduced into the inlet feed (Figure 46) along with 820 ppm hydrocarbon and 0.65% oxygen appears on the basis of two sets of points to shift the conversion curves to a more horizontal position, contrary to the behavior desired to match the experimental curve.

The simulation of a half reactor assuming symmetry (Figure 52) is similar to the "best" simulation, but requires a noticeably greater temperature increase to raise the CO conversion. This is in part due to proration of I_m strictly according to module volumes, which places a greater emphasis on the large plug flow exit section than on the stirred core and therefore tends to reduce the effectiveness of backmixing.

D. SENSITIVITY TO RESIDENCE TIME DISTRIBUTION AND MICROMIXEDNESS (I_m)

Results of "MIXONLY" simulations (Tables I and III) demonstrated that generally higher conversions result from plug flow residence time distributions due to the avoidance of early cell departures. If we consider sufficiently high temperatures, the same conclusion would be reached using the POF simulations. However, at normal operating temperatures this view must be modified.

In Figure 53, the sensitivity of conversions for CO to change in I_m is considered for the "best" simulation (Figure 47 and Figure 43, item 2) and for the all-plug-flow simulation of Figure 49. Two inlet temperature levels are considered: $T_{EXHAUST}$ = 1663°F and 2013°F. The first is near the upper limit of entering exhaust temperatures found in practice and the second outside the normal operating range.

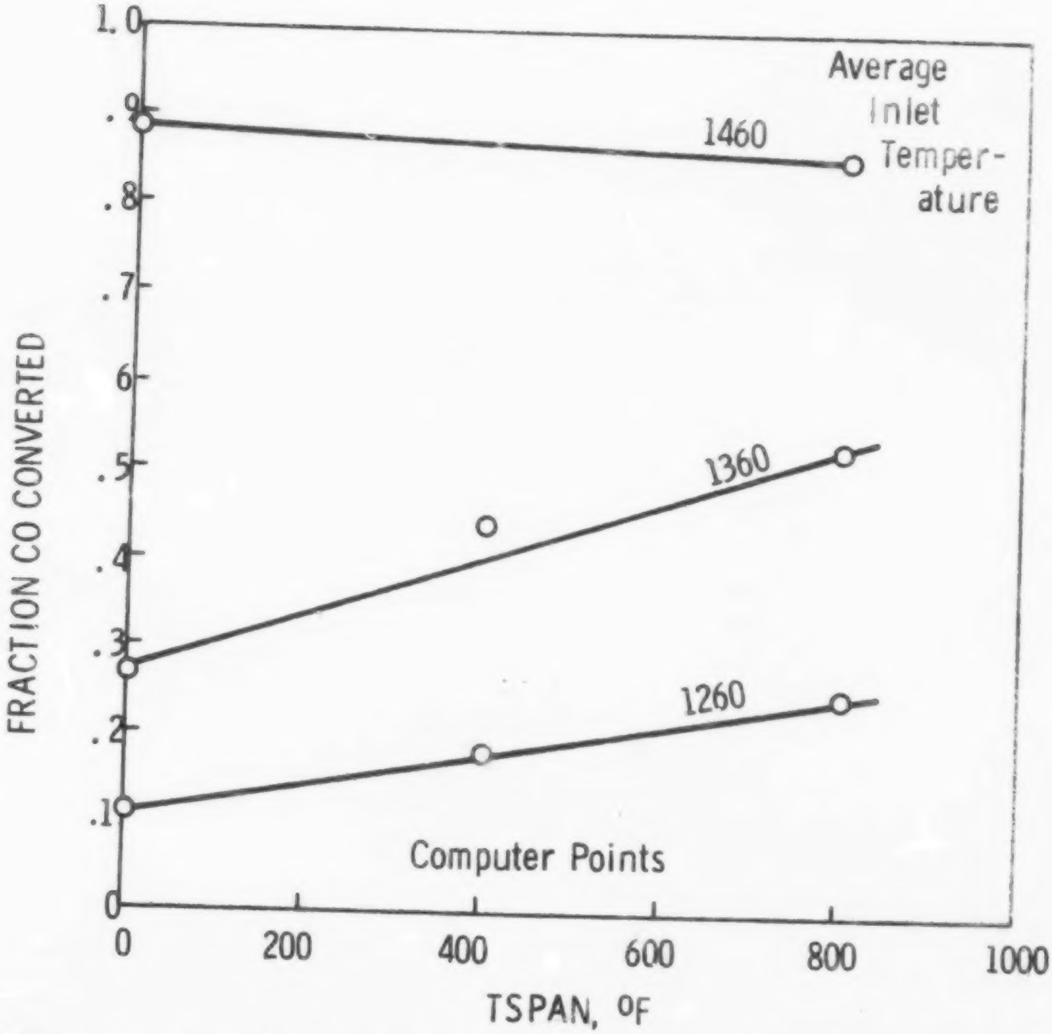

Figure 51. The effect of inlet exhaust temperature span (cyclic) on conversion. Pattern of flow for simulation shown in Figure 43, item 2.

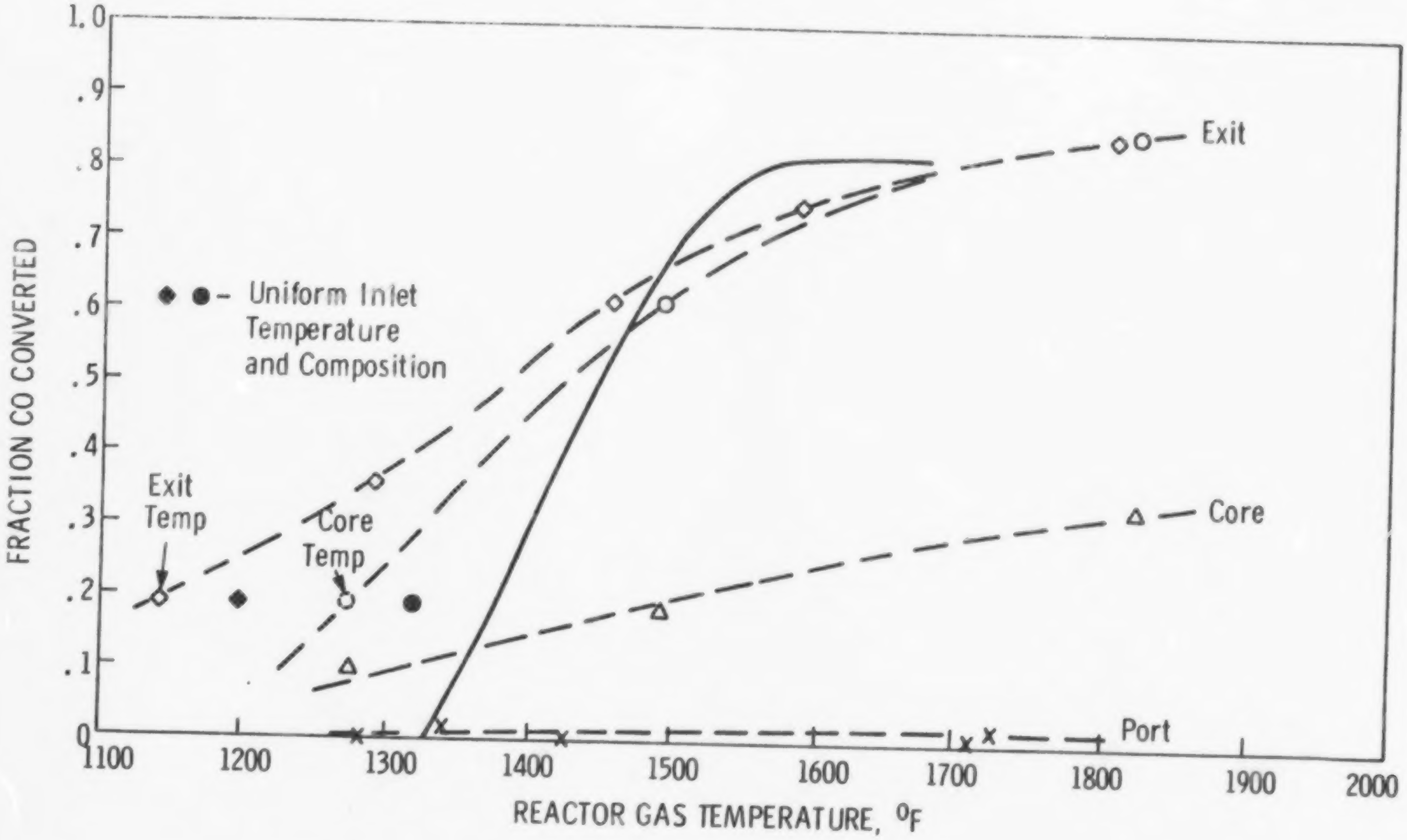

Figure 52. Simulation of a half reactor assuming symmetry. Cylinders 1 and 3 firing half the core and half the annulus.

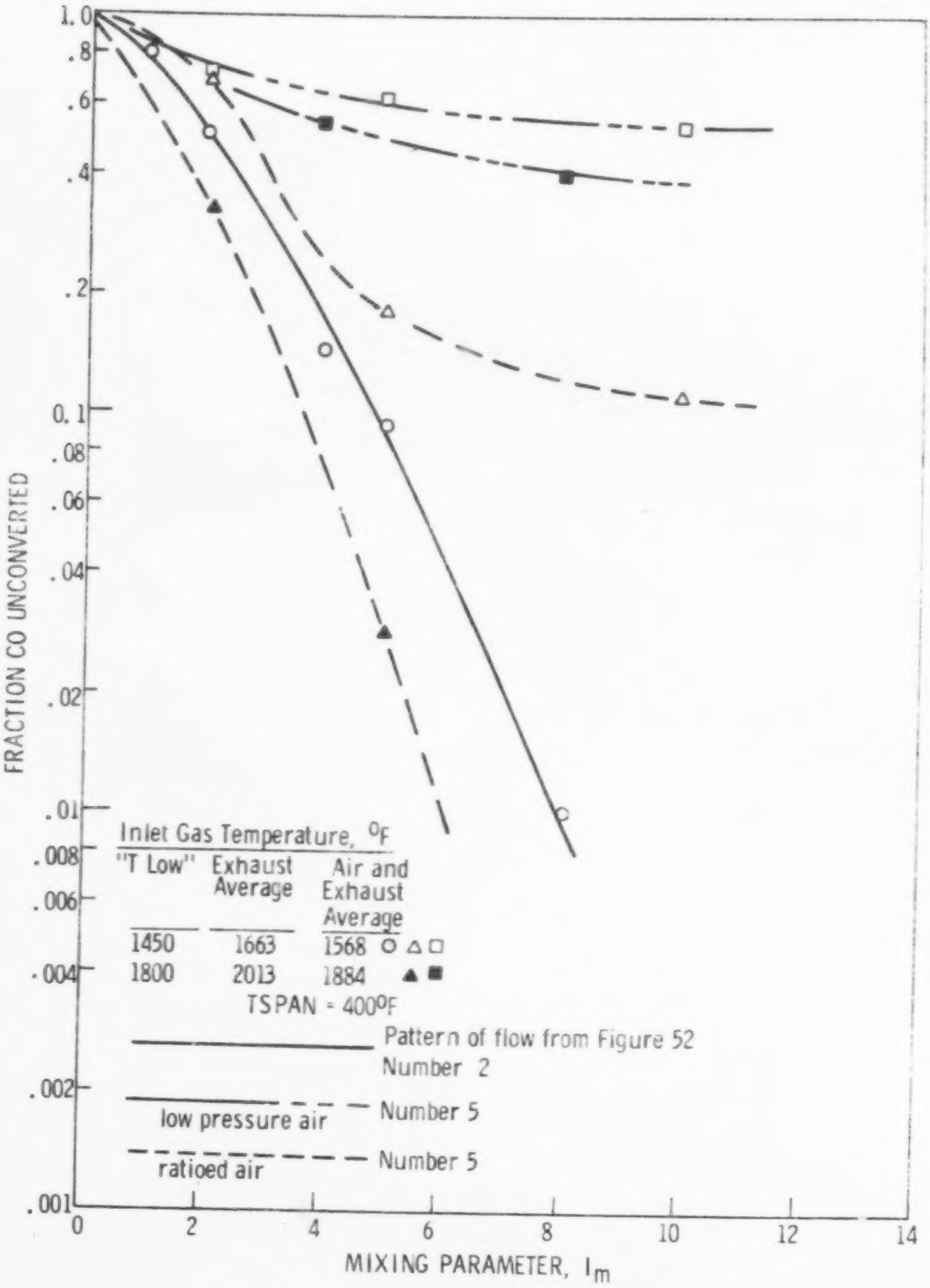

Figure 53. Sensitivity of simulation conversions to the mixing parameter, I_m. Comparison of the stirred-tank-with-plug-flow (number 2, Figure 43) and the all plug flow simulation (number 5, Figure 43) using low pressure and ratioed air. See note 2, Figure 46.

In Figure 53, the simulation that we have termed "best" (Figure 45, item 2) exhibits a rapid decline in the fraction CO unconverted at the lower inlet temperature to reach a level of 99% conversion at $I_m = 8$. At this lower temperature, the all-plug-flow simulation exhibits a much smaller change in fraction unconverted both in the case of low pressure air and of air ratioed to exhaust flow. In both cases, the fraction unconverted appears to have nearly leveled off at $I_m = 10$. For the low pressure air, this is due both to the maldistribution of air and exhaust and the persistence of low-temperature regions in the temperature distribution which are not eliminated by backmixing. With ratioed air, the maldistribution of flow is eliminated, but the temperature distribution still limits conversion.

Raising the inlet exhaust temperature by 350° raises the entire temperature distribution sufficiently to react any exhaust that mixes with air, causing the ratioed-air simulation to exhibit a high sensitivity to increased I_m, reaching 99% conversion at $I_m = 6$. Unfortunately, this is true only outside the range of acceptable operating temperature and a plug-flow, ratioed air reactor cannot be considered as an improved practical device.

For low pressure air, the plug flow simulation at the higher temperature shows only slightly improved conversion, because of the overriding effect of flow maldistribution. This simulation does allow blending of air and exhaust entering the reactor coincidentally from all ports; consequently, the 60% conversion at the higher temperature is an indication of the penalty associated with time maldistribution alone where backmixing is nearly eliminated (40 slugs per cycle).

To place the "best" simulation (Figure 45, item 2) into a familiar macromixing frame of reference, its sensitivity is plotted along with those for well-mixed stirred tanks in series (MIXONLY) in Figure 54. There exists a close correspondence between the "best" simulation and five stirred tanks. We recall that on the basis of the variance in the RTD, correspondence should be established with eight tanks in series: this difference is due at least in part to axial dispersion within slugs for the plug flow element of the "best" simulation (16 slugs per engine cycle).

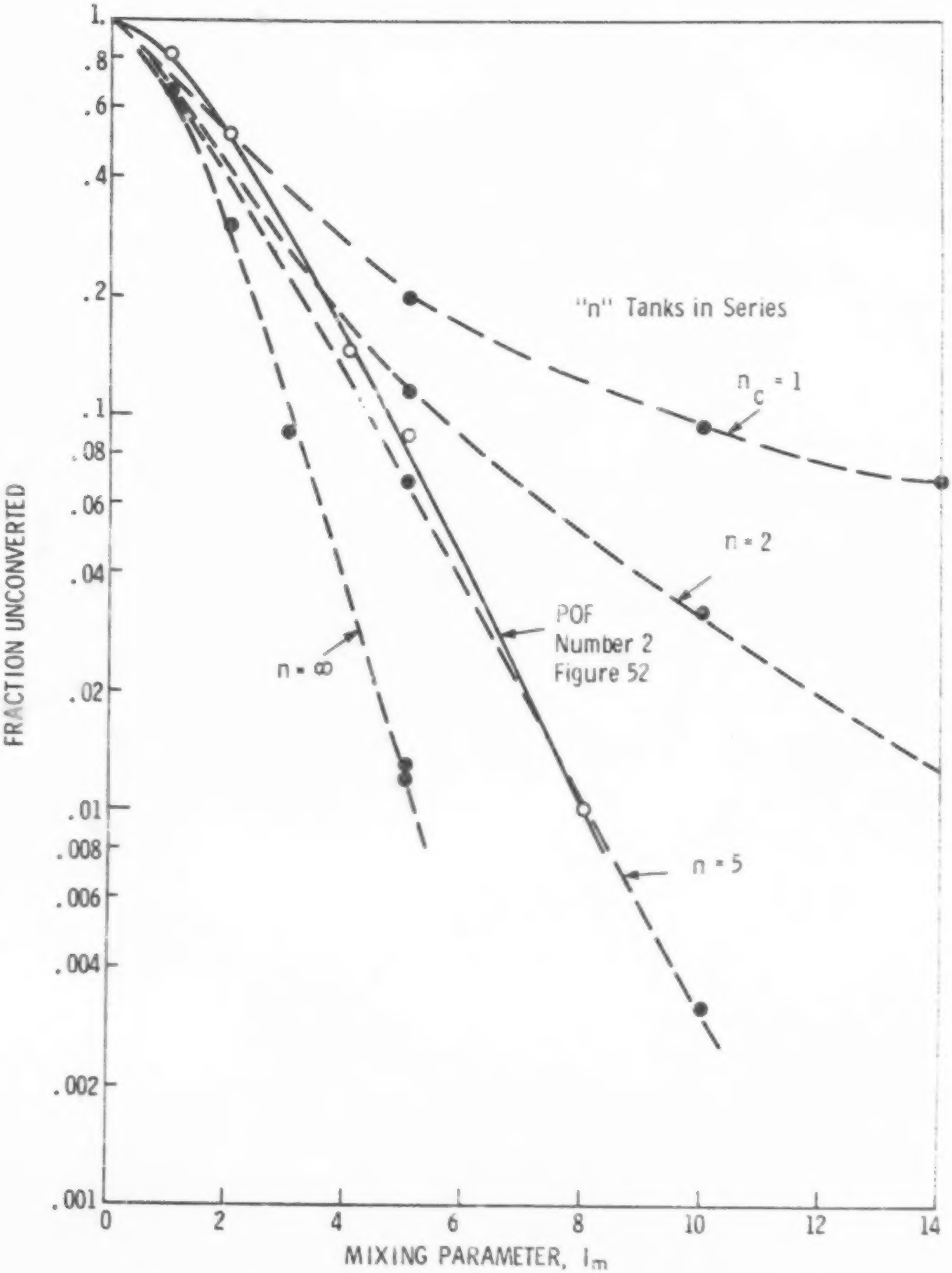

Figure 54. Comparison of the stirred tank-with-plug-flow simulation (number 2, Figure 43) with cell-wise stirred tanks in series. Simulation number 2 is run at an average inlet temperature of 1663°F. Tanks in series are for instantaneous reaction after mixing. See note 2, Figure 46.

MODELING REACTOR OPERATION DURING WARM-UP

Warm-up of the DuPont Model V reactor during unchoked engine operation with air injection has been characterized by a nonreactive period of several minutes during which reactions are largely quenched due to heat loss, followed by a transition to a lightoff condition that is gradual for hydrocarbon conversion but more abrupt for carbon monoxide. No experimental conversions have been determined for hydrogen during warm-up.

For a sufficiently high inlet temperature and/or high entering combustible concentration, the lightoff should occur at time zero. However, this was not observed for the range of conditions run on the Model V reactor.

Model building for the warm-up period has had the objective of developing a rapid computer simulation to predict the warm-up time required to achieve lightoff for various reactor designs and operating conditions. The computer program allows the user to designate a wide range of design specifications; the coupled reaction kinetics are restricted to zero-order oxidations in a continuous stirred tank reactor. This severe restriction on kinetics can be relaxed within the general framework of the existing model, but not without considerably complicating the calculations.

VI. Model Building for Unsteady State Operation

A. KEY FEATURES AND ASSUMPTIONS

All of the stationary state simulations of species conversions described in the previous sections solved for an unsteady state approach to the stationary state solutions (or periodic solutions) on a reactor time scale measured in tenths of a second. Changes in surface temperatures occur on a much longer time scale, measured in minutes. To reconcile these time scales without incurring the high cost of running an unsteady state simulation of species conversions for a simulation time of several minutes, the warm-up simulation was designed to compute steady state conversions and reactor gas temperature at intervals of several seconds, and then to extrapolate these gas temperatures for the purpose of computing more frequent estimates of the unsteady state heat balance on reactor parts and their rise in temperature.

Reactor gas temperature and chemical conversions are calculated as solutions for an ideal backmix reactor with continuous feed and feed properties. This assumption ignores all distributions of temperature and composition and causes the transition to a lightoff condition to proceed in a narrower range of time and temperature than would occur in practice. The assumption of zero-order kinetics is discussed in the subsequent section on method of solution.

The unsteady state simulation of surface temperatures integrates temperature change based on heat balance for as many components in a reactor as the user wishes to ascribe different average temperatures. All of the defined parts are assumed to have a uniform internal temperature. If insulation is present, it must be divided into thin layers.

Any defined part of a reactor can be caused to exchange heat with exhaust gas and/or ambient air by convection, or with any other part by radiation or conduction. Many of the possible paths of heat transfer will be redundant in a particular reactor design, and these will be excluded from the calculations by preassigning heat transfer coefficients of zero.

Heat transfer by radiation assumes a view factor that is appropriate to concentric cylinders or spheres, where each component is uniformly irradiated by an opposite surface. The contribution of radiation to the heat balance for a part is treated as an equivalent conductance term which can be lumped with convection and/or conduction in circumstances of parallel heat transfer to an infinite surrounding, across a closed gas space, or between connected parts. Heat transfer by convection is computed using coefficients that are obtained from steady flow correlations based on the usual Reynolds (Re), Prandtl (Pr), and Grashof (Gr) numbers. Calculations employ user-designated parameters describing reactor geometry, mass flow, and the division of mass flow into fractions passing each of the designated surfaces. Where specific data on convective heat transfer coefficients are available, the computed values can be adjusted.

B. REACTOR PARTS TEMPERATURE SIMULATION

The operation of the parts temperature simulation will be illustrated by referring to a thermal network (Figure 35) which corresponds to the DuPont Model V reactor with two layers of insulation at the outside and a wrapping on the insulation. The reactor itself is represented as six concentric parts: the core, two layers of radiation shield, and three layers of outer shell. Heat losses at the insulated ends are neglected. The insulation is treated as a half layer resistance at the inside and outside. The two other entities which exchange heat are the exhaust gas and ambient air, which brings the total number of heat exchange "bodies" to eleven.

All heat transfers are computed as a conductance, which we designate "HA," times a temperature difference. "HA" in the computer program is an array which reserves storage for conductances between all pairings of bodies in the thermal network, except that no storage exists for conductance directly

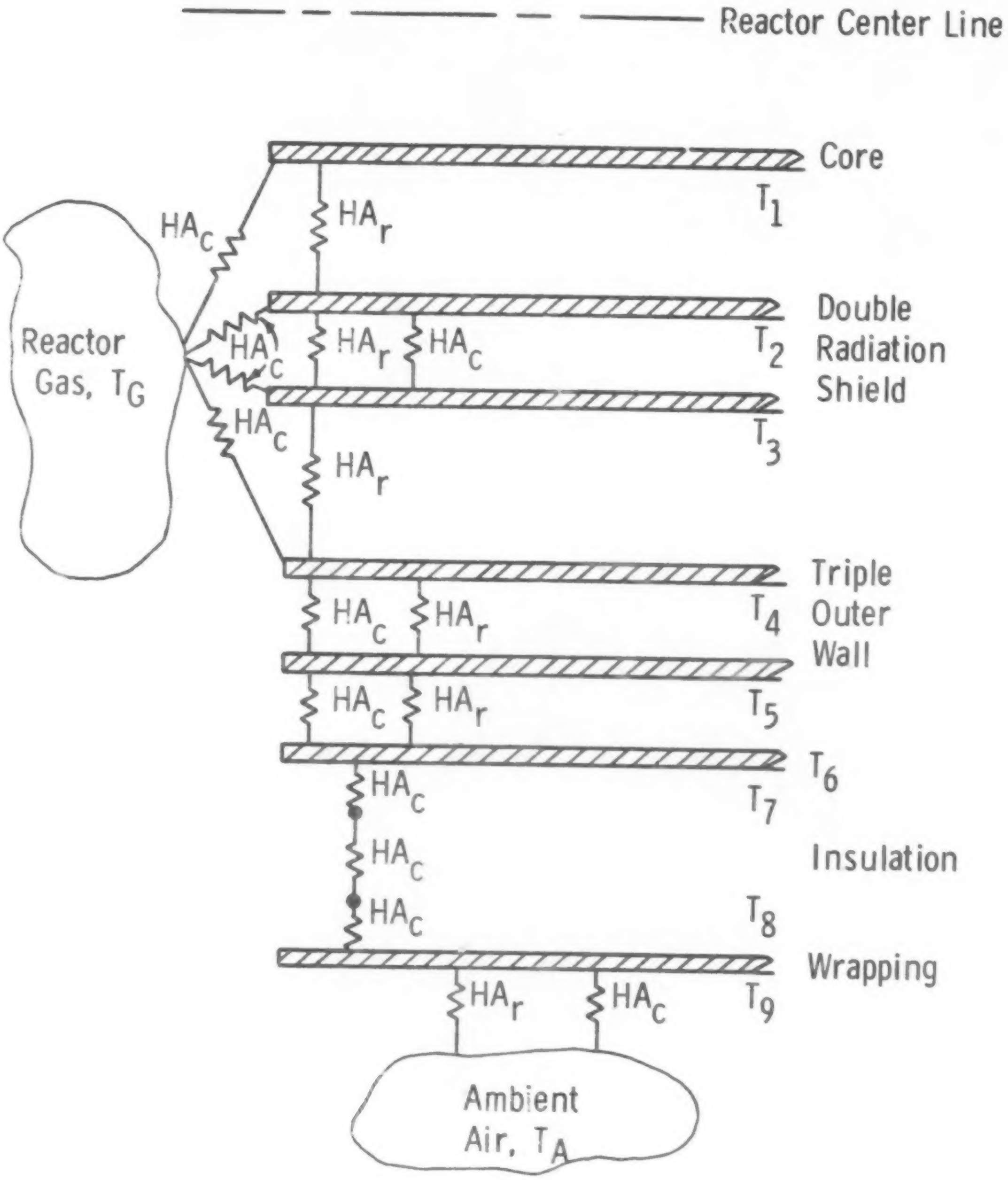
Reactor Center Line
Core
T_1
HA_c
HA_r
Double
Radiation
Shield
T_2
HA_c
HA_r
HA_c
T_3
HA_c
HA_r
Reactor
Gas, T_G
Triple
Outer
Wall
T_4
HA_c
HA_r
T_5
HA_c
HA_r
T_6
T_7
HA_c
HA_c
Insulation
HA_c
T_8
Wrapping
T_9
HA_r
HA_c
Ambient
Air, T_A

Figure 55. Thermal conductance network for the DuPont Model V reactor with external insulation.

between ambient air and exhaust. Where heat transfer between two bodies is both by radiation and by conduction or convection, there exist parallel conductances which we refer to as HA_r and HA_c, respectively.

There is assumed to exist only a single thermal resistance between any two parts, by virtue of neglecting internal resistance in parts in contact resistance between insulation and other parts.

For the thermal network shown in Figure 55, the computer program would reserve (9x11) storage locations for both HA_c and HA_r. Of the 198 paths for for heat exchange thus allowed, only 17 are used. The redundant paths are exempted from calculations by assigning zero initial values, which signal a null computation. The redundancy provides flexibility to the user in the thermal networks which can be represented.

Prior to each time that the part temperatures are integrated, a new reactor temperature has been computed from the coupled CSTR simulation. After two successive gas temperatures have been computed, the value used for computing heat transfer to reactor parts may be a linearly extrapolated value (optional). Integration of the parts temperatures proceeds over a designated number of steps before another gas temperature is computed. Step size is variable to limit the change in parts temperatures within designated bounds.

Conductances may be recomputed for each step in the parts temperature integration, or optionally may be computed only once after each new calculation of reactor gas temperature. The conductance calculations that are programmed into the simulation include the following:

Radiation between bodies i and j (21, p. 227).

$$HA_{r_{i,j}} = \frac{\sigma_r (T_i^4 - T_j^4)}{\left[\frac{1-\varepsilon_i}{A_i \varepsilon_i} + \frac{1}{A} + \frac{1-\varepsilon_j}{A_j \varepsilon_i}\right] (T_i - T_j)} \tag{VI-1}$$

Convection between air or exhaust and any part j.

$$HA_{c_{i,j}} = \sum_{s=1}^{2\text{ sides}} h_{j,s} A_{j,s} \tag{VI-2}$$

Where "h" is computed from steady flow correlations.

Forced convection in a closed conduit.

Laminar flow, RE < 2000. (25, p. 392)

$$\overline{Nu} = 8.57(\mathrm{RePrD}/L)^{.27}; \ (\mathrm{RePrD}/L) < .3 \qquad \text{(VI-3)}$$

$$\overline{Nu} = 10.02(\mathrm{RePrD}/L)^{.40}; \ (\mathrm{RePrD}/L) < .3 \qquad \text{(VI-4)}$$

Transition flow, 2000 < Re < 10,000 (31, p. sec, 10, p. 14)

$$\overline{h} = \frac{418\ G\ Cp\ (Re^{2/3} - 125)(1 + (D/L)^{2/3})}{Pr^{2/3}\ Re} \qquad \text{(VI-5)}$$

Fully turbulent flow, RE > 10,000 (26, sec. 10, p. 14)

$$\overline{Nu} = .023\ Re^{.8}\ Pr^{1/3} \qquad \text{(VI-6)}$$

Free convection outside a horizontal cylinder (21, p. 342)

$$\overline{Nu} = 0.53(\mathrm{GrPr})^{1/4} \qquad \text{(VI-7)}$$

Gas flow normal to the outside of a circular cylinder (21, p. 411)

$$\overline{Nu} = 0.536(Re)^{.496} \qquad \text{(VI-8)}$$

Convection and conduction across a narrow closed gas space (21, p. 347)

$$\overline{Nu} = .0712\ Gr^{.324}; \ Gr > 3500 \qquad \text{(VI-9)}$$

$$\bar{h} = \frac{k_f}{D}; \; Gr < 3500 \tag{VI-10}$$

Conduction through insulation

$$HA_c = \frac{k_t A}{\Delta L} \tag{VI-11}$$

The use of steady flow convective heat transfer correlations was dictated by an absence of any detailed measurement of heat fluxes within an exhaust reactor. However, all of these correlations are assigned variable leading coefficients so that the values can be adjusted by the program user. This was done, as described later, to adjust the change in parts temperatures to measured values.

When all conductances have been computed, a heat balance is performed on each reactor part and a temperature change computed for one integration step. For a part "j" in Figure 55, we sum the heat fluxes from all eleven heat exchange bodies.

$$T_j = T_{j_{last}} + \frac{\sum_{i=1}^{11} HA_{c_{i,j}} (T_i - T_j) + \sum_{i=1}^{11} HA_{r_{i,j}} (T_i - T_j)}{M_j C_{p_j}} \Delta t \tag{VI-12}$$

The simple Euler's method of integration shown is consistent with the approximate nature of this entire simulation. An option is provided, however, for a midpoint slope method.

C. SOLUTIONS FOR MULTIPLE OXIDATIONS IN A "CSTR"

A general method of solution will be outlined, and then assumptions will be invoked to reduce the complexity of the calculation.

Obtaining solutions for an ideal backmix reactor where more than one reaction is represented can be approached either as an initial value problem where an unsteady state approach is computed to the steady state solution (as in the program "EXHAUST"), or as the simultaneous solution of nonlinear algebraic equations derived from the steady state material and energy balances.

Efforts made to simplify and adapt the "unsteady-state-approach" program, "EXHAUST," to the warm-up problem did not produce an acceptably rapid version. The essential difficulty resulted from the fact that a short time step was required in the Runge-Kutta integration, which unavoidably implied unacceptable running costs on the computer. The alternative of solving nonlinear algebraic equations was used.

We wish to determine an exit temperature T and exit conversions X_i for $i = 1, \ldots, q$ combustible species which are assumed to be oxidized independently (no series reactions). Stoichiometry given by $\nu_{i,k}$ for specie "i" in reaction "k" is written for one mole of the oxidized species to cause rates of reaction r_k, $k = 1, \ldots, q$ to equal rates of "appearance" of species "i," $\overline{r}_i$, $i = 1, \ldots, q$.

Rates of reaction are assumed to have the following form and to involve an order dependence on any of the "m" species that are present:

$$\overline{r}_i = r_k = -A_k e^{-E_k/RT} \prod_{i=1}^{m} (PC_i)^{\eta_{i,k}} \qquad \text{(VI-13)}$$

From the material balance,

$$f_o C_{i_o} + \overline{r}_i V - f C_i = 0 \qquad \text{(VI-14)}$$

we obtain "q" equations of the form:

$$F_i \triangleq X_i - \dot{A}_i \prod_{j=1}^{q} (1-X_j)^{\eta_{j,k}} \prod_{j=q+1}^{q+net} \left(1 - \sum_{l=1}^{q} \nu_{j,l} X_l\right)^{\eta_{j,k}} e^{-E_k/RT}$$

$$i = k = 1, \ldots, q$$

$$\dot{A}_i \triangleq \frac{A_i V \left(\frac{f_o}{f} P\right)^b \prod_{j=1}^{m} C_{j_o}^{\eta_{i,j}}}{f_o C_{i_o}}; \quad b = \sum_{j=1}^{m} \eta_{j,k} \qquad \text{(VI-15)}$$

where

$$\frac{f}{f_o} = 1 - \sum_{k=1}^{q} \sum_{j=1}^{q\ act} \nu_{j,k} C_{j,o} X_j \qquad \text{(VI-16)}$$

The term f/f_o is 1 if all reactions are equilmolar or if mole compression is small enough to be ignored. If it cannot be ignored, the expression for f/f_o must be substituted into the functions F_i.

From the energy balance:

$$F_{q+1} \triangleq \sum_{j=1}^{m} C_{j,o} H_j(T_o) - \frac{1}{f_o} \sum_{k=1}^{P_r\ sinks} HA_{c_k} (T-T_k)$$

$$- \sum_{j=1}^{q} C_{j,o} (1-X_j) H_j(T) - \sum_{j=q\ act\ +\ 1}^{m} C_{j,o} H_j(T)$$

$$- \sum_{j=q+1}^{q\ act} \left[C_{j,o} + \sum_{k=1}^{q} \nu_{j,k} C_{k,o} X_k \right] H_j(T) \qquad \text{(VI-17)}$$

A solution is obtained when we find T and X_i, i = 1, ... q, which satisfy $F_i = 0$, i = 1, ... , q + 1. Because of the coupling that is introduced by assuming that the rate of a particular reaction is order dependent on species which are appearing or disappearing in other reactions, a solution must be approached by a multivariate search method or by an iteration such as Newton's method for vector functions. In the latter case, an approach to a solution is obtained from:

$$X_{i_n} = X_{i_{n-1}} + \Delta X_{i_{n=1}}, \quad i = 1, \ldots, q$$

$$T_n = T_{n-1} + \Delta T_{n-1}$$

Where ΔX_i and ΔT are the solution to the system of linear algebraic equations:

$$\left(\frac{\partial F_1}{\partial X_1}\right)_{n-1} \Delta X_{1_{n-1}} + \ldots + \left(\frac{\partial F_1}{\partial X_q}\right) \Delta X_{q_{n-1}} + \left(\frac{\partial F_1}{\partial T}\right)_{n-1} \Delta T_{n-1} + F_1 = 0$$

$$\left(\frac{\partial F_2}{\partial X_1}\right)_{n-1} \Delta X_{1_{n-1}} + \ldots \qquad + F_2 = 0$$

$$\left(\frac{\partial F_{q+1}}{\partial X_1}\right)_{n-1} \Delta X_{1_{n-1}} + \ldots \qquad + F_{q+1} = 0 \qquad \text{(VI-18)}$$

Here "n" refers to the step in the iteration. Given the fact that the nonlinear equations will in general possess several possible solutions, the particular solution that is obtained as well as the question of whether Newton's method will converge at all will depend heavily on the guess used to start the iteration.

To reduce the difficulty in searching for a solution we are aided by assumptions which reduce the interdependence between the several conversions X_i. For example, if order dependence for each reaction is limited to the oxidized specie and oxygen, we are left with only a two-dimensional search on oxygen conversion and temperature; i.e., the equations for F_i are reduced to

$$F_i = X_i - A_i^* e^{-E_i/RT} (1-X_i)^{\eta_{i,i}} (1-X_{q+1})^{\eta_{q+1,i}} = 0$$

$$i = 1,\ldots,q \qquad \text{(VI-19)}$$

Here if we have search values of X_{q+1} and T, the equations are solvable for X_i by a root finding method.

If we proceed to an order dependence of zero, we are reduced to a one-dimensional search on temperature alone, and the calculation of X_i is explicit,

$$X_i = A^* e^{-E/RT} \qquad \text{(VI-20)}$$

This assumption was used in the present work.

To justify this sweeping assumption, it should be noted that the reaction orders for carbon monoxide in the current study were close to zero (.20 ± 2σ = .100 for order with respect to CO and -.032 ± 2σ = .106 for order with respect to O_2. For hydrogen, no statistically satisfactory rate expression was obtained by the method of least-squares, and a rate equation for temperature dependence alone based on a plot of conversion versus temperature is the only estimate which can be safely offered. Finally, although hydrocarbon oxidation involves statistically valid orders, its contribution to a change in reactor gas temperature is only about 10% of that for total combustibles (based on a characteristic exhaust analysis of 4% CO, 1.6% H_2, and 500 ppm hydrocarbon). Hence some imprecision in simulated values of hydrocarbon conversion can be tolerated.

The strategy for finding a solution in the zero-order case depends solely on finding the exit gas temperature which satisfies both the energy balance (based on the inlet composition and temperature of exhaust, the air dilution fraction, and heat loss) and the material balances for the various reactive species (based on the exit temperature and reaction kinetics). This is equivalent to searching for the value of exiting gas temperature which satisfies the energy balance written

$$F_{q+1} = \sum_{j=1}^{m} C_{j,o} H_j(T_o) - \frac{1}{f_o} \sum_{k=1}^{P\ \text{sinks}} HA_{c_k} (T-T_k)$$

$$-\frac{f}{f_o} \sum_{j=1}^{m} C_j H_j(T) = 0 \qquad \text{(VI-21)}$$

with

$$C_j = \frac{f_o}{f} C_{j,o} \left(1 - A^* e^{-E_j/RT}\right) \qquad \text{(VI-22)}$$

The method used to find the exiting temperature begins as a one-directional search of uniform step size in temperature, using the fact that a positive direction of search is indicated where F_{q+1} is positive. As the search approaches a solution, the step size is reduced by application of Newton's method, or in the event that the solution is overshot, the half interval root-finding method is invoked.

The familiar possibility that a stirred tank reactor may exhibit more than one operating point for a given set of inlet conditions, which has been discussed at length by Schwing (29) for lightoff of a single reactant in a stirred thermal reactor, attests to the importance of both the starting point in the search and also the step size used. In the case where several reactions occur simultaneously, there exists in general the possibility of multiple solutions. Where multiple solutions exist, the solution actually obtained will depend both on the starting temperature and on the search step size, by virtue of the possibility of over shooting an entire region associated with some particular stable solution.

Because the warm-up computer program as used has no provision for introducing nonzero-order kinetics, use of the program with rate expressions which include order dependence requires averaging out this dependence. For hydrocarbon, which is fractional order in HC, O_2, NO, and O_2 for a total order of 1.7, the rate equation was corrected by inserting the log mean values of the order determining species for the 105 data sets used in the least-squares determination.

Least squares equation for hydrocarbon:

$$r_{HC} = 1.141\ e^{-29,336/RT}\ p_{HC}^{.238}\ p_{O_2}^{.537}\ p_{NO}^{.415}\ p_{CO}^{.512} \qquad \text{(VI-23)}$$

Rate equation for hydrogen corrected to zero order.

$$r_{HC} = .00325\ e^{-29,336/RT} \qquad \text{(VI-24)}$$

For carbon monoxide and hydrogen, zero-order equations are:

Zero-order rate equation for carbon monoxide

$$r_{CO} = .621\ e^{-33,800/RT} \qquad \text{(VI-25)}$$

Zero-order rate equation for hydrogen

$$r_{H_2} = 12660.\ e^{-52,000/RT}. \qquad \text{(VI-26)}$$

The conversions previously determined (Phase I) corrected on the basis of zero-order kinetics to a flow $f^* = 1.99 \times 10^{-4}$ lb moles/sec and inlet concentration $C_o^* = .006$ mole fraction, provide a measure of the uncontrolled variation in conversion for hydrogen under the assumption of zero-order kinetics. Corrections are shown for the data for carbon monoxide (Figure 56; $f^* = 2.98 \times 10^{-4}$, $C_o^* = .02$) and for hydrocarbon (Figure 57; $f^* = 1.99 \times 10^{-4}$, $C_o^* = .0004$).

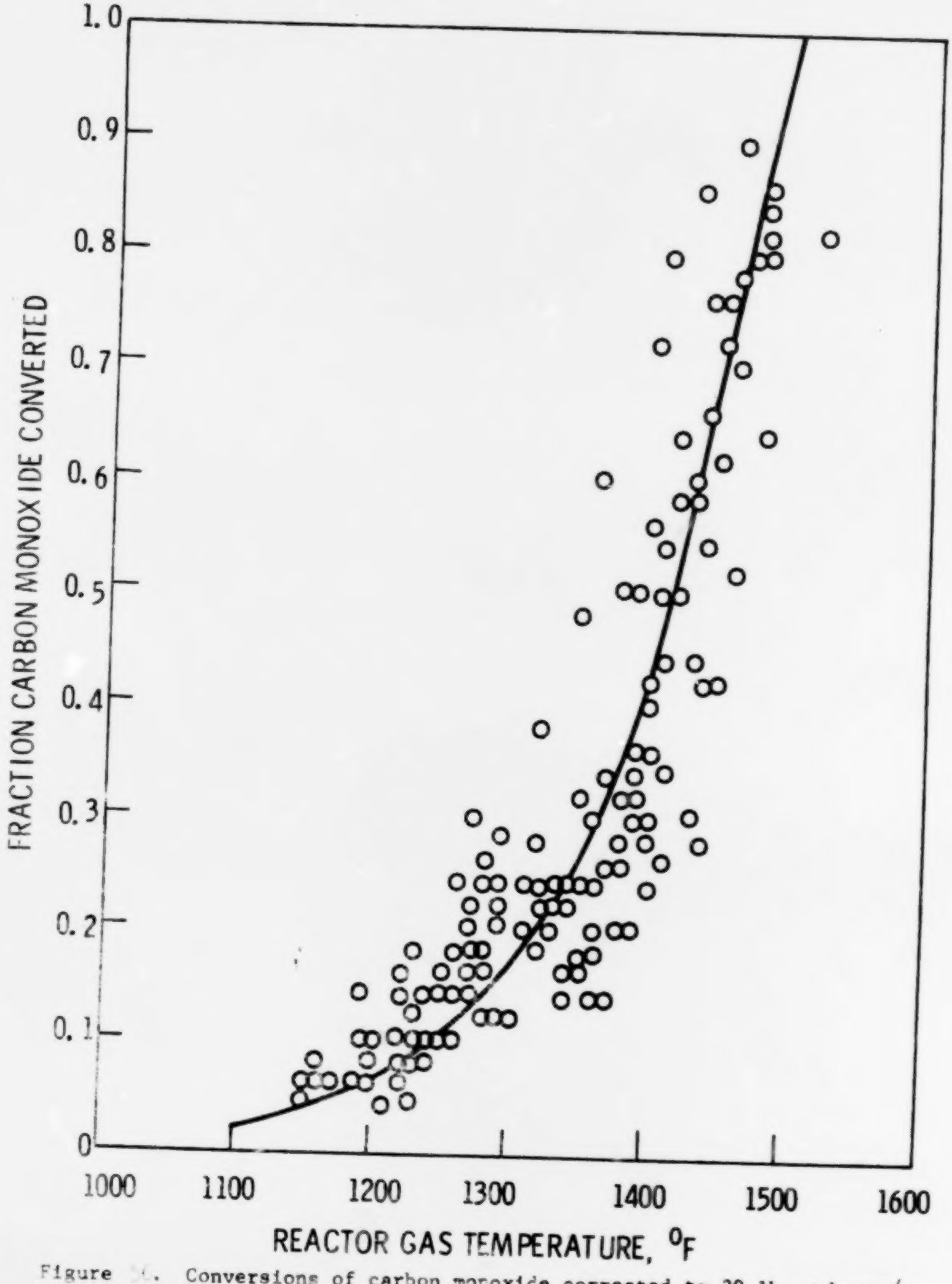

Figure 56. Conversions of carbon monoxide corrected to 30 lb. exhaust/hr and .02 mole fraction CO entering.

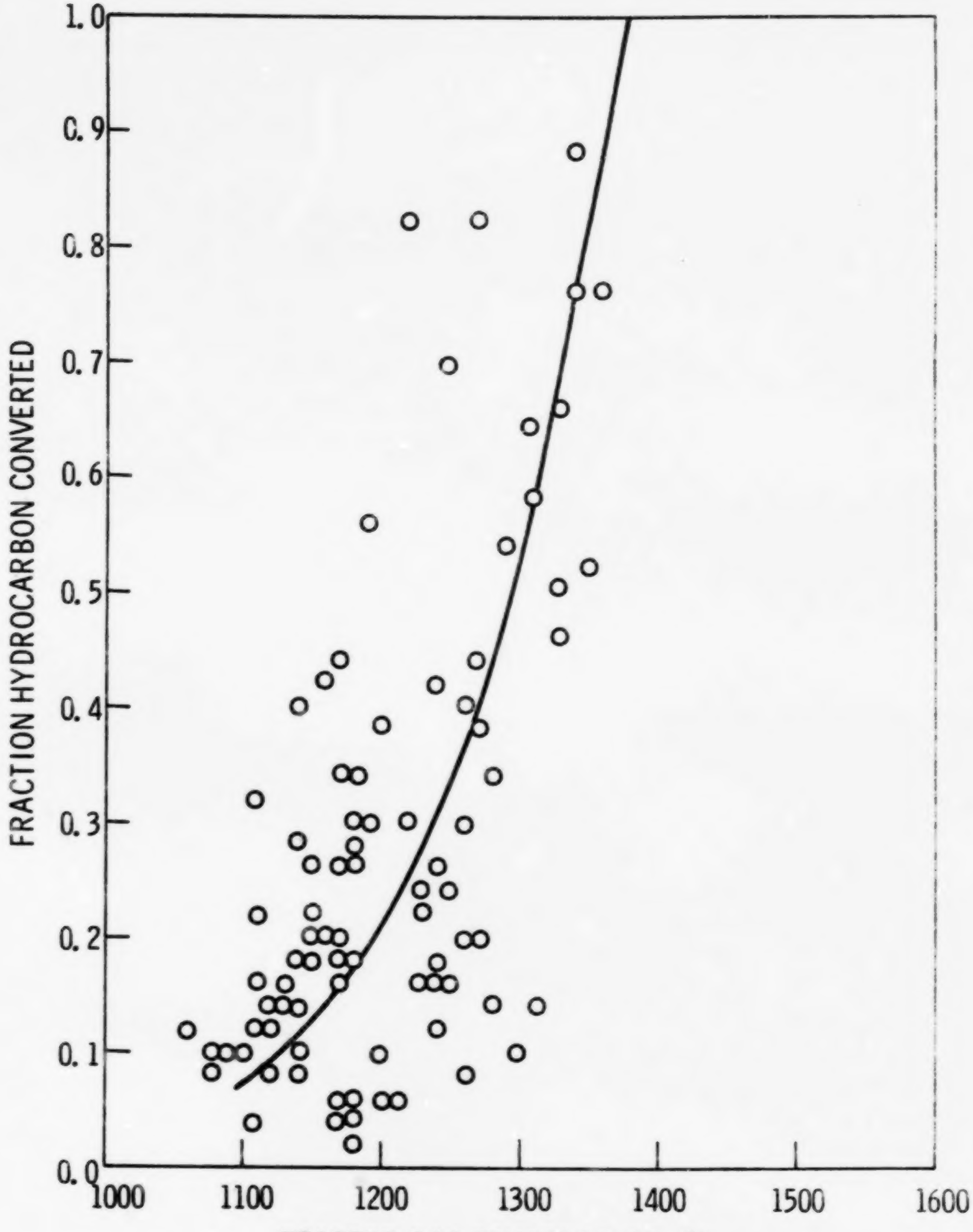

Figure 57. Conversions of hydrocarbon corrected to 20 lb exhaust/hr and 400 ppm hydrocarbon entering.

VII. Base Case Warm-Up Simulations for the DuPont Model V Reactor

Base case simulations on the DuPont Model V reactor were performed on six concentric cylinders representing—1 inner core, 2 and 3—the double radiation shield, and 4, 5, and 6—the three outer shells (see Figure 55). No insulation was included.

A. WARM-UP WITHOUT REACTION—THERMAL PARAMETER EVALUATION

The first simulations were run without appreciable reaction on 150 lb of exhaust per hour passing through the reactor for the purpose of testing the sensitivity of the model heat loss at steady state to changes in emissivities and convective heat transfer coefficients. Results (Figures 58, 59, and 60) allow approximate comparisons to be made with selected experimental results; however, no precise determination of "best" thermal parameters can be claimed in consideration of the complete mixing assumption made in modeling.

Model heat losses at steady state, expressed as temperature drop, are presented in Figure 58 for ranges of emissivities, convective coefficients, and inlet temperatures. Surface emissivities play a large role in determining heat loss, more so than exhaust-side convective heat transfer coefficients. The relative insensitivity to exhaust side convection at steady state is due to the fact that all inner surfaces are at high temperatures, approaching the gas temperature, whereas most of the temperature drop to ambient level is across the air spaces between the three outer shells (Figure 59).

Temperature measurements reported for the DuPont reactor by Blenk (3) indicate a temperature drop between core and outlet varying from 160° to 215° for unreacting exhaust in a range of approximately 1350° to 1750° inlet exhaust temperature. Since these values do not appear correlatable, no single value can be selected for comparison. However, based on the median value of approximately 190°F, we are directed to a model emissivity of .5 to .6 to match a 190°F drop at an inlet temperature of 1725°F.

A second group of experimental data that are available for comparison are the measurements of temperatures of concentric enclosures within the reactor at steady state. Experimental points (Figure 59) indicate that all of the surfaces in contact with exhaust exhibit temperatures differing from the core exhaust temperature of no more than about 200°F. The profile of parts temperatures with reaction (90% conversion of 3% CO) is slightly flatter than without, due to compensation for heat loss by heat of reaction. However, even with reaction the experimental gas temperature is indicated to drop by approximately the same 200°F between the core and the exit, according to both the CRC study and Blenk (3). This occurs even though oxidation of the combustible content

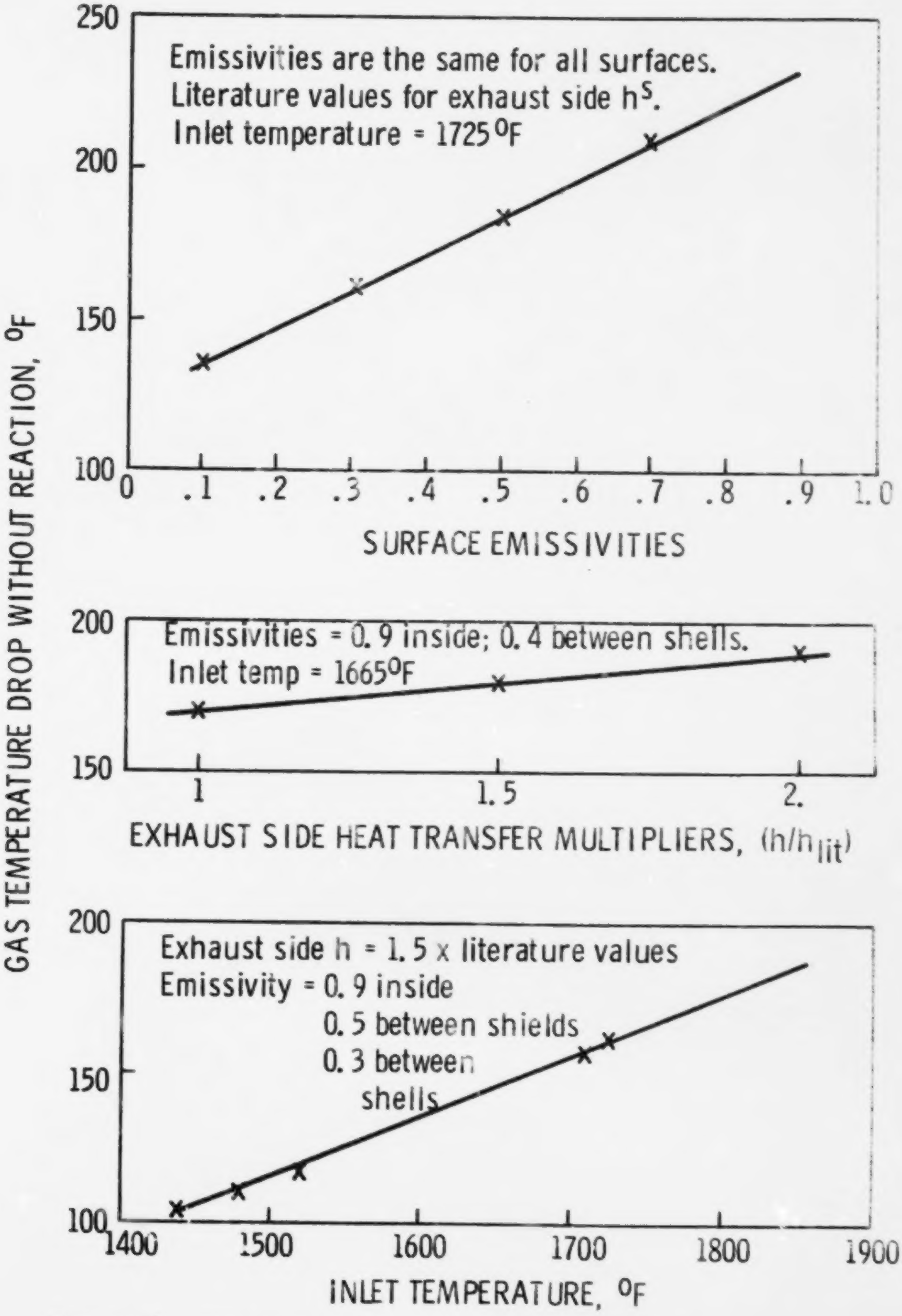

Figure 58. Simulated steady-state heat loss measured as drop in exhaust temperature. DuPont Model V reactor configuration. Mass flow = 150 lb/hr.

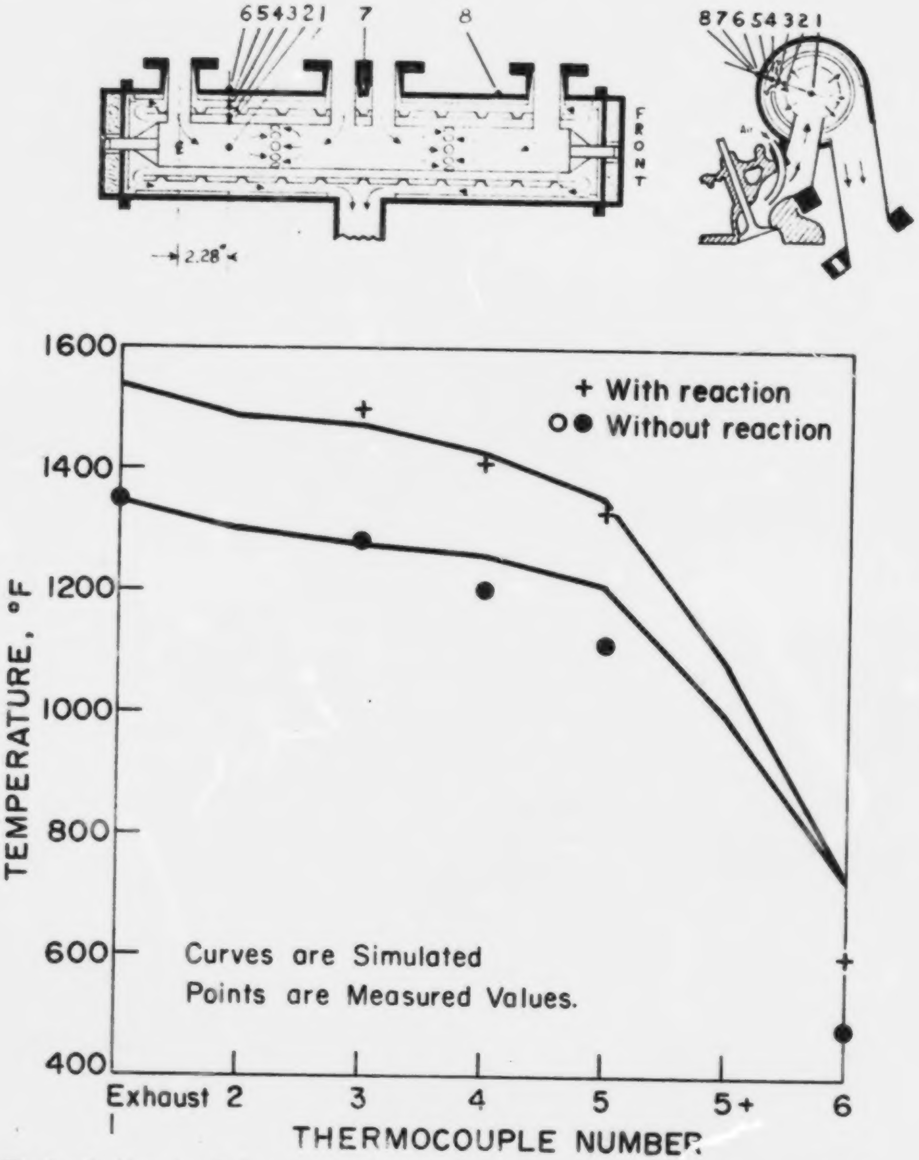

Emissivity in	0.9	0.9	0.5	0.9	0.3	0.3
out	0.9	0.5	0.9	0.3	0.3	0.3
Convective coefficients, Btu/hr/ft^2/°F						
	Exhaust-7.8	11.7	12.0	11.8		air-2.6
Equivalent radiative coefficient, Btu/hr/ft^2/°F						
	42.2	16.1	36.9	5.8	3.2	1.5

Figure 59. Steady-state metal temperature profiles.

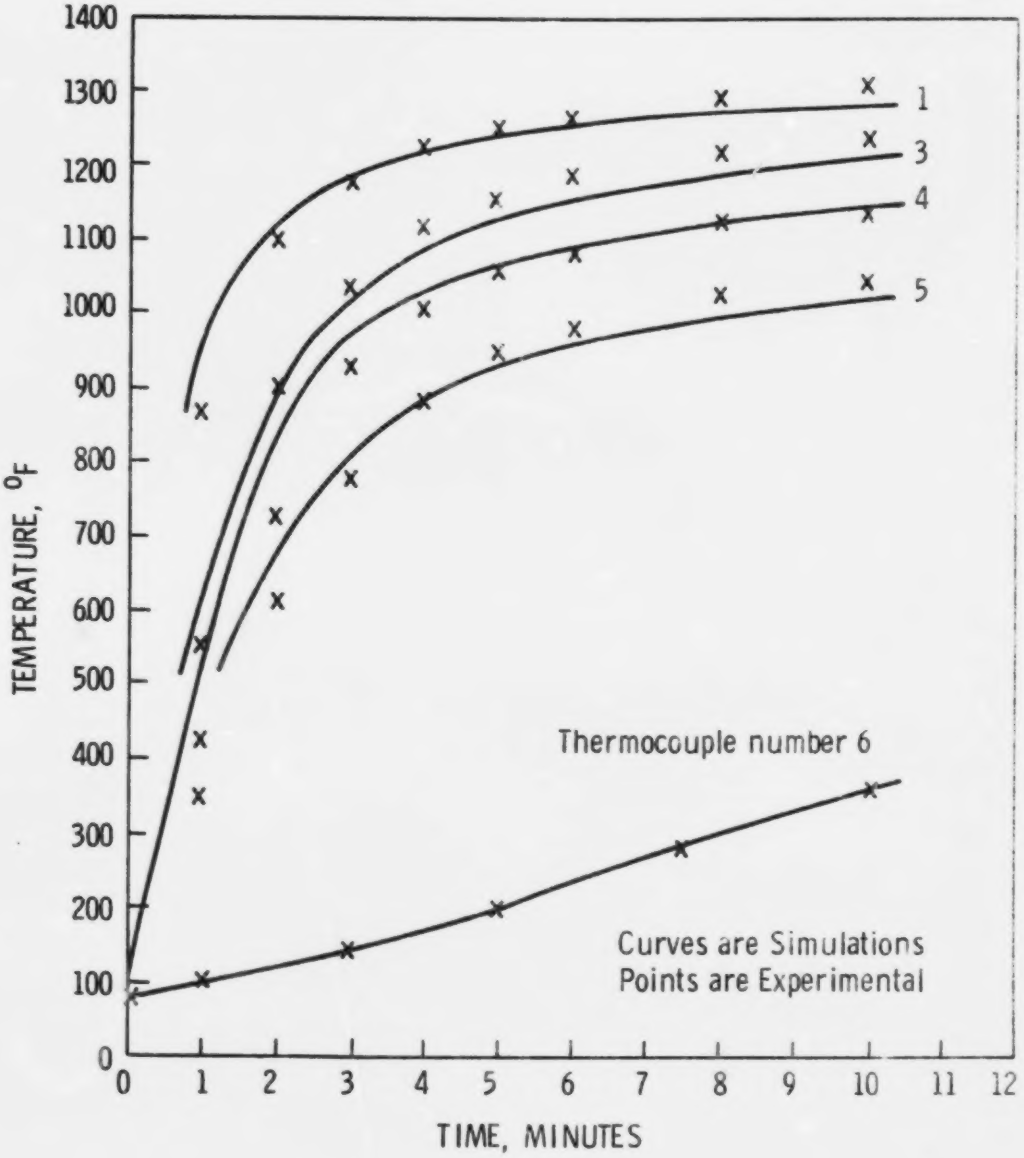

Figure 60. Warmup of the DuPont Model V. 1.-exhaust, 3 and 4 radiation shield, 5-inner shell, 6-outer shell. See Figure 59 for thermocouple locations.

(nominally 3% CO, 1% H_2, and 500 ppm HC) releases heat which would raise the temperature by 500°F. This persistent drop in temperature between the core and the exit during lightoff operation is an indication that a large portion of the reaction occurs in the core.

Given the experimental fact that gas temperature does drop after leaving the core, it is evident that a simulation based on complete mixing to a uniform gas temperature should predict less difference in metal temperatures, measured from the core outward to the shell, than would be observed experimentally. However, use of plausible emissivities for partially blackened metal (ε = .70 and .85), applied to all surfaces alike, and on convective coefficients up to double the steady-flow values (not graphed) caused the simulation metal temperatures progressing out from the core to drop more sharply than the experimental. To counter this behavior, it was assumed that emissivities in closed gas spaces were lower (more reflective) than those for surfaces darkened by contact with exhaust. By assuming an emissivity of .5 between the two layers of the heat shield and an even lower .3 between the three layers of outer sheel (polished stainless has ε = .2), the general agreement shown in Figure 59 between the simulations and measurements was obtained. The convective coefficients used were one and one half times values computed from steady-flow correlations. Agreement is better for the experimental points obtained with reaction. At the very outside surface of the reactor, the simulation temperature is high (due in part to neglect of the metal supports).

Values of the convective coefficients and equivalent radiative coefficients, HA_r/A, computed by the simulation are given in Figure 59. The convective coefficients on the exhaust side change negligibly during warm-up; convection at the outside surface based on an external air velocity of 8 ft/sec approximately doubles; and the radiative coefficients rise sharply from zero to their given values in proportion to $(T_1^4 - T_2^4)/(T_1 - T_2)$.

Figure 60 shows the unsteady-state approach to the metal temperature profile of Figure 59 (without reaction). Good agreement was obtained between the simulation and the experimental observations. That the simulation curves exhibit values that are higher than the observed values at 1 min can be attributed in part to the fact that the simulation treats hot exhaust entering a cold reactor whereas the experimental values represent start up of a cold engine and reactor. A good fit for the temperature transients, as shown, is very important to achieving useful estimates of time to lightoff. Furthermore, accuracy in the time constant for warm-up implies that the heat transfer parameters used are approximately correct.

The emissivities and convective coefficients shown in Figure 59 are representative of those used in subsequent simulations involving reaction, since the same heat transfer parameters are used. That these parameterr taken together are plausible representation of the heat transfer regime is supported by three aspects of the simulations without reaction just cited: (1) The total heat loss for gas passing through the reactor (Figure 58) checks experimentally observed values (approximately); (2) the temperatures of concentric shells in the reactor (Figure 59) check experimental profiles (approximately); and (3) the unsteady state warm-up traces (Figure 60) check experimental data very well. The 0.3 values of emissivity are the most difficult parameter values to accept; however, in the absence of insulation between the outer shells, emissivities must necessarily be low to preserve a large temperature drop. The other possibility is that the small closed spaces between these outer shells may have filled with insulating scale particles; which would produce an effect similar to a low emissivity, althought not changing with temperature in the same way.

Future work to obtain better values of heat transfer parameters could proceed by taking more data of the type shown and attempting to optimize by formally minimizing deviations indicated by the simulations; or more satisfactorily a detailed experimental study could be undertaken of the heat fluxes at surfaces throughout the reactor. Any optimization beyond the informal search that was conducted to establish the agreement cited is counter recommended by the severity of the assumptions in the existing simulation (especially a uniform gas temperature). If a detailed heat flux study were to be undertaken, consideration should be given to studying time variations in convective coefficients linked to the cyclic flow.

B. WARM-UP WITH LIGHTOFF

Base case warm-up simulations with reaction were performed for 150 lb of exhaust per hour at 4% CO, 1.6% H_2, and 500 ppm hydrocarbon. The experimental data on warm-up was obtained by presetting the test engine at a particular air/fuel ratio, typically 12.5/1, and running at that fixed ratio from time zero forward. This mode of operation is not characteristic of choked operating modes used in practice to acceleration reactor ligntoff and warm-up.

A typical comparison of simulated and experimental results is shown in Figure 61 for an entering exhaust temperature of 1600°F and air dilution ratio of DR = .25. Time to lightoff and the temperature of approximately 1200°F at the threshold to ignition are in agreement with experimental results. The lesser amount of tailing in simulations for hydrocarbon and CO concentrations (H_2 was not measured experimentally and is not plotted) have already been mentioned in relation to reaction order and mixing. The other difference is the greater temperature rise after ignition in the simulation, which is explained by the conversion which takes place beyond the core, where temperature was measured, in the actual reactor. In the simulation, the ideal backmix assumption causes the entire temperature rise associated with reaction to be evidenced throughout the reactor.

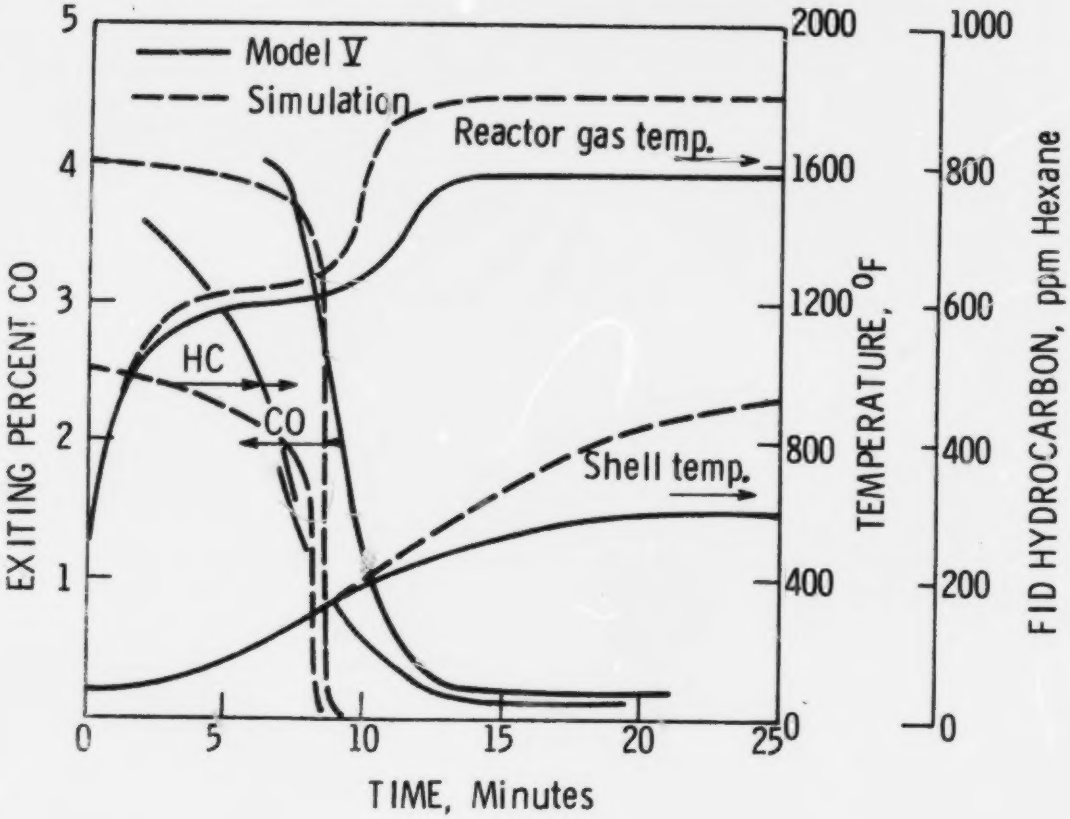

Figure 61. Comparison of experimental and typical simulated warmup for the DuPont Model V reactor.

By running simulations similar to the one in Figure 61 but different inlet temperatures and air dilution ratios, a map of time to ignition vs. inlet temperature and dilution ratio (Figure 62) was obtained. All of these simulations were conducted for an initial temperature of 1200°F in the CSTR, which caused the search to tend toward a low-coversion operating point at time zero. The dilution ratio of 0.148 represents the air fraction needed to stoichiometrically burn all combustible species. The lightoff curve for zero dilution ratio (no air) is a hypothetical curve representing the time required to bring the reactor gas temperature to 1300°F, which was approximately the temperature at which lightoff occurred when air was injected. This represents a limiting warm-up time which could perhaps be approached by shutting off air injection until a 1300°F reactor gas temperature was achieved and then slowly bleeding in air until ignition was established.

The base case simulations did not produce any immediate lightoff for the exhaust inlet temperatures (before air dilution) shown in Figure 61.

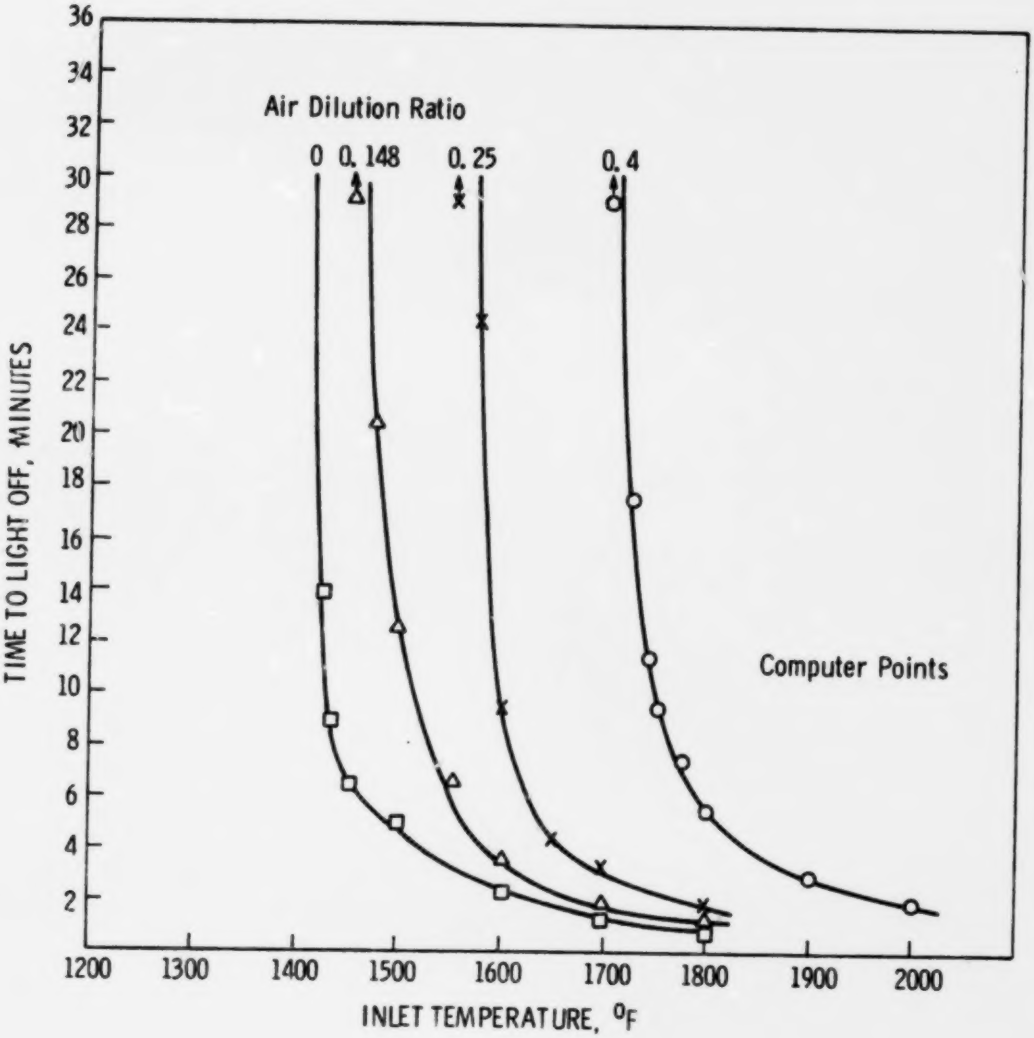

Figure 62. Simulation of lightoff for the DuPont Model V reactor. Base case: 4% CO, 1.6% H_2, 500 ppm HC.

VIII. Variations on the Base Case Warm-up Simulation

A. DESIGN AND OPERATION

A series of runs were made based on changes in design and combustible concentrations with air dilution ratios maintained the same as for base case. The variations made in the base case and results are given in Table IV and Figure 63. The discussion that follows relates to Figure 63, which represents simulation run at dilution ratio, DR = .25. Again, the initial temperature in the CSTR was set at 1200°F, tending to cause the search to approach at low conversion operating point at time zero.

A decrease in reactor diameter to 1/2 the base value while maintaining the same reactor length (points 1, Figure 63) caused the inlet exhaust temperature required to attain lightoff to increase by approximately 100°F. A fourfold decrease in reactor volume was here the controlling factor; the twofold reduction in heat transfer areas tended to counteract the volume change but was a smaller effect in the temperature range studied. Lightoffs at higher temperatures and earlier times were less affected due to the greater importance of heat loss in this region.

Doubling the reactor diameter (points 2, Figure 63) was actually detrimental at high inlet temperatures because of a controlling effect due to increased heat transfer area. However, at lower inlet temperatures and later times past start up, ignition was promoted by the longer residence time.

Reducing the combustible content (points 3, Figure 63) to 2% CO and 0.8% H_2 increased the inlet temperature for lightoff by approximately 50°F. In the context of the zero-order rate assumption and a low starting temperature in the search for an operating point, increasing the inlet reactant concentrations affects the lightoff of CO favorably only because of the larger temperature boost provided by reacting more of the readily oxidized hydrogen. Hydrocarbon, which was not changed in this simulation, would have a similar effect.

Increasing the combustible content from 4% CO, 1.6% H_2, to 8% CO, 3.2% H_2 (points 4, Figure 63) produced no appreciable effect. Interpretation of this result must again be tempered by realizing the obvious implications of the zero-order rate assumption. However, subject to this assumption, the greater hydrogen content has no effect simply because the primer effect of the lesser amount (1.6% H_2) was already sufficient to "ignite" the carbon monoxide. Increasing hydrogen content alone from 1.6% to 4% (points 5, Figure 63) had no effect for the same reason.

The existence of a triggering effect for hydrogen and hydrocarbon on the oxidation of carbon monoxide is very clearly evidenced in both simulations and

TABLE IV

TIME TO LIGHTOFF FOR VARIATIONS TO THE DUPONT MODEL V BASE CASE

(4% CO, 1.6% H_2, 500 ppm HC, 150 lb. exhaust per hour)

[2] Variation on base case, No.	AIR DILUTION RATIO 0.[1] Exhaust inlet temp., °F	0.1 Time to lightoff, minutes	0.148 Exhaust inlet temp., °F	0.148 Time to lightoff, minutes	0.25 Exhaust inlet temp., °F	0.25 Time to lightoff, minutes	0.4 Exhaust inlet temp., °F	0.4 Time to lightoff, minutes
1	1350	>25	1500	>25	1700	>25	1900	>25
	1400	9 1/2	1600	14	1725	15	1925	5
	1450	4	1650	4 1/2	1750	9	1950	4 1/2
	1600	1	1700	3 1/2	1800	4 1/2	2000	3
	1700	1	1800	2	1850	3		
					1900	2 1/2		
2	1350	>25	1450	>25	1450	>25	1600	>25
	1400	15 1/2	1475	16 1/2	1500	15 1/2	1650	13 1/2
	1450	9 1/2	1500	12	1550	9 1/2	1700	8 1/2
	1500	7 1/2	1600	6 1/2	1600	7 1/2	1750	6 1/2
	1600	4 1/2	1700	5	1700	4 1/2	1800	5 1/2
	1700	4			1800	4	1850	4 1/2
							2000	2 1/2
3	1425	15	1500	17 1/2	1600	23 1/2	1750	22 1/2
	1450	7 1/2	1550	8 1/2	1650	9 1/2	1800	9 1/2
	1550	5	1600	6	1700	5 1/2	1850	4 1/2
	1600	3	1700	4	1800	2 1/2	1950	3
4	1425	14	1500	12 1/2	1600	9 1/2	1750	11 1/2
	1450	9 1/2	1550	6 1/2	1650	4 1/2	1800	5 1/2
	1600	3	1700	2	1700	3 1/2	1900	3 1/2

TABLE IV (Contd.)

Variation on base case, No.[2]	0.[1]		0.148		0.25		0.40	
	Exhaust inlet temp., °F	Time to lightoff, minutes	Exhaust inlet temp., °F	Time to lightoff, minutes	Exhaust inlet temp., °F	Time to lightoff, minutes	Exhaust inlet temp., °F	Time to lightoff, minutes
5	1425	13 1/2	1475	19 1/2	1575	21 1/2	1725	16 1/2
	1450	7 1/2	1550	5 1/2	1650	4 1/2	1800	4 1/2
	1550	4			1750	2 1/2	1900	2 1/2
6	1350	>25	1425	19 1/2	1525	>25	1675	21 1/2
	1375	12	1450	11 1/2	1550	12 1/2	1700	10 1/2
	1400	7	1475	9 1/2	1575	9 1/2	1725	8 1/2
	1450	5 1/2	1525	6	1625	6	1775	5 1/2
	1550	4	1625	3 1/2	1725	3 1/2	1875	3 1/2
7.	1500	10	1500	>25	1650	8 1/2	1800	10 1/2
	1550	6	1575	5 1/2	1725	4	1875	5 1/2
	1650	3 1/2	1650	3	1800	2	1950	3 1/2
	1750	1 1/2	1800	1	1950	1	2100	1
8	1400	11 1/2	1400	>25	1550	13 1/2	1700	16 1/2
	1450	5 1/2	1425	17 1/2	1600	7 1/2	1750	9 1/2
	1500	1 1/2	1450	12 1/2	1650	3 1/2	1775	2 1/2
	1550	0	1525	4 1/2	1675	2 1/2	1800	1/2
			1600	0	1750	0		

NOTES TO TABLE IV

[1] Times to lightoff for an air dilution ratio of zero indicate the time required to reach a gas temperature of 1300°F within the reactor, which was the temperature which characterized lightoff for the base case.

[2] Variations to the DuPont Model V base case.

1 - reactor diameter 1/2xbase (1/4xvolume) with geometric similarity.

2 - reactor diameter 2xbase (4xvolume) with geometric similarity.

3 - low combustible entering; 2% CO, 0.8% H_2, 500 ppm HC.

4 - high combustible entering; 8% CO, 3.2% H_2, 500 ppm HC.

5 - high H_2/CO ratio; H_2/CO = 4%/4%.

6 - 1/2" asbestos insulation on outside of DuPont base case reactor.

7 - ceramic reactor - 1/16" thick core and shield, 1/8" thick shell.

8 - empty can with 1/2" asbestos insulation; no baffles.

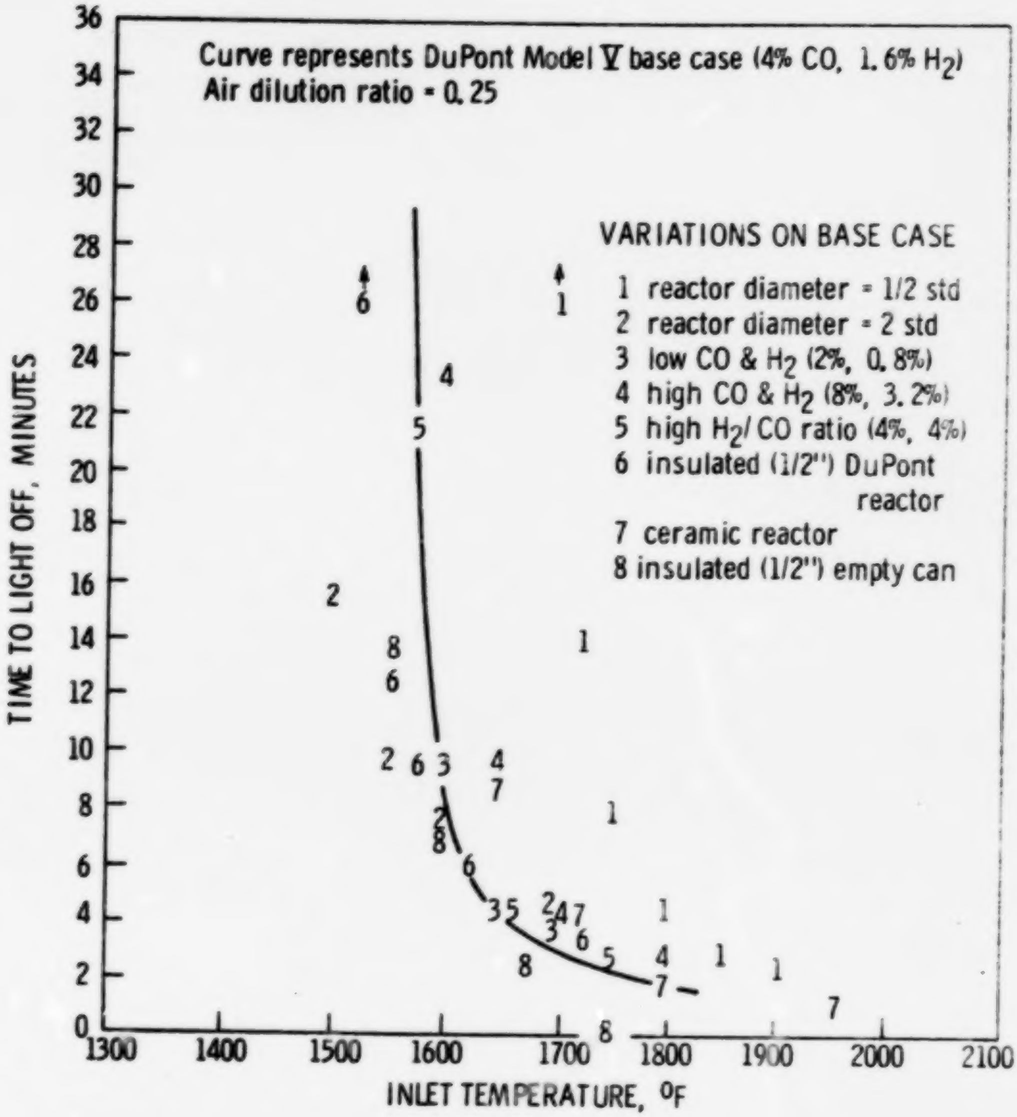

Figure 63. Deviations in time to lightoff for variations to the DuPont Model V base case.

in practice by the fact that at low entering combustible concentrations, these three major species may disappear one at a time with a rather long time lapse (minutes) between the successive events (this was particularly evident in the kinetics test reactor). At higher concentration, any time interval between events is bridged by the temperature rise due to the first specie oxidized, and all species disappear together in an avalanche ignition.

Returning to Figure 63 (points 6), placing 1/2 in. of asbestos insulation on the outside of the DuPont reactor retarded lightoff slightly at high inlet temperature in the period just following start up due to an added heat sink effect, it aided lightoff at lower temperatures due to the lesser heat loss with approach to steady state.

Simulations on a three-component ceramic reactor (Figure 63, points 7) having a 1/16 in. wall thickness for core and shield and a 1/8 in. shell indicated a slight deterioration in performance due to greater heat loss at the longer lightoff times approaching steady state. This may not represent a feasible design, and no general significance should be attributed to the result. It does, however, demonstrate that different materials of construction can be tested in the simulation.

The last design variation tested was a simulation of an empty insulated can (points 8, Figure 63), with no internal baffles to increase the mass and area for transient heat loss. In the region of short time to lightoff, this design was superior to all others and reached lightoff at time zero for an inlet exhaust temperature of 1750°F.

B. LIGHTOFF AT TIME ZERO

The simulation results shown in Figure 64 were run on the DuPont reactor configuration with a starting temperature of 3000°F to insure that a high temperature—high conversion solution would be the one approached provided it existed. At 8% CO, 3.2% H_2, and 1000 ppm HC (stoichiometric air rate), the approach to immediate lightoff is gradual, indicating that the role of change in heat loss after start-up remains important. That is, for the points along this approach, there existed no high-conversion solution at time zero, however, the low temperature solution is high enough to permit ignition as the heat loss declines after time zero.

At higher combustible contents, 12% and 16% CO, the existence of a high-conversion solution at time zero was evidenced at much lower inlet temperatures. However, if stable ignition did not occur at time zero as a result of the high initial temperature specified, the subsequent decline in heat loss was not sufficient to produce a transition to high conversion at a later time from the low temperature direction. Consequently, we obtain the sharp light-no light condition indicated in Figure 64.

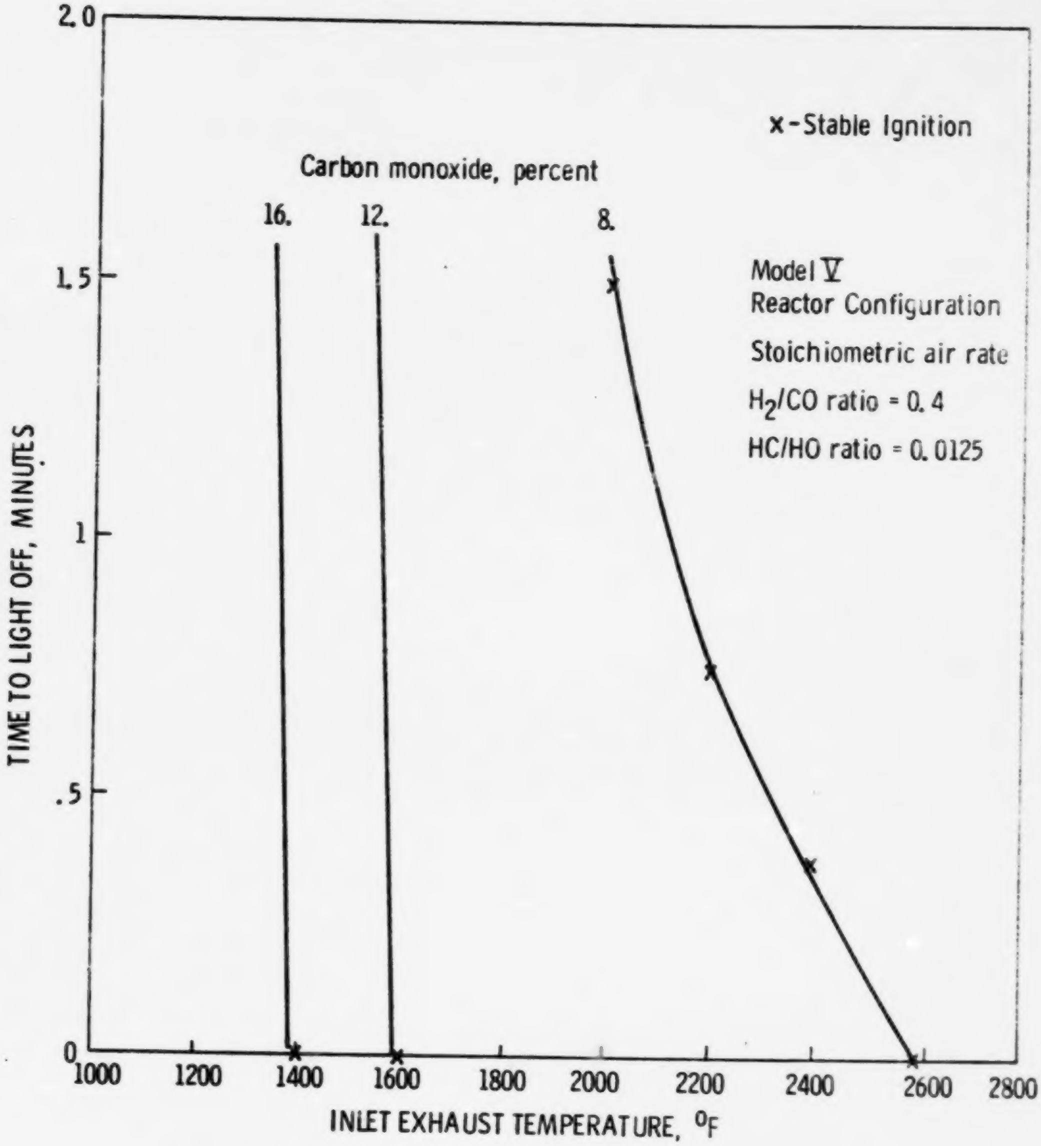

Figure 64. Approach to immediate lightoff.

Ignition at time zero in relation to inlet combustible concentrations is greatly influenced by the amount of heat loss occurring at start up. For a lower heat loss, the energy balance curve for a given feed concentration slopes more toward higher temperature (see Figure 67), causing a stable ignition to be achieved with less combustible. Returning to the simple insulated can, ignition from the high temperature side (an initial reactor temperature of 3000°F) was simulated and compared with previous results for a low temperature approach (Figure 64). Ignition at time zero for 4% CO was established at 1475°F from the high temperature side compared to 1750°F from the low. Again, use of the high temperature initial condition resulted in a sharp light-no light behavior. Since this is directly due to searching from the high temperature side *only at time zero* (the *initial* condition), the abruptness can be eliminated by searching from the high temperature side beyond time zero (Figure 65, "continuous ignition source"). Physically, this represents any continuing source of ignition, including hot regions in the temperature distribution of entering exhaust.

The "continuous-ignition-source" curve in Figure 65 was shown by a few isolated simulations to be highly sensitive to changes in feed concentrations. By changing the concentration from 4% CO to 3% and 5%, the time to lightoff at an entering exhaust temperature of 1350°F was observed to be changed to a time greater than 25 min and to zero (immediate lightoff), respectively. This contrasts very markedly with the low sensitivity to change in feed concentration observed for ignition approached from the low temperature side (Figure 63).

To better illustrate the simulation conditions which produced immediate lightoff, Figure 66 shows combinations of inlet exhaust temperature and feed CO concentration which produced complete reaction at time zero. All points were obtained by a high temperature approach to solutions. Because of higher heat loss, the DuPont reactor is indicated to require much higher inlet temperatures and/or inlet CO concentrations to achieve immediate lightoff than does the insulated can. Augmenting the hydrocarbon fraction, which was not simulated, would be expected to produce instant lightoff at lower concentration levels due to a much higher heat of reaction. This is an approach which could be taken to simulate warm-up on exhaust from a choked engine.

C. SUMMARY ON IGNITION EFFECTS

If we plot the amount of total combustible oxidized versus temperature for multiple oxidations in a CSTR, we obtain a material balance curve for which the amount converted tends to increase along with temperature in stages as shown in Figure 67. The zero-order assumption causes all segments of the curve to be concave upward. By increasing the amounts of the combustible types that are oxidized at lower temperatures, it is possible to cause the energy balance to shift past the right side of the material balance curve so that a high total conversion intercept is established in a low temperature

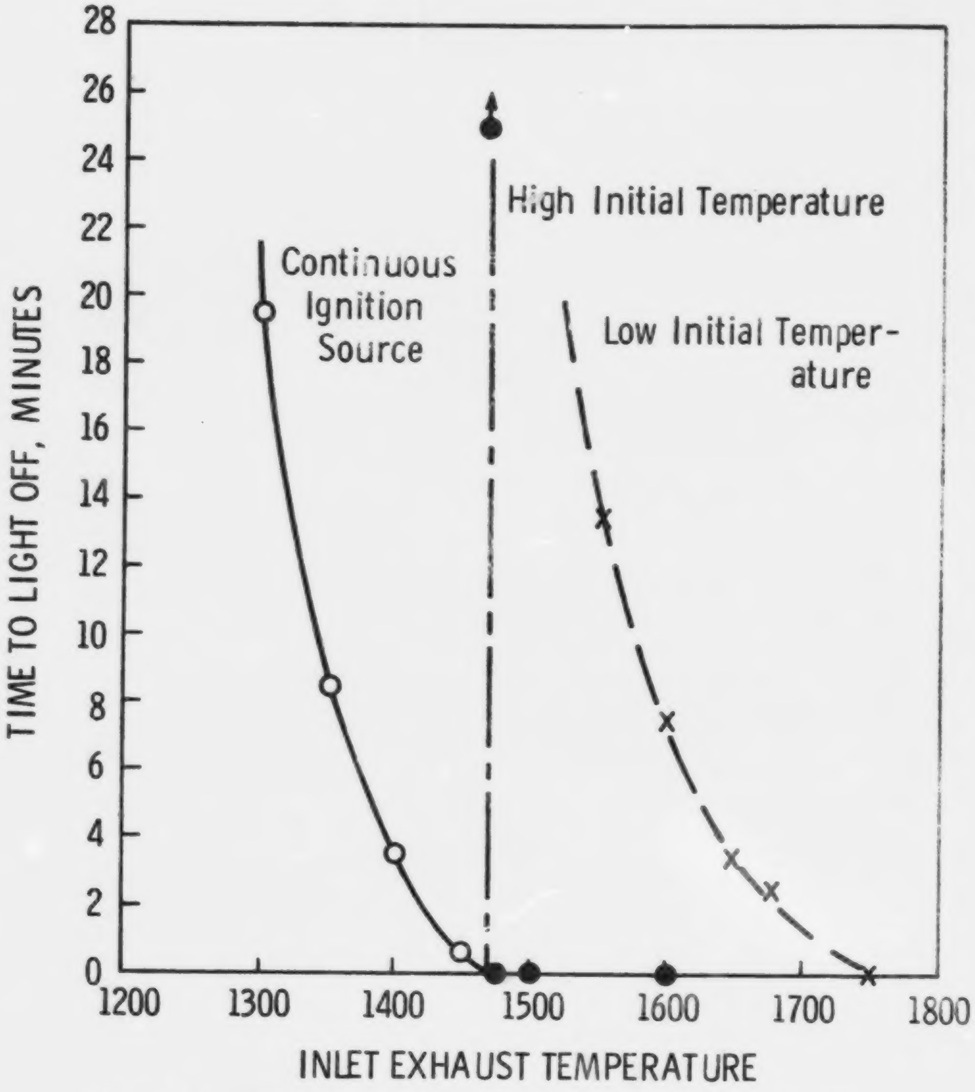

Figure 65. Simulated lightoff for insulated empty can.
X-T(time zero) = 1200°F; ● -T(0) = 2400°F;
O-continuous source of ignition;
f_m = 150 lb. exhaust/hr.; DR = .25;
V = 220 cu.in.;
Inlet mole fractions: CO = 4%, H_2 = 1.6%, HC = 500 ppm.

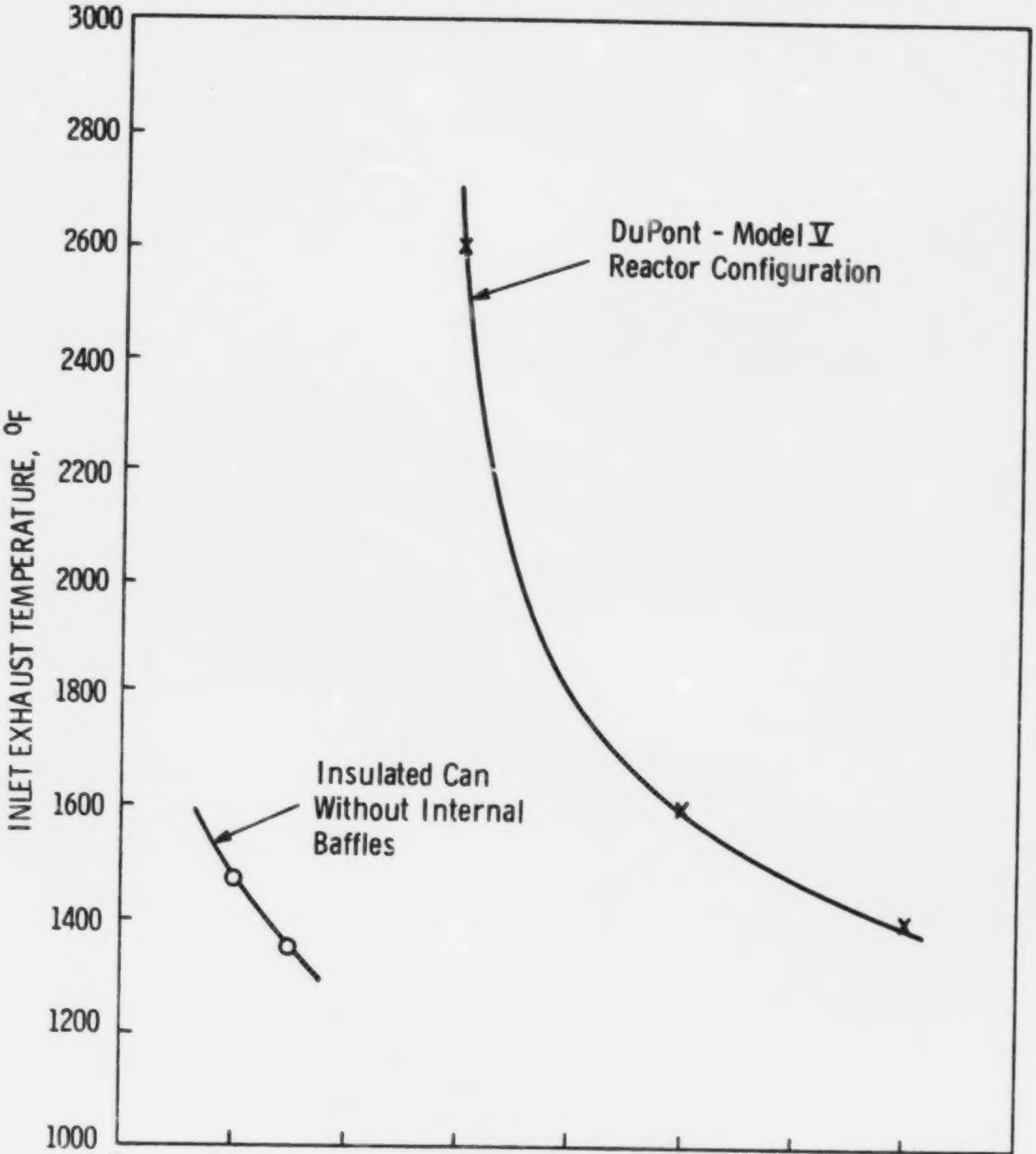

Figure 66. Warmup simulation of inlet properties required to achieve immediate ignition with stoichiometric air at 100°F. H_2/CO ratio = 0.4; HC/CO ratio = 0.012.

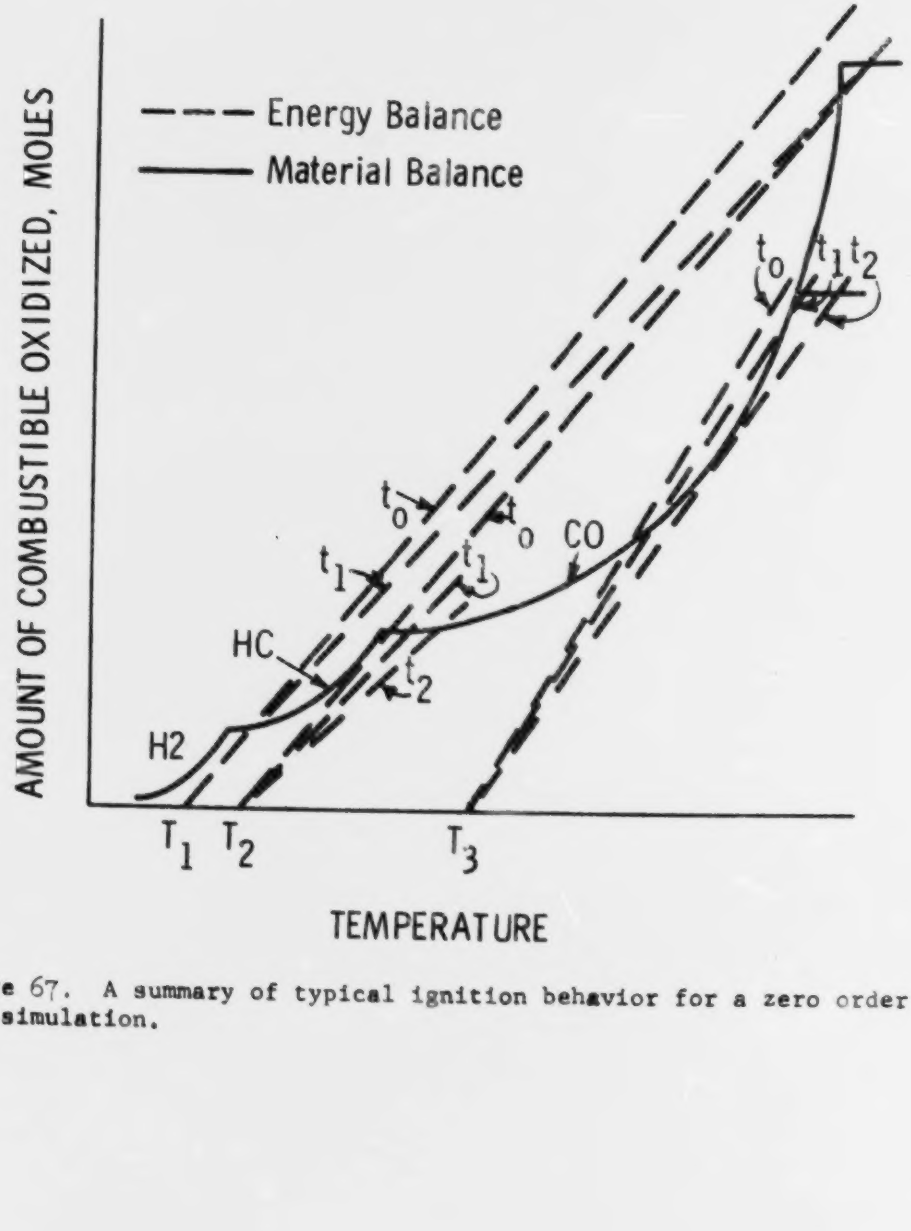

Figure 67. A summary of typical ignition behavior for a zero order CSTR simulation.

approach to a solution. Such a change in H_2 or HC is not shown in Figure 67, but can be visualized. This is the type of effect evidenced by changes in combustible concentration in Figure 63.

Referring to the energy balance lines in Figure 67, lines starting at the same inlet temperature (T_1, T_2, or T_3) but proceeding upward at different slopes are used to represent the shift in the energy balance with the progress of time past start up (t_o, t_1, ...) as heat losses are reduced. For the inlet temperature T_1 in Figure 67, no high conversion solution exists at time zero. If we increase inlet temperature slightly to T_2 and impose a high initial temperature, we do obtain a high conversion solution. If, however, the high temperature approach to a solution is invoked only at time zero, t_o, all subsequent solutions approached from low temperature at times t_1, t_2, ... , will exhibit low conversion. It is in this manner taht we obtain the light-no light ignition behavior shown in Figures 64 and 65. If, however, the approach to a solution continues to be from the high temperature side, the energy balance for T_1 at time t_1 does establish a high temperature solution and we obtain a "continuous-ignition source" result as is shown in Figure 65.

As the amount of total combustible is reduced, higher inlet temperatures are required to achieve lightoff (Figure 67, inlet temperature T_3). If the energy balance slopes are as shown at t_o, t_1, and t_2, it is possible to achieve three types of ignition for the same inlet temperature, T_3: (1) low conversion only at time t_o; (2) high conversion for a continuous-ignition-source approach at time t_1; and (3) a high temperature conversion from a low temperature approach at time t_2.

CONCLUSIONS AND USE OF RESULTS

IX. Summary and Conclusions

Reaction kinetics in the CRC study were determined at an experimentally verified stirred tank RTD; at a nonlimiting intensity of micromixing (based on simulations and high experimental conversions); and in contact with Hastelloy X and copper wall surfaces, without significant change in conversion. Tests were distributed reasonably evenly over the range of parameters. Results in a conversion range of 20 to 80% were linearly regressed to obtain least-squares values of the constants in an Arrhenius-type rate equation. A near-zero-order rate equation was determined for oxidation of carbon monoxide, which corroborated a test result of 99% conversion at 1687°F. Since simulations for first- or second-order reactions predict 99% conversion only at temperatures more than 1000°F higher than this, we are led to a strong conclusion that the near-zero-order kinetics are valid and that failure to achieve a close approach to complete conversion for CO in the DuPont reactor is due to incomplete mixing rather than order dependence.

Considering the blending of multiple cyclic inputs which characterizes the exhaust reactor problem, failure to approach complete conversion at a high temperature stationary state depends strongly on both the pattern of flow and the turbulent mixing intensity. Without a direct measurement of one or the other in a particular device, we cannot differentiate absolutely between the effect of a low backmix flow pattern which prevents maldistributed reactants from coming into proximity and a low mixing intensity which limits mixing after reactants are in proximity. "Proximity" implies a mixing scale, which for a one-phase system is a continuum of scales from molecular diameter to the system diameter, but which under the idealization of Danckwerts' (11) is considered to consist of distinct macro- and microscales of mixing.

Taken together the simulations run indicate three basic limitations on conversion due to mixing: departure of reactants from the reactor prior to cell-wise mixing due to insufficient micromixing intensity relative to a given flow pattern; lack of sufficient backmixing to blend mal-timed input of air and exhaust; and lack of sufficient backmixing to bring a low-temperature fraction of exhaust up to reaction temperature irrespective of timing of air injection. In all simulations, an improved conversion is indicated for an increase in the mixing intensity, I_m. An optimum flow pattern lies between the nonideal stirred tank and the nonideal plug flow reactor, since the first accentuates early departure and the second a persistence of maldistributions originating with input. Best simulated operation is indicated for a stirred tank core for backmixing followed by a plug flow exit section for preventing early departure.

The work of Corrsin (8) on turbulent reactors permits calculations of mixing intensity that are consistent with the geometry and performance of existing thermal exhaust reactors. Thus, this body of theory leads to estimates of the improvement which can be obtained.

Use of Corrsin's (8) theory requires that a length scale for turbulent variation in fluid properties be chosen in reference to the geometry of the reactor. Evangelista's (15,16) assumption that this length scale should be the sphere equivalent diameter of the reactor predicts conversions that are lower than the currently obtained experimental values. Use of the dimension of the inlet was found to give good agreement with experimental conversions.

In the kinetics test reactor having stirred tank flow, the calculation of mixing intensity from Corrsin's (8) theory based on the entire reactor volume predicts conversions that agree reasonably with experimental results. In the DuPont Model V reactor with a more dispersed flow, better agreement is obtained if an attenuation of mixing intensity through the reactor is assumed.

Experiments on the kinetics test reactor indicate that the early departure characteristic of a nonideal stirred tank are overcome sufficiently to yield 99+% CO conversion for surge-tank stabilized input for inlet dimensions which result in a pressure drop of 10 in. Hg. However, the large surge tank and the 10 in. Hg pressure drop are impractical in an engine mounted device.

Failure to reach essentially complete conversion in the DuPont Model V reactor is due to inadequate mixing rather than to a high order dependence on disappearing species. Cell simulations paralleling the operation of the DuPont reactor indicate that sufficient backmix blending can be accomplished in a network consisting of a nonideal stirred tank representing approximately one third the total reactor volume followed by a plug flow module so that simulation CO conversion for cyclic inputs can be increased to 99% or higher by sufficiently increasing mixing intensity. In an all plug flow simulation, conversions are kept below 50% for low pressure air and below 90% for ratioed air irrespective of mixing intensity due to persistence of maldistributions of reactant concentrations and temperature.

The actual flow pattern in the DuPont Model V reactor is not known. However, based on the best general correspondence between experimental and simulated conversions over a range of air injection fractions and reactor gas temperatures, a degree of backmixing which is consistent with 99% conversion for CO is inferred for high mixing intensities. Experimentally, it is indicated that no gross fraction of air leaves the reactor without coming into proximity with exhaust since a maximum conversion is approached with stoichiometrically equivalent air under favorable lightoff conditions.

The air dilution ratios and stoichiometric ratios that characterize operation of exhaust reactors fall in a range where mixing dependent conversions are importantly affected by them.

Simulated conversions for the DuPont reactor are very sensitive to an increase in the mixing parameter, I_m. The energy available in the exhaust blowdown occurring just after the exhaust valve opens is potentially capable of producing high mixing intensities and high conversions, based on an analysis using Corrsin's (8) theory of turbulent reactors. It has been tentatively concluded that failure to realize this potential is due to the essentially sequential input of air and exhaust which occurs with low pressure air injection. Sequential input of air and exhaust causes reactants to assume the dimension of the inlet port before they mix. The CO conversions obtained in the DuPont reactor are consistent with a mixing intensity I_m computed from this dimension and Corrsin's theory. Ratioed injection of air in close proximity to the exhaust valve would promote mixing based on the dimensions of the exhaust valve opening and the air jet. Mixing based on the maximum valve opening rather than the port diameter predicts an approximate doubling of the mixing intensity, I_m, and an increase in conversion from approximately 80 to 99%, based on simulation results only.

The use of ratioed air without sufficient backmixing would not have a beneficial effect because, in the absence of backmixing, a considerable proportion of the exhaust would remain at too low a temperature to react, despite adequate air.

Experimental results indicating 60% and higher conversions in the core of the DuPont reactor were matched by "POF" simulations only when the mixing parameter I_m was distributed in a manner that represented a decay of turbulence for flow passing through the reactor.

Reaction in the ports entering a reactor contribute only negligibly to the overall combustible conversion obtained. This is true for low pressure air injection because ports tend to be full of either air or exhaust alone due to zero air flow during peak exhaust flow. With ratioed air, significant reaction in the ports would occur in the high temperature peaks in the inlet flow.

The transition of conversions from a quenched low at start up to a high lightoff level occurs in practice after times ranging from a minute or less to an indefinite period. Modeling of warm-up is used to characterize the effects of design and operation on this time lapse to lightoff.

Lightoff involving a rapid transition at a time after start up occurs as the result of declining heat loss in a reactor which must be at least partially backmixed. For plug flow, exit conversion would be uniquely determined by inlet conditions and heat loss. However, with backmixing there exit multiple operating states and transitions between them; and the initial reactor temperature and perturbations in temperature are introduced as additional determining factors. In an ideal stirred tank, this ignition phenomenon is amenable to relatively simple analysis based on simultaneous solutions to material and energy balances on reactor contents.

Modeling warm-up to predict time to ignition is prohibitively expensive (on the computer) if numerical integration of unsteady state gas properties is performed continuously over a simulation of several minutes. Therefore, only changes in wall temperatures are integrated over the entire period, whereas gas temperature is updated periodically at intervals of several seconds and either extrapolated or treated by means of step increases.

Neglecting cyclic input, solutions for gas temperature and species conversions for multiple reactions are obtainable either by integrating from a last condition to a new quasi steady state (negligible change in wall temperature occurs during the time span of integration) or by solving simultaneous nonlinear algebraic equations representing the steady state. Since there exist in general several steady states, a well behaved method of solution must be sought taking into consideration the initial condition, perturbation conditions, and step size.

Integrations performed on properties of reactor contents are unstable unless a very short time step is used, since property changes occur on a time scale determined by residence time in the reactor. Therefore, the cost of even periodic computations remains prohibitively high.

Simultaneous solution of the algebraic equations is a one-dimensional search problem involving only explicit functions in the case of zero-order reactions. Oxidation of CO is indicated to be essentially zero order in this study; oxidation of H_2 is assumed to be zero order; and HC normally affects the energy balance only slightly. Thus, for these reactions a simple search strategy is a workable and useful method of solution. To investigate reaction order effects on warm-up, the computer simulation developed must be generalized by using a multivariate search strategy or Newton's method for vector valued functions.

Convective heat transfer coefficients and emissivities used in warm-up simulations on the DuPont reactor satisfy measured warm-up curves and steady state metal temperature profiles. Change in exhaust side coefficients from steady flow values obtained for literature correlations to twice these values has little affect on steady state heat loss, but does affect rate of metal warm-up. Change in emissivities between $\varepsilon = .1$ and .9 has an important effect at steady state, indicating sensitivity to the effectiveness of heat shielding.

Simulated ignition proceeds more abruptly than observed ignition, which can be attributed to either the assumption of CSTR flow, or zero-order reactions, or both. For most simulation conditions, H_2, HC, and CO disappear nearly simultaneously; however, at low inlet concentrations they disappear consecutively with a time lapse between, which agrees with tests on the kinetics test reactor.

The ignition behavior of a particular reactor design operating on a given inlet exhaust composition is characterized by running simulations of time to lightoff versus inlet temperature and air injection fraction. Such simulations can also be run for a low initial temperature for reactor contents, a high initial temperature, or a continuing high perturbation temperature (indicating a continuing source of ignition such as hot particulate matter or a hot segregated gas fraction).

Simulations for variations in design and operation using the DuPont reactor as a base case and starting at a low initial temperature indicated the following: changes in reactor diameter may either increase or decrease time to lightoff depending on the relative importance of change in area compared to change in reactor volume; under the prevailing assumptions including low initial temperature, a change in the inlet concentration of combustible affects time to ignition only to the extent that H_2 and CH as the more readily oxidizable species boost the temperature to promote oxidation of CO; insulation at the outside of the reactor slightly increases time to an ignition occurring immediately after start up but reduces it thereafter; removal of baffles produces an important reduction in time to lightoff.

Immediate lightoff at start up is predicted by simulations run at a high initial temperature, provided that inlet combustible concentration is high. The combustible concentration required is far lower in the absence of internal baffles than it is for the DuPont Model V design.

If a simulation approaches a solution from a high temperature only at time zero, there exists a critical inlet exhaust temperature which sharply separates immediate lightoff from indefinite unlit operation. However, if a simulation approaches a solution from a high temperature each time a new gas temperature is computed, to represent a continuing source of ignition, lightoff occurs below this critical temperature beyond time zero and an increase in inlet combustible concentration shifts lightoff sharply toward shorter times and lower temperatures. Since there exists a high temperature spike in the temperature distribution of the incoming exhaust, the simulations based on continuous ignition represent the most likely operating mode for a reactor.

X. Use of Results

It is established that stationary state conversions are limited by poor mixing which can be improved, rather than by an order dependence on disappearing species which could not be altered. Thus, justification exists for further simulations coordinated with experimental work to optimize the design and operating cycle of exhaust reactors at their stationary state.

Optimization for the high temperature stationary state is concerned with finding the reactor configuration which establishes the best pattern of flow together with the air injection location, timing, and pressure which best utilizes exhaust blowdown turbulence to accomplish mixing.

The work of Corrsin (8) provides a basis for correlating mixing intensities with reactor size and inlet geometry. However, the efficiency factor in the correlation is not known precisely, and should be determined more exactly for geometries that apply to exhaust reactors. For a known RTD, a "MIXONLY" type simulation could be fit to conversions for a very rapid reaction (possibly an oxidation at high temperature) to establish the effective mixing intensity for various inlet jet sizes and jet locations. By determining mixing efficiencies first for various simple geometries and then their combinations, a firm basis would be established for relating overall mixing effectiveness with complex geometries.

An extension of work on mixing efficiencies would be the determination of the distribution of mixing intensities where the intensity is decaying due to dissipation of turbulence or increasing due to generation of turbulence. An experiment might determine the distribution of conversions for a rapid exothermic reaction by measuring temperature distribution by optical methods. A PATTERN OF FLOW type cell mixing simulation could be used to fit the measured temperature or conversion distribution, and thereby infer a pattern of mixing intensity. Kattan and Adler (20) did essentially this for a rapid reaction in a plug flow reactor. Development of characteristic patterns of decay or growth of mixing intensity for flow through various geometries would provide a greatly improved basis for design in relation to geometry.

Further global-type simulations of complex reactors, similar to current simulations paralleling experimental work on the DuPont Model V reactor, should be carried forward to better determine the interrelation between cyclic input, extent and location of backmixing, and intensity and distribution of cell micromixing in determining reactant conversions. The optimal relative size of a nonideal stirred tank module and plug flow module in series should be investigated. A plug flow leading element should be added and air input ratioed to determine the advantage, if any, of reacting the combustibles in the inlet temperature spike prior to backmixing.

Distribution of heat losses should be further investigated from the viewpoint that reactions are accelerated by temperature rise in a reactor core where heat loss is low whereas they are decelerated by temperature drop in an outer annulus due to a high rate of heat loss. The amount of mixing that is accomplished in the core is coupled with heat loss and kinetics in determining the amount of temperature rise that will occur in the core to extend reaction into the annulus.

The warm-up simulation program can be used in present form to investigate further the effect of insulation and surface emissivities on the distribution of heat losses at stationary state. These heat losses can then be used as motivated estimates for mixing simulations.

A second tie in between warm-up and stationary state which should be simulated is the trade off that would be indicated for elimination of baffles to achieve earliest lightoff but also to surrender control of mixing geometry. The detailed effects of geometry on mixing limited conversion would have to be resolved before this trade off could be evaluated.

The ignition phenomenon of exhaust reactors should be further simulated using inlet combustible concentrations that are characteristic of choked engine operation. Simulations should be run in a pattern which would establish both the inlet combustible concentration and air injection fraction versus time which yield the lowest integrated emission during warm-up.

Cell mixing simulations can be used to check for bias introduced into the determination of activation energies and reaction orders provided that the experimental conditions and the distribution of data points in relation to conversion level are known.

Further simulations in the areas mentioned would be more profitable if certain extensions were made in existing simulation programs. These include:

The MICROMIX PATTERN OF FLOW simulation should be modified by addition of an executive iteration loop to handle backflow.

MIXONLY PATTERN OF FLOW should include both parallel modules and backflow. An energy balance feature for determining temperature distribution would also be useful.

WARM-UP should be extended to handle nonzero-order reactions.

The facility of WARM-UP to treat subvolumes should be extended to an ideal stirred tanks in series representation of gas temperature(s) and species conversions. Further coupling with "MICROMIX POF" should be considered.

APPENDIX A

MIXING AND REACTOR THEORY

1. MIXING IN REACTOR DESIGN

This appendix contains further information on the present state of mixing theory, in conjunction with chemical reactors.

A great deal of information about the state of mixing for the models described in Chapter I and for reactors in general can be obtained from the external, or exit residence time distribution. For simple models such as recycle or tanks in series, such residence time distributions can be expressed in a simple algebraic formulae:

Residence time distribution for a recycle model:

$$f(t) = \sum_{j=1}^{\infty} \frac{\gamma^j}{(1+\gamma)j} \delta (t - j\tau^*); \qquad (A-1)$$

$$\tau^* = \frac{v}{(1+\gamma)v_o} \qquad (A-2)$$

Residence time distribution for n ideal tanks stirred in series:

$$f(t) = \left(\frac{n}{\tau_T}\right)^n \frac{t^{n-1}}{(n-1)!} e^{-nt/\tau} \qquad (A-3)$$

These formulae are obtainable from the unsteady differential material balance with the aid of LaPlace transforms, as outlined by Levenspiel and Bischoff (23) for the case of tanks in series.

Conversions cannot be obtained unambiguously from kinetics and the RTD except in the very special case of a first-order reaction occurring without thermal effects on a single steady inlet flow of uniform composition. Levenspiel (22) points out that an average exiting composition computed from

$$\bar{c} = \int_{t=0}^{t=\infty} c(t)\, f(t)\, dt \qquad (A-4)$$

will be the correct exiting composition for order 1,
an upper bound for orders greater than 1,
a lower bound for orders less than 1;

subject to the qualifications in input given above. The stipulation of a single inlet is of obvious necessity if we consider that the arguments up to this point have had nothing to say concerning the extent of blending between separate entering streams.

To understand first the cause of ambiguity where there exists a single uniform input but order differs from 1, we turn to the concept of local mixedness introduced by Danckwerts (11). Working with a stirred tank residence time distribution, he assumed the following two limiting circumstances:

(1) Inflowing material is dispersed on a molecular scale in a time much less than τ, a condition described as complete micromixing. This condition has been implied for all discussion on ideal stirred tanks up to this point.

(2) Inflowing material is broken into cells which are far smaller than the tank and are uniformly dispersed through it, but which contain nevertheless a very large number of molecules which remain together for their entire stay in the reactor. This condition he described by saying that the fluid was completely "segregated." The length scale of segregatedness is not specified, and it is not directly important so long as there are a sufficiently large number of cells to be representative of the segregated property distributions that are now possible within the reactor.

Extents of conversion calculated for the above two cases are indicated by Zwietering (39) to show greater conversion for the completely segregated case when reaction order is greater than 1 and greater conversion for the completely micromixed case when order is less than 1. This still of course implies a single or premixed feed, since segregated cells of different reactants would not react at all in the segregated case.

Danckwerts (11) proceeded to define an index of segregatedness based on the ages of material within the system. He first defined a point age, α_p, which is the average age of material in one particular cell. If materials are uniformly distributed down to the molecular level, this average or point age will be the same for any defined cell containing a large number of molecules, and the distribution of point ages will be a delta function positioned at the mean age, $\delta(\bar{\alpha})$. However, if material is entirely segregated, point ages will possess the same distribution as the molecules.

The index of segregation proposed by Danckwerts (11) was the ratio of statistical variance in point ages to be the statistical variance in molecular ages, both internal to the system.

$$J \triangleq \text{Var}\ \alpha_p/\text{Var}\ \alpha. \tag{A-5}$$

For a completely micromixed stirred tank, the variance in point ages is zero; thus J = 0. For a segregated stirred tank, the variance in point ages equals the variance in molecular ages, and J = 1.

To obtain a better perspective on the significance of segregatedness, consider again conversion for a zero-order reaction in n ideal stirred tanks in series. Recall that conversion was indicated to be independent of n, and therefore apparently unaffected by flow pattern per se. In consideration of the early-departure property of a single ideal stirred tank, we can visualize this lack of dependence on pattern of flow only by considering the immediate dispersal on a molecular scale as in effect hiding low inlet concentrations to prevent immediate departure of all but a very small, second-order amount of reactant. However, if a reactant enters and remains segregated in one cell, early departure of that cell removes a not insignificant amount of reactant, and conversion is lowered. This intuititive reasoning is lent rigor by the fact that it is confirmed by calculations. Furthermore, we observe in this example evidence of the fact that kinetics and residence time distribution do not alone determine conversion.

If we apply the definition of Danckwerts' "J" to an ideal plug flow reactor, we see that all molecules at a "point" must possess the same age since all entered at essentially the same time. Consequently, point age and molecular age are synonomous, and J = 1. This argues that an ideal plug flow reactor is always completely segregated.

It is demonstrated that J may assume values from 0 to 1 for an ideal stirred tank but must be precisely 1 for an ideal plug flow reactor. In general, J can approach a limit of 1 for any residence time distribution since complete segregation as defined is always possible. However, complete micromixing to produce point ages that are everywhere the same depends directly on the random mixing occurring throughout a stirred tank. Therefore a value of J = 0 can be approached only for a CSTR residence time distribution; for an arbitrary RTD, the value of J will approach some lower bound between 0 and 1.

One further word concerning zero-order reactions; independence between conversion and the number of ideal tanks in series indicates that the increased tendency for early departure in going from plug flow to stirred tank flow must be cancelled out by a greater allowable extent of micromixing. Since the locus of this effect leads to the J = 0 bound for n = 1, we could be tempted to assume that the ideal tanks in series models provide a lower bound on J for all n, however, this has been demonstrated to be untrue based on the maximum mixedness concept of Zwietering (39), which is discussed next.

Zwietering (39) considered the bounding affect of residence time distribution on micromixing and devised two very clever models which represent, respectively, the minimum mixedness and maximum mixedness consistent with any arbitrary RTD

Minimum mixedness model:

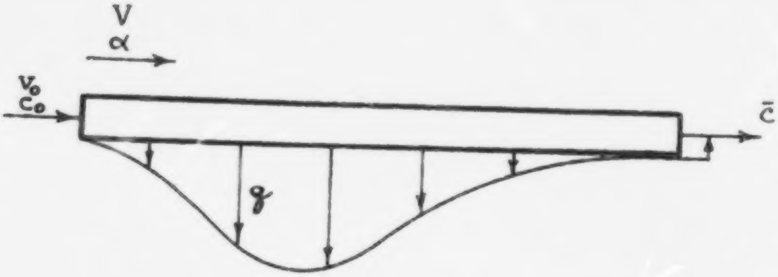

The minimum mixedness model consists of a plug flow reactor with side exits. Since all molecules at a given point in the plug flow reactor are of the same age, altering the distribution of side flow at points along the length of the reactor is a direct means of establishing any desired residence time distribution. Because of the complete segregation of material remaining within the reactor, we are assured that variance in point age equals variance in molecular age, and J = 1. A property that is demonstrated to coincide with segregatedness in this model is that mixing occurs as late as possible, i.e., at the reactor exit. Since each increment of material in the reactor acts independently, we can obtain the average exit concentration form:

$$\bar{c} = \int_0^\infty c(t)\ f(t)\ dt \tag{AI-4}$$

Parametric equations relating side flow q and displaced volume V for a designated residence time distribution are given by Zwietering (39).

Maximum mixedness model:

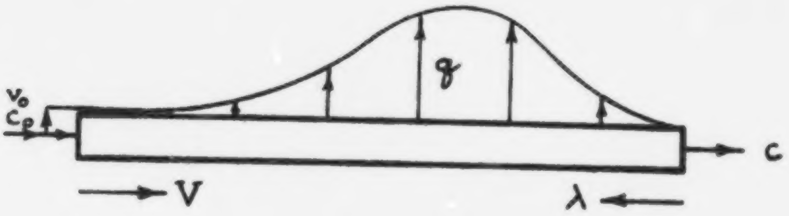

Any desired RTD can also be established with side entrance to a plug flow reactor, as illustrated above. In this case, all material at a given point in the reactor will possess the same life expectancy λ, and the differential equation for the model is written in terms of λ as follows:

$$\frac{dc}{d\lambda} - \frac{f(\lambda)}{1-F(\lambda)} (c - c_o) - r(c) = 0 \qquad \text{(A-6)}$$

This equation can be solved by integrating from $\lambda = \infty$ to $\lambda = 0$ if we have $c(\lambda = \infty)$ as a boundary condition at the left of the reactor, which is obtainable from the differential equation by noting that $dc/d\lambda\ (\lambda = \infty) = 0$. If the RTD is given by data, we do not know $\lim f(\lambda)/1-F(\lambda)$ as $\lambda \to \infty$, and a starting value for c must be estimated for some "large" λ (perhaps 3 or 4 times the mean resident time). Zwietering (39), by expressing age α as a function of life expectancy λ and using the definition $J = \mathrm{Var}(\alpha_p)/\mathrm{Var}(\alpha)$, was able to prove that this model satisfies sufficient conditions for J_{min}, and hence that the model is indeed a maximum mixedness model. The intuitive counterpart of this proof is that the model mixes feed and reactor contents at the earliest time possible.

In order to compute conversions for intermediate micromixedness, it is necessary to assume some history for groups of molecules, or cells, as they pass through the reactor. The issue in question is which molecules should be given opportunity to mix, and when in the sense for example that molecules in the minimum mixedness model are allowed to mix only with other molecules of the same age or with molecules at the exit from the reactor.

There exists in the literature two classes of intermediate mixedness models: extensions of Zwietering's min and max models through combination of the two, and cell models wherein mixing is accomplished by coalescence and redispersal of cells.

Villermaux and Zoulalian (37) have proposed a parallel combination of minimum and maximum mixedness models with inlet flow divided between the two.

Intermediate mixedness model:

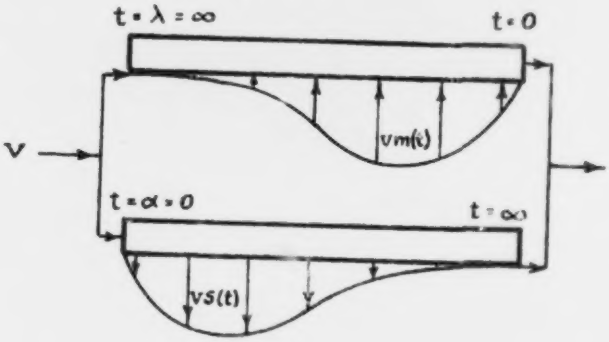

The state of mixedness is defined by a function of residence time, g(t), such that

$$s(t) = g(t)f(t)$$

$$m(t) = (1-g(t))f(t) \text{ and}$$

$$s(t) + m(t) = f(t).$$

Complete segregation is indicated where $g(t) \equiv 0$. Outlet conversion is computed by weighting the conversions from the minimum and maximum mixedness sections, which are obtainable from the differential equations already given for the min and max modules.

i.e.,

$$\bar{X} = \int_0^\infty X_s(t)\ g(t)\ f(t)dt + \left[\ \int_0^\infty (1-g(t))\, f(t)dt\right]\ X_m(o) \tag{A-7}$$

Weinstein and Adler (38) proposed a similar parallel model with g(t) equal to the step function U(t* - t), which is to say that material corresponding to the early portion of the residence time distribution from $t = 0$ to $t = t^*$ is directed through a minimum mixedness model, and that corresponding to $t = t^*$ to $t = \infty$ through a maximum mixedness model. Villermaux has pointed out that Weinstein and Adler made the error of integrating the maximum mixedness conversion to $\lambda = 0$, whereas its contribution should vanish for $\lambda < t^*$.

Series combinations of minimum and maximum mixedness models have also been proposed by Weinstein and Adler (38) and by Ng and Rippin (24). In the model of Ng and Rippin, it is assumed that material entering a reactor remains for a period of time in a poorly mixed region which is represented by minimum mixedness and then proceeds to a well mixed region around an impeller which is represented by maximum mixedness. Material is assumed to be transferred from the min to the max environment in proportion to the amount remaining in the first, and therefore in accordance with diffusional transfer. While this concept is simple, its execution is exceptionally involved.

The cell model concept of mixing which treats intermediate micromixedness by averaging properties for selected cells was introduced by Curl (10) to treat mixing of droplets in a dispersed phase. This model assumes that droplets themselves are uniformly dispersed throughout a well-stirred flow reactor and that the spread in concentration among drops tends to be averaged out by coalescences and redispersals for randomly selected drops. The model as developed further assumed that the drop opulation remains constant, that all drops are the same size, that departure from the reactor as well as coalescence involves randomly selected drops (due to stirred tank flow), that perfect mixing to a single concentration occurs when two drops coalesce, and that redispersals occur immediately after coalescences.

While the random coalescence cell model is physically motivated by dispersed droplets, it is entirely consistent with Danckwerts' original definition of micromixedness and may legitimately be proposed as a mechanism for describing intermediate mixedness for any system that has a stirred-tank flow pattern. Even prior to considering the mathematical description of the model, it is intuitively evident that the transition from complete segregation to complete mixedness can be accomplished by defining a rate of coalescence or "interaction frequency," ω_I, that assumes values from 0 to ∞.

The very special integro-differential equation derived by Curl (10) for this model was developed by performing a material balance on a concentration interval c to $c + dc$ of the concentration distribution $p(c)$. Based on the parameters ω_I defined as the fraction of cells coalescing per second and ω_r defined as the fraction of cells leaving per second ($\omega_r = 1/\tau$), the equation is as follows:

$$\begin{matrix}\text{Rate of}\\ \text{Change}\end{matrix} = \begin{matrix}\text{Flow}\\ \text{In}\end{matrix} - \begin{matrix}\text{Flow}\\ \text{Out}\end{matrix} - \begin{matrix}\text{Loss by}\\ \text{reaction}\end{matrix} + \begin{matrix}\text{Coalescence}\\ \text{into } c \text{ to } c{+}dc\end{matrix} - \begin{matrix}\text{Coalescence out}\\ \text{of } c \text{ to } c{+}dc\end{matrix}$$

$$\frac{\partial p(c)}{\partial t} = \omega_r p_o(c) - \omega_r p(c) - \frac{\partial [r p(c)]}{\partial t}$$

$$+ 4\omega_i \int_o^c p(c')p(2c-c')dc' - \omega_i p(c) \qquad \text{(A-8)}$$

No analytical solution is known for this equation, but it can be solved numerically either by treating the equation directly or by applying the Monte Carlo method to the original conditions describing the model. The equation has been solved numerically at steady state by Curl (10) for zero- and second-order reactions on a single feed concentration. Evangelista (15) describes a method of steady state solution based on the moments of the concentration distribution, which applies for high mixing intensities where the quotient ω_r/ω_i is close to zero and can be used in power expansions of "p" and its moments.

Spielman and Levenspiel (33) solved Curl's model by the Monte Carlo method to determine conversions for zero- and second-order reactions on a single inlet stream and for second-order reaction on two inlet streams carrying different reactants. The Monte Carlo method because of its simplicity is very easy to use for discretized systems compared to more cumbersome numerical methods, but it exacts a penalty in running time on a computer if large number of cells are to be treated.

The mixing intensity parameter used in correlation by Spielman and Levenspiel (33) was $I/2 = \omega_i/2\omega_r$, which is the number of coalescences that occur during the time interval between entering droplets. To avoid the cumbersome quotient notation we will denote this parameter as I_m.

The cell coalescence principle of Curl's model was extended by Kattan and Adler (20) to treat the mixing of separate reactant streams in a plug flow reactor. Here coalescence occurs only for cells occupying the same axial position, and the cells are thereby available to coalesce act as a miniature batch reactor with a reaction time equal to time of flight through the reactor. Kattan and Adler used this to fit experimental data by allowing the coalescence rate to change as a function of axial position.

2. THEORY OF AN IDEALIZED TURBULENT MIXER

In order to make use of cell models for treating mixing in reactors, it is necessary that we have a practical estimate of the mixing parameters ω_i and I_m based on obtainable system parameters. The work of Corrsin (8,9) on the scale up of stirred tanks leads to such an estimate, based on an assumption of homogeneous isotropic turbulence. A summary of this work and its relation to current mixing parameters follows.

From the work of Corrsin, the mean square fluctuation in concentration $\overline{C^2}$ in a homogeneous turbulent field obeys:

$$\frac{d\overline{c^2}}{dt} = -2D_v \sum_{i=1}^{3} \overline{\frac{\partial c^2}{\partial x_i}} \tag{A-9}$$

Under the assumption of a homogeneous isotropic field, the three mean-square components are equal and have one common value $2\overline{C^2}/l_m^2$, where this defines ℓ_m, the microscale of turbulence. Hence

$$\overline{\left(\frac{\partial c}{\partial x_i}\right)^2} = 6\,\frac{\overline{c^2}}{\ell m^2} \tag{A-10}$$

and

$$\frac{d\overline{c^2}}{dt} = -12\,\frac{D_v}{\ell m^2}\,\overline{c^2}\,. \tag{A-11}$$

From this equation, it is established that variance in concentration decays exponentially with a decay constant of $12D_v/\ell_m^2$, which we will define as β. It remains to express β in system parameters, and then to establish a correspondence with ω_i and I_m.

For a Schmidt number $N_{sc} \leq 1$, Corrsin ([illegible]) has derived an engineering expression for β as follows:

$$\beta = \frac{3-N_{sc}^2}{2\,\eta_m^{1/3}} \left(\frac{\pi}{5}\right)^{2/3} \left(\frac{g_c P_m}{L_c^2 M_r}\right)^{1/3} \tag{A-12}$$

where η_m is an efficiency,
N_{sc} is Schmidt Number,
L_c is the integral scale of concentration fluctuations,
M_r is the mass in the reactor, and
P_m is the mixing power applied to the reactor.

Corrsin in an earlier publication (8) indicates that $\eta \approx 1/2$; and since for CO and air, $N_{sc} \approx .82$ at 100°K (1340°F), we obtain, approximately,

$$\beta = 1.07 \left(\frac{g_c P_m}{L_c^2 M_r} \right)^{1/3} \tag{A-13}$$

Corrsin's earlier publication (8) differs from the latter (9) by about a factor of 2, and predicts a leading coefficient of approximately 1/2 after correction is made for an arithmetic error.

To establish a correspondence between β and ω_i, we return to the intego-differential equation for Curl's random coalescence model. This equation can be solved for the special case of batch mixing to establish the relationship of ω_i to the decay of variance in concentration, and therefore its relationship to β.

In Appendix B, a general formula is developed for moment equations for the concentration distribution p(c). For batch mixing without feed ($\omega_r = 0$) and without reaction ($r = kC^{\eta}$), this formula reduces to:

$$\frac{dm_k}{dt} + \left(1 - \frac{1}{2^{k-1}}\right) \omega_i m_k = \omega_i \sum_{j=1}^{k-1} a_{k,j} m_j m_{k-j} \tag{A-14}$$

$$a_{1,j} \equiv 0, \quad j = 1 \text{ and } 0$$

$$a_{k,1} = \frac{k-1}{2^{k-1}}, \quad k = 2, 3, \ldots$$

$$a_{k,k-1} = \frac{1}{2^{k-1}}, \quad k = 3,4,\ldots$$

$$a_{k,j} = \frac{1}{2}\left(a_{k-1,j-1} + a_{k-1,j}\right), \quad k = 4,5,\ldots \quad j = 2,\ldots,k-2$$

For k = 1,

$$\frac{dM_1}{dt} = 0 \text{ or } M_1 = M_{1_o}. \tag{A-15}$$

This of course only confirms what we already know; that the average concentration M_1 remains constant. However for k = 2,

$$\frac{dm_2}{dt} + \frac{\omega_i}{2} m_2 = \frac{\omega_i}{2} m_1^2 \tag{A-16}$$

$$m_2 = K e^{-\frac{\omega_i}{2} t} + m_{1,0}^2 \tag{A-17}$$

$$\overline{c^2} = \text{variance} = \sigma^2 = m_2 - m_1^2 = \sigma_o^2 e^{-\frac{\omega_i}{2} t} \tag{A-18}$$

Thus, with reference to ω_i, variance decays exponentially with a decay constant $\omega_i/2$: $\beta = \omega_i/2$, and $I_m = \omega_i \tau/2 = \beta\tau$.

3. SELECTION OF A MODEL TYPE FOR EXHAUST REACTOR SIMULATION

With reference to the review on reactor modeling, we recognize that a simulation of exhaust reactor performance should include provisions for altering both the pattern of flow and the degree of intermediate micromixing, or conversely segregatedness. The latter can be roughly viewed as the effectiveness of "local" mixing, recognizing however that the pattern of flow sets bounds that are related to the selection of the material that is allowed to mix.

Selection of a model type was guided by the necessity for handling the mixing of separate streams, where the rates of flow and properties of these streams vary cyclically. All of the literature models representing combinations of Danckwerts' minimum and maximum mixedness devices have been developed for steady flow to a single inlet and a single inlet concentration. Extension to treat the conditions of exhaust reactors, if possible, would require a high degree of mathematical sophistication.

By treating micromixedness in terms of functions that are single valued in J and which cause J to vary over a range from 1 to J_{min}, the class of models proposed by Villermaux and Zoulalian (37) and others does not allow differences in local segregation within a plug flow device, where J = 1. This is the result of assuming that micromixedness is an effect occurring in only one dimension. This view is satisfactory for a single or premixed feed entering an ideal plug flow device only because of the one-to-one correspondence between concentration and position, z. One-to-one correspondence between position and concentration is retained in the intermediate mixedness models because of the assumption that material transferred into Danckwerts' maximum mixedness model is instantaneously mixed with the material already at that position.

A more general view of the mixing problem is easily constructed. First, the ideal plug flow assumption can be relaxed to permit radial segregation, as in the cell model for progressive mixing of separate streams in a plug flow reactor proposed by Kattan (20). Beside segregation introduced in the feed, there exist in any real device internally generated property distributions which may be radially oriented. For reactors that are not radially symmetric, we could add a third dimension; and in general we could continue to relax stated or implied assumptions to treat the distributed mass transfer that we refer to as "mixing" with respect to an arbitrary set of dimensions: e.g., add to the three Euclidean dimensions-time, temperature, velocity, energy, a length scale on turbulence, state, density, ... This is not a useful approach (it is a lack of an approach); but to point it out does emphasize that a model does not represent an entirely general approach to mixing simply because it allows us to treat any arbitrary residence time distribution and intermediate values of "J" as a defined measure of "micromixedness."

What Villermaux and Zoulalian's (37) models (and other similar models) represent are a very special geometric flow pattern for given functions f(t) and s(t). That selection of f(t) and a s(t) value corresponding to a given "J" does not provide an unambiguous description of mixing has been shown by counter example: i.e., when Rippin (27) applied his model to the RTD for two ideal backmix reactors in series ($I_m = \infty$) at a mixedness given by the two-tank value of "J," conversion predicted for second-order reaction differed from that obtained from the two-tanks-in-series model itself. Since the "two-parameter" approach of specifying f(t) and J does not produce a unique result, there exists no compelling reason to follow it except where it is computationally convenient or there exists a particular geometric motivation for such a model. In view of the apparent difficulties in extending the approach to exhaust reactors, this type of modeling was dropped from consideration.

Cell models fashioned after those of Curl (10) for the stirred tank and Kattan and Adler (20) for plug flow have no inherent limitation in regard to number of inlet streams or periodicity of flow and inlet properties. The periodicity does however necessitate solution of the unsteady approach to a quasi-steady cyclic performance. In Curl's equation (10), application to exhaust reactor design involves replacing

$$\omega_r p_o(c) \text{ by } \sum_{j=1}^{k} \omega_{r_j}\, p_{o_j}\, (c_{i,t}) \tag{A-19}$$

for $j = 1,2,\ldots, k$ inlet streams and $i = 1,2,\ldots, m$ chemical species; similarly making the c' concentration a vector valued function of time; writing a similar dispersion equation for distribution of temperature, including provision for distributed heat loss; and making reaction rates appropriate functions of concentrations and temperature. For Curl's model per se, the method of treating moments of distributed properties was developed (Appendix B) sufficiently to show that the resulting differential equations were not a closed set. Evangelista's method of moments involving expansion in powers of (ω_r/ω_i) does not apply to low levels of mixing intensity and is unsatisfactory for that reason. Further, any treatment of these moments is still restricted to consideration of a stirred tank residence time distribution only.

In view of the complexity and the restrictions that result from treating Curl's equation or the corresponding moments, it was decided to pursue a Monte Carlo method of solution to the cell-wise models. The Monte Carlo approach applies for both stirred-tank and plug-flow flow patterns; it places no severe limitation on treatment of multiple inlets, periodicity, numerous species concentrations, temperature distribution, expressions for reaction rates, or extent and distribution of heat loss; and it allows the building of complex flow patterns by series and parallel combination of nonideal plug flow and stirred tank modules. Use of the flow pattern modules is also a geometrically motivated approach which readily allows a correspondence to be visualized between a model and the particular reactor which it represents; this is generally not true when specifying f(t) and J.

The Monte Carlo method applied to reaction coupled with cell-wise mixing in a network of reactor modules accounts for both "axial" dispersion and "local" segregation without solving a split boundary value problem as in the axial dispersion model or an integro-differential equation problem as in the random coalescence cell model approached from an analytical standpoint.

Reproducibility using the Monte Carlo method is determined by the total number of cells transiting a simulation module. A bias is introduced by the number of cells that are used to represent the contents of a module, with the correct number determined by the module size and the size of actual droplets or eddies. Viewed as a representative sample, the number of cells used is not critical so long as bias is satisfactorily small.

Spielman's (33) use of 500 cells to represent an arbitrarily large population caused unnecessary expense in running simulations, since current runs on 100 cells produced very nearly the same results for the case of mixing with instantaneous reaction. Even for only 10 cells in the reactor, the bias is comparable to the standard error of estimate for a throughput of 100 cells. Thus, first estimates can be obtained relatively inexpensively using a few cells. In the instance of a very small reactor volume or subvolume and a relatively large eddy size, a small number of cells will provide the best approximation of the true result.

Convergence to average stationary state conversions occurs in three or four mean residence times in a cell-wise mixed stirred tank. However, computation of variances and values of Danckwerts' (11) "J" necessitates a longer period of simulation, out to about ten mean residence times, because the weight given to the tails on the distributions of residence time and cell properties.

Combinations in series or parallel of Danckwerts' (11) minimum and maximum mixedness models (min-max models) as proposed in most general form by Villermaux and Zoulalian (37), were concluded to be inapplicable to treatment of multiple segregated reactant streams. All models of this type impose a rule of correspondence between the RTD and degree of micromixing by defining a function (or parameter) which causes the Danckwerts' "J" to vary from "1" to a minimum value by apportioning flow. Regardless of the apportionment, an element of entering feed is caused, under Danckwerts' original assumptions, to be immediately mixed with reactor contents at a point or points within the reactor, with no provision for mixing between points. Thus, for a plug flow RTD, feed from multiple inlet streams would necessarily be mixed at the inlet point and would remain segregated from other reactor contents in passing through the reactor; no progressive mixing as proposed by Kattan and Adler (20) is allowed.

Adaptation of a min-max type model to progressive mixing of streams would necessitate introducing partial mixing at Danckwerts' (11) points.

Partial mixing at a point would necessitate the introduction of cells and slugs of cells or their equivalent, as in the "POF" simulation, which would destroy the simplicity of the min-max model class and invalidate our ability to solve comparatively simple differential equations by standard numerical methods. Alternatively, we would be forced back to using the Monte Carlo method, with the min-max model supplying the rules for selecting cells that coalesce or leave the reactor.

If cell coalescence is used, it is deemed more desirable and practical to use geometry and flow to motivate mixing rules than to use the RTD in the context of a min-max model. The network flow and coalescence model, as developed in the MICROMIX PATTERNS OF FLOW simulation program, possesses ability to treat segregated feed; cyclic operation; multiple reactions; distribution of temperature under the influence of inlet temperatures, heat of reaction, and heat loss; the distribution of heat loss among cells and among modules; and distribution of mixing intensities among modules. The module network approach contains the nonideal stirred tank and the nonideal plug flow bounds as subsets. The solely mixing limited bound (instantaneous reaction) can be investigated by removing the kinetics and substituting a rule of complete disappearance for the limiting reactant in each coalescence.

Danckwerts' (11) "J" defined as the ratio of internal variance for point ages to that for molecular ages is not a sufficient index of "mixedness" for a system receiving segregated feed. This is true simply because "J" reflects only that segregation which is related to age, whereas segregation entering in the feed originates independently from age. In the specific instance of a series of nonideal stirred tanks, the value of "J" is related to both the number of tanks "n" and the cell mixing intensity, I_m. For instantaneous reaction, mixing limited conversion depends overwhelmingly on I_m and only slightly on changes in "J" that are independent of I_m (i.e., only slightly on the number of tanks).

An alternative "index," which is sensitive to segregation determined both by the feed and by internal mixing, is the conversion level that is attained for an infinitely rapid reaction. Its value for steady inlet flow of segregated reactant streams goes from 0 to a stoichiometric limit (100% conversion for the limiting reactant) as I_m goes from 0 to ∞, irrespective of flow pattern. For given cyclic inlet flows and concentrations, the solely mixing limited conversion goes from 0 to a maximum that is determined both by stoichiometry and backmixedness.

The solely mixing limited result provides an upper bound on conversion as temperature is increased. For a cell-wise-mixed stirred tank receiving feed at one temperature, the material balance curve (conversion versus temperature) has been observed to characteristically follow the curve for $I_m = \infty$ (ideal CSTR) until the mixing limited maximum is approached and then to asymptotically tend toward that maximum as temperature is further increased. This behavior is sufficiently regular to permit good estimates of the material balance for coupled mixing and kinetics to be obtained solely from the ideal CSTR curve and the "MIX ONLY" maximum in many cases.

APPENDIX B

MOMENTS OF THE CONCENTRATION DISTRIBUTION FOR CURL'S RANDOM COALESCENCE MODEL APPLIED TO A REACTION VELOCITY OF ORDER η, $r = -kc^{\eta}$

Starting with Curl's (10) equation for the random coalescence model, we

$$\frac{\partial p(c)}{\partial t} = \omega_r p_o(c) - (\omega_r + \omega_i)p(c) - \frac{\partial r p(c)}{\partial c} + 4\omega_i \int_o^c p(c')p(2c - c')dc', \qquad (B\text{-}1)$$

substitute $-kc^{\eta}$ for r (η a positive integer or zero) and take the partial derivative of the reaction term:

$$\frac{\partial r p(c)}{\partial c} = -k\left[c^{\eta} \frac{\partial p(c)}{\partial c} + \eta c^{\eta-1} p(c)\right]. \qquad (B\text{-}2)$$

We then proceed to take the LaPlace transform of the first equation, focusing attention first on the integral term.

$$L\left[4\omega_i \int_o^c p(c')p(2c - c')dc'\right] = 4\omega_i \int_o^{\infty} e^{-cs} \int_o^c p(c')p(2c - c)dc'dc \qquad (B\text{-}3)$$

Recognizing that the product $p(c')p(2c - c')$ is symmetric in c' about any point c, we change the integral $\int_o^c$ to $1/2 \int_o^{2c}$; and since $p(2c - c')$ is zero for all $c' > 2c$, this is equal to the integral $1/2 \int_o^{\infty}$. Then, substituting $\gamma = 2c - c'$ we obtained:

$$L[\qquad] = 2\omega_i \int_o^{\infty} e^{-c'\frac{s}{2}} p(c')dc' \int_o^{\infty} e^{-\gamma\frac{s}{2}} p(\gamma)d\gamma, \qquad (B\text{-}4)$$

or

$$L[\qquad] = \omega_i \hat{p}^2\left(\frac{s}{2}\right). \qquad (B\text{-}5)$$

The LaPlace transform of the entire original equation is then:

$$\frac{\partial \hat{p}}{\partial t} = \omega_r \hat{p}_o - (\omega_r + \omega_i)\hat{p} + k(-1)^{\eta}\partial^{\eta} \frac{(s\hat{p}(s))}{\partial s^{\eta}} + k\eta(-1)^{\eta-1} \frac{\partial^{\eta-1} p(s)}{\partial s^{\eta-1}} + \omega_i \hat{p}^2\left(\frac{s}{2}\right) \qquad (B\text{-}6)$$

To obtain moment equations for the transformed equation, we use the property of the kth moment given by

$$m_k = (-1)^k \lim_{s \to o} \frac{\partial^k p}{\partial s^k} \tag{B-7}$$

Applying this property, we obtain

$$\frac{\partial m_1}{\partial t} + \omega_r m_1 = \omega_r m_{1_o} - km_\eta, \tag{B-8}$$

where m_{1_o} is the first moment of the feed.

By successively taking partial derivatives with respect to s and taking the limit as $s \to 0$, we find

$$\frac{\partial m_2}{\partial t} + (\omega_r + \frac{\omega_i}{2})m_2 = \omega_r m_{2_o} + 1/2\omega_i m_1^2 - 2km_{\eta+1} \tag{B-9}$$

$$\frac{\partial m_3}{\partial t} + (\omega_r + 3/4\omega_i)\ m_3 = \omega_r m_{3_o} + 3/4\omega_i m_1 m_2 - 3km_{\eta+2} \tag{B-10}$$

$$\frac{\partial m_4}{\partial t} + (\omega_r + 7/8\omega_i)\ m_4 = \omega_r m_{4_o} + 1/2\omega_i m_1 m_3 + 3/8\omega_i m_2^2 - 4km_{\eta+3} \tag{B-11}$$

$$\frac{\partial m_5}{\partial t} + (\omega_r + 15/16\omega_i)\ m_5 = \omega_r m_{5_o} + 5/16\omega_i m_1 m_4 + 5/8\omega_i m_2 m_3 - 5km_{\eta+4} \tag{B-12}$$

$$\frac{\partial m_6}{\partial t} + (\omega_r + 31/32\omega_i)\ m_6 = \omega_r m_{6_o} + 3/16\omega_i m_1 m_5 + 15/32\omega_i m_2 m_4 + 5/16\omega_i m_3^2 - 6km_{\eta+5} \tag{B-13}$$

$$\vdots$$

Or in general the kth moment equation is

$$\frac{\partial m_k}{\partial t} + (\omega_r + (1 - \frac{1}{2^{k-1}})\omega_i)m_k = \omega_r m_{k_o} + \omega_i \sum_{j=1}^{k-1} a_{kj} m_j m_{k-j} - km_{\eta+j-1} \tag{B-14}$$

where we define

$$a_{1,0} = 0$$

$$a_{k,1} = \frac{k-1}{2^{k-1}}, \; k = 1,2,\ldots$$

$$a_{k,k-1} = \frac{1}{2^{k-1}}, \; k = 3,4,\ldots$$

$$a_{k,j} = \frac{a_{k-1,j-1} + a_{k-1,j}}{2}, \; \begin{array}{l} k = 4,5,\ldots \\ j = 2,\ldots,k-2 \end{array}$$

For a zero-order reaction ($\eta = 0$) at steady state,

$$\omega_r m_1 = \omega_r m_{1_o} - km_o; \tag{B-15}$$

and if we set $m_o = 1$, we obtain for $\bar{c} = m_1$ and $c_o = m_{1_o}$

$$\bar{c} = c_o - \frac{k}{\omega_r} = c_o - k\tau, \; \tau \leq \frac{c_o}{k} \; . \tag{B-16}$$

This suggests that for a given τ, $\bar{c}$ is independent of mixing frequency, ω_1, which is not true. This discrepancy results from ignoring the delta function singularity in the solution at $c = o$, which as pointed out by Curl (10) represents the fraction of cells in which reactant has been completely consumed.

For first-order reaction ($\eta = 1$) at steady state,

$$\omega_r m_1 = \omega_r m_{1_o} - km_1; \tag{B-17}$$

and for $m_{1_o} = c_o$, $\bar{c} = c_o \; 1/1 + k\tau$. Since for a first-order reaction the reactant concentration of a cell reaches zero only as time goes to infinity, we are not concerned with a singularity at $c = o$; and the last result confirms that the average conversion for $\eta = 1$ is independent of ω_1. This conclusion is invalid for feed comprised to two or more different streams, where cells enter at different concentration.

For integer values of η greater than 1, the moments equations for $j = 1,2,\ldots, k$ are not a closed set since the reaction term in the kth equation, being of the form $km_{\eta+j-1}$, will always introduce the $(k+1)^{th}$ or higher moment for $\eta = 2,3,\ldots$. Thus regardless how far we extend the sequence of equations, there will always be one more unknown (moment) than there are equations. We can by scaling concentration so that $c < 1$ cause higher moments to become small and essentially zero for some sufficiently large k. This would close the set. There remain however many additional mathematical complexities in dealing with multiple inlet streams, temperature dependence and heat loss, competing reactions, and the extension of cell-wise mixing to nonstirred residence time distributions.

APPENDIX C

DANCKWERTS' "J" FACTOR FOR STIRRED TANKS IN SERIES AT $I_m = \infty$

In order to evaluate "J" from the definition given by Danckwerts (11),

$$J = \mathrm{Var}(\alpha_p)/\mathrm{Var}(\alpha), \tag{C-1}$$

we must find the internal age distributions $\Phi(\alpha_p)$. The first of these we obtain from

$$\phi(\alpha) = \frac{1}{\tau}\,[1 - F(\alpha)]; \tag{C-2}$$

the second is calculated directly based on the fact that all point ages in the ith tank will have the same value as the mean age in the ith tank

$$(\alpha_{pi} = \tau_T \cdot i/n). \tag{C-3}$$

To find $\Phi(\alpha)$, we start with the material balance on a tracer concentration in the ith tank of "n" equal size tank:

$$C_{i-1} - C_i = \frac{\tau_T}{n}\,\frac{dC_i}{dt} \tag{C-4}$$

By taking the LaPlace transform of this equation, it can be shown that the exit residence time distribution for n tanks in series is:

$$f_n(t) = \left(\frac{n}{\tau_T}\right)^n \frac{t^{n-1}}{(n-1)\,!}\, e^{-nt/\tau_T} \tag{C-5}$$

Evaluating the step function $F_n(t)$ from the definition

$$dF_n(t) = f_n(t)dt, \tag{C-6}$$

we integrate by parts (repeatedly) to obtain:

$$F_n(t) = 1 - [(\frac{n}{\tau_T})^{n-1} \frac{1}{(n-1)!} t^{n-1} e^{-nt/\tau_T} \tag{C-7}$$

$$+ (\frac{n}{\tau_T})^{n-2} \frac{1}{(n-2)!} t^{n-2} e^{-nt/\tau_T}$$

$$+ \dots$$

$$+ (\frac{n}{\tau_T})^{1} \frac{1}{1!} t^{1} e^{-nt/\tau_T}$$

$$+ e^{-nt/\tau_T}] .$$

And, by substitution of α for t into $\phi(\alpha) = \frac{1}{\tau}[1 - F(\alpha)]$,

$$\phi(\alpha) = \frac{1}{\tau_T} [(\frac{n}{\tau_T})^{n-1} \frac{1}{(n-1)!} \alpha^{n-1} e^{-n\alpha/\tau_T} \tag{C-8}$$

$$+ (\frac{n}{\tau_T})^{n-2} \frac{1}{(n-2)!} \alpha^{n-2} e^{-n\alpha/\tau_T}$$

$$+ \dots$$

$$+ \frac{n}{\tau_T} \alpha e^{-n\alpha/\tau_T}$$

$$+ e^{-n\alpha/\tau_T}] .$$

Variance, the second moment about the mean σ^2, is computed from the first and second moments about the origin m_1 and m_2.

$$m_1(\alpha) = \int_0^\infty \alpha\phi(\alpha)d\alpha \tag{C-9}$$

Integration of $\alpha\Phi(\alpha)$ is simplified by noting that only those terms involving the factor $\alpha^{0}e^{-n\alpha/\tau T}$ will contribute to the integral, all others being zero.

$$m_1(\alpha) = \tau_T [\frac{n}{n^2} + \frac{n-1}{n^2} + \frac{n-2}{n^2} + \dots + \frac{1}{n^2}] = \frac{T}{n^2} \sum_{i=1}^{n} (n-i+1) \tag{C-10}$$

Similarly, $m_2(\alpha)$ is evaluated from $\int_0^\infty \alpha^2(\alpha)d\alpha$.

$$m_2(\alpha) = \frac{\tau_T^2}{n^3} \sum_{i=1}^{n} [(n - i + 1)(n - i + 2)] \quad (C\text{-}11)$$

And,

$$\text{Var}(\alpha) = \sigma^2 = m_2(\alpha) - [m_1(\alpha)]^2 \quad (C\text{-}12)$$

$$\text{Var}(\alpha) = \frac{T^2}{n^3} \left\{ \sum_{i=1}^{n} (n - i + 1)(n - i + 2) - \frac{1}{n} [\Sigma (n-i+1)]^2 \right\} \quad (C\text{-}13)$$

For point ages in the ith tank,

$$\alpha_{p_i} = \frac{i}{n}\tau_T \quad (C\text{-}14)$$

$$\phi(\alpha_p)_i = \frac{1}{n}\delta(\alpha_p - \alpha_{p_i}); \quad (C\text{-}15)$$

so that

$$m_1(\alpha_p) = \sum_{i=1}^{n} \left(\frac{i}{n}\tau_T\right)\left(\frac{1}{n}\right) = \frac{\tau_T}{n^2} \sum_{i=1}^{n} i \quad (C\text{-}16)$$

$$m_2(\alpha_p) = \sum_{i=1}^{n} \left(\frac{i}{n}\tau_T\right)^2 \left(\frac{1}{n}\right) = \frac{\tau_T^2}{n^3} \sum_{i=1}^{n} i^2 \quad (C\text{-}17)$$

$$\text{Var}(\alpha_p) = \frac{\tau_T^2}{n^3} \left\{ \sum_{i=1}^{n} i^2 - \frac{1}{n} \left[\sum_{i=1}^{n} i\right]^2 \right\}. \quad (C\text{-}18)$$

And finally,

$$J = \text{Var}(\alpha_p)/\text{Var}(\alpha) \quad (C\text{-}19)$$

$$J = \frac{\sum\limits_{i=1}^{n} i^2 - \frac{1}{n} \left[\sum\limits_{i=1}^{n} i\right]^2}{\sum\limits_{i=1}^{n} (n-i+1)(n-i+2) - \frac{1}{n} \left[\sum\limits_{i=1}^{n} (n-i+1)\right]^2} \quad (C\text{-}20)$$

REFERENCES FOR PHASE II

1. Bell, R. L. and Babl, A. L., "On the Extension of the Method of Moments to a Cascade of Well Mixed Discrete Stages with Backflow Between Stages," Chemical Engineering Science, 20, Dec. 1965, pp. 1001-1006.

2. Bird, R. B., Stewart, W. E., and Lightfoot, E. N., Transport Phenomena, Wiley, 1960, 24.

3. Blenk, M. H., and Franks, R.G.E., "Math Modeling of an Exhaust Reactor," SAE, Paper No. 710607, Mid-Year Meeting, January 7-11, 1971, Montreal, Quebec, Canada.

4. Brownson, D. A., and Stebar, R. F., "Factors Influencing the Effectiveness of Air Injection in Reducing Exhaust Emissions," SAE Transactions, 1966, 74.

5. Cantwell, E. N., and Pahnke, A. J. (DuPont), "Design Factors Affecting the Performance of Exhaust Manifold Reactors," SAE Transactions, 1966, 74.

6. Cantwell, E. N., Rosenlund, I. T., Barth, W. J., Kinnear, F. L., and Ross, S. W., "A Progress Report on the Development of Exhaust Manifold Reactors," SAE, Paper No. 690139, International Automotive Engineering Congress, Detroit, Michigan, January 13-17, 1969.

7. Chandler, J. M., Smith, A. M., and Struck, H. J., "Development of the Concept of Non-flame Exhaust Gas Reactors," SAE, Paper No. 486 M, National Automobile Week, March 1962.

8. Corrsin, S., "Simple Theory of an Idealized Turbulent Mixer," AIChE Journal, 3, No. 3, Sept. 1957, pp. 329-330.

9. Corrsin, S., "The Isotropic Turbulent Mixer: Part II, Arbitrary Schmidt Number," AIChE Journal, 10, No. 6, Nov. 1964, pp. 870-877.

10. Curl, R. L., "Dispersed Phase Mixing: I. Theory and Effects in Simple Reactors,: AIChE Journal, 9, No. 2, March 1963, pp. 175-181.

11. Danckwerts, P. V., "The Effect of Incomplete Mixing on Homogeneous Reactions," Chemical Reaction Engineering, 12th Meeting. Europ. Fed. Chem. Engrg., Amsterdam, 1957.

REFERENCES FOR PHASE II (Continued)

12. Daniels, W. A. (General Motors), "Engine Variable Effects on Exhaust Hydrocarbon Composition (A Single-Cylinder Engine Study with Propane as the Fuel)," *SAE*, Paper No. 670124, Automotive Engineering Congress, Detroit, Michigan, January 9-13, 1967.

13. Deans, H. A., and Lapidus, L., "Effects of Non-Ideal Flow Represented by a Tanks-In-Series Model," *AIChE Journal*, 6, 1960, pp. 656-663.

14. Dryer, F., Naegeli, D., and Glassman, I., "High-Temperature Oxidation Reactions of Carbon Monoxide," *Western States Section Combustion Institute* Preprint No. 71-26, 1971.

15. Evangelista, J. J., Katz, S., and Shinnar, R., "Scale-up Criteria for Stirred Tank Reactors," *AIChE Journal*, 15, No. 6, pp. 843-853.

16. Evangelista, J. J., Shinnar, R., and Katz, S., "The Effect of Imperfect Mixing on Stirred Combustion Reactors,". *Twelfth Symposium (International) on Combustion*. Poitiers, France, July 1968.

17. Gillespie, B., and Carberry, J. J., *I. and E. C. Fund.*, 5, 1966, 164.

18. Glass, W., Kim, D. S., and Kraus, E. J. (Esso), "Synchrothermal Reactor System for Control of Automotive Exhaust Emissions," *SAE*, Paper No. 700147, Automotive Eng. Contress, Detroit, Michigan, Jan. 12-14, 1970.

19. Horn, F.J.M., and Parish, T. D., "The Influence of Mixing on Tubular Reactor Performance," *Chem. Eng. Sci.* 22, Dec. 1967, pp. 1549-1560.

20. Kattan, A., and Adler, R. J., "A Stochastic Mixing Model for Homogeneous, Turbulent, Tubular Reactors," *AIChE Journal*, 18, 8, 1967, 585.

21. Kreith, F., *Principles of Heat Transfer*, International Textbook Company, 1965.

22. Levenspiel, O., *Chemical Reactor Engineering*, John Wiley and Sons, Inc., 1962.

23. Levenspiel, O., and Bischoff, K. B., "Patterns of Flow in Chemical Process Vessels," *Advances in Chemical Engineering*, 4, 1963, pp. 95-108.

24. Ng, D.Y.C., and Rippin, D.W.T., "The Effect of Incomplete Mixing on Conversion in Homogeneous Reactions," *Third European Symposium on Chemical Reaction Engineering*, Amsterdam, Sept. 1964, p. 161. Pergamon Press, Oxford, 1965.

REFERENCES FOR PHASE II (Continued)

25. Patterson, D. J., *et al.*, "Kinetics of Oxidation and Quenching of Combustibles in Exhaust Systems of Gasoline Engines," *Annual Progress Report No. 2 to CRC*, 1970-71.

26. Perry, R. H., Chilton, C. H., and Kirkpatrick, S. D., *Chemical Engineers' Handbook*, McGraw-Hill Book Company, 1963.

27. Rippin, D.W.T., "Segregation in a Two-Environment Model of a Partially Mixed Chemical Reactor," *Chem. Eng. Sci.*, 22, 1967, pp. 247-251.

28. Rippin, S.W.T., *I. and E. C. Fund.*, 6, 1967, 488.

29. Schwing, R. C. (General Motors), "An Analytical Framework for the Study of Exhaust Manifold Reactor Oxidation," *SAE* preprint 700109, Jan. 1970.

30. Shinnar, R., and Naor, P., "Residence Time Distribution in Systems with Internal Reflux," *Chem. Eng. Sci.*, 22, Oct. 1967, pp. 1369-1381.

31. Sigworth, H. W., Jr., Myers, P. S., and Uyehara, O. A., "The Disappearance of Ethylene, Propylene, n-Butane, and 1-Butane in Spark-Ignition Engine Exhaust," *SAE*, Paper No. 700472, Mid-Year Meeting, Detroit, Michigan, May 18-22, 1970.

32. Sondreal, E. A., Kadlec, R. H., and Carnahan, B., "Computer Programs for Reactor Design," *Coordinating Research Council*, APRAC-CAPE 8-68, New York, New York. (Unpublished computer listings with documentation on file.)

33. Speilman, L. A., Levenspiel, O., "A Monte Carlo Treatment for Reacting and Coalescing Dispersed Phase Systems," *Chem. Eng. Sci.*, 20, 1965, pp. 247-254.

34. Stainthrop, F. P., and Sudall, N., "Backmixing in a Rotating Disc Contractor," *Trans. Inst. of Chem. Eng.*, 42, 1964, pp. T193-T208.

35. Tabaczynski, R. J., Heywood, J. B., and Keck, J. C., "Time-Resolved Measurements of Hydrocarbon Mass Flow-Rate in the Exhaust of a Spark-Ignition Engine," *SAE*, Paper No. 720112, Automotive Engineering Congress, Detroit, Michigan, Jan. 10-14, 1972.

36. Terukatsu, M., and Vermeulen, T., "Diffusion and Back-Flow Models for Two-Phase Axial Dispersion," *I. and E. C. Fund.*, 2, Nov. 1963, pp. 304-320.

REFERENCES FOR PHASE II (Concluded)

37. Villermaux, J., and Zoulalian, A., "State of Mixedness of Fluid in a Continuous Reactor—With Respect to a Model of Weinstein and Adler," Chem. Eng. Sci., 24, 1969, pp. 1513-17.

38. Weinstein, H., and Adler, J., "Micromixing Effects in Continuous Chemical Reactors," Chem. Eng. Sci., 22, 1967, pp. 65-75.

39. Zwietering, T. N., "The Degree of Mixing in Continuous Flow Systems," Chem. Eng. Sci., 11, No. 1, 1959, p. 1.

NOMENCLATURE FOR PHASE II

Symbol	Quantity Letter Symbols
$a_{k,j}$	a coefficient in the k^{th} moment equation for the property distribution p(c) belonging to the product $a_{k,j} \cdot m_j \cdot m_{k-j}$.
a_i, b_i, c_i, and d_i	constants in specific heat equations
A	area, sq. ft.
A_k	the preexponential term in the rate equation for a reaction "k".
c	concentration, lb moles/cu.in.
$C_{j,i}$	mole fraction of specie "i" in cell "j".
C_i	mole fraction of specie "i".
C_p	specific heat (at constant pressure), Btu/lb mass °F or Btu/lb mole °F.
D	diameter, ft.
D_L	axial dispersion coefficient, ft^2/sec.
D_v	molecular diffusivity, ft^2/sec.
DR	dilution ratio for exhaust with air; volumetric air flow (stream 2)/volumetric exhaust flow (stream 1).
E_k	activation energy for reaction "k", cal/gmole.
f_m	mass flow rate, lb mass/hr.
f(t)	exit age distribution function, dimensionless.
F(t)	dimensionless tracer response to a step input; $F(t) = \int_0^t f(t)dt$.
F_i	functions defined by the material and energy balance, which are to be minimized (to zero) to solve for operating temperature and conversions in a CSTR.
g(t)	a function of time having value less than or equal to 1 used in Villermaux and Zoulalian's (46) mixedness model. $g(t) \equiv 1$ implies complete segregation and $g(t) \equiv 0$ complete segregation.

NOMENCLATURE FOR PHASE II (Continued)

Symbol	
G	mass velocity or flow rate per unit area, lb_m/hr.sq.ft.
Gr	Grasshof number = $\beta_T\ g\ L^3\ \Delta\ T\ \rho^2/\mu^2$
h	gas phase heat transfer coefficient, Btu/hr.sq.ft.°F.
H_i	the enthalpy of a pure specie, "i", Btu/lb mole
ΔH_{r_k}	heat of reaction for a reaction k represented by stoichiometry $\nu_{i,k}$, Btu, for the reaction as written.
HA_c	thermal conductance by conduction or convection, Btu/hr °F.
HA_r	thermal conductance, Btu/hr.°F.
I_m	the number of coalescences occurring per unit of residence frequency, $I_m = \varpi_i/2\omega_r$
J	Danckwerts' (12) index of segregation: $J = \text{var}\ (\alpha)/(\alpha_p)$, internal ages.
k	reaction rate constant, $(\text{cu.in/lb mole})^{1-\eta}$/sec.
k_f	thermal conductivity of a fluid at the mean film temperature, Btu/hr.ft.°F.
k_t	thermal conductivity, Btu/hr.ft.°F.
L	length, ft.
L_c	the "integral scale of turbulence", ft.
L_r	sphere equivalent reactor diameter, ft.
m	the total number of chemical species in a simulation.
$m(t)$	$= (1-g(t))f(t)$.
m_k	the k^{th} moment of a property distribution; $m_k \triangleq \int_0^\infty p(c)\ c^k\ dc$
M	mass, lb mass.

NOMENCLATURE FOR PHASE II (Continued)

Symbol	
M_c	mole contents of a cell, lb moles.
M_r	mass in the reactor, lb_m.
M_{w_i}	molecular weight of a species "i".
n	number of tanks in a tanks in series model.
N_c	the number of cellsin a cell-wise mixed reactor module.
$p(c)$	the normalized distribution function for concentration, $(\int_0^\infty p(c)dc = 1)$.
P_r	the number of parts in the thermal simulation of a reactor.
P	pressure, psia.
P_i	partial pressure of specie "i", psia.
P_m	mixing power in Corrsin's (9,10) engineering correlation for β, ft lb_f/sec.
q	the number of oxidizable chemical species, or the number of reactions.
q_{act}	the number of active species, which appear as reactants or products in any reaction, as opposed to inert species.
Q	heat loss from a reactor or reactor module, Btu/hr.
$\bar{r}_i$	the rate of "appearance" of a specie "i", lb moles/sec. cu.in.
r_k	the rate of a reaction "k", lb moles/sec.cu.in.
R	gas law constant, 1.987 cal/gmole °K or 18540.psi cu.in./lb mole °R.
s	the LaPlace transform variable defined by $L[(f(t)] = \int_0^\infty e^{-ts} f(t)d\,t$.

NOMENCLATURE FOR PHASE II (Continued)

Symbol	
$s(t)$	a fraction of the residence time distribution function defined by $s(t) = g(t)\ f(t)$, used in Villemaux and Zoulalian's (46) mixedness model.
SR	the stoichiometric ratio of oxygen to the oxidized specie (s).
t	time, seconds or hours.
T	temperature, degrees F, except °R for radiant heat transfer and °K in Arrhenius term.
TLOW	a computer variable for the low temperature assumed during cycling of temperature, °F.
TSPAN	the span of temperature change for cycling exhaust temperature, °F.
u	velocity, ft/sec.
$U(t^{*}-t)$	the unit step function at $t = t^{*}$.
v	volumetric flow rate, ft^3/sec.
v_m	molar flow rate, lb moles/sec.
V	reactor volume, cu.in.
V_c	volume of a single cell, cu.in.
X_i	chemical conversion of specie "i"; fraction converted into product.
X_m	conversion in a maximum mixedness reactor.
X_s	conversion in a segregated reactor.
y	fractional length through a reactor, z/L.
z	length

NOMENCLATURE FOR PHASE II (Continued)

Symbol	Greek Letter Symbols
α	age, sec.
α_p	average age at a point, as defined by Danckwerts (12), sec.
β	a constant for the decay of turbulence defined by $\frac{d\overline{C^2}}{dt} = - \beta \overline{C^2}$.
β_T	temperature coefficient of volume expansion, 1/°R.
γ	recycle ratio.
γ_c	ratio of specific heats, C_ρ/C_v.
$\delta(t)$	Dirac delta function, representing an idealized pulse occurring at time zero.
ε	emissivity for radiation.
η or $\eta_{i,k}$	reaction order (of a specie "i" in a reaction "k".)
η_m	mixing efficiency.
λ	life expectance, sec.
μ_i	viscosity of a pure specie, "i", lb_m/ft.sec.
$\nu_{i,k}$	a stoichiometric coefficient for a specie "i" in a reaction "k"; negative value indicates a reactant and positive value a product.
ρ	density, lb_m/ft^3.
τ	mean residence time, sec.
τ_T	mean residence for a system, as for example all tanks in a tanks in series model, sec.
σ	one unit of standard deviation for a normally distributed statistic.
σ_r	Stefan-Boltzman constant, Btu/hr.sq.ft.$°R^4$.

NOMENCLATURE FOR PHASE II (Concluded)

Symbol	
σ^2	variance, or the second moment about the mean, for the propeity distribution p(c); $\sigma^2 = \int_0^\infty p(c)\ (c-\bar{c})^2\ dc$.
$\phi(\alpha)$	the internal age distribution.
ω_i	the fraction of cells coalescing per second, equal to two times the number of coalescences per second devided by the number of cells in the reactor.
ω_r	the residence frequency, $1/\tau$.

DIMENSIONLESS GROUPS

$\overline{Nu}$	average Nusselt number, $\bar{h}D/k_f$
Pe	Peclet number = $L\ u/D_L$
Pr	Prandtl number = $C_p\mu/k_f$
Re	Reynolds number = $Du\rho/\mu$
N_{SC}	Schmidt number, $\mu/\rho D_v$
Gr	Grasshof number = $\beta_T\ g\ L^3\ \Delta\ T\ \rho^2/\mu^2$

DETAILED PROGRESS - PHASE III

SPECIAL INSTRUMENTATION DEVELOPMENT AND MEASUREMENTS

A. SUBTRACTIVE COLUMN HYDROCARBON ANALYSIS

1. Purpose

For assessing thermal reactor performance or for that matter performance of any emission control device, it is desirable to determine not only the reduction possible in total hydrocarbon emission but also the reduction in reactive constituents. In our study the subtractive column technique of Sigsby[1] was selected for a measure of reactivity change since our laboratory did not possess adequate gas chromatographic capability and because this technique allowed relatively rapid determinations to be made. Thus data could be obtained for a variety of operating points. Olefinic exhaust content was used as the reactivity measure. Experimental results were reported in a number of curves in both the First and Second Annual Progress Reports.

2. Equipment

According to Sigsby, the subtractive column subdivides the hydrocarbons into three subgroups, olefins plus acetylenes, aromatics, and paraffins. Two scrubbers are used. Olefins and acetylenes are removed by a mercuric sulfate-sulfuric acid scrubber and aromatics are removed by a palladium sulfate-sulfuric acid scrubber. A flame ionization detector (FID) is used as the hydrocarbon detector.

Figure 1 shows a flow schematic of The University of Michigan system. The unit has three parallel paths. The exhaust sample is directed either through path S_1 (total hydrocarbons), S_2 (total minus olefins and acetylenes), or S_3 (total minus olefins, acetylenes, and aromatics). Provisions were made for zeroing the FID and for backflushing with dry nitrogen. A master timer selects the flow path and controls sampling and backflushing. Details of construction are included in Ref. 1 and are not repeated here.

---

[1] Klosterman, D. L., and J. E. Sigsby, "Application of Subtractive Techniques to the Analysis of Automotive Exhaust," Environmental Science and Technology, 1, No. 4, April 1967, p. 309.

Preceding page blank

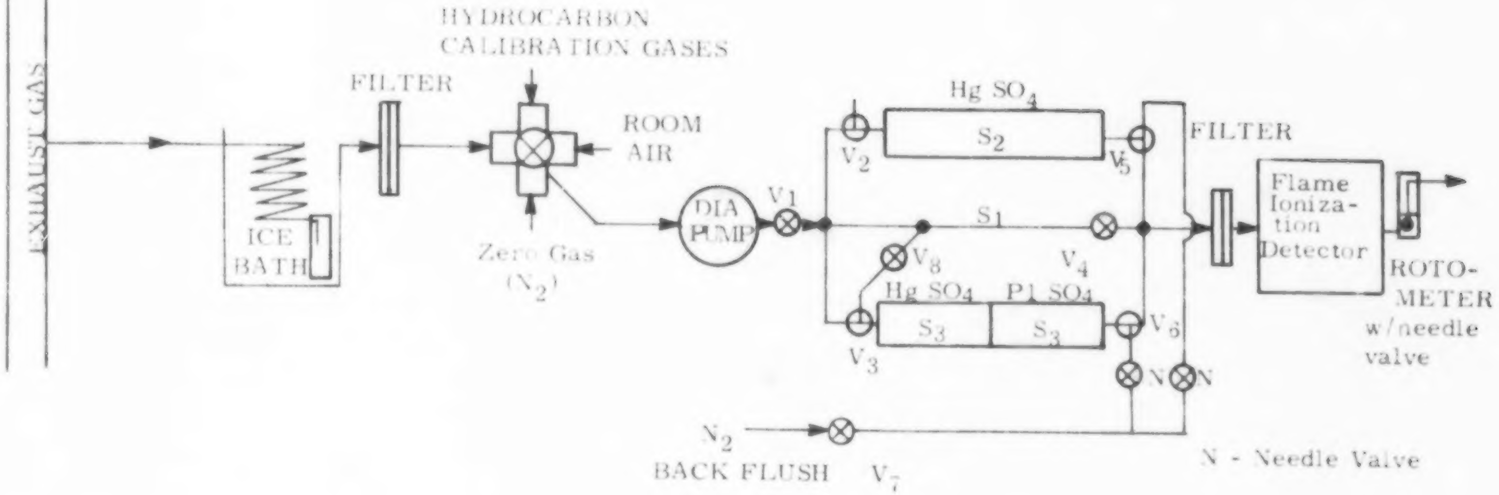
EXHAUST GAS
ICE BATH
FILTER
HYDROCARBON CALIBRATION GASES
ROOM AIR
Zero Gas (N_2)
DIA PUMP
V_1
V_2
Hg SO_4
S_2
V_5
S_1
V_8
V_4
Hg SO_4
Pd SO_4
S_3
S_3
V_3
V_6
N
N
FILTER
Flame Ioniza- tion Detector
ROTO- METER w/needle valve
N_2
BACK FLUSH V_7
N - Needle Valve

Posi- tion	Sample Seen by FID	Flow Path	Scrubber	Operation of Valves $V_{7,8}$	V_1	$V_{2,5}$	$V_{3,6}$	V_4
1	Back flush	S_2S_3	All	On	Off	Off	Off	On
2	Paraffins and benzene	S_3	$HgSO_4$ and Pd	Off	On	Off	On	Off
3	Total olefins	S_2	$HgSO_4$	Off	On	On	Off	Off
4	Total or zero	S_1	None	Off	On	Off	Off	On

Figure 1. Flow schematic of University of Michigan subtractive column-flame ionization hydrocarbon analysis system. The subtractive analyzer is patterned after that of Sigsby, Ref. 1.

3. Experimental Verification

A. GAS CHROMATOGRAPHIC COMPARISON

Results from a detailed G.C. analysis were compared to subtractive column results to determine the performance of The University of Michigan unit on exhaust gas. Since our laboratory lacked the necessary G.C. capability, arrangements were made to check our unit against a Beckman GC-4 at the Ford Motor Company Engineering Staff. Tests were run using exhaust from an idling 2000 cc Pinto. Three series of tests were run.

In the first test, exhaust was passed through the olefin + aromatic subtractor columns and then to the G.C. The following results were obtained (ppmc):

Paraffins	Olefins & Acetylenes	Aromatics	Total
1087	19	44	1150

Our analyzer would report 1150 ppmc as paraffins rather than the correct 1087. Thus the error in reporting paraffins was +63/1087 or +5.8%. Our analyzer overestimated the paraffin content of the exhaust by 5.8%.

In the second test exhaust gas was passed through the olefin subtractor only. The results were:

Paraffins	Olefins & Acetylenes	Aromatics	Total
1344	27	1130	2501

Our analyzer would report 2501 ppmc as paraffins and aromatics rather than the correct 2474. Thus the error in reporting paraffins plus aromatics was +27/2474 or +1.1%. The error in reporting aromatics alone must be estimated since the emission base line shifted between tests. If we assume that the subtractive column would report paraffins 5.8% too high, then an estimated value would be: 1344 x 1.058 = 1420 ppmc. By differencing, we find 2501 - 1420 = 1081 to be the aromatic content that would be reported by the subtractive column. The error is 1130 - 1081 or 49 ppmc. Thus the subtractive column underestimated aromatics by 49 ppmc or -49/1130 = -4.3%.

In the final test, exhaust was passed directly into the G.C. The results were:

Paraffins	Olefins & Acetylenes	Aromatics	Total
1384	1905	1435	4722

In the above test paraffins plus aromatics were 2817 ppmc. From Test 2, this may be assumed to be 1.1% lower than the subtractive column would yield. The subtractive column value would be 2817 x 1.011 = 2848 ppmc. The subtractive column prediction of olefins plus acetylenes would then be 4722 - 2848 = 1874. This is too low by 1905 - 1874 = 31 ppmc or -31/1905 = -1.6%.

Based on G.C. results one can conclude that the subtractive column class results differed from G.C. class results as below in Table I:

TABLE I

SUBTRACTIVE COLUMN—G.C. COMPARISONS

Class	Percent Error
Acetylenes + Olefins	-1.6
Aromatics	-4.3
Paraffins	+5.8

Since acetylenes were about 7.7% of the total in these tests, interpreting the subtractive column results to be olefins rather than olefins plus acetylenes would overestimate olefin content by 5.8%.

Considering the nonparaffin constituents which broke through in Test 1, 14 were olefins and 6 aromatics. Of the 14 olefins, 7 were either 2 or 3 ppmc, the rest were less. Of the 6 aromatics, the ppmc contributions were:

Constituent	ppmc After Sub.
Benzene	3
Toluene	17
Ethyl benzene	5
Xylenes	6
Mono substituted ethyl benzenes	8
Di substituted ethyl benzene	5
Total	44

Only 1 or 2% of the smaller aromatics broke through but virtually all of the large aromatics did. This result is different from that of Sigsby. In his tests virtually no larger aromatics broke through but a large percentage (>80%) of benzene did. Fortunately the concentration of the larger aromatics was small.

B. CALIBRATION GAS COMPARISON

Additional evaluations, reported in the First Annual Progress Report, page 27, were made with the following calibration gases (as analyzed by the manufacturer).

paraffinic: 4620 ppmc propane in nitrogen
aromatic: 315 ppmc toluene plus 282 ppmc benzene in nitrogen—597 ppmc
olefinic: 100 ppmc acetylene, 150 ppmc propylene, 101 ppmc ethylene, and 205 ppmc 1—butene in nitrogen—total 556 ppmc

These gases were used to check the day to day operation of the unit.

Results were:

a. With propane the analyzer worked perfectly (no olefins or aromatics reported).

b. With the aromatic calibration gas about 60% of the benzene broke through to be reported as paraffins (no olefins reported). It was found that flowing dry nitrogen through the aromatic subtractor improved benzene retention. However, benzene scrubbing efficiency was variable.

c. All the acetylene in the olefinic calibration gas was reported as an olefin (no paraffins or aromatics reported).

4. Conclusions

In conclusion, within the limitations of the vehicle tests with shifting baseline exhaust emission levels, the subtractive columns were very accurate (better than 6%) in reporting the classes. The major drawback was that acetylene was reported as an olefin. Results with the calibration gases confirmed the acetylene reporting problem and in addition demonstrated variability in benzene retention. Thus the subtractive column is somewhat limited in accuracy by these problems but was concluded to give a reasonable indication of exhaust reactivity changes particularly if a fuel with fixed aromatic content is used. Some improvement in accuracy can be made by estimating the acetylene content of the exhaust and correcting the olefinic results accordingly. Estimation of acetylene content in exhaust gas is discussed in the following section.

B. GAS CHROMATOGRAPHIC STUDIES OF EXHAUST ACETYLENE

1. Purpose

Gas chromatographic analysis for acetylene was performed on a number of exhaust samples at various engine air-fuel ratios, air injection fractions, and with and without exhaust reaction suppression. The objective was to estimate acetylene content both in engine exhaust and reactor exhaust. For these tests the engine was run at 1800 rpm, 30 BHP and MBT spark. Manifold vacuum was 11-13 in. Hg.

2. Sampling Technique

A total of 12 samples of exhaust gas from the 350 CID Chevrolet engine were taken at a point downstream from the duPont thermal reactor. In all cases the samples were passed through an ice bath and then collected in 500 cc stainless steel cylinders maintained at 110°-120°C. Usually, several days passed before the contents of the cylinders were withdrawn for G.C. analysis. However, immediately before and after each sample collection the exhaust gas was measured on-line with an FID and a subtractive column analyzer to determine total hydrocarbons, paraffins, olefins, and aromatics. In some cases quench coils at the engine exhaust ports just ahead of the reactor were turned off and the reactor was simply acting as an exhaust manifold. The conditions of sampling for each run are given in the right-hand column of Table II. Also presented are the air-fuel ratio in the feed to the engine and the concentrations determined by the FID. The air fraction added, as given under Sampling Conditions, refers to the air pumped directly into the reactor to oxidize the incompletely burned fuel in the exhaust issuing from the engine.

3. Gas Chromatograph Operation

Dual columns were employed in the heated oven section of a Perkin-Elmer 800 gas chromatograph. The columns were 1/8 in. O.D. by 4 ft long, wound in spirals, and packed with Poropak-N. This packing gave an excellent separation of the light hydrocarbons. In order to obtain sharp peaks for the components in a reasonable time temperature programming was employed. Beginning with an initial temperature of 60°C, the oven was raised 10°C/min. This caused some

TABLE II

FID AND SUBTRACTIVE COLUMN ANALYSES

Sample	Air Fuel Ratio	Total Hydrocarbon (ppm)	Paraffin (ppm)	Aromatic (ppm)	Olefin (ppm)	*Sampling Conditions
A	11.5	1290	640	340	310	Quench coils on, no air added to reactor
B	13.2	800	318	232	250	"
C	14.65	630	200	180	250	"
D	16.45	510	162	133	215	"
E	17.45	530	200	160	170	Quench coils off, no air added to reactor
F	12.05	940	435	260	245	"
G	13.38	326	84	67	175	Quench coils off, added air fraction .167
H	13.38	38.5	4	10	24.5	" .359
I	11.73	152	52	27	73	" .131
J	11.73	950	402	209	339 Did not ignite	" .123
K	13.42	418	92	99	227	" .535
L	17.33	560	205	172	183	Quench coils on, no air added to reactor

*Exhaust cooling coils were used to quench after-reactions in the exhaust ports of the engine. Thus, results reflecting either a high or low degree of after-reaction were obtained.

baseline drift after the propane-propylene peak. Consequently, no attempt was made to analyze for the concentration of the higher molecular weight species.

An Infotronics electronic integrator, Model CRS-10H, was used in conjunction with the G.C. to determine the peak areas.

4. Data Analysis

The light hydrocarbon content of the samples was calculated from G.C. results by comparing the ratio of the peak area to the sample pressure (P.A./Pr), of each of the light end components in the sample with the same ratio for an olefinic standard.* The olefinic standard was reported to contain ethylene (50.7 ppm), acetylene (49.9 ppm), propylene (50.7 ppm), and 1-butene (51.[illegible] ppm). Since the standard did not contain known amounts of methane and ethane (two important components of the actual exhaust samples analyzed), their content in the samples was estimated from the following relations:

$$\text{ppm methane} = \left(\frac{\text{P.A.}}{\text{Pr}}\right)_{\substack{\text{methane}\\ \text{in sample}}} \times \left(\frac{2}{1.05}\right) \frac{50.7}{\left(\frac{\text{P.A.}}{\text{Pr}}\right)_{\substack{\text{ethylene in}\\ \text{standard}}}}$$

$$\text{ppm ethane} = \left(\frac{\text{P.A.}}{\text{Pr}}\right)_{\substack{\text{ethane in}\\ \text{sample}}} \times \left(\frac{1}{1.05}\right) \frac{50.7}{\left(\frac{\text{P.A.}}{\text{Pr}}\right)_{\substack{\text{ethylene in}\\ \text{standard}}}}$$

In the first equation the factor of 2 corrects for the carbon atom/mole difference between methane and ethylene; while the factor 1/1.05 is an estimate of the correction for the different responses of paraffins and olefins in the FID detector.

Duplicate runs were made with the standard and the samples. The results of the analyses are reported in Table III, as ppm of each component converted to its hexane equivalent. This conversion was accomplished by multiplying the actual ppm of each component by the carbon ratio; i.e., the carbon atoms of a given species divided by 6, which is the number of carbons in hexane.

---

*Standard prepared by Scott Research Laboratories, Inc. Composition stated to be accurate to ±[illegible]% or better.

TABLE III

HEXANE EQUIVALENT OF COMPONENTS DETERMINED BY GC ANALYSIS

Sample	Component ppm Hexane				
	CH_4	C_2H_6	C_2H_4	C_2H_2	$C_3H_6 + C_3H_8$
A	81.0	4.4	63.7	53.4	33.9
B	24.5	7.4	28.7	22.0	9.4
C	12.8	6.5	26.1	15.9	5.9
D	5.7	3.6	23.6	10.8	3.4
E	3.3	2.0	6.0	5.6	0.32
F	45.5	5.6	55.7	40.0	37.8
G	28.3	2.4	71.5	18.5	11.0
H	1.5	0.04	3.9	1.9	0.34
I	30.8	0.95	25.9	9.9	8.0
J	68.8	6.2	79.1	42.6	55.8
K	22.1	2.9	7.8	16.0	0.38
L	3.3	---	2.5	3.7	0.27

The olefin content, listed in Table II, includes acetylenic (triple bond) components. The "true" olefin content has been estimated by deducting the acetylene content given by G.C. analysis from the olefin content given by FID and subtractive column analysis. The "true" olefin content is given in Table IV as ppm hexane and also as a percentage of the total hydrocarbons, while the acetylene content is given as a percentage of both true olefins and of total hydrocarbons.

As indicated in Table II, samples A-D and L were taken with the quench coils on, samples E and F had the quench coils off but no air added to the exhaust, and samples G-K had the quench coils off and air added to the reactor to effect after-reaction. It was observed, however, that for sample J there was no rise in the temperature of the reactor indicating that the air-exhaust mixture did not ignite.

Figure 2 shows total hydrocarbons, % "true" olefins, and % acetylene for samples A-F, J, and L as a function of the air-fuel ratio, A/F. Figure 3 shows the same results for samples at A/F ≅ 13.3 and 11.73 as a function of volume fraction added air in the reactor. Figures 4 and 5 show the percentage of acetylene in the olefins determined by the FID and subtractive column analyzer for the sample sets corresponding to Figures 2 and 3, respectively.

Although the methane, ethane, ethylene, acetylene, and propane-propylene combination contents of the exhaust were determined, the principal interest here is in the acetylene content for correction of the FID-subtractive column olefin results. From Figures 2 and 4 (no after-reaction), it is seen that the correction to the FID olefin is a function of the A/F ratio; although there was some scatter in the results. Figure 4 shows that acetylene as a percent of total olefins decreased nearly linearly from 16% at 11:1 A/F to 2% at 18:1 A/F. Likewise, acetylene varied from 4 to 2% of the total HC content (Figure 2). After-reaction (in the reactor) had little effect on acetylene as a percent of remaining olefins (Figure 5) but did affect acetylene as a percent of total HC (Figure 3).

5. Conclusion

Our conclusion, based upon these limited tests, with a single Indolene fuel is that the FID-subtractive column olefin results can be corrected for acetylene content through the A/F ratio variations according to Figure 4 with no additional correction needed for air injection. Thus, for estimating olefin content from subtractive column analysis, "true olefin %" equals value observed from subtractive column analysis divided by

$$\left(1 + \frac{\%\ \text{in Figure 4}}{100}\right)$$

TABLE IV

CORRECTED OLEFIN CONTENT OF SAMPLES

Sample	Total Hydrocarbon ppm Hexane	"True" Olefin ppm Hexane	"True" Olefin % Total Hydrocarbon	Acetylene % Total HC	% Total Olefin*
A	1290	257	19.9	4.14	17.2
B	800	228	284	2.75	8.79
C	630	234	37.2	2.52	6.35
D	510	204	40.2	2.04	5.02
E	530	164	31.0	1.06	3.30
F	940	205	21.8	4.25	16.4
G	326	157	47.9	5.68	10.6
H	38.5	22.6	58.9	4.93	7.75
I	152	63	41.7	6.51	13.6
J	950	296	31.2	4.49	12.6
K	418	211	50.5	3.83	7.04
L	560	179	31.9	0.66	2.02

*Total olefin includes acetylene.

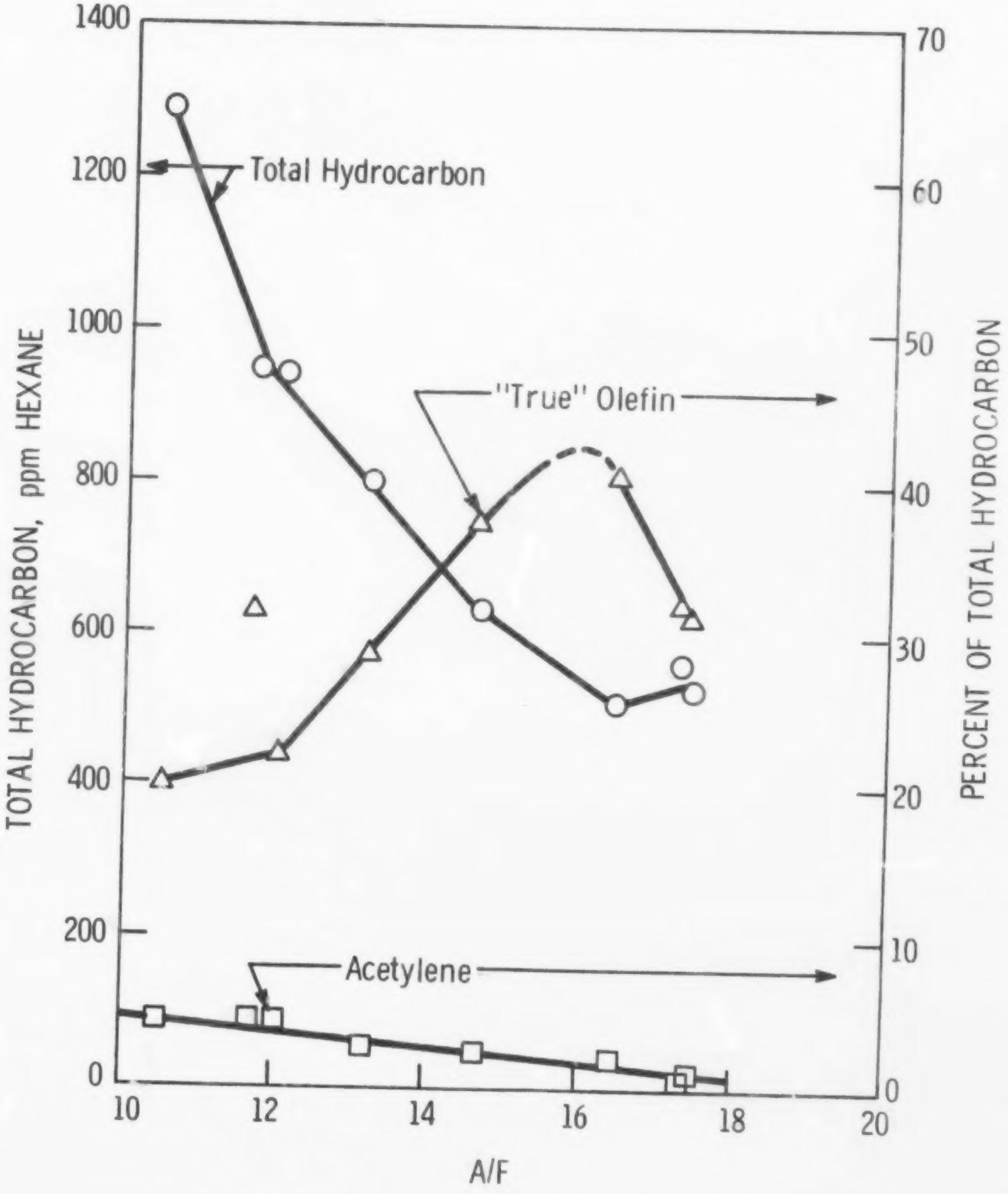

Figure 2. Results for samples without after-reaction.

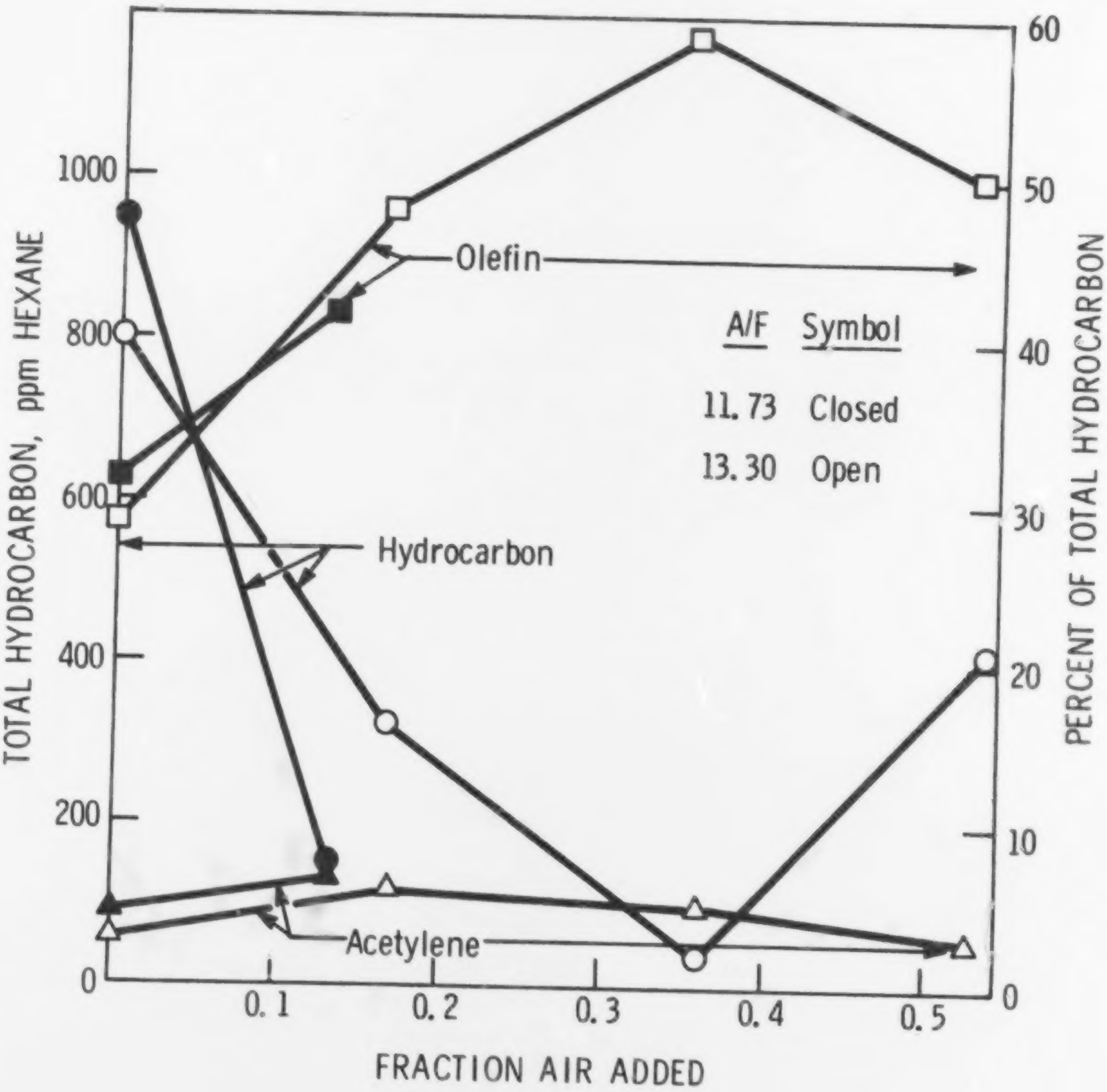

Figure 3. Results for samples with after-reaction. A/F ~ 13.3 and 11.73.

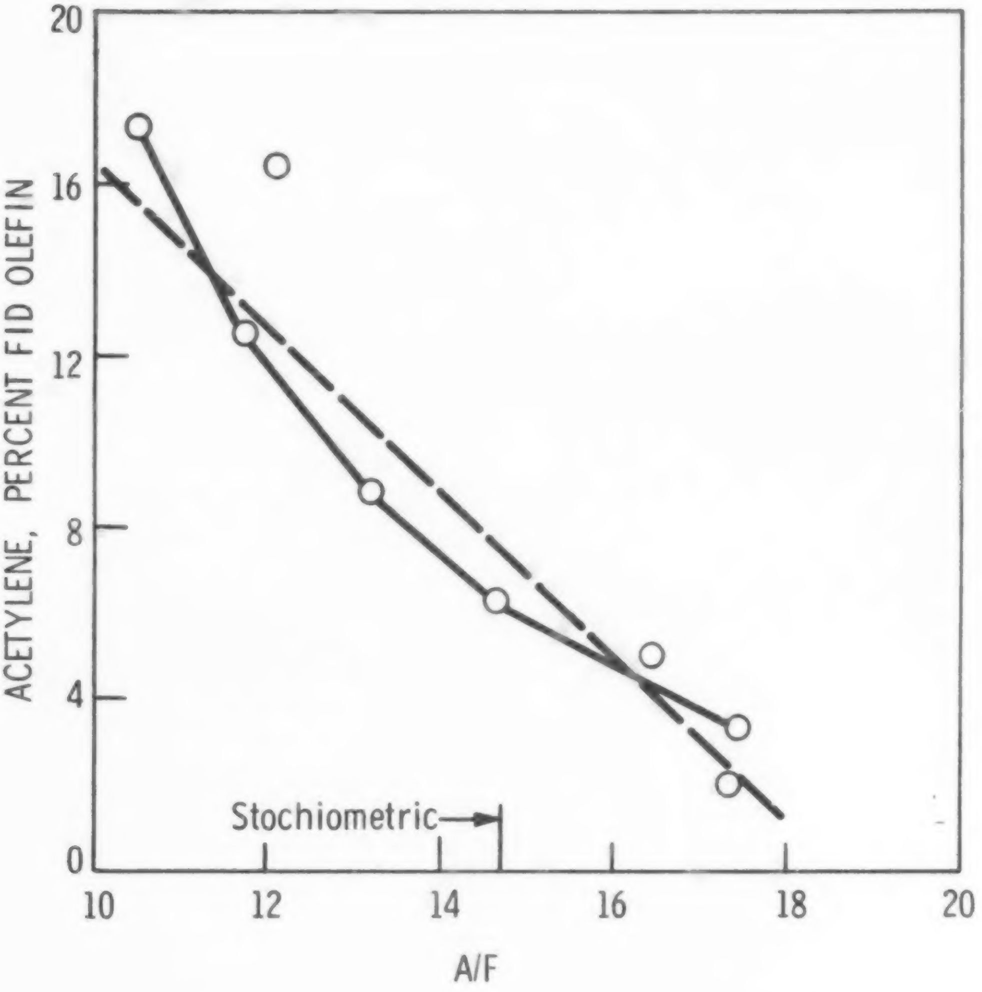

Figure 4. Results for samples without after-reaction.

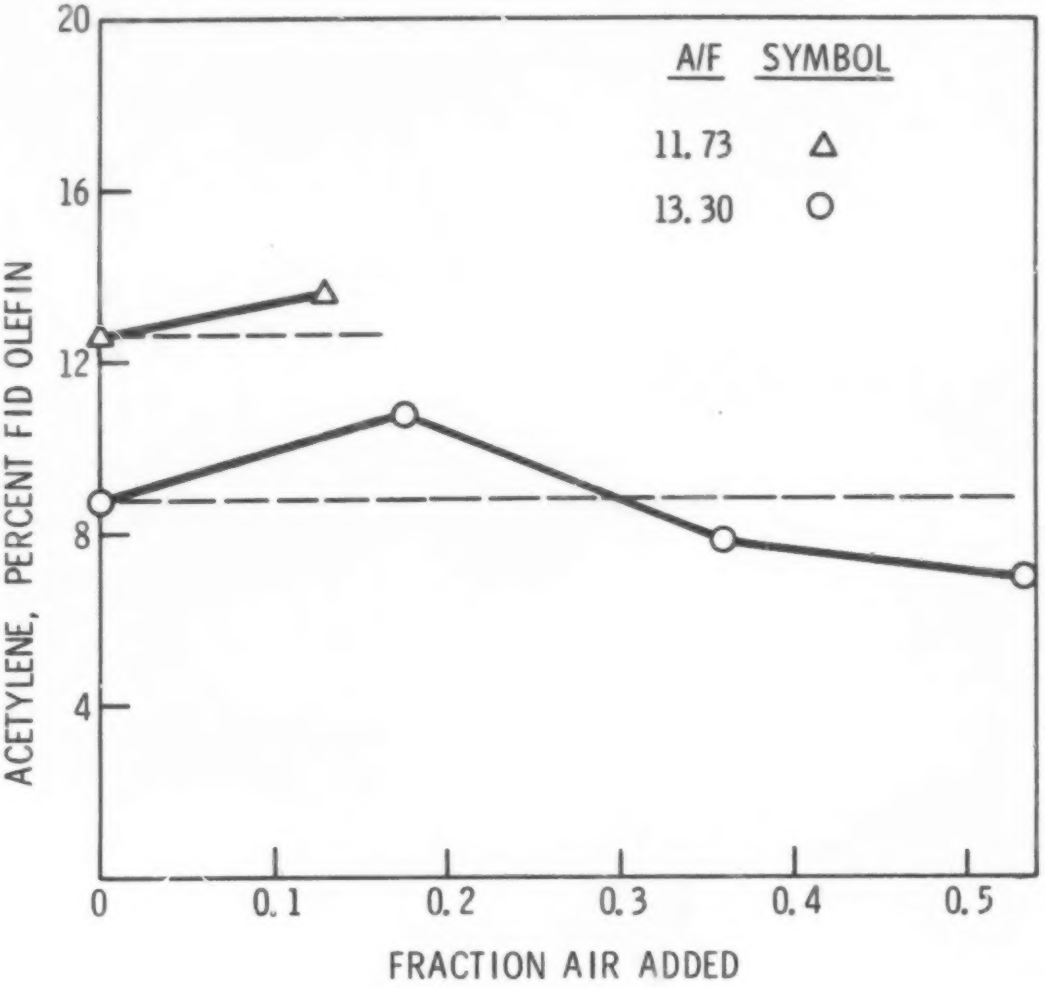

Figure 5. Results for samples with after-reaction. A/F ~ 13.3 and 11.73.

C. MEASUREMENT OF INSTANTANEOUS ENGINE EXHAUST VELOCITY AND TEMPERATURE

The studies in Phase II of this project brought out the fact that the reactor model was quite sensitive to the exhaust enthalpy input to the reactor. Since an accurate experimental determination of the enthalpy input requires good measurements of both instantaneous engine exhaust velocity and temperature, and since no known conventional techniques were available for getting these measurements, developmental work was undertaken on a new technique which appeared promising for both the velocity and temperature measurements.

The method used laser-schlieren photography with a rotating-mirror slit-streak camera. The laser-schlieren system was used to detect turbulent eddies in the exhaust as they moved with the exhaust stream. The average eddy-spatial-velocity was assumed to be equal to the exhaust stream velocity. By projecting the eddy schlieren image through a narrow slit and moving the slit image at a fixed rate across a sheet of Polaroid film, Figure 6, a photograph was obtained which gave continuous records of both eddy position and time, over a short-time interval. The slope of the resulting image at any point gave instantaneous velocity. Figure 7 is an example of such a photograph.

Unsuccessful measurements of instantaneous gas temperature were also attempted using the same technique for measuring the speed of a spark-induced low amplitude shock wave in the gas stream. Since sound velocity is proportional to $T^{1/2}$, the gas stream temperature can, in theory, be estimated from the measured sound velocity. Good results were obtained in open air and in a motored engine, but the interference generated by the hot exhaust resulted in too low a signal-to-noise ratio for reliable measurements.

1. The Measurement of Engine Exhaust Velocity

The laser-schlieren optical system and associated timing and synchronization circuits are shown in Figures 8 and 9. Exhaust gas velocity as a function of crankangle was obtained from photographs such as shown in Figure 10, and the result from an early run is shown plotted in Figure 11. Specifications of the engine used in this work are summarized in Table V.

The photographic procedure required that the camera mirror be properly phased with the engine rotation so that any preselected portion of the engine cycle can be photographed. This phasing was accomplished with the circuit shown in Figure 9, and required that both engine and mirror be in their proper positions for the recording of an event. The mirror had to be at the position where the slit image was at the start of its sweep across the photographic

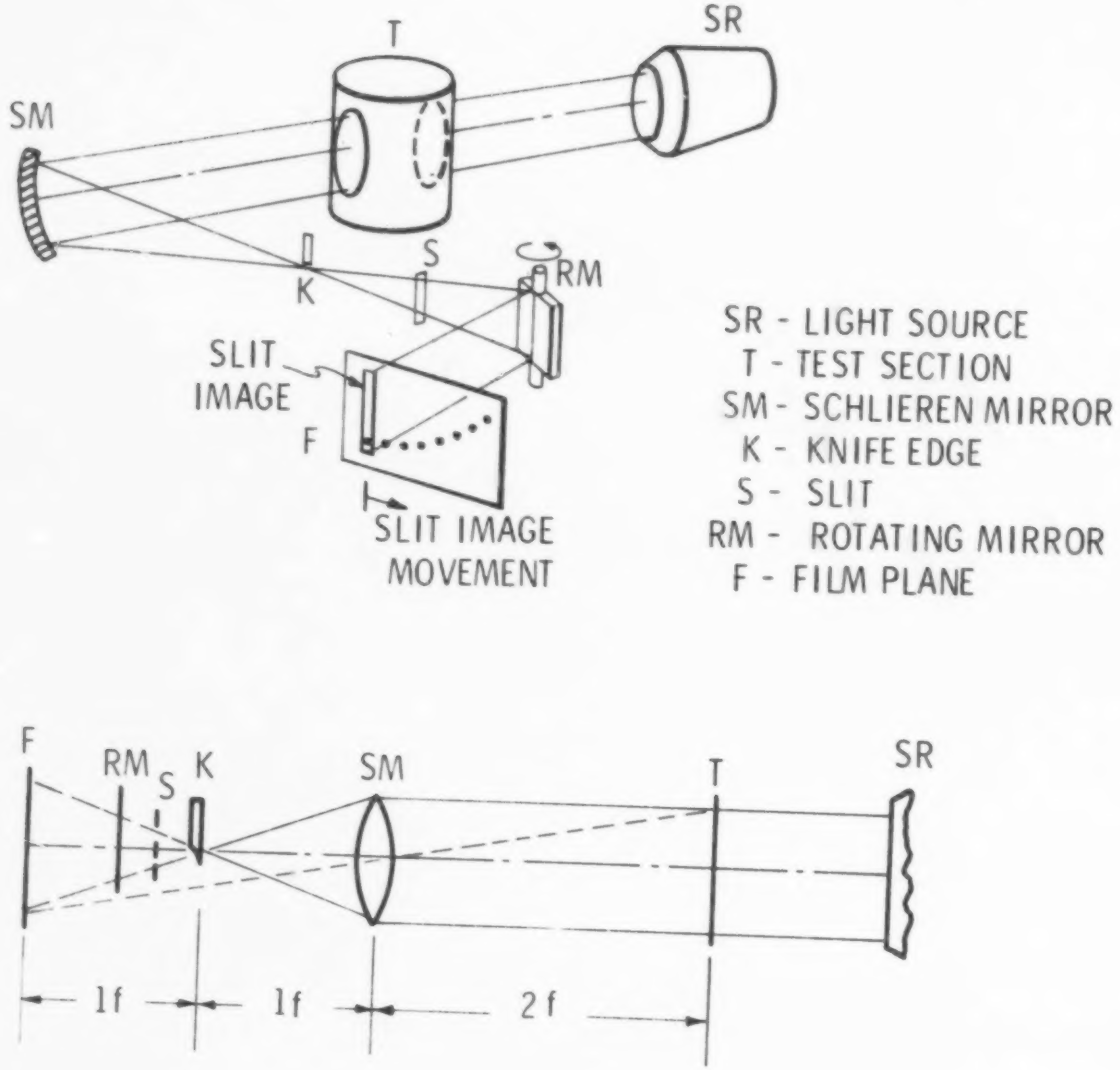
T
SR
SM
K
S
RM
SLIT IMAGE
F
SLIT IMAGE MOVEMENT
SR - LIGHT SOURCE
T - TEST SECTION
SM - SCHLIEREN MIRROR
K - KNIFE EDGE
S - SLIT
RM - ROTATING MIRROR
F - FILM PLANE
F
RM
S
K
SM
T
SR
1f
1f
2f

Figure 6. Schematic diagram of laser-schlieren optical system.

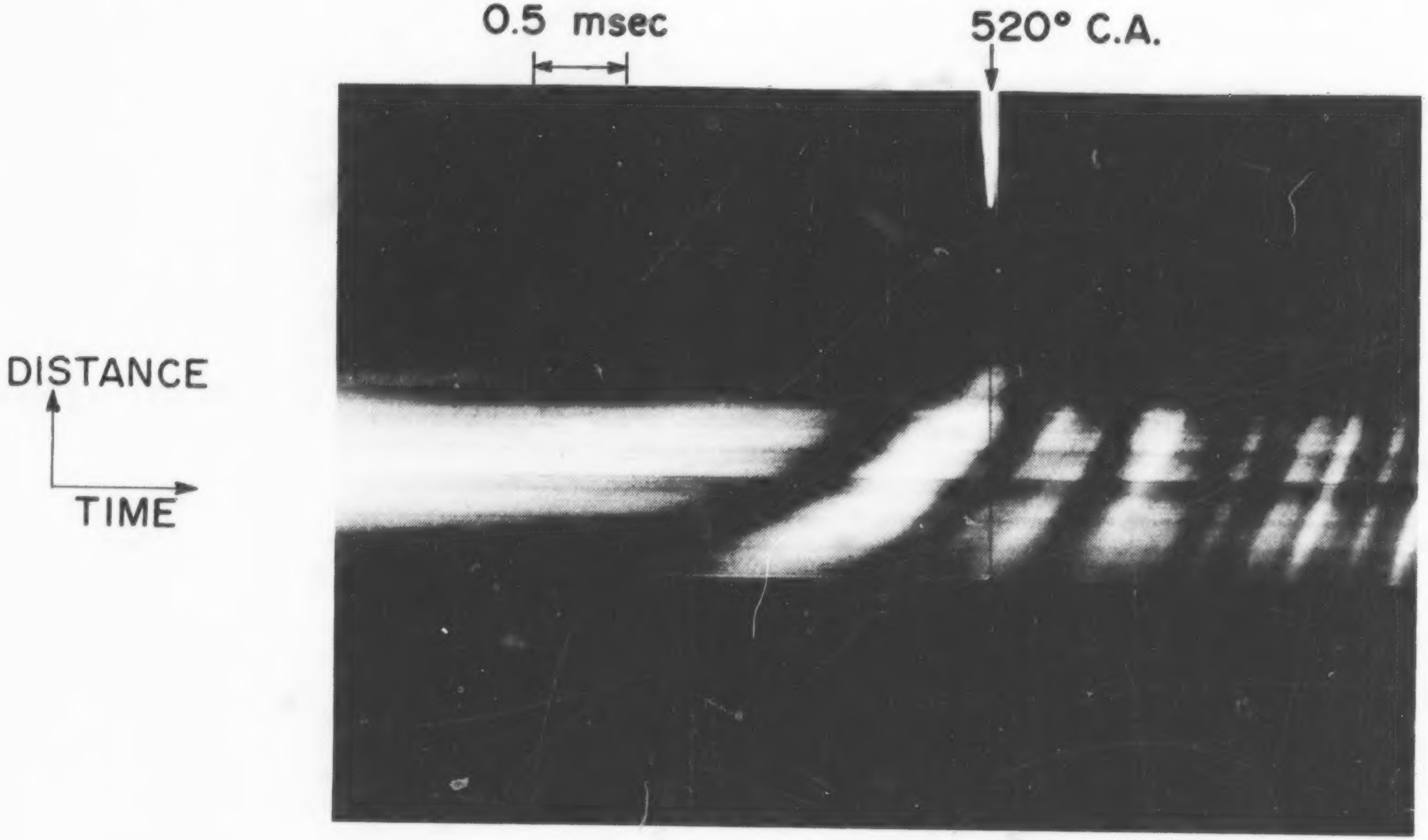
0.5 msec
520° C.A.
DISTANCE
TIME

Figure 7. Streak schlieren photograph showing the start of the exhaust process. Engine speed is 600 rpm. Exhaust valve opens at 500° C.A.

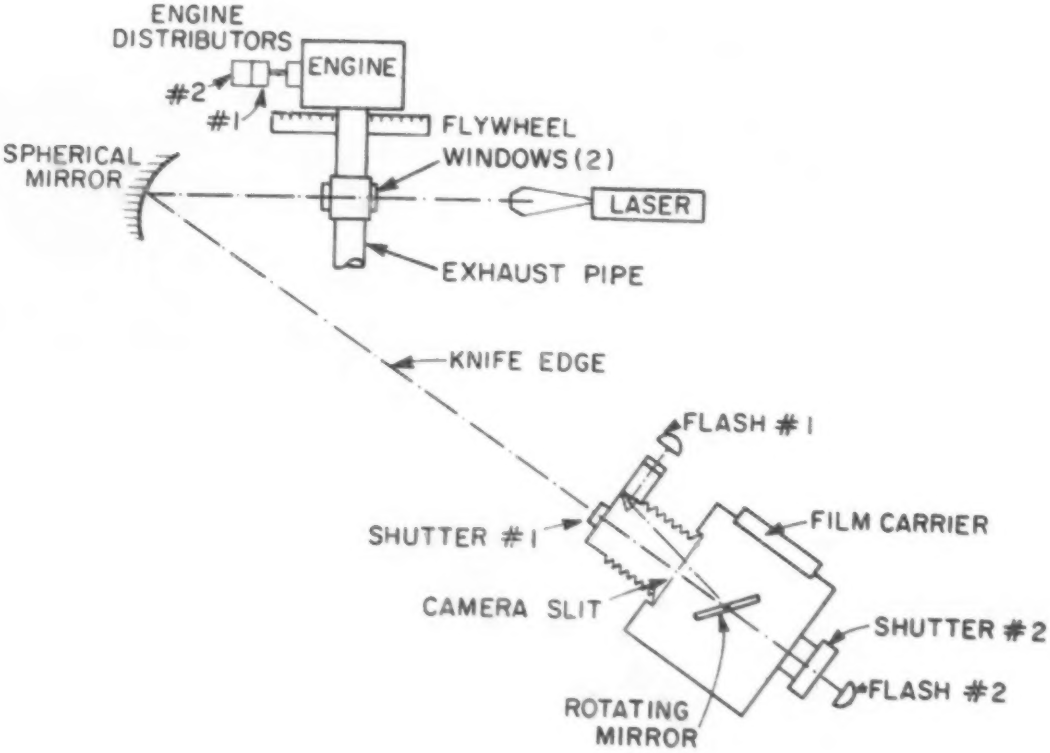
ENGINE DISTRIBUTORS
ENGINE
#2
#1
FLYWHEEL
WINDOWS (2)
SPHERICAL MIRROR
LASER
EXHAUST PIPE
KNIFE EDGE
FLASH #1
SHUTTER #1
FILM CARRIER
CAMERA SLIT
SHUTTER #2
FLASH #2
ROTATING MIRROR

Figure 8. Exhaust velocity measurement system. Mechanical and optical schematic.

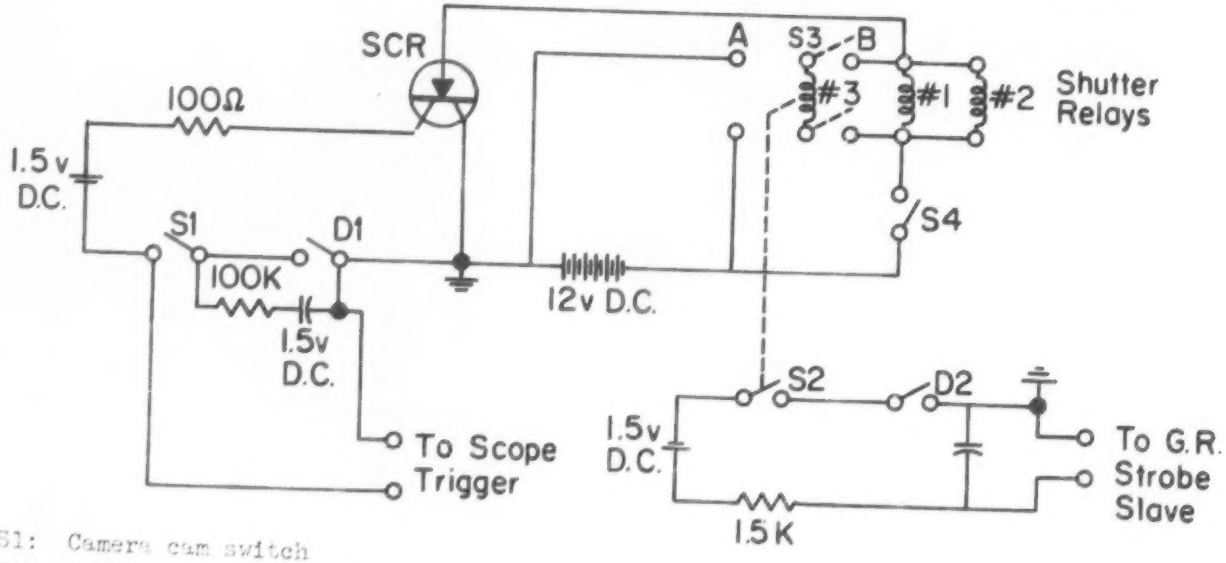
SCR
100Ω
1.5v D.C.
S1
D1
100K
1.5v D.C.
12v D.C.
A
S3
B
#3
#1
#2
Shutter Relays
S4
S2
D2
1.5v D.C.
1.5K
To Scope Trigger
To G.R. Strobe Slave

S1: Camera cam switch
S2: Switch operated by relay #3
S3: Manual DPDT switch
S4: Manual ON-OFF switch
D1: Engine distributor #1
D2: Engine distributor #2

Figure 9. Electrical schematic.

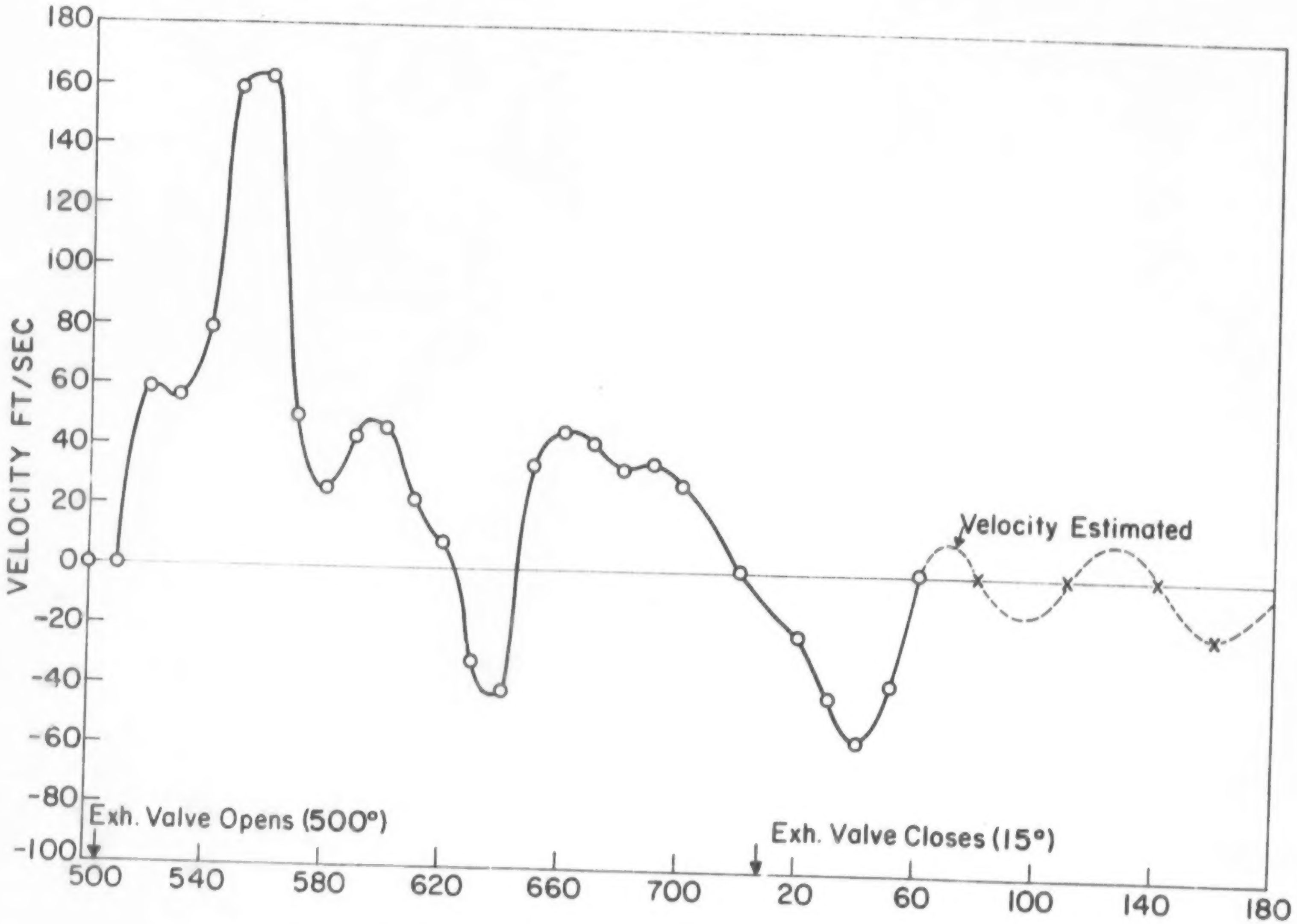

Figure 10. Velocity as a function of crankangle. Engine speed = 600 rpm.

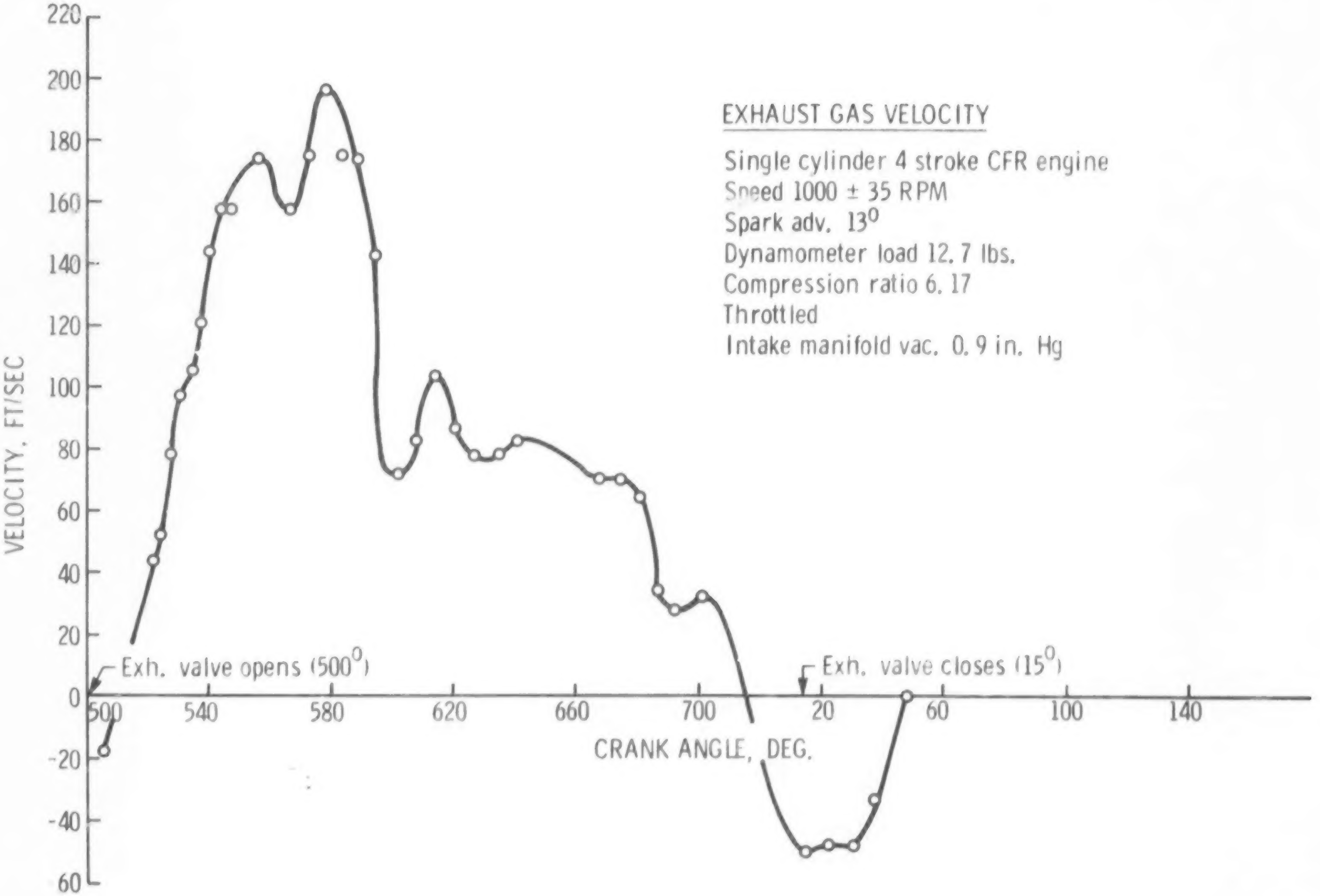

Figure 11. Exhaust gas velocity vs. crankangle. Engine speed = 1000 rpm.

TABLE V

ENGINE SPECIFICATIONS

(ASTM-CFR Single Cylinder 4-Stroke Spark-Ignition Engine)

		Valve Timing
Compression ratio	4 to 10	
Bore	3.25 in.	I.V.O. 10 atdc
Stroke	4.50 in.	I.V.C. 34 abdc
Displacement	37.33 in.^{3}	E.V.O. 40 bbdc
Speed	600 ± 6 rpm	E.V.C. 15 atdc
Spark advance	15° btdc	

plate, with the engine at the selected crankangle position. At the proper times, the phasing cam on the mirror shaft closed S1 (see Figure 9) for a few degrees of rotation, while an auxiliary distributor on the engine performed a similar phasing function by closing D1. Only when the mirror and engine were in proper phase would both S1 and D1 be closed simultaneously to trigger the SCR. In turn, the SCR opened shutter #1 to admit the schlieren image, shutter #2 to admit the repetitive timing mark signal and closed S2. A short time later distributor cam D2, which was phased to lag D1, closed D2 and fired the strobe light to record the bright single timing mark on the photograph (see Figure 7). The same strobe, but with S3 in position A, was used to illuminate the flywheel to get an exact crankangle reading at the time of this strobe flash.

Figure 7 is a typical photographic result and shows the initial movement of the exhaust gas as the exhaust valve starts to open. The repetitive timing marks at the top of the photograph give time intervals of 1/2 msec and the bright single mark indicates an engine crankangle position of 520°. The total vertical dimension of the schlieren image corresponds to slightly over 1/2 in. at the exhaust pipe. The slope of the image at any position gives ($\Delta x/\Delta t$) or velocity and the measured result for this photograph shows that the instantaneous velocity at 520° crankangle is 59 ft/sec. Similar results over the entire portion of the exhaust cycle were made and the results are shown plotted in Figure 10.

Figure 11 shows similar results obtained at an engine speed of 1000 rpm. A peak velocity of approximately 200 ft/sec was observed compared with 160 ft/sec for the engine speed of 600 rpm. This increase of velocity was expected since mass flowrate increases as engine speed increases. However, the first flow reversal shown in the curve for 600 rpm was not observed in the latter test. It is believed that the first flow reversal was due to a pipe elbow located upstream of the test section and later removed for the test at 1000 rpm. The occurrence of the flow reversal just before the closing of the exhaust valve was about the same in both cases.

These results show excellent agreement with respect to the opening and closing of the exhaust valve, give reasonable values for the exhaust velocity, and show an expected oscillation of the gas flow after the exhaust valve closes.

An attempt was made to obtain an instantaneous schlieren picture of the exhaust gas flow using a short-duration, high-intensity spark as a light source replacement for the laser. The objective was to investigate the possible effects of the secondary flows, created by a pipe elbow just upstream of the test section, on the flow reversal shown in Figure 10. The effort was not successful due to erratic operation of the spark light source. Later the elbow was removed with a consequent optical system rearrangement.

2. The Attempted Measurement of Instantaneous Exhaust Temperature

Having obtained preliminary data on exhaust velocity measurement, studies were started to consider the system changes required for measuring exhaust gas temperature. As proposed, exhaust temperatures were to be obtained indirectly by measuring the speed of spark-induced pressure waves. The speed of sound at a typical exhaust temperature is of the order of 2000 ft/sec. To obtain reasonable time scales on the schlieren-streak photographs, the required rotating mirror speeds turn out to be several thousand revolutions per minute. An additional requirement was that the camera shutter open very quickly so as not to miss the event. It was also found that when the camera was operated at high mirror speeds of about 1000 rpm, the camera unit vibrated due to a slight unbalance of the rotating mirror and mount.

To avoid these difficulties, a new method was investigated for detecting the schlieren image utilizing photodiodes as light detectors. Instead of the streak photograph technique, several photodiodes were mounted at the film plane along the axis of the exhaust pipe image to detect the passage of the schlieren image of the spark-induced pressure wave. As the pressure wave moves down the exhaust pipe, its image passes over each of the photodiodes in turn, generating pulses which are displayed on the single sweep of an oscilloscope. The distance between successive pulses gives the time for passage of the wave over a known distance and thus gives velocity from ($\Delta x/\Delta t$).

The photodiode used in this work was the Hewlett-Packard Pin Photodiode 5082-4205 with a response time of less than 1 nsec. The detection circuit and the dimensions of the photodiode are shown in Figures 12 and 13. This one-channel amplifier was built to test the feasibility of the new method. The perliminary test results indicated adequate sensitivity and excellent time response. However, the system was found to be extremely sensitive to slight building vibrations. Efforts to vibration-isolate the system were reasonably successful, even though some vibration "noise" still appeared on the oscilloscope.

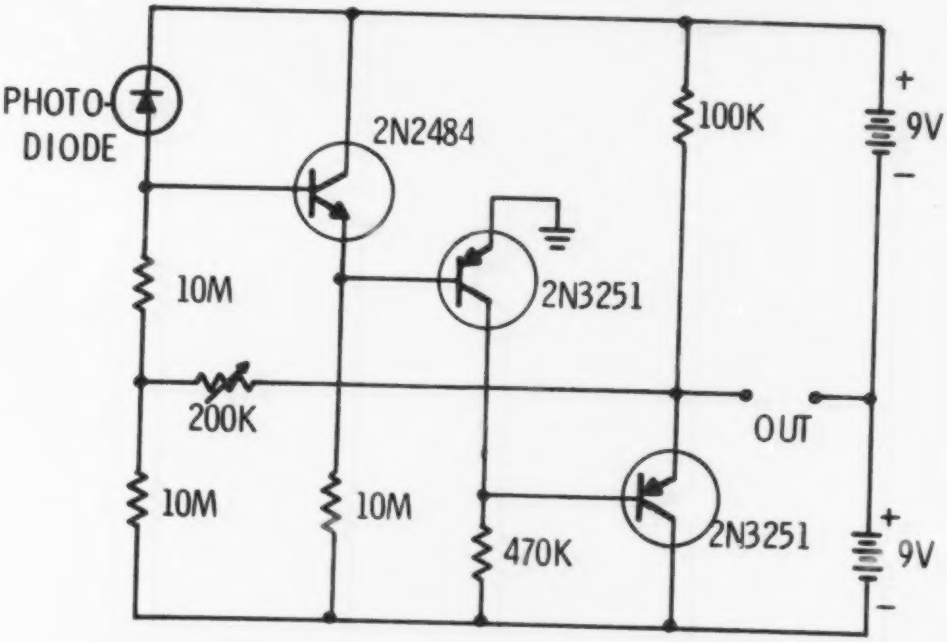
PHOTO-DIODE
2N2484
2N3251
100K
+
9V
−
10M
200K
OUT
10M
10M
470K
2N3251
+
9V
−

Figure 12. Photodiode amplifier circuit.

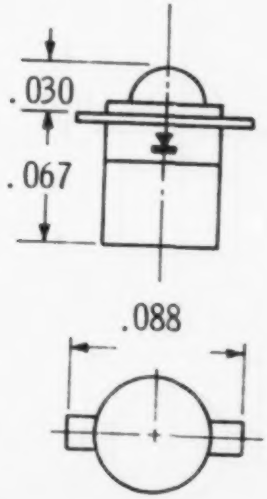

Figure 13. Dimensions of Hewlett-Packard pin photodiode 5082-4205.

Following these initial tests, two more channels were added to the photodiode-amplifier unit with the detector photodiodes spaced 1/4 in. apart. Time response of each channel was checked using a high frequency strobotac. The result was excellent, far exceeding the requirements.

The spark electrodes and triggering circuit for the sound wave generator are shown in Figure 14.

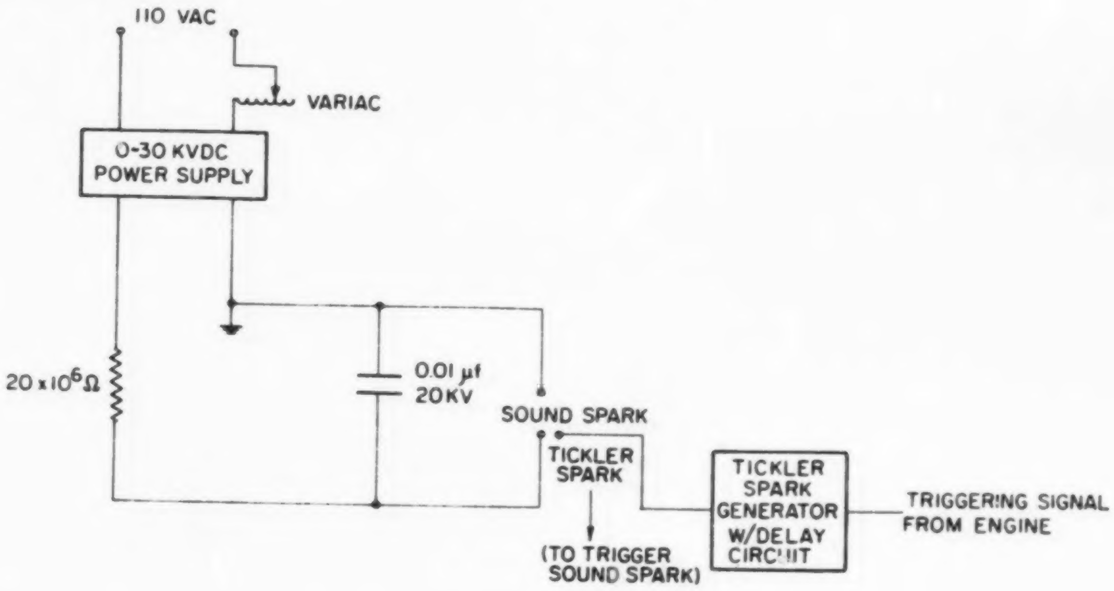
110 VAC
VARIAC
0-30 KVDC POWER SUPPLY
20 x 10⁶ Ω
0.01 µf 20KV
SOUND SPARK
TICKLER SPARK
(TO TRIGGER SOUND SPARK)
TICKLER SPARK GENERATOR W/DELAY CIRCUIT
TRIGGERING SIGNAL FROM ENGINE

Figure 14. Spark circuit.

Tests on the spark wave form showed good repeatability in both timing and wave amplitude. Measurements of the speed of sound in free air at room temperatures were carefully performed in order to determine the radius of the spark wave at which the speed of the wave approached that of the sound wave. It was found that the speed of the spark wave becomes identical to the speed of sound at a distance as close as 5/8 in. from the spark electrodes.

Typically the exhaust gas temperature ranges from 1600°R to 2500°R, and the pressure is nearly atmospheric except during the blowdown period, so that the ideal gas assumption holds with reasonable accuracy. The equation for the speed of sound for an ideal gas, $a = \sqrt{kgRT}$, was used to convert the measured speed of sound to gas temperature. The specific heat ratio, k, and the gas constant, R, were obtained from Hottel's combustion chart as functions of the fuel-air ratio. Figure 15 shows the variation of the speed of sound vs. fuel-air ratio.

Figure 16 and 17 show the signal of the spark wave recorded on the scope while the test section was open to the air at 72°F. The time delay between two signals was measured to be 9.6 µsec. The equivalent distance between two

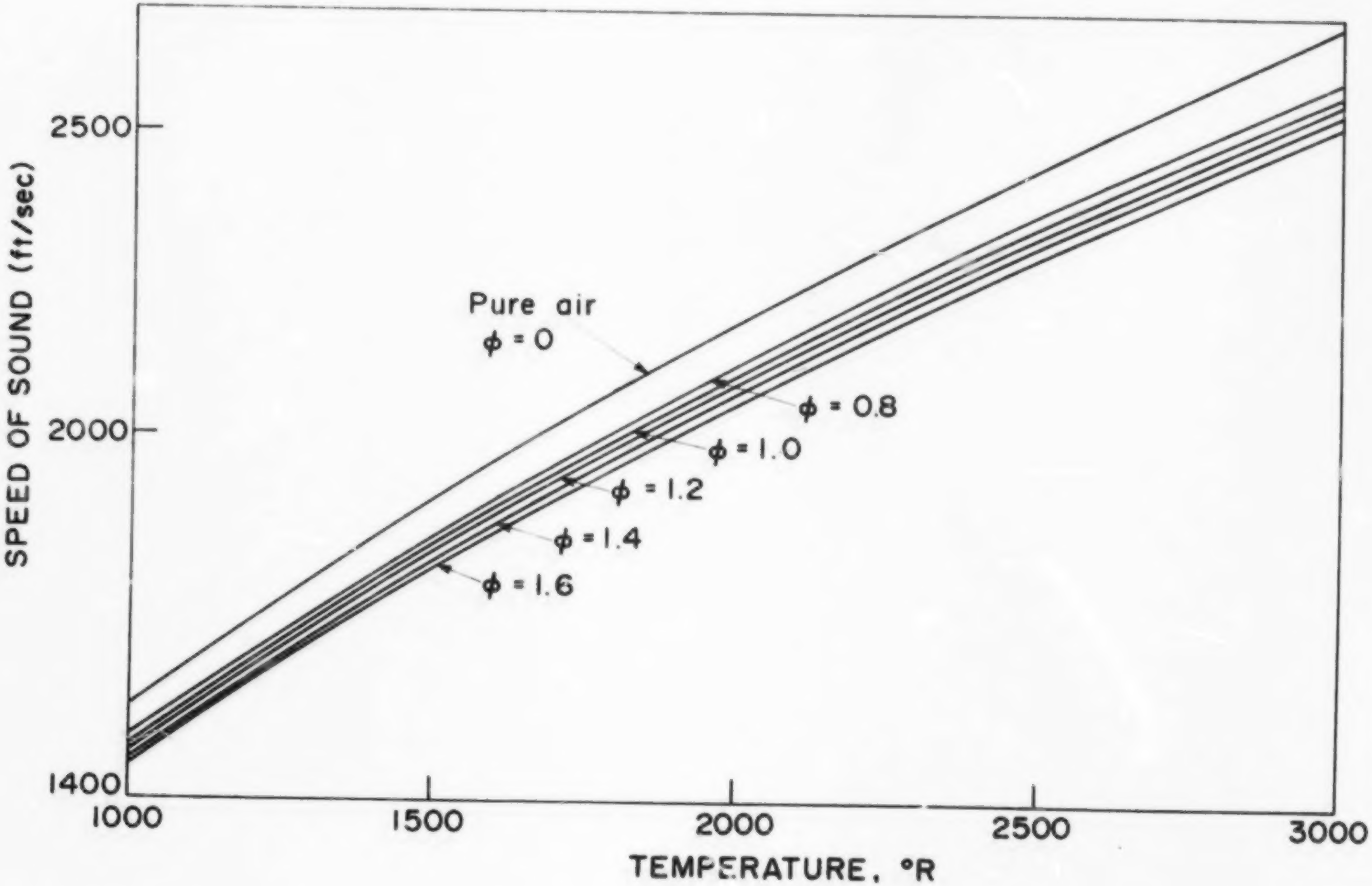

Figure 15. Speed of sound in exhaust gas as a function of temperature and equivalence ratio.

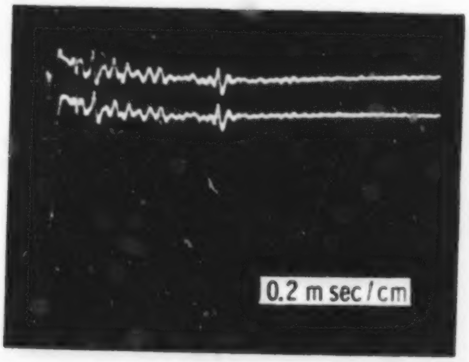

Figure 16. Photodiode signals from velocity of sound measurements in room air at 72°F.

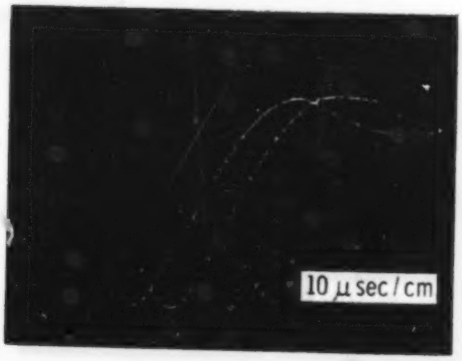

Figure 17. Photodiode signals with expanded time scale.

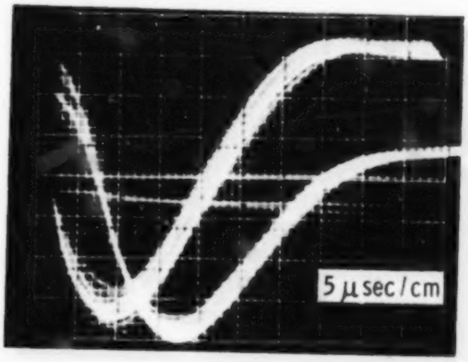

Figure 18. Photodiode signals showing repeatability.

photodiodes at the test section was 0.132 in., taking into account the optical magnification factor. The calculated velocity of the air at 72°F was 1130 ft/sec and the measured velocity was 1145 ft/sec.

Figure 18 shows the repeatability of the spark wave. Even though slight variations in the magnitude of the signal are evident, the main interest in our measurement was the time delay between the two signals. This difference was repeatable.

The spark electrodes were next mounted in the exhaust pipe to determine the effects of the exhaust gas flow on the spark characteristics. The electrodes were sealed into Norton's alundum thermocouple tubes with Sauereisen Electrotemp Cement Powder No. 8. This cement was particularly suitable for the electric insulation at high voltages and temperatures.

It was found that due to the water vapor in the exhaust gas, the spark breakdown voltage in the hot exhaust dropped to approximately one third of that in atmospheric air. As a result, triggering of the spark system became irregular and the spark intensity was too weak to generate a reasonably sharp signal.

After several attempts with minimum system changes the problem was solved by employing a double spark method. In this system, two spark gaps are connected in series by a floating electrode. The spark gap at the high voltage side, called the "triggering spark gap," is triggered by a tickler spark located outside of the exhaust pipe. The second spark gap, the "sound spark gap," is located in the test section. The sound spark is discharged instantly when the triggering spark gap is ionized by the tickler spark. Good control of the spark system was possible with this arrangement.

Subsequent attempts to measure the sound-wave signal in the exhaust gas flow were unsuccessful due to the low signal-to-noise ratio, the noise coming from the exhaust eddies, and the building vibrations.

At first, it was thought that the position of the test section was affected by the thermal expansion of the exhaust pipe due to the hot exhaust gas. This would alter not only the shape of the signal but the sensitivity of the system. A plain glass window with an adjustable angular position was installed to allow quick adjustments of the beam direction. Following these adjustments, it was still not possible to detect useful signals.

Further tests were made by motoring the engine while the engine remained hot to examine whether or not the exhaust gas itself was the main factor that caused the difficulty. With the engine motoring, the shape and intensity of the sound signal appeared to be as good as that obtained in atmospheric air.

Despite considerable effort to solve the "noise" problem, the measurement of exhaust gas temperature using the speed-of-sound method was not successful.

The sound wave signal could not be detected in the presence of the hot exhaust gases. It was concluded that the sound wave signal was obscured by the background noises which were generated by the density eddies of the exhaust gas itself. Several checks were made before reaching this conclusion. Various optical effects such as the position shift of the test section due to the thermal expansion of the pipe, the orientation of the photodiode plate relative to the location of the spark electrodes, and the position of the knife-edge, were examined carefully without any success. A high-pass filter circuit was constructed and used to eliminate the low-frequency signals from the exhaust gas.

Since no problems were encountered in detecting the sound wave in still air or a motored engine, the problem appears to be caused by the exhaust gas eddies. When the exhaust gas is introduced into the test section, the light is deflected not only by the sound wave but by the density fronts of the gas itself. The magnitudes of these deflections were observed to be approximately of the same order. Since these two effects are independent of each other, the net output signal from the combined schlieren effect would be completely random. Since this is a basic difficulty associated with the measuring technique itself, further continuation of the work was not pursued.